



UNIVERSITAT DE
BARCELONA

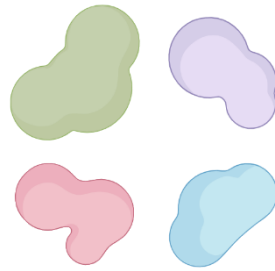
Understanding the genotype-phenotype relation between *PIK3CA* variant signalling and vascular malformations

Louis Maes

ADVERTIMENT. La consulta d'aquesta tesi queda condicionada a l'acceptació de les següents condicions d'ús: La difusió d'aquesta tesi per mitjà del servei TDX (www.tdx.cat) i a través del Dipòsit Digital de la UB (diposit.ub.edu) ha estat autoritzada pels titulars dels drets de propietat intel·lectual únicament per a usos privats emmarcats en activitats d'investigació i docència. No s'autoritza la seva reproducció amb finalitats de lucre ni la seva difusió i posada a disposició des d'un lloc aliè al servei TDX ni al Dipòsit Digital de la UB. No s'autoritza la presentació del seu contingut en una finestra o marc aliè a TDX o al Dipòsit Digital de la UB (framing). Aquesta reserva de drets afecta tant al resum de presentació de la tesi com als seus continguts. En la utilització o cita de parts de la tesi és obligat indicar el nom de la persona autora.

ADVERTENCIA. La consulta de esta tesis queda condicionada a la aceptación de las siguientes condiciones de uso: La difusión de esta tesis por medio del servicio TDR (www.tdx.cat) y a través del Repositorio Digital de la UB (diposit.ub.edu) ha sido autorizada por los titulares de los derechos de propiedad intelectual únicamente para usos privados enmarcados en actividades de investigación y docencia. No se autoriza su reproducción con finalidades de lucro ni su difusión y puesta a disposición desde un sitio ajeno al servicio TDR o al Repositorio Digital de la UB. No se autoriza la presentación de su contenido en una ventana o marco ajeno a TDR o al Repositorio Digital de la UB (framing). Esta reserva de derechos afecta tanto al resumen de presentación de la tesis como a sus contenidos. En la utilización o cita de partes de la tesis es obligado indicar el nombre de la persona autora.

WARNING. On having consulted this thesis you're accepting the following use conditions: Spreading this thesis by the TDX (www.tdx.cat) service and by the UB Digital Repository (diposit.ub.edu) has been authorized by the titular of the intellectual property rights only for private uses placed in investigation and teaching activities. Reproduction with lucrative aims is not authorized nor its spreading and availability from a site foreign to the TDX service or to the UB Digital Repository. Introducing its content in a window or frame foreign to the TDX service or to the UB Digital Repository is not authorized (framing). Those rights affect to the presentation summary of the thesis as well as to its contents. In the using or citation of parts of the thesis it's obliged to indicate the name of the author.



Understanding the genotype-phenotype relation
between *PIK3CA* variant signalling and
vascular malformations

Doctoral thesis entitled

Understanding the genotype-phenotype relation between *PIK3CA* variant signalling and vascular malformations

Comprensió de la relació genotip-fenotip entre la senyalització de les variants del gen *PIK3CA* i les malformacions vasculares

For obtaining the academic degree

Doctor of Philosophy

Doctor per la Universitat de Barcelona

Submitted by

Louis Maes, MS

Doctoral programme in Biomedicine

Faculty of Medicine

At the University of Barcelona



**UNIVERSITAT DE
BARCELONA**

Barcelona, 2025

Dr. Mariona Graupera

Thesis director

Dr. Ana Angulo-Urarte

Thesis director

Dr. Fransesc Viñals

Tutor

Louis Maes, MS

PhD candidate

Affidavit

The work entitled "Understanding the genotype-phenotype relation between *PIK3CA* variant signalling and vascular malformations" has been carried out by Louis Maes in the Endothelial Pathobiology and Microenvironment laboratory at the Josep Carreras Leukaemia Research Institute (IJC) under supervision of Dr. Mariona Graupera and Dr. Ana Angulo-Urarte. The information derived from the literature has been duly acknowledged in the text and a list of references is provided. No part of this work was previously presented for another degree or diploma at this or any other institution.

Financial support

This work received the following financial support:

- European Union's Horizon 2020 Research and Innovation Programme under the Marie Skłodowska-Curie grant agreement No. 955534 ("PIPgen")

Throughout this period, experimental work and training was performed at iOnctura (Geneva, Switzerland) and in the laboratory of Dr. Bart Vanhaesebroeck (University College London Cancer Institute) as part of secondments funded by "PIPgen".



Institut de Recerca
CONTRA LA LEUCÈMIA
Josep Carreras



“I can never be all the people I want and live all the lives I want. I can never train myself in all the skills I want. And why do I want? I want to live and feel all the shades, tones and variations of mental and physical experience possible in my life. “

Sylvia Plath

Acknowledgements

It's amazing how time passes faster the older we get. I still remember how working during COVID in my master's thesis motivated me to pursue a PhD abroad. Soon thereafter, I packed my bags and left to work in the Endothelial Pathobiology and Microenvironment lab. Since then, I have continued to grow and learn both professionally and personally. I have learned many lessons during my years in Barcelona, and it has been a crazy ride. This thesis recapitulates a lot of these lessons and in every page lies loads of work, consideration, frustration, but also so much happiness and pride. One of the lessons I learned is that life is not always about the destination, and it's not really about the journey either, but about the company that we meet along the way. I can say that I have been truly blessed with the most amazing laboratory, friends, and family. Sincerely, I could not have done this without you. It is because of all of you that this chapter in my life is truly remarkable and unforgettable.

First, I want to thank the one and only **Mariona**. Thank you for letting me be part of your wonderful group and for introducing me to the PIPgen network. With your care and advice, you have seen me grow and change into the person I am today. You are a truly inspirational person (seriously, I don't know how you are able to manage it all). Above all, I want to thank you for believing in me.

Ana, your upbeat attitude is inspirational. Getting introduced to the world of PI3K and vascular malformations was a pleasure because of your optimism. Thank you for all the support over the years, and specifically I want to thank you for your patience with me.

I would like to thank my tutor Dr. **Fransesc Viñals**. Next, I would like to thank the members of the defence committee, Dr. **Eulalia Baselga**, Dr. **Ana Fonseca**, and Dr. **Benoit Bilanges**. I feel honoured to discuss my work with you.

I would like to thank all people involved with my secondments. First, all the lovely people of **iOnctura**, I learned a great deal during my time in Geneva, thank you for introducing us to the complicated world of the biotech/pharma industry. Next, I would like to thank Dr. **Bart Vanhaesebroeck** for not only welcoming me into his lab, but also his home. Staying in your lab was a big learning experience for me. Thank you to the kind members of your lab that made me feel at home instantly. A special thanks to **Alberto**, **Sara**, **Benoit**, and **Grace**, for helping me complete my experiments, your expertise was highly valued.

I would like to thank everyone involved in the PIPgen network. This was truly a special opportunity through which I learned so much and helped me feel connected to the PI3K field. **Laia**, best project manager EVER! Thank you for all your work, the memories and lessons will not be forgotten. To all my fellow PIPgeners, **Alberto, Ilaria, Ane, Manu, Shal, Leqi, Devi, Sara, Sanzhar, Ivana, Shanlin, Maria, Janki, and Fatemeh**, I am so proud of what you have achieved and can't wait to see you all evolve into experienced PhDs!

Then, this experience simply would not have been the same without the amazing members of the ONA lab. I will always cherish the many memories, from calçotadas to parties, small breakfasts, coffee breaks, mental breakdowns, and even trips to Mallorca, Perarrúa, and the Delta de l'Ebre. Most importantly, you have all shaped me into the person I am today, and with that I mean you have seen me change my clothing style and hairstyle 1000 times. Thank you all for being such an amazing lab and making me feel welcome in Barcelona. To the "seniors", **Sandra, Leonor, Frede**, thank you for your expertise and making science fun. Your advice on the climbing wall or on the train from Toulouse are all greatly appreciated. To **Quim**, thank you for the scientific advice, but mostly for tremendously helping me setting up my life here in Barcelona. To the past members of the lab, **Judith, Anabel, Helena, and Saray**. You are all fantastic scientists, and it was a pleasure learning from you. Judith, you are like an older sister and your advice meant so much to me. Anabel, I didn't know they made scientists this good-looking! Simply, you are an amazing person. Helena, thank you for all your lessons and sharing a desk with me, you are simply the best! Next, my princess and twin **Odena**, I should dedicate this thesis to you for all the help you have given me, both academic and administrative! To all the PhD's still working hard, I am very proud of you, and I have no doubts you will all be amazing PhD researchers soon! **Margot** and **Xabi**, thank you for being my style icons over the years, a true science twink and handler combo. It was fun sharing the petit ONA lab for a little while. My favourite Catalan girl and little sister **Ari**. Ets un cas com un cabàs! You know you can count on me for a little coffee (with napolitana). El Mas Grande **Jose**, you are one of kind, please, never change. You are a truly inspirational guy, and I had a blast working with you! **Ane**, thank you for letting me eavesdrop when you were doing complicated analysis at our desk, I learned a lot from you! **Alba**, you are dramatic, but I love you for it. I will miss our many laughs and tears; I could not ask for a better desk partner. To my fellow guiris, **Manu, Hielke, and Marta**. It was absolutely fantastic getting to know you all, and we share so many memories I cannot even begin to list them. Thank you so much for making this experience unforgettable. To the newer members of the lab, **Elena, Annamaria, Maria, and Laisa**.

You are all wonderful people, and I wish you the best of luck for the future. You know who to call if you want a little party or need someone to drive your car out of a difficult situation.

Then, I would like to thank some special people that have changed my life considerably over the years. **Eve** (aka Buddheve), thank you for being my roommate. I will miss our many balcony chats and crazy nights, but most importantly, P4L. The feral trio would not be complete of course without my girlie **Kathleen**. You are both amazing people and I love you to death. Next, **Adri**, **Lauren**, and **Livi**, my besties, thank you for letting my queen out with y'all over the past year.

En tot slot, aan mijn vrienden en familie thuis. Bedankt om er altijd voor mij te zijn desondanks mijn impulsieve en zotte ideeën. **Papa**, **mama**, en mijn lieve **zussen**, dankuwel voor alle steun de afgelopen jaren, thuiskomen voelt altijd geweldig door al de moeite die jullie voor mij doen. Aan **Mamie** en **Papy**, **Bomma** en **Bompa**, bedankt voor de wonderlijke momenten en er steeds voor mij te zijn. **Maarten**, **Belén**, **Julie**, **Julia**, en **Laura**, bedankt voor al de mooie reizen en de ongelooflijke momenten, jullie zijn natuurlijk altijd welkom in Barcelona, of waar ik ook ben.

Contents

Acknowledgements	9
Abstract	15
Resum	17
List of figures	19
List of tables	20
List of non-standard abbreviations	21
Introduction	23
1. PI3K α signalling	23
1.1 The PI3K protein family	23
1.2 Class IA PI3K structure, function, and signalling	24
1.3 Pathogenic variants of the PIK3CA gene: from cancer to congenital disorders	28
2. PROS, vascular pathologies and related molecular drivers	31
2.1 Classification of PROS	31
2.2 Vascular malformations	34
2.3 Diagnosis and treatment of vascular malformations	36
3. Vascular development	38
3.1 The mammal circulatory system	38
3.2 Vascular origins and growth	40
3.3 Sprouting angiogenesis	41
3.4 Molecular regulators of endothelial cells during angiogenesis	44
3.5 Vessel maturation and stabilization	46
3.6 PI3K α signalling in the endothelium	48
Hypothesis and aims	53
Materials and methods	55
1. Animal husbandry and care	55
1.1 Mouse colony maintenance	55
1.2 Transgenic mouse models	55
1.2.1 <i>Pik3ca</i> ^{H1047R} , generated by <i>Kinross et al.</i> (268)	55
1.2.2 <i>Pik3ca</i> ^{E545K} , generated by <i>Robinson et al.</i> (269)	56
1.2.3 <i>Pik3ca</i> ^{E726K}	56
1.2.4 Cre lines	57
1.2.5 mTmG reporter line, generated by <i>Muzumbar et al.</i> (272)	57
1.3 Mice genotyping (tail lysis and PCR)	57
2. <i>In vivo</i> experiments	58
2.1 <i>in vivo</i> Cre-mediated recombination of <i>Pik3ca</i> mutations	58
2.2 Mouse retina isolation and immunostaining	59
2.3 Embryo isolation and immunostaining	60
2.4 Confocal microscopy	61
2.5 Image analysis and quantification	61
2.5.1 Localization and quantification of vascular lesions	61
2.5.2 Vascular area: IB4	62
2.5.3 Recombinant endothelial cell area: GFP	62
2.5.4 Endothelial cell number: ERG	62
2.5.5 PI3K α pathway activation: p-S6	62
2.5.6 MAPK pathway activation: p-ERK	62
3. Recombinant protein experiments	63
3.1 Generation of <i>PIK3CA</i> mutant plasmids	63
3.2 Bacmid transformation and preparation	64

3.3 Sf9 insect cell transfection and amplification	64
3.4 Protein purification	65
3.5 ADP glo	65
4. <i>In vitro</i> experiments	66
4.1 Mouse heart endothelial cell isolation and culture	66
4.2 <i>In vitro</i> Cre-mediated recombination of <i>Pik3ca</i> mutations	67
4.3 Analysis of recombination with PCR	67
4.4 Protein extraction and immunoblotting	68
4.4.1 Signalling in basal, starved, and iFBS-stimulated conditions	68
4.4.2 Signalling in VEGFC and EGF-stimulated conditions	68
4.4.3 Protein extraction and immunoblotting	69
4.5 RNA extraction and qPCR	70
4.5.1 Expression of <i>Ang2</i> , <i>Cxcr4</i> , <i>EphB4</i> , <i>Itga9</i>	70
4.5.2 Expression of <i>Vegfr1</i> , <i>Vegfr2</i> , <i>Vegfr3</i> , and <i>Egfr</i> in starved and EGF-stimulated conditions	70
4.5.3 RNA extraction, cDNA synthesis and qPCR	70
4.6 Confluency assay	71
4.7 EdU-incorporation assay	71
4.8 Scratch-wound assay	72
5. Statistical analysis	72
Results	73
I. Objective 1: Studying the activating <i>PIK3CA</i> mutations in the developing vasculature in mice.	73
1.1. Vascular malformations generated by the <i>PIK3CA</i> variants during angiogenesis.	73
1.2. Vascular malformations generated by the <i>PIK3CA</i> variants during vascular remodelling.	82
1.3. Tolerability of <i>Pik3ca</i> ^{E545K} expression during embryonic development.	88
II. Objective 2: Elucidating <i>PIK3CA</i> variant kinase activity and signalling differences in cultured endothelial cells.	93
2.1. Variant effect on PI3K α 's kinase activity.	93
2.2. Characterization of recombination between the different <i>Pik3ca</i> mutant constructs <i>in vitro</i> .	95
2.3 Signalling differences between the <i>PIK3CA</i> variants <i>in vitro</i> .	97
2.4 Cellular processes affected by <i>PIK3CA</i> variants <i>in vitro</i> .	107
III. Objective 3: Exploring the signalling differences between <i>Pik3ca</i> ^{H1047R} and <i>Pik3ca</i> ^{E545K} <i>in vivo</i> during vascular malformation development.	113
3.1. Validation of PI3K α activation in <i>Pik3ca</i> ^{E545K} .	113
3.2. Study of MAPK signalling in <i>Pik3ca</i> ^{H1047R} and <i>Pik3ca</i> ^{E545K} .	121
Discussion	127
I. Objective 1: Studying the activating <i>PIK3CA</i> mutations in the developing vasculature in mice.	128
II. Objective 2: Elucidating <i>PIK3CA</i> variant kinase activity and signalling differences in cultured endothelial cells.	133
III. Objective 3: Exploring the signalling differences between <i>Pik3ca</i> ^{H1047R} and <i>Pik3ca</i> ^{E545K} <i>in vivo</i> during vascular malformation development.	138
Conclusions	143
References	145

Abstract

Vascular malformations (VMs) represent a diverse group of diseases with complex yet poorly understood underlying mechanisms. Causative gain-of-function mutations in *PIK3CA* have been associated with the onset of these disorders. The pathological diversity has made scientific research challenging, however, recent advances in genetically engineered mouse models have provided tools for spatiotemporal control of *PIK3CA* activation, offering an opportunity to investigate vascular processes such as angiogenesis and vascular remodelling, and the effect of *Pik3ca* variant expression.

In this thesis, we addressed the knowledge gap in understanding the genotype-phenotype relationship of three common *PIK3CA* variants found in VMs: *PIK3CA*^{H1047R}, *PIK3CA*^{E545K}, and *PIK3CA*^{E726K}. Using conditional mouse models, we studied these variants by expressing them in endothelial cells (ECs) during key stages of vascular development. We also examined mouse embryonic lethality and intracellular signalling pathways associated with these variants in cultured mouse ECs and *in vivo*.

Our results revealed significant phenotypic and molecular differences between the *PIK3CA* variants. *In vivo*, *Pik3ca*^{H1047R/WT} and *Pik3ca*^{E545K/WT} expression caused extensive vascular hyperplasia and increased EC numbers during active angiogenesis. *In vitro*, *Pik3ca*^{H1047R/WT} expression strongly activated PI3K α -AKT and MAPK signalling pathways, upregulated VEGFR2 and VEGFR3, and slightly downregulated EGFR. By contrast, *Pik3ca*^{E545K/WT} expression induced less robust PI3K α -AKT activation, potential MAPK downregulation, and mild upregulation of VEGFR2, VEGFR3, and EGFR. Conversely, *Pik3ca*^{E726K/WT} expression caused only mild vascular phenotypes and modest PI3K α -AKT activation, suggesting this mutation leads to milder VM phenotypes.

These findings shed light on the distinct molecular mechanisms underlying the vascular phenotypes associated with these *PIK3CA* mutations. Furthermore, the observed differences between the variants in these regulators of angiogenesis reveal potential targets for therapeutic intervention. This work highlights the utility of conditional mouse models in advancing our understanding of VM disease progression, paving the way for future research into personalized medicine for patients suffering from VMs.

Keywords: Clinical Genetics (320102), Angiology (320117), Cardiovascular Pathology (320704), Pathology (320700)

Resum

Les malformacions vasculares (MV) formen un grup divers de malalties amb mecanismes subjacents complexos però poc compresos. Les mutacions causants de guany de funció a *PIK3CA* s'han associat amb l'aparició d'aquestes malalties. La diversitat patològica ha fet que la recerca científica sigui un repte; tanmateix, els avenços recents en models de ratolí genèticament modificats han proporcionat eines per al control espaciotemporal de l'activació de *PIK3CA*, oferint una oportunitat per investigar processos vasculares com l'angiogènesi i la remodelació vascular, així com l'efecte de l'expressió de variants de *Pik3ca*.

En aquesta tesi, aprofundim en la manca de coneixement de la relació genotip-fenotip de tres mutacions freqüents de *PIK3CA* trobades en MV: *PIK3CA^{H1047R}*, *PIK3CA^{E545K}* i *PIK3CA^{E726K}*. Utilitzant models de ratolins condicionals, hem estudiat aquestes mutacions expressant-les en cèl·lules endotelials (CEs) durant etapes clau del desenvolupament vascular. També hem examinat la letalitat embrionària i les vies de senyalització intracel·lular associades amb aquestes mutacions en CEs cultivades i *in vivo*.

Els nostres resultats han identificat diferències fenotípiques i moleculars significatives entre les variants de *PIK3CA*. *In vivo*, l'expressió de *Pik3ca^{H1047R/WT}* i *Pik3ca^{E545K/WT}* va causar una hiperplàsia vascular extensa i un augment del nombre de CEs durant l'angiogènesi activa. *In vitro*, l'expressió de *Pik3ca^{H1047R/WT}* va activar fortament les vies de senyalització PI3K α -AKT i MAPK, va induir un augment de l'expressió VEGFR2 i VEGFR3, i una disminució lleugera de l'expressió EGFR. Per contra, l'expressió de *Pik3ca^{E545K/WT}* va induir una activació menys robusta de PI3K α -AKT, una possible regulació a la baixa de MAPK, i una lleugera regulació a l'alça de VEGFR2, VEGFR3 i EGFR. L'expressió de *Pik3ca^{E726K/WT}* va causar només fenotips vasculars lleus i una activació modesta de PI3K α -AKT, suggerint que aquesta mutació condueix a fenotips de MV més suaus. Aquests resultats il·lustren els mecanismes moleculars diferents subjacents als fenotips vasculars associats amb aquestes mutacions de *PIK3CA*. A més, les diferències observades en alguns reguladors de angiogènesis entre les variants revelen possibles dianes per a la intervenció terapèutica. Aquest treball destaca la utilitat dels models de ratolí condicionals per avançar en la comprensió de la progressió de les MV, obrint camí per a futures investigacions en medicina personalitzada per als pacients que pateixen MV.

Paraules clau: Genètica Clínica (320102), Angiologia (320117), Patologia Cardiovascular (320704), Patologia (320700)

List of Figures

Introduction

Figure 1.1. <i>PIK3CA</i> and <i>PIK3R1</i> genes and inhibitory contacts.	25
Figure 1.2. Important steps in the activation of PI3K α .	26
Figure 1.3. <i>PIK3CA</i> gene and reported variants in PROS.	30
Figure 2.1. Classification of PROS disorders.	32
Figure 2.2. How strength of variant activation correlates with tolerability during embryonic development.	33
Figure 3.1. Composition of the main vessel types in the cardiovascular system.	40
Figure 3.2. Tip/stalk cell differentiation during early angiogenesis.	42
Figure 3.3. Endothelial differentiation during embryonic development.	46

Results

Figure 1.1.1. <i>In vivo</i> strategies for overactivation of <i>PIK3CA</i> with <i>Pik3ca</i> mutant mouse models.	74
Figure 1.1.2. <i>In vivo</i> injections scheme to study overactivation of <i>PIK3CA</i> with <i>Pik3ca</i> mutant mouse models.	75
Figure 1.1.3. Occurrence of <i>Pik3ca</i> ^{H1047R} , <i>Pik3ca</i> ^{E545K} , and <i>Pik3ca</i> ^{E726K} -driven vascular malformations during angiogenesis.	75
Figure 1.1.4. <i>Pik3ca</i> ^{H1047R} -driven vascular malformations in mouse retinas.	77
Figure 1.1.5. <i>Pik3ca</i> ^{H1047R} -driven vascular malformations with increased amounts of endothelial cells in mouse retinas.	78
Figure 1.1.6. <i>Pik3ca</i> ^{E545K} -driven vascular malformations in mouse retinas.	79
Figure 1.1.7. <i>Pik3ca</i> ^{E545K} -driven vascular malformations with increased amounts of endothelial cells in mouse retinas.	80
Figure 1.1.8. <i>Pik3ca</i> ^{E726K} -driven vascular malformations in mouse retinas.	81
Figure 1.1.9. <i>Pik3ca</i> ^{E726K} -driven vascular malformations with increased amounts of endothelial cells in mouse retinas.	82
Figure 1.2.1. <i>In vivo</i> injection scheme to study overactivation of <i>PIK3CA</i> with <i>Pik3ca</i> mutant mouse models.	83
Figure 1.2.2. Occurrence of <i>Pik3ca</i> ^{H1047R} , <i>Pik3ca</i> ^{E545K} , and <i>Pik3ca</i> ^{E726K} -driven vascular malformations during vascular remodelling.	83
Figure 1.2.3. <i>Pik3ca</i> ^{H1047R} expression during vascular remodelling in mouse retinas.	85
Figure 1.2.4. <i>Pik3ca</i> ^{E545K} expression during vascular remodelling in mouse retinas.	86
Figure 1.2.5. <i>Pik3ca</i> ^{E726K} expression during vascular remodelling in mouse retinas.	88
Figure 1.3.1. Embryos of <i>Tie2-Cre-</i> ; <i>Pik3ca</i> ^{E545K/WT} , <i>Tie2-Cre+</i> ; <i>Pik3ca</i> ^{WT/WT} and <i>Tie2-Cre+</i> ; <i>Pik3ca</i> ^{E545K/WT} at E11.5.	90
Figure 1.3.2. Stereoscope images of embryos of <i>Tie2-Cre-</i> ; <i>Pik3ca</i> ^{E545K/WT} , <i>Tie2-Cre+</i> ; <i>Pik3ca</i> ^{WT/WT} and <i>Tie2-Cre+</i> ; <i>Pik3ca</i> ^{E545K/WT} at E10.5.	91
Figure 1.3.3. Confocal images of embryos of <i>Tie2-Cre-</i> ; <i>Pik3ca</i> ^{E545K/WT} , <i>Tie2-Cre+</i> ; <i>Pik3ca</i> ^{WT/WT} and <i>Tie2-Cre+</i> ; <i>Pik3ca</i> ^{E545K/WT} at E10.5.	92
Figure 2.1.1. Determination of optimal enzyme concentration and comparison of enzyme activity for wild-type and mutant PI3K α in basal conditions.	94
Figure 2.1.2. Determination of optimal enzyme concentration and comparison of enzyme activity for wild-type and mutant PI3K α in pY-stimulated conditions.	95
Figure 2.2.1. Determination of recombination in EC- <i>Pik3ca</i> ^{E545K/WT} and EC- <i>Pik3ca</i> ^{E726K/WT} with different treatments of 4-OHT.	96
Figure 2.2.2. Validation of the recombination in the three heterozygous EC- <i>Pik3ca</i> ^{H1047R/WT} , EC- <i>Pik3ca</i> ^{E545K/WT} , and EC- <i>Pik3ca</i> ^{E726K/WT} .	97
Figure 2.3.1. Comparison of PI3K α pathway activation between EC- <i>Pik3ca</i> ^{H1047R/WT} , EC- <i>Pik3ca</i> ^{E545K/WT} , and EC- <i>Pik3ca</i> ^{E726K/WT} <i>in vitro</i> .	98
Figure 2.3.2. Comparison of MAPK pathway activation between EC- <i>Pik3ca</i> ^{H1047R/WT} , EC- <i>Pik3ca</i> ^{E545K/WT} , and EC- <i>Pik3ca</i> ^{E726K/WT} <i>in vitro</i> .	99

Figure 2.3.3. Impact of EC- <i>Pik3ca</i> ^{H1047R/WT} , EC- <i>Pik3ca</i> ^{E545K/WT} , and EC- <i>Pik3ca</i> ^{E726K/WT} on transcription of <i>Ang2</i> , <i>EphB4</i> , <i>Cxcr4</i> , and <i>Itga9</i> .	101
Figure 2.3.4. Regulation of PI3K α -AKT pathway activation in EC- <i>Pik3ca</i> ^{H1047R/WT} and EC- <i>Pik3ca</i> ^{E545K/WT} in VEGFC and EGF-stimulated conditions <i>in vitro</i> .	103
Figure 2.3.5. Regulation of MAPK pathway activation in EC- <i>Pik3ca</i> ^{H1047R/WT} and EC- <i>Pik3ca</i> ^{E545K/WT} in VEGFC and EGF-stimulated conditions <i>in vitro</i> .	104
Figure 2.3.6. Impact of EC- <i>Pik3ca</i> ^{H1047R/WT} and EC- <i>Pik3ca</i> ^{E545K/WT} on transcription of <i>Vegfr1</i> , <i>Vegfr2</i> , <i>Vegfr3</i> , and <i>Egfr</i> expression in starved and EGF-stimulated conditions.	106
Figure 2.4.1. Impact of EC- <i>Pik3ca</i> ^{H1047R/WT} and EC- <i>Pik3ca</i> ^{E545K/WT} on confluency in normal growth conditions <i>in vitro</i> .	108
Figure 2.4.2. Impact of EC- <i>Pik3ca</i> ^{H1047R/WT} and EC- <i>Pik3ca</i> ^{E545K/WT} on confluency in starvation conditions <i>in vitro</i> .	109
Figure 2.4.3. Impact of EC- <i>Pik3ca</i> ^{H1047R/WT} and EC- <i>Pik3ca</i> ^{E545K/WT} on proliferation in normal growth conditions <i>in vitro</i> .	110
Figure 2.4.4. Impact of EC- <i>Pik3ca</i> ^{H1047R/WT} and EC- <i>Pik3ca</i> ^{E545K/WT} on migration in normal growth conditions <i>in vitro</i> .	111
Figure 2.4.5. Impact of EC- <i>Pik3ca</i> ^{H1047R/WT} and EC- <i>Pik3ca</i> ^{E545K/WT} on migration in starvation conditions <i>in vitro</i> .	112
Figure 3.1.1. Recombination in <i>Pik3ca</i> ^{E545K/WT} mouse retinas with different doses of 4-OHT.	114
Figure 3.1.2. <i>In vivo</i> injection scheme to study overactivation of <i>PIK3CA</i> with <i>Pik3ca</i> mutant mouse models.	114
Figure 3.1.3. <i>Pik3ca</i> ^{H1047R} -driven vascular malformations in mouse retinas with 2.5 mg/kg 4-OHT injection.	116
Figure 3.1.4. <i>Pik3ca</i> ^{E545K} -driven vascular malformations in mouse retinas with 2.5 mg/kg 4-OHT injection.	118
Figure 3.1.5. P-S6 (S235/236) levels in <i>Pik3ca</i> ^{E545K} -expressing mouse retinas with 2.5 mg/kg 4-OHT injection.	120
Figure 3.1.6. P-ERK (T202/Y204) levels in <i>Pik3ca</i> ^{H1047R} -expressing mouse retinas with 2.5 mg/kg 4-OHT injection.	122
Figure 3.1.7. P-ERK levels in <i>Pik3ca</i> ^{E545K} -expressing mouse retinas with 2.5 mg/kg 4-OHT injection.	124

List of Tables

Introduction

Table 2.1. Classification of vascular malformations (VMs) depending on their functional characteristics and the associated mutated gene.	35
--	----

Materials and methods

Table 1.1. Primers and conditions for the PCR reaction used to genotype animal constructs.	58
Table 2.1. Primary antibodies for retinal immunostaining.	60
Table 2.2. Secondary antibodies for retinal immunostaining.	60
Table 2.3. Primary antibodies for embryo immunostaining.	61
Table 2.4. Secondary antibodies for embryo immunostaining.	61
Table 3.1. Primers designed for mutagenesis.	64
Table 4.1. Reagents used for mouse heart EC isolation and culture.	66
Table 4.2. Primers and conditions to verify <i>Pik3ca</i> mutant construct recombination.	68
Table 4.3. Primary antibodies used for immunoblotting.	69
Table 4.4. Fluorescent secondary antibodies used for immunoblotting.	69
Table 4.5. Primers used for qPCR.	71

Results

Table 1.3.1. Viability table of <i>Tie2-Cre</i> ; <i>Pik3ca</i> ^{E545K/WT} embryos.	89
--	----

List of non-standard abbreviations

4-OHT	4-hydroxy-tamoxifen
ABD	Antigen binding domain
AJ	Adherent junction
ANG1/2	Angiopoietin 1/2
ARAP3	ArfGAP With RhoGAP Domain, Ankyrin Repeat And PH Domain 3
ATP	Adenosine 5'-triphosphate
CLOVES	Congenital Lipomatous asymmetric Overgrowth of the trunk with lymphatic, capillary, venous, and combined-type Vascular malformations, Epidermal naevi, Scoliosis/Skeletal and spinal anomalies
CTF	Corrected total fluorescence
CXCR4	C-X-C chemokine receptor type 4
DCMO	Diffuse Capillary Malformation with Overgrowth
DLL4	Delta-like 4 ligand
EC	Endothelial cell
ECM	Extracellular matrix
EdU	5-ethynyl-2-deoxyuridine
EGF	Epidermal growth factor
EMA	European medicines agency
EMP	Erythron-myeloid progenitor cell
eNOS	Endothelial nitric oxidase
EPHB4	Ephrin type-B receptor 4
ERK	Extracellular signal-regulated kinase
etOH	Ethanol
FCD	Focal cortical dysplasia
FDA	Food and drug administration
FOXO1	Forkhead box O transcription factor 1
GAP	GTPase-activating protein
GFP	Green fluorescence protein
GPCR	G-protein coupled receptor
HMEG/DMEG	Megalencephaly
HUVEC	Human umbilical vein endothelial cell
IB4	Isolectin B4
IF	immunofluorescence
IGF	Insulin-like growth factor
ITGA9	Integrin α 9
KLF2	Krueppel-like factor 2
LM	Lymphatic malformation
MAPK	Mitogen-activated protein kinase
MCAP	Megalencephaly-capillary malformation-polymicrogyria syndrome
MMP	Metalloprotease
mTOR	Mechanistic target of Rapamycin
NICD	Notch intracellular domain
NRARP	Notch-regulated ankyrin repeat protein
PC	Pericyte
PDGFB	Platelet derived growth factor B
PDGFR β	Platelet derived growth factor receptor β
PDK1	Phosphoinositide-dependent kinase 1

PGF	Placental growth factor
PH	Pleckstrin homology domain
PI3K	Phosphoinositide 3-kinase
PIP2	phosphatidylinositol 4,5-bisphosphate
PIP3	phosphatidylinositol 3,4,5-trisphosphate
PROS	<i>PIK3CA</i> -related overgrowth spectrum
PTEN	Phosphatase and Tensin homology
qPCR	Quantitative polymerase chain reaction
RBD	Ras binding domain
RTK	Receptor tyrosine kinase
Sf9	<i>Spodoptera frugiperda</i>
SH2	Src homology domain
TGF β	Transforming growth factor β
TIE2	Tyrosine kinase with immunoglobulin-like and EGF-like domains 2
TJ	Tight junction
VE-Cadherin	Vascular endothelial cadherin
VEGF	Vascular endothelial growth factor
VEGFR	Vascular endothelial growth factor receptor
VM	Vascular malformation
VPS34	Vacuolar protein sorting 34
vSMC	Vascular smooth muscle cell
WT	Wild type

Introduction

1. PI3K α signalling

For an organism to survive, its cells require control over important processes such as proliferation, survival, migration, and metabolism. To coordinate these processes, cells must continuously sense their environment, integrate external and internal signals, and provide the appropriate response. This is achieved through intricate signalling networks composed of receptors, enzymes, and transcription factors which receive, transmit, and process molecular signals to elicit specific cellular responses. A key component of such a signalling network is **phosphoinositide 3-kinase (PI3K)**. It was first identified in 1988 as a critical mediator of intracellular signalling (1). Additional research revealed PI3K activity influences fundamental cellular behaviours, including growth, differentiation, metabolism, and cell death (2). Mutations in the gene encoding PI3K can disrupt these cellular processes, leading to a range of human diseases, such as cancer, overgrowth syndromes, immune deficiencies, and metabolic disorders (3). Despite extensive research, the mechanisms underlying the context-dependent regulation of PI3K remain incompletely understood. Further exploration of how PI3K signalling influences different cellular environments could reveal novel therapeutic strategies for targeting PI3K-associated diseases.

1.1 The PI3K protein family

The PI3K lipid kinase family contains 8 members, subcategorized into 3 classes. **Class I PI3Ks** form obligate heterodimers between a catalytic subunit and regulatory subunit. Depending on the regulatory subunit, class I PI3Ks are divided into subclasses, class IA and IB. The class IA comprises 3 isoforms, p110 α , p110 β , and p110 δ , encoded by the *PIK3CA*, *PIK3CB*, and *PI3KCD* genes. These catalytic isoforms interact with 5 regulatory subunits, p85 α and splicing variants p55 α and p50 α encoded by *PIK3R1*, p85 β encoded by *PIK3R2*, and p55 γ encoded by *PIK3R3*. This interaction is non-specific and depends on cellular context and availability (4, 5). Class IB includes one kinase p110 γ encoded by *PIK3CG* and regulatory subunits p101 encoded by *PIK3R5*, and p87 encoded by *PIK3R6* (6). All class I PI3Ks use ATP to convert phosphatidylinositol 4,5-bisphosphate (PIP₂) into phosphatidylinositol 3,4,5-trisphosphate (PIP₃) at the cellular membrane (7).

Class II contains 3 members, PI3K-C2 α , PI3K-C2 β , and PI3K-C2 γ , encoded by *PIK3C2A*, *PIK3C2B*, and *PIK3C2G*. These monomers are able to catalyse 2 reactions at the cellular membrane: conversion of PI4P into PI(3,4)P₂, or conversion of PI into PI3P (8). By facilitating these conversions, these kinases contribute to vesicle trafficking and membrane dynamics. Specifically, PI3K-C2 α regulates clathrin coating during endocytosis and performs a scaffolding function during mitotic spindle formation (9, 10). PI3K-C2 β regulates mTORC1 signalling and regulates cell growth (11). While the other members are ubiquitously expressed, PI3K-C2 γ is only expressed in the liver where it regulates AKT2 function (12).

Class III contains one enzyme VPS34, encoded by *PIK3C3*, which converts PI into PI3P. This enzyme forms large, tetrameric protein complexes (complex 1 or complex 2) and plays a role in vesicle trafficking and autophagosome formation (13, 14).

1.2 Class IA PI3K structure, function, and signalling

The genes encoding for the catalytic subunits of **class IA PI3Ks** (*PIK3CA*, *PIK3CB*, *PI3KCD*) consist of 5 domains; the p85 binding domain (ABD) which facilitates the interaction with the p85 regulatory subunit, a Ras binding domain (RBD) for interaction with Ras, a C2 domain which facilitates membrane interactions, a helical domain, and a kinase domain (15). Once encoded, p110 catalytic subunits will be degraded unless stabilized by interaction with the regulatory subunit p85, which simultaneously inhibits the lipid kinase function (16) (see **Figure 1.1**). The PI3K complex is then activated by various upstream signalling events, allowing the pathway to respond to environmental cues with precise spatial and temporal control. This ensures that PI3K signalling generates a specific and appropriate cellular response. Generally, the intracellular

signalling response is finetuned by PI3K's location at the plasma membrane, the amount of substrate binding to the RTK, the duration of the extracellular signal, the type of receptor, the control via Ras and other interactions, and autophosphorylation and ubiquitination of the p85 regulatory subunit (17, 18).

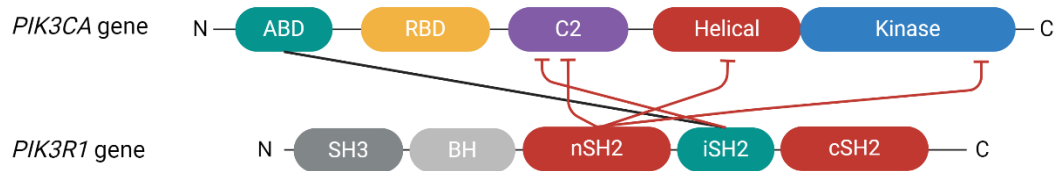


Figure 1.1. *PIK3CA* and *PIK3R1* genes and inhibitory contacts.

The 5 domains of *PIK3CA* gene encoding p110 α and the 5 domains of the *PIK3R1* gene encoding p85 α , p55 α , and p50 α . The ABD closest to the N-tail, followed by the RBD, C2, helical, and kinase domains. The ABD domain interacts with the iSH2 domain (black line), resulting in 4 inhibitory contacts between the 2 subunits (red lines). Figure modified from (16).

Class IA PI3K activity is primarily regulated by **receptor tyrosine kinases (RTK)**. RTK are present at the plasma membrane and are activated by substrates from the cellular environment. Interaction with their substrate will cause dimerization of 2 RTK subunits, followed by their cross-phosphorylation on phosphotyrosine (pY) residues on the intracellular part of the receptor. These pY sites control distinct cellular pathways since they can be recognized by cellular domains on kinases or other adaptor molecules, which will propagate the signal further downstream. The p85 regulatory subunit contains a Src homology domain (SH2) domain that can recognize a phosphorylated YXXM motif of a RTK (19). This interaction will localize the PI3K complex at the plasma membrane, where it will perform its catalytic function. Moreover, the interaction between the RTK and p85 will cause a conformational change in the complex and relieve the inhibitory contacts between 2 PI3K subunits (20). This both activates the catalytic domain of the PI3K complex, and reveals lipid binding surfaces required for tight connection with the plasma membrane (15). As a result, the p110 catalytic subunit is activated at the plasma membrane to convert PIP₂ to PIP₃ (see **Figure 1.2**).

Class IA PI3K activity is further enhanced by the membrane-bound G protein **Ras** (21). *In vitro* studies suggested that RTKs and G-proteins can directly bind PI3K at distinct sites, resulting in synergistic activation (22, 23). Two models have been proposed to explain how G-proteins enhance PI3K activity: the membrane recruitment model, where G-proteins increase PI3K's membrane localization, and the enzyme activation model, where G-proteins enhance PI3K's catalytic activity (23). Both models are not mutually exclusive, since Ras isoforms are known to recruit PI3K to the membrane (24), while

structural studies indicated that Ras binding also induces conformational changes that regulate PI3K activity (25). However, current evidence remains inconclusive on the precise mechanism by which Ras amplifies PI3K activation and how this affects downstream signalling responses.

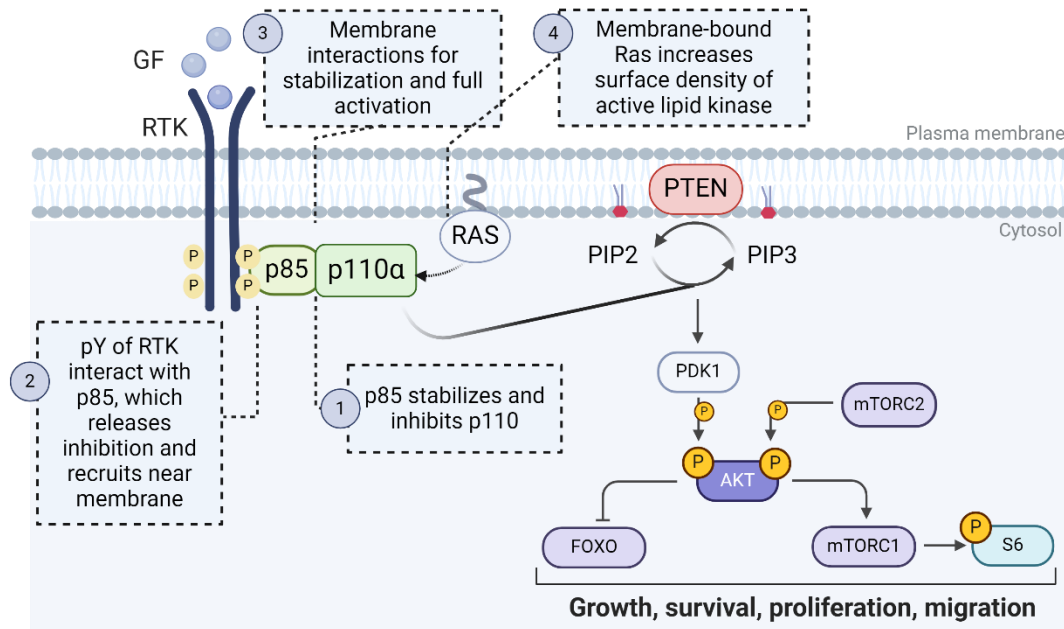


Figure 1.2. Important steps in the activation of PI3Kα.

1) The heterodimer PI3Kα protein will form by interactions between the regulatory subunit p85 and the catalytic subunit p110α, these interactions will stabilize the complex but prohibit catalytic activity. 2) Once the cell receives signals from its environment, RTK will active and autophosphorylate on tyrosine residues. These can be recognized by p85. Interaction between RTK and p85 will relieve the inhibitory contact of p85 on p110α, activating the enzyme. 3) PI3Kα can be further activated by integration into the plasma membrane. 4) p110α also contains a Ras binding domain for interactions with membrane-bound Ras. This interaction can also further activate the enzyme. The activated PI3Kα will convert PIP2 into PIP3 at the membrane, this conversion is antagonized by PTEN. PIP3 acts as a second messenger to many proteins, most notably, it will activate AKT activation, which will influence cell processes such as growth, survival, proliferation, and migration.

PIP3 at the plasma membrane acts as a second messenger since it can be recognized by proteins containing a Pleckstrin homology (PH) domain. These proteins include kinases, adaptors, Guanine Exchange Factors (GEFs), and GTPase Activating Proteins (GAPs) (15). Hereby, PI3K influences multiple signalling cascades, most notably the AKT-mTOR pathway (26).

The **AKT** protein family consists of 3 isoforms: AKT1, AKT2, and AKT3. AKT1 and AKT2 are ubiquitously expressed, while AKT3 is predominantly found in the liver, endocrine tissues, and the brain (27). AKT interaction with PIP3 at the plasma membrane will first promote phosphorylation by PDK1 on T308 and subsequently by mTORC2 on S473. Once AKT is fully activated, its lifespan is relatively short. However, it can activate many

effectors including other lipid kinases, transcription factors, metabolic enzymes, E3 ubiquitin ligases, cell cycle regulators, and others. Together, these will regulate cell growth, survival, proliferation, and metabolism (28).

One of the key AKT substrates is Tuberous Sclerosis Complex 2 (TSC2), which inhibits the small GTPase Rheb. Phosphorylation of TSC2 by AKT relieves its inhibitory effect on Rheb. Activated Rheb promotes **mTORC1** activation, which is a critical regulator of protein synthesis, autophagy, and cell growth (29). Additionally, AKT phosphorylates and inhibits **FOXO** transcription factors, excluding them to the cytosol for degradation. Hereby, AKT reduces their ability to drive the expression of pro-apoptotic genes such as BIM and PUMA, thus promoting cell survival (30).

AKT also plays a crucial role in metabolic regulation. It phosphorylates **Glycogen Synthase Kinase 3 (GSK3)**, inhibiting its activity and thereby promoting glycogen synthesis (31). In adipose and muscle tissues, AKT-mediated phosphorylation of AS160 (TBC1D4) enhances glucose uptake by facilitating GLUT4 vesicle translocation to the plasma membrane, a key process in insulin signalling (32). Furthermore, AKT activates MDM2, leading to the degradation of p53, thereby reducing apoptosis, which can contribute to tumorigenesis in cancer cells (33).

While AKT is a major effector of PI3K, several important signalling branches operate **independently of AKT**. For instance, ARAP3 is a GAP which is directly activated by PIP3 and regulates the small GTPase RhoA, which controls cytoskeletal dynamics and cell migration (34). Similarly, DOCK180, a GEF, is recruited by PIP3 to activate Rac1, influencing actin cytoskeleton remodelling and cell motility (35). Another key pathway involves Serum- and Glucocorticoid-Induced Kinase (SGK), which shares overlapping substrates with AKT but has distinct regulatory roles in ion transport and cell survival (36). Additionally, Bruton's Tyrosine Kinase (BTK), a PH domain-containing kinase activated by PIP3, is critical for B-cell receptor signalling and plays a fundamental role in immune cell activation (37).

The reaction from PIP2 to PIP3 by PI3Ks at the plasma membrane is antagonized by **Phosphatase and Tensin homology lipid phosphatase (PTEN)**, resulting in inhibition of cell survival, growth, and proliferation (38). This phosphatase adds another layer of control over the PI3K pathway, since PTEN expression, location, stability, and activity are regulated by other protein-protein interactions and post-translational modifications (38).

We discussed some of PI3K's main pathway signalling components and the resulting control over processes such as proliferation, survival, and metabolism. However, how

the different cell and environmental contexts determine the signalling output remains underexplored. Since class IA PI3K pathway alterations are implicated in many human diseases, it is of crucial importance that these cellular contexts are investigated. This could unravel new mechanistic insights in pathway activation and elucidate new therapeutic targets (15).

1.3 Pathogenic variants of the *PIK3CA* gene: from cancer to congenital disorders

Given that PI3K α plays a critical role in essential cellular processes, disruptions in this signalling pathway can lead to severe consequences for the organism. Since its discovery, PI3K α activity has been linked to pathological cell growth and oncogenesis (39-42). First, somatic mutations in the *PIK3CA* gene were found causative for colorectal cancer (39). Since then, ***PIK3CA* somatic mutations** have been found in 24 to 46% of endometrial cancer, 20 to 32% of breast cancers, 20 to 27% of bladder cancer, 14 to 23% of cervical cancers, 13 to 28% of colorectal cancer, and 12 to 15% of head-and-neck cancer (40). This makes *PIK3CA* one of the most commonly mutated oncogenes (41, 42). These mutations are missense gain-of-function mutations, resulting in increased PI3K α pathway activation through different mechanisms, promoting tumour transformation and even multipotency (43-45).

In cancer, mutations have been found all over the *PIK3CA* gene, except the Ras binding domain. Yet, more than 80% of oncogenic *PIK3CA* mutations cluster at three specific sites, known as oncogenic **hotspot variants** (40). These include two mutations in the helical domain, where glutamic acid (E) is replaced by lysine (K) at positions 542 (**E542K**) and 545 (**E545K**), and one mutation in the kinase domain, where histidine (H) is replaced by arginine (R) at position 1047 (**H1047R**).

The oncogenic hotspots have since been extensively studied, and research regarding their activating mechanism reveals how they promote oncogenic transformation. The **H1047R** variant induces conformational changes which modify several aspects of the protein's kinase activity (46-48). Firstly, the H1047 position in the WT enzyme stabilizes the activation loop of the kinase domain via a hydrogen bond. H1047R disrupts this hydrogen bond, resulting in a release of this activation loop and hereby increasing kinase activity. Secondly, the gain in flexibility at the C-terminal with H1047R facilitates better interaction with the plasma membrane, further enhancing the kinase activity of the enzyme. Lastly, the inhibitory interaction between the iSH2 domain on p85 α with the ABD on p110 α is disrupted with H1047R, allowing the catalytic subunit more mobility. These specific conformational changes have important consequences for the regulation of this

variant. Namely, growth factor stimulation and the resulting interaction between RTK and PI3K α can further cause overactivation with this variant (48-50). However, disruption of the Ras interaction with PI3K α did not affect the oncogenicity of H1047R, suggesting this variant does not require Ras activation for oncogenic transformation (49).

The **E545K** and E542K variants have a different activating mechanism. The inhibitory contacts between both subunits are facilitated by the E545 and E542 residues of WT p110 α (46). These variants cause the disruption of salt bridges between the subunits, causing partial disengagement and relieving the inhibitory contacts on p110 α (46). The dissociation of the two subunits mimics activation via RTK, meaning this variant renders the protein into a basally active state, and further activation via RTK does not affect its overactivation (47, 48). Interestingly, the oncogenic potential of these variants required the interaction with Ras (48-50).

An interesting aspect is the occurrence of double *PIK3CA* variants found in 13% of all *PIK3CA*-related cancers (51). This phenomenon was most frequently observed in breast, uterine, and colorectal cancer. Often, the 2 mutations were found on the same allele, and included combination of a hotspot mutation with a non-hotspot mutation such as **E726K**, M1043L/I, or E453Q/K. How these double variants occur remains unknown, but they showcased increased oncogenic potential, likely due to enhanced dissociation between the PI3K α subunits and increased membrane binding.

Apart from their oncogenic potential, *PIK3CA* variants have been described in benign overgrowth lesions as well. This field of study only developed in the past decade, with new pathologies still being discovered that are related to *PIK3CA*. The umbrella term ***PIK3CA*-related Overgrowth Spectrum** or **PROS** was coined to combine these benign pathologies (52). While oncogenic hotspot variants such as E545K, E542K, and H1047R are found in PROS patients, causative mutations in other regions of the gene are commonly found in patients with PROS as well (53, 54) (see **Figure 1.3**).

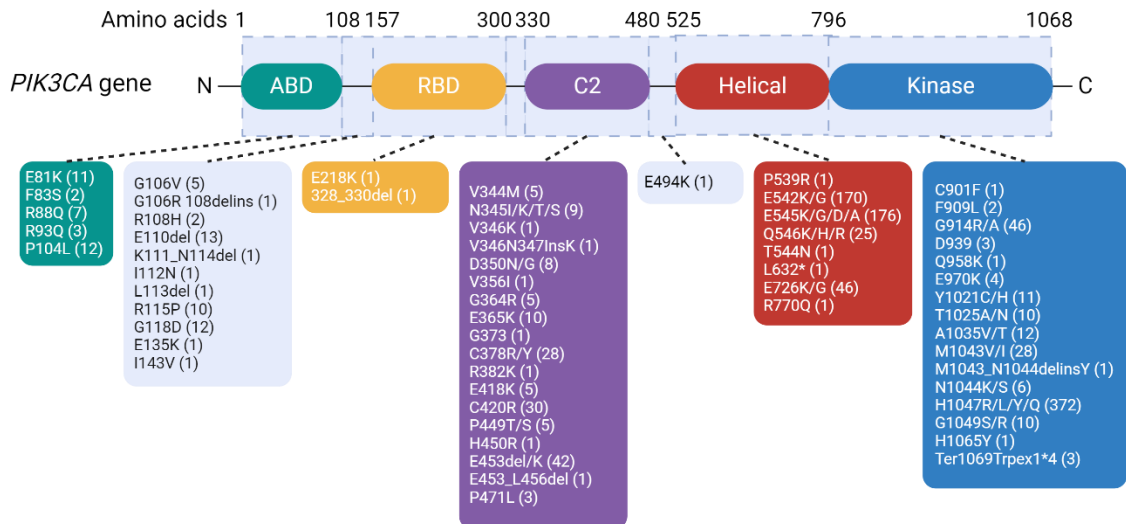


FIGURE 1.3. *PIK3CA* gene and reported variants in PROS.

The 5 domains of *PIK3CA* gene. The ABD closest to the N-tail, followed by the RBD, C2, helical, and kinase domains. Mutations found in PROS for each domain are listed. Figure modified from (55).

One explanation for the distinct variant patterns between tumours and PROS is that oncogenic variants typically exhibit stronger gain-of-function activity (52-55). In contrast, many PROS-related variants activate PI3K α only mildly, making them insufficient to drive oncogenic transformation (54, 55). This notion is supported by advances in sequencing technologies, which have offered new insights into the **relationship between specific variants and PROS phenotypes**. For instance, the E726K variant is more commonly associated with conditions such as MCAP, a disease characterized by widespread tissue overgrowth originating from multiple germ layers (56-58). Conversely, oncogenic hotspot variants are more frequently linked to isolated phenotypes, such as isolated brain overgrowth seen in conditions like Megalencephaly (HMEG/DMEG) or Focal Cortical Dysplasia (FCD), as well as lymphatic malformations (59). Research indicates that most *PIK3CA* variants linked to PROS are gain-of-function mutations, although the precise mechanisms driving their activation remain largely unknown (60, 61). In PROS, multiple *PIK3CA* mutations have even been identified within the same lesion, although it remains unclear whether these mutations arise within the same cells or occur in cis or trans configurations (62, 63).

2. PROS, vascular pathologies and related molecular drivers

First, *PIK3CA* hotspot variants were associated with benign skin lesions, called epidermal nevi or seborrheic keratoses (64). Then, more pathologies characterized by **asymmetric overgrowth** were linked with activating variants of *PIK3CA* (65-67). These disorders arise during embryogenesis due to stochastic activation of *PIK3CA*, causing pathway overactivation and resulting in overgrowth of tissues (66, 68).

2.1 Classification of PROS

PROS disorders include overgrowth of mainly mesoderm- and neuroectoderm-derived tissues (69). These include brain, fibro-adipose tissues, skin, bone, muscle, and often the vasculature. These pathologies are highly diverse, making categorization challenging. *Mirzaa et al.* proposed to distinguish between **isolated and syndromic PROS** (68). Isolated PROS are tissue overgrowth occurring locally affecting one tissue type or body part. Syndromic PROS are conditions with widespread manifestations affecting several tissues, which can present other features as well (see **Figure 2.1**).

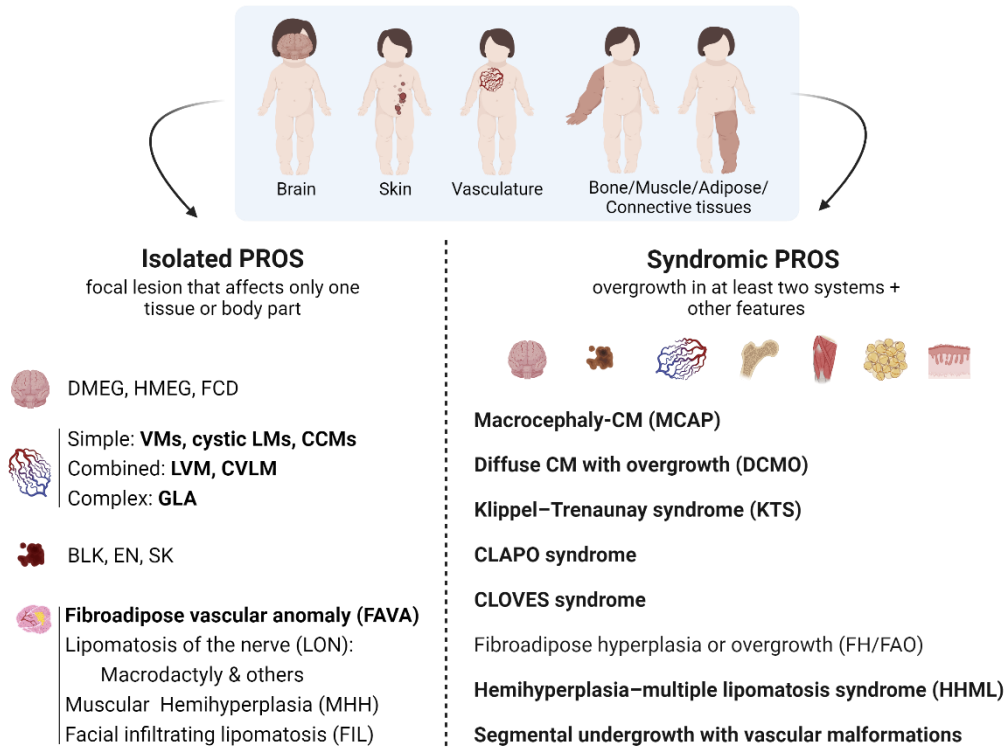


Figure 2.1. Classification of PROS disorders.

With PROS, patients display overgrowth of neuroectoderm and endoderm-derived tissues such as brain, skin, vasculature, bone, muscle, and fibroadipose tissues. PROS disorders can be categorized as isolated and syndromic PROS depending on how many tissues and locations they affect. Isolated PROS include Dysplastic/Hemimegalencephaly (DMEG/HMEG), Focal Cortical Dysplasia (FCD), Vascular malformations such as Venous Malformations (VMs), Lymphatic Malformations (LMs), Cerebral Cavernous Malformations (CCMs), Lymphatic-Venous Malformations (LVMs), Capillary-Venous-Lymphatic Malformations (CVLM), Generalized Lymphatic Anomalies (GLA), skin lesions such as Benign Lichenoid Keratosis (BLK), Epidermal Nevi (EN), Seborrhic Keratosis (SK), and combined tissue lesions which are locally affected such as FibroAdipose Vascular Anomaly (FAVA), Lipomatosis of the Nerve (LON), Macrodactyly, Muscular Hemihyperplasia (MHH), and Facial Infiltrating Lipomatosis (FIL). Syndromic PROS include Megalencephaly-Capillary Malformation (MCAP), Diffuse capillary malformation with overgrowth (DCMO), Klippel-Trenaunay syndrome (KTS), Capillary vascular malformation of the lower lip, Lymphatic malformation of the head and neck, Asymmetry and Partial/generalized Overgrowth (CLAPO), Congenital Lipomatous Overgrowth, Vascular malformation, Epidermal nevi, and Skeletal/Spinal abnormalities (CLOVES), FibroAdipose hyperplasia or overgrowth (FAO), HemiHyperplasia-multiple lipomatosis (HHML), and segmental undergrowth with vascular malformations. Picture modified from (55).

When activating *PIK3CA* variants stochastically occur during embryonic development, they lead to a mosaic pattern of overgrowth (53). Hence, the affected tissues in patients contain only a small proportion of cells carrying the variant (59). The timing and location of the mutation will determine the clinical manifestation. Other factors may contribute to PROS formation as well, such as cell-extrinsic factors that modify the PI3K α pathway activity (69). These **cell-autonomous** and **extrinsic determinants** of PROS are likely why PROS disorders are so diverse (55).

Oncogenic hotspot variants that occur during the zygotic stage proved to be lethal (70). This is supported by expression of *Pik3ca*^{H1047R/WT} in mice, which is fatal during early embryonic development (71, 72). These data imply the presence of an **activation threshold** during embryonic development which, when crossed, proves fatal. If a *PIK3CA* variant's activating potential remains below this threshold, the activated cell could expand into multiple cell lineages, leading to a widespread phenotype when it occurs during early embryonic development (55). In contrast, variants that generate a stronger activation of PI3K α may only be tolerated later in embryonic development, causing lineage-specific lesions (54, 55). However, this relation between the severity of the phenotype, the variant allele frequency, and the activating potential of the *PIK3CA* mutation remains unclear (54) (see **Figure 2.2**).

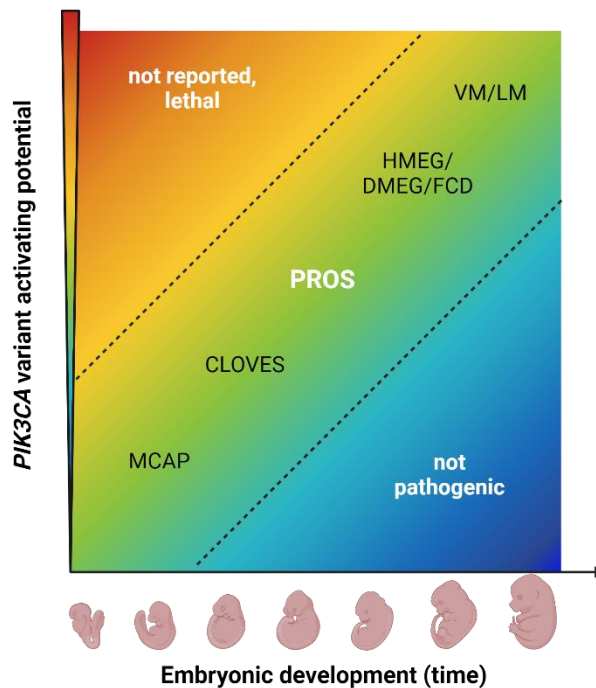


Figure 2.2. How strength of variant activation correlates with tolerability during embryonic development.

In PROS, mutations show an intriguing pattern of distribution. Some strongly activating variants are likely lethal during embryonic development if they occur at early stages (red area). If these occur during later stages, they cause local phenotypes such as LM or Megalencephaly. On the other hand, less strong variants are not lethal if they arise during early development, and mutated clones can expand into multiple cell lineages and spread out into multiple locations, as seen in PROS diseases such as MCAP or CLOVES. MCAP = Megalencephaly-Capillary Malformation-Polymicrogyria Syndrome, CLOVES = Congenital Lipomatous asymmetric Overgrowth of the trunk with lymphatic, capillary, venous, and combined-type Vascular malformations, Epidermal naevi, Scoliosis/Skeletal and spinal anomalies, HMEG/DMEG = Hemimegalencephaly and Dysplastic Megalencephaly, FCD = Focal Cortical Dysplasia, VM/LM = Vascular or Lymphatic Malformation.

Lastly, adipose and **vascular tissues** are most affected in PROS phenotypes (69, 70). This is supported by cell type-specific isolation and sequencing of patient-derived overgrown tissues, which revealed mutations in blood and lymphatic endothelial cells (69, 73, 74), fibroblasts (65, 75-77), and adipocytes (78, 79). These tissues are highly responsive to metabolic needs. Therefore, extrinsic factors such as signalling cues from the environment are likely of importance during the development of PROS. This notion is supported by research relating *PIK3CA*-related vascular lesions to growth factor stimulation (73, 80, 81).

2.2 Vascular malformations

Vascular overgrowth or **vascular malformations (VMs)** can occur as isolated lesions or combined into syndromic PROS (55, 82). A VM entails the formation of a defective blood or lymphatic vessel, growing aberrantly during embryonic development. Like PROS, VMs entail a wide variety of phenotypes depending on the size of the lesion, the affected vessel type, the location of the lesions, and the presence or absence of overgrowth of other tissues. VMs can be classified depending on how many vessel types they affect. Simple VMs are restricted to one vessel type, such as capillary, venous, or arteriovenous malformations, while combined VMs affect multiple vessel types, such as capillary-venous malformations, lymphatic-venous malformations, or capillary-lymphatic-venous malformations.

In general, VMs are functionally categorized into two types: **slow-flow** and **fast-flow** lesions. Slow-flow lesions include capillary, lymphatic, or venous malformations, or combinations thereof. Fast-flow lesions refer to arteriovenous malformations, characterized by wrongful connection of arteries and veins (see **Table 2.1**). Interestingly, this type of malformation has never been associated with *PIK3CA* mutations, but with mutations in the MAPK signalling pathway (83, 84). Why mutations in *PIK3CA* are not found in arteriovenous malformations remains unknown.

	Type of Malformation	Name	Mutated Gene	Nature of the Lesion
High Flow	Arteriovenous Malformations (AVM)	Sporadic arteriovenous malformations	<i>RASA1, MAP2K/MEK, KRAS, NRAS, BRAF, ENG, ALK</i>	Somatic
		Hereditary hemorrhagic telangiectasia (HHT)	<i>ENG, ALK1/ACVRL1, GDF2, SMAD4/MADH4</i>	Hereditary
		Capillary-arteriovenous malformations (CM-AVMs)	<i>RASA1, EPHB4</i>	Somatic/hereditary
Slow Flow	Capillary Malformations (CMs)	Capillary malformations (CM)	<i>GNAQ, GNA11</i>	Somatic
		Cutis Marmorata Telangiectatica Congenita (CMTc)	<i>Unknown, possibly GNA11</i>	Somatic
		Sturge-Weber Syndrome (SWS)	<i>GNAQ</i>	Somatic
		Pigmentovascular phakomatosis	<i>GNAQ, GNA11</i>	Somatic
	Venous Malformations (VeMs)	Common venous malformations (VM)	<i>TEK, PIK3CA</i>	Somatic
		Verrucous venous malformations	<i>MAP3K3</i>	Somatic
		Fibroadipose vascular anomalies (FAVA)	<i>PIK3CA</i>	Somatic
		Cerebral cavernous malformations (CCM)	<i>KRIT1, CCM2, PDCD10</i>	Somatic/hereditary
		"Blue rubber bleb nevus" syndrome	<i>TEK</i>	Somatic
		Venous anomalies associated with PTEN	<i>PTEN</i>	Hereditary
		Mucocutaneous venous malformations	<i>TEK</i>	Hereditary
		Glomangiomas Varicose veins	<i>GLMN, FOXC2</i>	Hereditary
	Lymphatic Malformations (LMs)	Lymphatic malformations (LM)	<i>PIK3CA</i>	Somatic
		Generalized lymphatic anomalies (GLA)	<i>PIK3CA</i>	Somatic
		Kaposiform lymphangiomatosis (KLA)	<i>NRAS</i>	Somatic
		Congenital pulmonary lymphatic malformations	<i>CCBE1</i>	Hereditary
		Primary lymphedema	<i>FLT3, VEGFR3</i>	Hereditary
		Other cases of lymphedema	<i>FOXC2, GJC2, KIF11, SOX18, PTPN14, CCBE1, FAT4, ADAMTS3, GATA2</i>	Hereditary
	Associated with other pathologies	Parkes Weber Syndrome	<i>RASA1</i>	Somatic
Maffucci Syndrome		<i>IDH1-IDH2</i>	Somatic	
CLOVES Syndrome (PROS)		<i>PIK3CA</i>	Somatic	
CLAPO Syndrome (PROS)		<i>PIK3CA</i>	Somatic	
Proteus Syndrome		<i>AKT1</i>	Somatic	
KTS Syndrome (PROS)		<i>PIK3CA</i>	Somatic	
MCAP Syndrome (PROS)		<i>PIK3CA</i>	Somatic	
DCMO Syndrome (PROS)		<i>PIK3CA</i>	Somatic	

Table 2.1. Classification of vascular malformations (VMs) depending on their functional characteristics and the associated mutated gene.

Vascular malformations can be divided into high-flow malformations, which include arteriovenous malformations (AVM), or low-flow malformations, which include venous (VeM), capillary (CM), or lymphatic (LM) malformations. We can also find vascular malformations associated with complex syndromes. Each type of malformation has been associated with certain genetic mutations of either germline or somatic origin, as indicated on the right side of the table. Table adapted from (85).

In **venous malformations**, the lesions are characterized by enlargement of the veins with increased tortuosity and reduced mural cell coverage, resulting in defective vessel function (55). Interestingly, 60% of venous malformations are caused by activating mutations in *TEK* (encodes for the TIE2 receptor upstream of PI3K α) and 20 to 25% by mutations in *PIK3CA* (86-88), both leading to overactivation of PI3K α . In mice, studies showed that mosaic expression of *Pik3ca*^{H1047R} under the endogenous promoter in the mesoderm during embryonic development led to venous malformations exclusively (89). These venous malformations were caused by increased EC proliferation and displayed reduced mural cell coverage (89, 90).

Activating mutations in *PIK3CA* are commonly found in **lymphatic malformations (LMs)** as well (91, 92). Interestingly, the cancer hotspots are commonly found in LMs, and recent studies indicated helical domain mutations (E542K and E545K) are more represented than kinase domain (H1047R), although more information and epidemiological studies are needed to confirm the significance of this phenomenon (59). Genetic expression of *Pik3ca*^{H1047R/WT} in mice lymphatic ECs revealed that early embryonic expression resulted in macrocystic lesions, and late embryonic or postnatal expression resulted in microcystic lesions, showcasing that the type of cell (progenitor or differentiated cell), timing, and the used mice model can influence the pathology of LMs (93).

Capillary malformations can be isolated lesions characterized by dilated capillaries near the skin surface or can be part of complex PROS disorders such as MCAP and DCMO (94). In these lesions, non-hotspot activating mutations in *PIK3CA* have been commonly described (58, 59, 84).

2.3 Diagnosis and treatment of vascular malformations

Only in recent years have *PIK3CA* variants been identified as a cause of many overgrowth diseases. As a result, data on the prevalence of PROS is limited, with estimates ranging from 1 in 20,000 to 1 in 30,000 (95). Due to PROS being rare, clinicians are often unaware of the full range of possible disease phenotypes, leading to patients frequently requiring multiple consultations before the condition is correctly identified and treated. Currently, vascular malformations are primarily treated with **surgical removal** and/or **sclerotherapy** (69). However, these treatments are not always feasible, as the ability to remove the malformation depends on its location or whether the lesion is widespread. Moreover, after surgery, surrounding tissue will release growth factors necessary for the healing process, which often results into the regrowth of a

vascular lesion. The molecular mechanisms that govern VM formation need to be better understood so targeted therapies can be designed. Nowadays, tissue biopsies followed by sequencing are used for diagnosis, although this does not always reveal causative mutations in *PIK3CA* since the variant allele frequency in lesions is usually low (59).

Research in the mechanisms of PI3K α signalling in cancer and PROS revealed some parts of the pathway that are druggable. As a result, some progress has been made regarding the molecular treatment of vascular malformations. The first targeted therapy for PROS was Sirolimus or **Rapamycin**, an allosteric mTOR inhibitor that was repurposed from its use in cancer treatments (96). Recently, Rapamycin use was approved by the European Medicines Agency (EMA) and the Food and Drug Administration (FDA) for the treatment of patients with PROS and VMs (97-99). Here, a reduced volume of vascular lesions was observed, although patients presented several adverse effects. Regardless, Rapamycin became part of the standard of care in patients with PROS (100, 101).

AKT can also be targeted. **Miransertib** was developed and used on a compassionate basis to treat patients with PROS and VMs (102-104). Some therapeutic efficacy was reported in the treatment of VMs in mice (73), and clinical trials are ongoing for the treatment of VMs.

Lastly, **PI3K inhibitors** are also being developed to treat PROS or VMs. Often, these are repurposed from their use to treat certain cancers. For example, Copanlisib (BAY 80-6946/Aliqopa) is the only pan-PI3K inhibitor approved by the FDA to treat relapsed follicular lymphoma (105). Moreover, Taselisib (GDC-0032), a pan-class I PI3K inhibitor, was developed for treatment of PROS and resulted in reduced pain and bleeding in patients, but the trial was terminated due to on-target adverse effects (106). PI3K α isoform-specific inhibitors are preferred to diminish these adverse effects. Alpelisib (BYL719/Piqray) is a PI3K α -selective inhibitor and is approved by the FDA for treatment of HR+, HER2-, locally advanced or metastatic breast cancer with a *PIK3CA* mutation (107). Interestingly, Alpelisib treatment showed promising results in mice with CLOVES or lymphatic malformations (108). Since, Alpelisib has been used on a compassionate basis in some patients with PROS with varying levels of success (109-111). Still, side effects such as hyperglycaemia, stomatitis, aphthous ulcers, and diarrhoea are often reported (112, 113). Nonetheless, retrospective multicentric studies such as EPIK-P1, showed promising results and accelerated the approval of Alpelisib by the FDA for PROS patients of at minimum 2 years old (114). Phase 2 randomized controlled trial EPIK-P2

(NCT04589650) will compare the results of Alpelisib to placebo-treated controls in patients with PROS (115).

PI3K inhibitors often showcase high toxicity and **pathway reactivation**, making treatments challenging. The PI3K pathway is tightly regulated by feedback loops. Namely, research demonstrated increased levels of RTK expression with inhibition of PI3K, which reactivates the PI3K pathway (115, 116). Hence, there is growing interest in dual treatment to counteract this pathway reactivation. For instance, dual treatment with PI3K inhibitors and anti-ER therapies in oestrogen receptor (ER)-positive cancers (116).

New inhibitors are being developed to specifically target **mutant forms of PI3K α** . LOXO-783, an inhibitor highly selective for H1047R, was able to kill several tumour cell types containing the *PIK3CA*^{H1047R} mutation (117, 118). In a phase 1 trial for treatment of breast cancer (PIKASSO-01, NCT05307705), LOXO-783 showed activity without adverse effects for WT PI3K α (119). RLY-2608 and RLY-5836 are 2 pan-mutant PI3K α inhibitors with demonstrated *in vivo* efficacy and acceptable safety profiles in solid tumour patients which are being tested in phase 1 clinical trials for advanced breast cancer (NCT05216432 and NCT05759949) (120). Regardless, these drugs are not yet available for patients with PROS or VMs, and more research is needed before patients will be able to benefit from these mutant-selective inhibitors.

3. Vascular development

3.1 The mammal circulatory system

The circulatory system or cardiovascular system in mammals comprises a complex network of blood and lymphatic vessels. This network is responsible for the transport of nutrients, hormones, water, and oxygen to every cell in the body, and the collection and removal of metabolic waste (121, 122). To perform its crucial functions, the circulatory system consists of distinct vessel types and organs. The **cardiovascular system** comprises the heart, a muscle that pumps blood directly in the aorta and other branching arteries, the blood then disperses into smaller and smaller vessels, arterioles, until the vessels become small enough for gas exchange to take place in the capillaries. Collecting venules transport the oxygen-poor blood back into large veins and transport it back to the heart (123). A whole other vessel system exists in our bodies as well, the **lymphatic system**. Lymphatic vessels form collecting ducts in all tissues to collect lymph, a fluid rich in immune cells, proteins, and metabolic waste (124). This waste gets collected into the veins and redistributed throughout the body (121). The lymphatic

system also contains lymph nodes, where collected pathogens are displayed to immune cells to fight infections. To summarize, the lymphatic system plays important roles in fluid regulation, nutrient absorption, and the immune system.

To perform their respective functions, the vessels of the circulatory system require specialization. Typically, the large blood vessels are composed of the tunica intima, the tunica media, and the tunica externa (125, 126). The tunica intima or the innermost layer is built from **endothelial cells (ECs)** covered by a basement membrane. The tunica media is made of mural cells and elastic fibres. This layer is particularly thick and muscular in arteries that need to withstand high blood pressure. The tunica externa or outermost layer is a collagen-rich structure that stabilizes the vessel. Morphologically, arteries are muscular, narrow, and straight, to withstand the rapid blood flow. Veins are more irregular and larger; and contain the highest volume of blood of all the vessels. Capillaries are very thin vessels with a high surface area to allow optimal gas exchange. Another interesting difference is the distinct pattern of mural cells that cover each vessel type. These mural cells are important in the maintenance of the vessel structure and integrity (127). Arteries are covered by many vascular smooth muscle cells (vSMC) aligned perpendicularly to the blood flow to support and reinforce the vessel (128). In veins, mural cells are less abundant and less organized. In capillaries, pericytes cover the vessel which provide mechanical stability (see **Figure 3.1**).

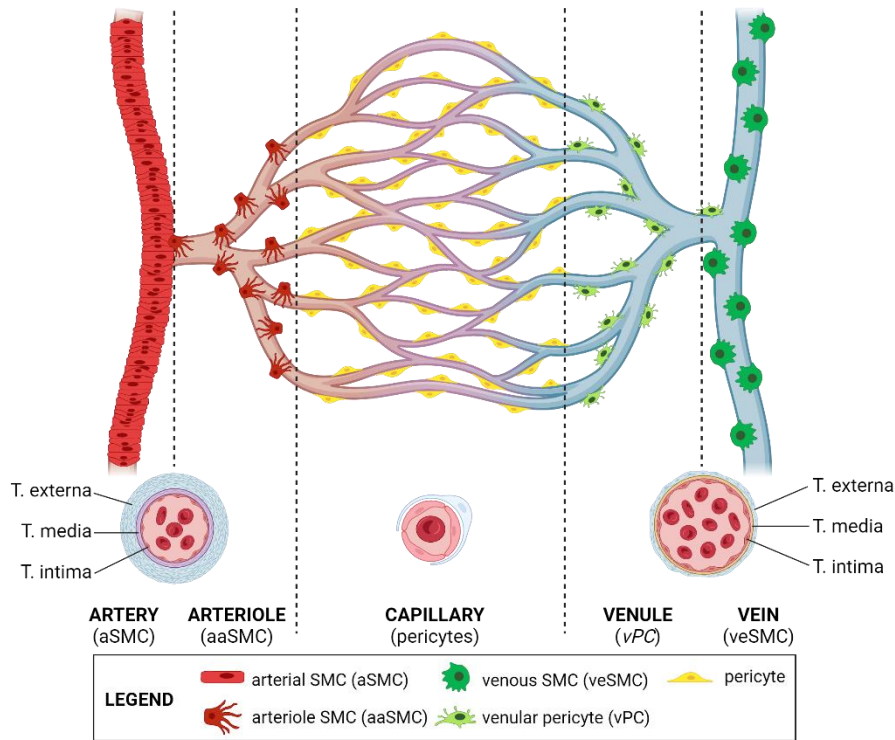


Figure 3.1. Composition of the main vessel types in the cardiovascular system.

Structure of the main blood vessel types: arteries, arterioles, capillaries, venules, and veins. Big vessels consist of 3 layers, Tunica externa, tunica media, tunica intima. The tunica intima is made from endothelial cells. These are enveloped by mural cells, depending on the vessel type. Figure modified from *Van Splunder et al.* (128).

3.2 Vascular origins and growth

The formation of the circulatory system is one of the first events during embryonic development and organogenesis in vertebrates (129). During early embryogenesis, a population of mesoderm-derived cells differentiate into hemangioblasts, which will further divide into two progenitor subpopulations: hematopoietic precursor cells that will develop into mature blood cell types, and endothelial precursor cells, known as angioblasts (130). Angioblasts cluster together to form structures called "blood islands" (131). These blood islands mark the first step in vasculature formation, where a primitive vascular network is established through a process known as **vasculogenesis**. Under the influence of growth factors, angioblasts within the blood islands undergo lineage commitment, giving rise to endothelial cells, while hematopoietic precursor cells develop into blood cells (132). Remarkably, new studies found other origins for ECs, namely erythron-myeloid progenitor cells (EMPs) derived from the yolk sac (133, 134).

Then, this primitive vascular network will respond to the hypoxic signals from its environment by expansion and remodelling. The formation of new blood vessels from

existing ones is called **sprouting angiogenesis**. The new vessels will specialize to create a hierarchical system of large vessels and smaller branches will form (135). The growth of the vascular network will require specialization of certain vessels for optimal blood transport depending on the tissues needs. Therefore, ECs will differentiate into different subpopulation depending on the tissue and vessel type they are part of. For example, capillaries in the liver and bone marrow contain fenestrations to allow permeability for nutrients, protein, and blood cells, while in the brain, the capillaries tightly maintain the blood-brain barrier. However, another process called intussusceptive angiogenesis, where vessels split and duplicate into new ones, has also been observed in physiological and pathological contexts, though this process remains poorly understood (136-138).

Many processes involved in vascular development are reactivated during tissue regeneration, scarring, and pathological conditions (139, 140). Understanding the mechanisms behind these events is therefore essential for advancing research and treatment across numerous diseases. Even in adulthood, the vasculature remains highly responsive to the metabolic needs of surrounding tissues. For example, during menstrual cycles, pregnancy, muscle angiogenesis, and similar situations, blood vessels must undergo expansion, remodelling, and maturation (141, 142). To adapt to these changing conditions, ECs continuously monitor their environment and respond accordingly.

3.3 Sprouting angiogenesis

Sprouting angiogenesis is a complex process, requiring strict regulation on a cellular and molecular level. In general, the process consists of 5 steps: 1. sprouting initiation, 2. sprout elongation, 3. anastomosis and lumen formation, 4 remodelling of the vessel and maturation, and 5. establishment of vessel quiescence (121).

Tissue hypoxia triggers the expression of pro-angiogenic growth factors, which will kickstart the formation of a new vessel via sprouting angiogenesis. The first step is the local degradation of the basement membrane around the ECs and mural cells by EC-secreted metalloproteases (MMPs) (143). This allows for some ECs to expand outwards with the growth factor gradient from their environment. Some ECs will differentiate into **tip cells**, containing many filopodia that will monitor the environment for vascular endothelial growth factors (VEGF) and spearhead the formation of the new vessel (121). The surrounding ECs, called **stalk cells**, will closely follow the tip cells and actively proliferate to form the new vessel (144, 145). Specifically, VEGFA binds to the VEGFR2 receptor which causes the differentiation into migrating tip cells. In turn, the tip cells will

express DLL4, which will interact with Notch receptors on nearby ECs to induce their differentiation into stalk cells (146-148). Here, tip cell identity will be suppressed in the nearby stalk cells due to the Notch-controlled expression of VEGFR1, a high-affinity decoy receptor for VEGFA with low activity (149). Notch will also activate other genes such as *Hes*, *Hey*, *Pten*, and *Nrarp*, which will further maintain stalk cell differentiation and identity (150, 151). NRARP will promote Wnt/ β -catenin signalling to regulate the stalk cell proliferation to facilitate the growth of the new vessel (152). VE-cadherin will mediate the rearrangement of cell junctions, allowing the dynamic rearrangement of the stalk cells into a new vessel (153). Last, the stalk cells will reestablish the basement membrane for vessel stability. Interestingly, pharmacological inactivation of Notch or DLL4 leads to an increased amount of tip cells and therefore sprout hyperplasia (146, 147) (see **Figure 3.2**).

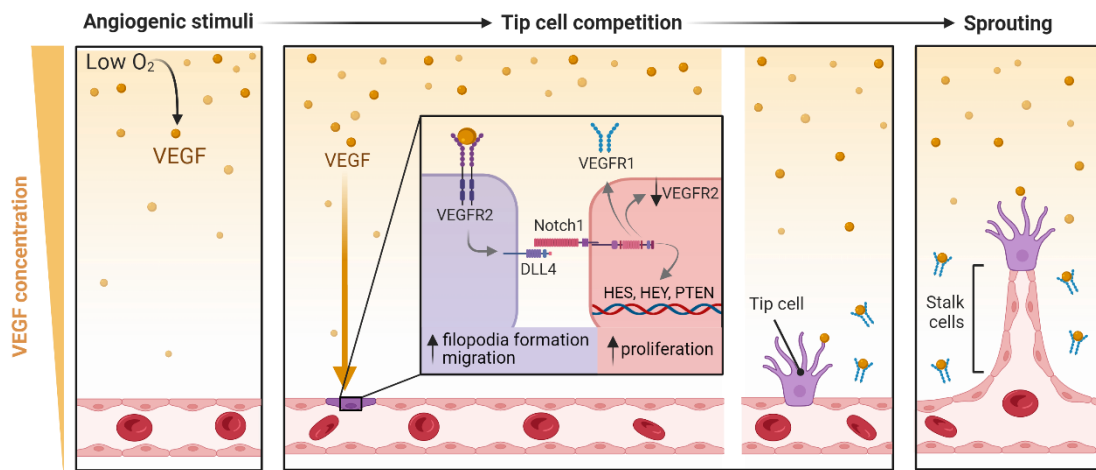


Figure 3.2. Tip/stalk cell differentiation during early angiogenesis.

VEGFR and Notch signalling play central roles during tip/stalk cell differentiation. Cells will compete for tip cell specification and induce stalk cell differentiation in neighbouring cells. Hypoxia in tissues will cause VEGFA production, which binds to VEGFR2 receptors expressed on all ECs. This will kickstart the ECs differentiation into a migrating tip cell with filopodia according to the VEGFA gradient. Neighbouring stalk cells will support the formation of the new vessel by rearranging and proliferating.

Anastomosis is the process of two vessels making contact and joining, initiated by the contact of a tip cell with another ECs, though the cellular mechanism of this process remains poorly understood (121). Macrophages are closely associated to tip cells at positions where vessel joining occurs, and likely prime tip cells for anastomosis (154). Subsequently, a lumen needs to be formed in the newly sprouted vessel to start the blood flow. Multiple mechanisms have been proposed for the mechanisms of lumen formation (155, 156). One mechanism entails the hollowing of stalk cells (157). Intracellular pinocytotic vacuoles will form adjacently in the neighbouring stalk cells of the new vessel,

which will eventually join and expand to form the lumen. Another mechanism proposes the junction-mediated dynamic EC rearrangement and establishment of the apical polarity of the ECs (158-161). The apical side will be coated in negatively charged glycoproteins, following repulsion which aids in the formation of the lumen (162). When the lumen forms, blood flow starts in the new vessel. However, additional maturation steps are required for the vessel to be stable and functional.

New blood vessels require a tight connection between the ECS for their functions, while also allowing for permeability and signal transmission between the blood and the surrounding tissue/ECM. These connections are formed by multi-protein complexes that can be categorized in two types of junctions: **tight junctions** (TJs) and **adherent junctions** (AJs). TJs are located between ECs near the lumen to maintain vessel integrity and regulate permeability (163). In the brain, TJs are crucial for maintaining the blood-brain barrier (164). These junctions are made from proteins that are part of the claudin and occludin families, among others. On the other hand, AJs are located in more basal positions, in addition to regulating permeability, they are important contributors of initiating contact and regulating interactions between ECS, and controlling cytoskeleton rearrangements (163, 165). AJs mainly consist of proteins such as cadherins and catenins. The transmembrane protein VE-Cadherin, specifically, was proven crucial for EC function. Artificial VE-Cadherin deficiency or truncation caused mice embryonic lethality due to vascular defects (166). VE-Cadherin can form complexes with VEGFR2 and members of the TGF β family, therefore playing a major role in EC differentiation, growth, and stability (167).

Another crucial process during the formation of new blood vessels is the establishment of arterial, capillary, and venous identity in ECs. The **arterial and venous specification** is determined by genetic and epigenetic factors and influenced by the surrounding microenvironment and shear stress. The identity of ECs is determined by the expression of certain molecular markers that are essential for their morphology and function. Lineage tracing studies have shown that there is a widespread conversion from venous into arterial ECs (168, 169). Moreover, gene expression trajectory studies demonstrated that ECs from veins and capillaries will undergo molecular conversion into arterial ECs and migrate to form the arteries (170, 171). Specifically, tip cells that spearhead the formation of new vessels will change their fate and migrate against the flow to ultimately occupy the artery (172-174).

3.4 Molecular regulators of endothelial cells during angiogenesis

The angiogenic process is governed by several molecular pathways. The **VEGF/VEGFR** pathway is the principal angiogenic growth factor pathway that modulates vessel formation and growth through VEGF receptor tyrosine kinases (VEGFRs). There are 5 VEGF ligands in mammals, VEGFA, VEGFB, VEGFC, VEGFD, and PGF, that can be secreted by hypoxic tissues (175). Their distribution and gradient will determine the fate of the ECs (176). The ECs will perceive and interpret these factors through their receptors, VEGFR1, VEGFR2, and VEGFR3.

VEGFA plays a central role in angiogenesis, its binding to the receptor **VEGFR2** (or KDR/Flk-1 in mice) will cause autophosphorylation of both receptor subunits on tyrosine positions, which can be recognized by effector kinases which will kickstart downstream signalling cascades important in regulating EC proliferation, survival, migration, and permeability (176). One important downstream pathway mediated by VEGFR2 signalling is the PLC γ -PKC-MAPK pathway, crucial for endothelial proliferation (177). Interestingly, downregulation of VEGFA results in mice embryonic lethality due to abnormal blood vessel formation (178). **VEGFR1**, on the other hand, acts as a decoy receptor for VEGFA, with high affinity for VEGFA but poor tyrosine kinase activity, demonstrating that the VEGF pathway is subjected to tight regulation. Studies in mice showed that deficiency of either VEGFR1 or VEGFR2 resulted into early embryonic lethality due to vascular defects but with opposing phenotypes. VEGFR1 deficiency resulted in overproliferation of ECs and vascular disorganization, while VEGFR2 ablation caused a lack of vessel formation due to reduced EC proliferation (178-180).

VEGFB and **PGF** are dispensable during embryogenesis, since genetic knock-out in mice models of either revealed no embryonic lethality. These are ligands for VEGFR1, and only under pathological conditions have they been described to contribute to angiogenesis (181).

VEGFC and **VEGFD** show strong affinity for **VEGFR3** (or FLT4), which is expressed mainly on lymphatic ECs where they play an important role in lymphangiogenesis (182-184). They showcase weak affinity to VEGFR2 as well, finetuning the EC response to extracellular VEGF signals. VEGFC downregulation caused mice embryonic lethality due to severe lymphatic defects and accumulation of fluids, while VEGFD knock-out did not cause mice embryonic lethality (184-188). During mice embryonic development, VEGFR3 is expressed in all endothelial cells, including in angiogenic sprouts. Absence of VEGFR3 during early embryogenesis results in reduced sprouting and reduced vascular density of all vessels in mice (189). In mature vascular networks, VEGFR3

becomes exclusively restricted to the lymphatic ECs (190). Other studies showed an important role of VEGFR3 in regulating vascular permeability (191).

The **Notch** pathway is another crucial signalling pathway during vascular development. The Notch family consists of 5 ligands DLL1, DLL3, DLL4, Jagged1, and Jagged2, and 4 receptors Notch1, Notch2, Notch3, and Notch4 (192). The interaction between a ligand and any Notch receptor will cause the dissociation of the Notch intracellular domain (NICD), which will translocate to the nucleus and regulate the transcription of Notch-regulated genes, such as *Hes*, *Hey*, and *Dll4* (146, 147). ECs mainly express the Notch1 and Notch4 receptors, along with the DLL1, DLL4, and Jagged1 ligands. The DLL4/Notch1 signalling axis directs the endothelial tip/stalk specification necessary for the formation of new vessels. Jagged1 activation will subsequently counteract the DLL4/Notch1 axis and cause equilibrium during angiogenic growth (193). Multiple studies on the role of Notch have demonstrated its essential functions during angiogenesis. Specifically, the inactivation of Notch1 or DLL4 lead to dysregulation of angiogenic processes, such as increased sprouting, branching, and filopodia formation (147-150).

The differentiation from venous or capillary cells into arterial ones is governed by **EPH-Ephrin** interactions. Veins exclusively express the EPHB4 receptor, while arteries express its specific ligand Ephrin-B2. An interaction between EPHB4 and Ephrin-B2 causes cellular repulsion and is necessary to establish arterial and venous fates (194-196). Moreover, EPHB4 activation will transmit an intracellular signal for adhesion molecules and integrins to enable invasion of surrounding tissues (197, 198). Ephrin-B2 activation, on the other hand, promotes intracellular VEGFR2 signalling through endocytosis. This will result into Notch pathway activation and inhibit the expression of transcription factor COUP-TFII, a hallmark of venous identity (199-201). Another chemokine receptor **CXCR4** is preferentially expressed in arterial ECs and has been shown to be necessary in the development of arteries (202-204). Blood flow-associated shear stress also guides EC differentiation, since flow induces expression of the transcription factor KLF2, an arterial EC marker (205) (See **Figure 3.3**)

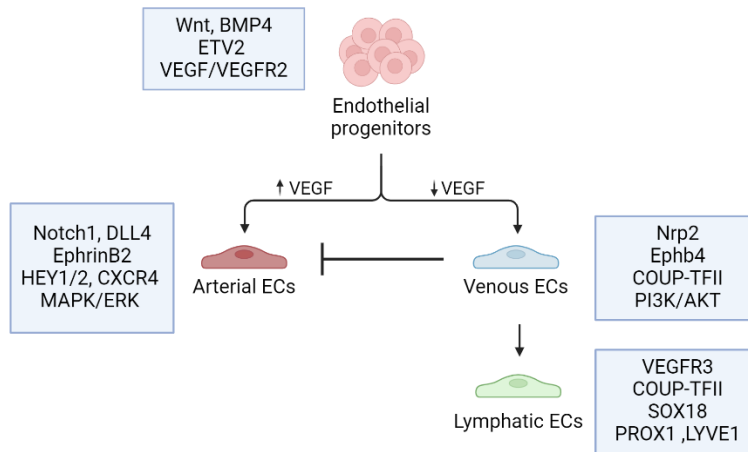


Figure 3.3. Endothelial differentiation during embryonic development.

Arteriovenous specification is guarded by molecular pathways during embryonic development. Endothelial progenitors will differentiate into venous or arterial ECs, with distinct molecular profiles. These molecular drivers maintain the equilibrium, interactions between the pathways inhibit and safeguard venous/arterial specification.

3.5 Vessel maturation and stabilization

Vessel maturation involves the formation of EC junctions, recruitment of supporting mural cells, reconstruction of the extracellular matrix (ECM), and the establishment of vessel quiescence (206). The initiation of blood flow will activate certain signalling pathways which regulate vessel remodelling into the final network. For instance, the endothelial transcription factor KLF2 is upregulated upon initiation of blood flow *in vitro*, and genetic knock-out in mice embryos *in vivo* proved its role in aiding the stabilization of the vessel wall (205, 207). Once vascularization and subsequent gas exchange takes place, the surrounding tissue will no longer emit hypoxic growth factor signals, which finally will induce blood vessel quiescence (208).

Mural cells play a crucial role in the maturation of blood vessels. Not only do they envelop the ECs to stabilize the blood vessel structure, but they also specialize to play a direct role in endothelial signalling, proliferation, migration, and formation and organization of the ECM (127). The term mural cells refers to multiple cell types including vascular smooth muscle cells (vSMCs) and pericytes (PCs). The vSMCs will encompass large vessels such as arteries and veins, while PC are more commonly found in smaller vessels such as arterioles, venules, and capillaries (128). Research regarding the PC is still recent and ongoing, yet it is clear they form a heterogeneous cell type across tissues (209). Although some molecular markers such as NG2, PDGFR β , α SMA, and desmin have been used to identify PCs, they are not completely PC-specific, and expression can vary depending on the tissue (128). One important interaction between ECs and PCs is

through PDGFR β , where EC secrete the ligand PDGFB to recruit PCs expressing the receptor PDGFR β . Additionally, PDGFB also stimulates the proliferation of vSMCs and induces the differentiation of mesenchymal progenitors into mural cells (210). Inactivation of either PDGFB or PDGFR β in mice results in vascular dysfunction due to lack of mural cell coverage during embryonic development (211-213). Interactions from mural cells to ECs are also governed via the Angiopoietin (ANG)-TIE2 receptor signalling pathway. ANG1 is secreted by PCs and binds to TIE2 receptors on ECs, promoting EC survival and quiescence. The antagonist of ANG1, ANG2, is secreted by ECs to regulate and control this interaction and facilitates PC detachment during the initiation of sprouting angiogenesis. This balance between ANG1 and ANG2 regulates the recruitment and attachment of PCs during vessel maturation and maintains the equilibrium of the vascular network (210, 214). The correct interactions between ECs and mural cells is crucial for vessel maturation, in fact, alterations in mural cell coverage or unstable junctions are hallmarks of defect vascular systems in diseases such as diabetic retinopathy, venous malformations, and some solid tumours (128).

Another important entity that regulates vessel maturation is the **ECM** and its constituents by interacting with EC receptors. The ECM comprises a complex network of (glyco)proteins, proteoglycans, and polysaccharides that provide adhesive and mechanical support to the blood vessels and participate in physiological functions through growth factor interactions (215). The ECM mainly consists of interstitial matrix and the basement membrane. The interstitial matrix is composed of collagens, elastic fibres, and glycoproteins and contains pro-angiogenic growth factors such as VEGF, IGF, PDGFB, ANG, and TGF β to facilitate the sprouting of new vessels (215). The basement membrane encapsulates the ECs and mural cells, supporting coordination of cell morphology, gene expression, proliferation, and migration. The ECM is highly dynamic depending on environmental cues, and undergoes remodelling, growth, and decomposition where necessary. For example, the degradation of the basement membrane is one of the first steps during sprouting angiogenesis (216).

Vascular remodelling actively occurs through different processes to form the final vascular bed. A lack of VEGF signals can induce EC apoptosis and therefore cause the degradation of certain vessels where they are not needed in a process called vascular pruning (217, 218). ECs also differentiate and migrate into certain vascular niches to remodel the vasculature, driven by local changes in blood flow (219).

Lastly, when the surrounding tissue no longer sends hypoxic signals, the blood vessels will establish a **quiescent steady state**. Even though the vessels seem stable and

unchanged, this state requires active processes such as auto- and paracrine signalling to maintain cell survival and the integrity of the vessel. VEGF signalling plays a role here by autocrine signalling in ECs, which activates the PI3K/AKT signalling pathway to promote survival but not proliferation (121, 220). Other pathways such as ANG1/TIE2 and BMP9/ALK1 also mediate EC survival (221). Shear stress caused by blood flow plays a major role in maintaining vessel integrity by signalling via KLF2 and nitric oxide production (205).

3.6 PI3K α signalling in the endothelium.

Over the past decade, research has elucidated important roles for **PI3K α signalling in the endothelium**. Genetic targeting of the components of the PI3K α signalling pathway in mice revealed embryonic lethality due to vascular defects. It was demonstrated that vascular biology is selectively governed by PI3K α and no other class I PI3Ks (222-224). On the other hand, sustained overactivation of PI3K α in ECs caused issues with vascular remodelling in mice, resulting in embryonic lethality (71). Meanwhile, additional research showcased the influence of PI3K α signalling on remodelling of cellular junctions in ECs, maintaining venous identity and repressing atrial differentiation, EC proliferation, migration, and metabolism (225-228). Moreover, genetic targeting of the regulatory subunits of class IA PI3Ks (p85 α , p55 α , p50 α , and p85 β) also revealed haemorrhage formation and embryonic lethality, which could be rescued by single copy retention of p85 α (229). These data point towards a crucial function for PI3K α in endothelial biology.

Even though PI3K α signalling is crucial in vascular biology, other **class I PI3K isoforms** play limited roles as well. For instance, PI3K β inhibits PI3K α function in the context of cardiac ischemia (230). Upregulation of PI3K δ in ECs has also been observed in inflammatory circumstances, where it regulated key cellular processes (231). More importantly, PI3K β signalling was found crucial for pericyte proliferation and maturation. This interaction is governed by PDGFR β , which contains the YXXM motif and can hereby directly recruit and activate the PI3K complex (232, 233).

VEGFR, TIE2, EGFR, PDGFR β , and ERBB receptors all rely on PI3K signalling to a certain extent to transform the signals they receive into a cellular response. Studies showed that **VEGFR2** and **VEGFR3**, and not VEGFR1, can activate the PI3K α pathway (234). Specifically, activated VEGFR2 recruits adaptor proteins of the Src kinase family which will serve as binding sites of the PI3K α complex. Other coreceptors, such as VE-Cadherin, integrins, and NRP1, and heterodimer formation with other VEGFRs, will finetune the signal (235, 236). Of note, VEGFRs do not have a YXXM motif to create the

binding sites for the PI3K α complex, so adaptor molecules are necessary for the VEGFR-PI3K α activation to occur (237). Though, the VEGFC/VEGFR3 axis also interacts with PI3K α indirectly. VEGFC-stimulated lymphatic ECs showcased no changes in AKT activation with disruption of the RBD in p110 α (238).

The **ANG/TIE axis** plays crucial role in vascular maturation by attracting mural cells. ANG1 is expressed by mural cells and activates the TIE2 receptor expressed on ECs. TIE2 can directly interact with p85 α through its pY sites, and hereby activate the PI3K α signalling pathway, which will control EC survival and vessel stabilization (239, 240). Additionally, PI3K α inhibits FOXO1 activity, a transcription factor for ANG2, the antagonist of ANG1 that is expressed by EC to form an autocrine finetuning mechanism (235).

The **Epidermal Growth Factor Receptor (EGFR)** is another RTK that plays a significant role in endothelial cell function, particularly in processes such as angiogenesis and vascular homeostasis (241). Activation of EGFR in endothelial cells can influence blood pressure regulation, endothelial dysfunction, and atherogenesis. Upon ligand interaction, EGFR will dimerize and autophosphorylate, and adaptor molecules will further influence the downstream signalling response. This includes the regulation of the PI3K α -Akt pathway (242). This activation promotes endothelial cell migration and survival, essential for new blood vessel formation (243). Furthermore, EGFR signalling can modulate the expression of VEGF, thereby indirectly influencing PI3K α pathway activity (244). Thus, EGFR serves as a pivotal regulator in endothelial biology, with its interplay with the PI3K pathway being central to vascular development and pathology.

AKT is one of the most prominent downstream effectors of PI3K α in the endothelium. For example, prolonged activation of AKT1 in the mouse endothelium causes structurally abnormal vessels (245), while AKT1 knock-out (but not AKT2 or AKT3) results in defective angiogenesis and limited vessel growth (246, 247). Additionally, AKT activation induced the production of hypoxia-inducible factors, HIF1 and HIF2, in ECs and other cell types. This promoted the expression and secretion of VEGFs and stimulated angiogenesis. Moreover, AKT activation also regulated endothelial nitric oxide synthase (eNOS), important in NO metabolism. NO is important for regulating blood flow through vasodilation and for stimulating angiogenesis (248, 249).

AKT also regulates the transcription factor **FOXO1** in ECs. Specifically, AKT phosphorylates FOXO1, resulting in its nuclear exclusion and degradation (250). FOXO1 inhibits EC proliferation by inhibiting glycolysis and oxidative phosphorylation via MYC (251). It appeared that genetic ablation of FOXO1 resulted in mouse embryonic lethality

due to aberrant vascular growth (252-254). *In vitro*, EC-specific FOXO1 knockout showed reduced EC migration and sprout formation (250).

Mechanistic Target of Rapamycin or **mTOR** also plays a critical role in the transfer of signalling downstream of class I PI3Ks (255). mTOR can act in 2 serine-threonine kinase protein complexes, mTORC1 and mTORC2. mTORC1 regulates processes such as mRNA translation and biomass synthesis, but also autophagy and lysosome production. mTORC2 influences proliferation and survival process due to its phosphorylation of AKT on S473 (255). Experimental deletion of some mTOR complex components in knockout mice models revealed central roles for these complexes in angiogenesis (256), resulting in increased production of proangiogenic factors (HIF1 and VEGFA) and EC proliferation, and therefore increased vessel growth in heart, kidney and liver (257, 258). Moreover, pharmacological inhibition of mTORC1 with Rapamycin resulted in a reduced proliferation and migration of ECs (259). How exactly mTOR complexes regulate ECs function remains elusive, likely mTORC1 acts as a metabolic sensor in ECs during the angiogenic process (260), while mTORC2 modulates the response to extracellular signal and controls cell survival and cytoskeleton organization (261).

We previously mentioned that the phosphatase **PTEN** antagonizes the reaction of class I PI3Ks, hence, PTEN function is also crucial in vascular biology. EC-specific targeting of PTEN in mice lead to increased amount of PIP3, resulting in haemorrhage formation and embryonic lethality (262) and inactivation in zebrafish demonstrated increased angiogenesis (263). Moreover, PTEN regulated angiogenesis and stalk cell proliferation both through its phosphatase and scaffolding function (264).

Lastly, we mentioned the importance of arteriovenous specification of ECs during the angiogenic process. This process is tightly governed by the antagonistic roles of both the PI3K α pathway and the **Mitogen-Activated Protein Kinase (MAPK) pathway**. In mice embryos, for instance, EC destined for arterial positions display high levels of ERK signalling (an important effector of the MAPK pathway), while cells with venous identity do not (170, 172). There is also direct interaction between the 2 pathways. Activated AKT in ECs can inhibit Raf1, upstream of ERK, and hereby inhibit MAPK signalling and maintaining venous specification (227, 228). In zebrafish, similar interactions have been observed, where venous specification was governed by increased PI3K α signalling during blood vessel formation (265), and suppression of PI3K α boosted arteriogenesis (227). In Human Umbilical Vein ECs (HUVECs), PI3K α activity also showcased an inhibitory effect on MAPK signalling (266). Moreover, TIE2 receptor deficiency led to decreased PI3K signalling, resulting in defective vein formation during mice

embryogenesis and postnatal development (267). In general, research showed an important role for PI3K α in maintaining venous identity through multiple interactions with MAPK signalling.

Hypothesis and aims

Gain-of-function mutations in the *PIK3CA* gene are causative for venous and lymphatic vascular malformations. These activating *PIK3CA* mutations span the whole gene, although hotspots have been identified such as H1047R and E545K. Both variants are frequently found in certain cancers and PROS. The E726K variant is rarely found in tumours, but commonly present in some types of PROS such as MCAP. The impact of E726K on PI3K α signalling and the mechanism of pathogenesis is poorly studied.

This thesis focusses on comparing the phenotypes caused by expression of H1047R, E545K, and E726K in blood vascular malformations. We hypothesized that the *PIK3CA* variants affect endothelial PI3K α signalling differently, which consequently determines the vascular phenotype *in vivo*. To address this question, we have used conditional mouse models which allow expression of the variants under the endogenous *Pik3ca* promoter. Using the pan-endothelial CreER^{T2} mouse line, we can control expression of the mutations in endothelial cells. We used the mouse retinas as an *in vivo* model and primary heart endothelial cells derived from the mouse models as an *in vitro* model.

This thesis is organized into three objectives:

- 1. Objective I:** Studying the activating *PIK3CA* mutations in the developing vasculature in mice.
- 2. Objective II:** Elucidating *PIK3CA* variant kinase activity and signalling differences in cultured endothelial cells.
- 3. Objective III:** Exploring the signalling differences between *Pik3ca*^{H1047R} and *Pik3ca*^{E545K} *in vivo* during vascular malformation development.

Materials and methods

1. Animal husbandry and care

1.1 Mouse colony maintenance

The animals used for this project were housed in individually ventilated and autoclaved cages in pathogen-free facilities and with *ad libitum* access to water, maintained at a stable temperature of 21°C under a 12-hour light/dark cycle to ensure animal welfare and experimental reproducibility. The experimental procedures were performed in agreement to the guidelines and regulations established by the Catalan Ministry of Agriculture, Livestock, Fisheries and Food, and the Ethical Committee of the Comparative Medicine and Imaging Centre of Catalonia (CMCiB), and the international AAALAC accreditation (association for Assessment and Accreditation of Laboratory Animal Care international).

1.2 Transgenic mouse models

The study of the vascular malformations and intracellular signalling required the use of various genetically modified mouse models (*Mus musculus*, strain C57BL/6J). These mice were designed to enable inducible expression of specific constructs. Usually, the gene of interest was flanked by LoxP sequences, recognizable for the Cre recombinase enzyme (Cre/lox recombinase system). The Cre recombinase excises the flanked sequence, leading to genetic modification. This strategy enables spatiotemporal control of genetic modification.

1.2.1 *Pik3ca*^{H1047R}, generated by Kinross *et al.* (268)

The *Pik3ca*^{H1047R} mice harbour an inducible mutation in the *Pik3ca* gene. The construct is placed under the endogenous *Pik3ca* promoter, allowing natural transcriptional regulation. The mini-gene strategy was used for this construct. The construct was

designed so that the wild-type (WT) structure is retained, only exon 20 is flanked by LoxP sequences and contains a STOP-codon at its end. Downstream, the duplicate of exon 20 was included, but here the point mutation (CAT to AGG) was incorporated that replaces histidine at position 1047 with arginine (H1047R). This results into the normal expression of the *Pik3ca* gene in absence of Cre recombinase, however, with Cre recombinase active, the WT exon 20 is excised and the mutated exon 20 will be expressed. In the animal models, the mutation was maintained in heterozygosity to replicate the genetic conditions found in diagnosed patients with vascular malformations.

1.2.2 *Pik3ca*^{E545K}, generated by Robinson et al. (269)

The *Pik3ca*^{E545K} mice harbour an inducible mutation in the *Pik3ca* gene. The construct is placed under the endogenous *Pik3ca* promotor, allowing natural transcriptional regulation. A knock-in strategy was used for this model. The construct was designed so that the wild-type (WT) structure is retained, except exon 9 contains the point mutation (GAG to AAG) so that glutamic acid at position 545 is replaced with lysine (E545K). Upstream of the coding sequence, a LoxP-STOP-LoxP sequence was placed. This results in no expression of the *Pik3ca* gene in absence of Cre recombinase for this allele, however, with Cre recombinase active, the LoxP-STOP-LoxP sequence is excised and the mutated *Pik3ca* will be expressed. In the animal models, the mutation was maintained in heterozygosity to replicate the genetic conditions found in diagnosed patients with vascular malformations. Also, this construct in homozygosity is not viable due to absent expression of *Pik3ca*.

1.2.3 *Pik3ca*^{E726K}

The *Pik3ca*^{E726K} mice harbour an inducible mutation in the *Pik3ca* gene. The construct is placed under the endogenous *Pik3ca* promotor, allowing natural transcriptional regulation. The mini-gene strategy was used for this construct. The construct was designed so that the wild-type (WT) structure is retained, only exons 13-20 are flanked by LoxP sequences and contains a STOP-codon at its end. Downstream, the duplicate of exons 13-20 was included, but here the point mutation (GAG to AAG) was incorporated that replaces glutamic acid at position 726 with lysine (E726K). This results into the normal expression of the *Pik3ca* gene in absence of Cre recombinase, however, with Cre recombinase active, the WT exons 13-20 are excised and the mutated exons 13-20 will be expressed. In the animal models, the mutation was maintained in heterozygosity to replicate the genetic conditions found in diagnosed patients with vascular malformations.

1.2.4 Cre lines

- ***Pdgfb-CreER^{T2}***. PDGFB (Platelet-derived growth factor B) is a ligand for the PDGFR α and PDGFR β receptors. It is expressed in endothelial cells (ECs), therefore the inducible Cre line is expressed ubiquitously in blood and lymphatic ECs, with activity reported starting from embryonic day E11.5. Generated by *Claxton et al.* (270).

- ***Tie2-Cre***. *Tie2* encodes for the TEK tyrosine kinase receptor. It is expressed in endothelial cells (ECs), therefore the constitutive Cre line is expressed ubiquitously in blood and lymphatic ECs, with activity reported starting from embryonic day E7.5. Generated by *Kisanuki et al.* (271).

1.2.5 mTmG reporter line, generated by *Muzumbar et al.* (272)

The mTmG mouse line (membrane-Tomato membrane-GFP) is a Cre-dependent dual receptor that expresses membrane-bound Tomato fluorescent protein before Cre-mediated excision, and GFP after excision. This reporter allows for visualization of recombined cell populations (GFP+). It is expressed ubiquitously under control of the *Rosa26* promoter.

1.3 Mice genotyping (tail lysis and PCR)

Tail biopsies were collected from adult mice upon weaning or from newborn mice for genotyping prior to retina isolation. For genotyping embryos, embryo yolk sacs were used. Biopsies were lysed using 50 mM NaOH at 100°C for 15 mins, followed by neutralisation using 1 M Tris-HCl pH 7.4. Samples were vortexed, centrifuged at full speed for 1 min, and DNA collected for DNA amplification by PCR and subsequent detection in 1.5% agarose (Promega, V2111) gels visualized with SYBR Safe DNA Gel Stain (Invitrogen, S33102-5). Primer sequences and PCR conditions are summarised in **Table 1.1**.

Gene	Primer sequence (5'-3')	PCR reaction	PCR conditions
<i>Pik3ca</i> ^{H1047R}	FW1: TTGGTTCCAGCCTGAATAAAGC FW2: TCCACACCATCAAGCAGCA RV: GTCCAAGGCTAGAGTCTTTCCGG	1.5 µL DNA 2.5 µL 10X buffer 2.5 µL 10 µM dNTPs 2.5 µL 10 µM primers mix 0.125 µL Titanium DNA polymerase 15.875 µL H ₂ O	95 °C, 10 min 35X: - 95 °C, 30 sec - 55 °C, 30 sec - 72 °C, 40 sec 72 °C, 5 min
<i>Pik3ca</i> ^{E545K}	FW: GCTGGGATTACAGGTGTTCC RV: GTGGAGGCAGGAGCATAAG	2 µL DNA 3 µL 10X buffer w/o Mg ²⁺ 3 µL 15 µM MgCl ₂ 3 µL 10 µM dNTPs 3 µL 10 µM primers mix 0.25 µL EcoTaq DNA polymerase 15.75 µL H ₂ O	95 °C, 10 min 35X: - 95 °C, 30 sec - 55 °C, 30 sec - 72 °C, 40 sec 72 °C, 5 min
<i>Pik3ca</i> ^{E726K}	FW: ACTGCCTGGCTCCATGTATT RV: GGGAATTCAGCTCAGGTCCT	1.5 µL DNA 2.5 µL 10X buffer 2.5 µL 10 µM dNTPs 2.5 µL 10 µM primers mix 0.125 µL Titanium DNA polymerase 15.875 µL H ₂ O	94 °C, 3 min 35X: - 94 °C, 30 sec - 60 °C, 30 sec - 72 °C, 45 sec 72 °C, 7 min
<i>Pdgfb-CreER</i> ^{T2}	FW: CCAGCCGCCGTCGCAACT RV: GCCGCCGGGATCACTCTCG	2 µL DNA 3 µL 10X buffer w/o Mg ²⁺ 3 µL 15 µM MgCl ₂ 3 µL 10 µM dNTPs 3 µL 10 µM primers mix 0.25 µL EcoTaq DNA polymerase 15.75 µL H ₂ O	94 °C, 4 min 35X: - 94 °C, 30 sec - 57.5 °C, 30 sec - 72 °C, 1 min 72 °C, 5 min
<i>Tie2-Cre</i>	FW: CTAGAGCCTGTTTTGCACGTTC RV: GGGAAGTCGCAAAGTTGTGAGTT	2 µL DNA 3 µL 10X buffer w/o Mg ²⁺ 3 µL 15 µM MgCl ₂ 3 µL 10 µM dNTPs 3 µL 10 µM primers mix 0.25 µL EcoTaq DNA polymerase 15.75 µL H ₂ O	94 °C, 3 min 35X: - 94 °C, 30 sec - 60 °C, 30 sec - 72 °C, 45 sec 72 °C, 7 min
<i>R26-mTmG</i>	FW1: CTCTGCTGCCTCCTGGCTTCT FW2: CGAGGCGGATCACAAGCAATA RV: TCAATGGGCGGGGGTCGTT	2 µL DNA 3 µL 10X buffer w/o Mg ²⁺ 3 µL 15 µM MgCl ₂ 3 µL 10 µM dNTPs 3 µL 10 µM primers mix 0.25 µL EcoTaq DNA polymerase 15.75 µL H ₂ O	94 °C, 5 min 35X: - 94 °C, 30 sec - 61 °C, 45 sec - 72 °C, 1 min 72 °C, 5 min

Table 1.1. Primers and conditions for the PCR reaction used to genotype animal constructs.

2. In vivo experiments

2.1 in vivo Cre-mediated recombination of *Pik3ca* mutations

Given the use of inducible Cre lines, Cre recombinase activity required the presence of 4-OH-Tamoxifen (4-OHT) (Merck, H7905). The induction of recombination in postnatal mouse pups was carried out by intraperitoneal injection of 4-OHT using a Hamilton syringe (Sigma-Aldrich, 21325U). The dose and timing of 4-OHT administration depended on the purpose of each experiment, with lower doses used to achieve greater mosaicism (fewer recombinant cells). Doses ranged from 25 to 2.5 mg/kg were injected from an original stock solution of 10 mg/mL 4-OHT, diluted in pure, sterile ethanol (Merck, 64-17-5) and stored at -20°C.

2.2 Mouse retina isolation and immunostaining

Depending on the objective and scientific question addressed in each experiment, the induction of recombination and isolation of retinas were carried out at different developmental stages. Animals were injected with 4-OHT at P1 or P15, and retinas were isolated at P7 or P21, all following the same protocol.

Postnatal animals were sacrificed by decapitation (P7) or cervical dislocation (P21), a fragment of the tail was collected for subsequent genotyping, and the eyes were isolated. The eyes were quickly immersed in 4% paraformaldehyde (PFA, Sigma-Aldrich, 158127) (diluted in phosphate-buffered saline (PBS)) and incubated for 1 hour at 4°C. After fixation, the eyes were rinsed with PBS 3 times 10 mins at room temperature, and the retinas were isolated. First, an incision was made on the surface of the eye, allowing the cornea and lens to be removed and exposing the retina. Here, hyaloid structures and other tissue remnants were removed. Once isolated, the retinas were fixed again in 4% PFA for 1 hour at 4°C. After this time, the tissue was washed with PBS 3 times 10 mins at room temperature and stored at 4°C until immunofluorescence (IF) staining was performed.

Retinas were then permeabilised overnight in permeabilization buffer (1% BSA, 0.3% Triton X-100 in PBS) at 4 °C, followed by incubation with primary antibody diluted in permeabilization buffer overnight at 4 °C (**Table 2.1**). Afterwards, retinas were washed in PBST (0.1% Tween-20 in PBS) 3 times 10 mins at room temperature. Next, the retinas were incubated with Pblec (1% Tween-20, 1 mM CaCl₂, 1 mM MgCl₂, 1 mM MnCl₂ in PBS at pH6.8) for 30 mins at room temperature. Secondary antibodies were diluted in Pblec in retinas incubated for 2 hours at room temperature (**Table 2.2**). Lastly, retinas were washed 3 times 10 mins at room temperature and mounted on a microscopy slide in Mowiol (Calbiochem, 475904).

To study phospho-proteins, the protocol was adapted to keep the phospho-sites intact. Fixation times in 4% PFA were reduced to 30 mins. After isolating the retinas, they are kept in 100% methanol at -20 °C. Once IF was performed, retinas were incubated with 75%, 50%, 25% methanol and lastly PBS for 10 mins each at room temperature. Permeabilization buffer (3% horse serum, 3% BSA, and 0.3% Tween-20 in PBS) was used and secondary antibodies were diluted in ½ of the permeabilization buffer.

Antigen	Company	Catalogue number	Species	Dilution
ERG	Abcam	AB92513	Rabbit	1:300
GFP	Abcam	AB13970	Chicken	1:300
p-S6 (S235/236)	Cell Signalling Tech.	4857	Rabbit	1:100
p-ERK (T202/204)	Cell Signalling Tech.	9101	Rabbit	1:200

Table 2.1. Primary antibodies for retinal immunostaining.

Antibody	Fluorophore	Company	Catalogue number	Dilution
Goat anti-chicken	Alexa Fluor 488	Invitrogen	A11008	1:300
Donkey anti-rabbit	Alexa Fluor 647	Life Tech	A31573	1:300
Isolectin GS-IB4 Alexa-568		Invitrogen	I21412	1:300

Table 2.2. Secondary antibodies for retinal immunostaining.

2.3 Embryo isolation and immunostaining

Timed matings were set up in the evening between a male carrying the *Tie2-Cre* line and a female carrying the *Pik3ca^{E545K}* line. The following morning, animals were separated, and a check was conducted to determine the presence of the vaginal plug in the female. The presence of a plug in the morning is considered embryonic day 0.5 (E0.5). Pregnancy monitoring was conducted by weighing females where the plug had been observed.

Pregnant females were sacrificed by cervical dislocation, an abdominal incision was made to remove the set of embryos within the uterus. The uterus was immediately immersed in PBS and kept cold (4°C) until the subsequent isolation of embryos. The entire isolation procedure was performed ensuring the embryos were constantly kept in PBS. First, the uterine chain was broken to separate the embryos individually. Both the embryo and the embryonic sac surrounding it were preserved for genotyping. The embryos were individually fixed in 4% PFA for 4 hours or overnight at 4°C. Finally, the PFA solution was replaced, and the embryos were washed before being stored in PBS until further whole-mount staining.

To perform whole-mount staining using immunofluorescence (IF), embryos were permeabilized throughout the day or overnight using a permeabilization buffer (0.3% Triton X-100 diluted in PBS) at 4°C. Subsequently, they were submerged throughout the day or overnight in blocking buffer (1% BSA, 0.3% Triton X-100 in PBS).

Next, the embryos were incubated overnight with the primary antibody (**Table 2.3**) diluted in blocking buffer at 4°C. The following day, embryos were washed for 15 mins with

PBST, after which the embryos were incubated with the secondary antibodies (**Table 2.4**) diluted in blocking buffer for 2 hours at room temperature. After incubation, 5 15-minute washes with PBST were performed. Then, embryos were incubated in progressively increasing concentrations of glycerol to allow clearing. Initially, they were incubated overnight in 25% glycerol diluted in PBS, followed by an increase to 50% glycerol for the entire day, and finally incubated in 90% glycerol overnight. All glycerol incubations were carried out at 4°C. Once the embryos were cleared, they were placed on concave slides and covered with ProLong Gold mounting medium and a coverslip.

Antigen	Company	Catalogue number	Species	Dilution
Endomucin	Santa Cruz Biotechnology	Sc-65495	Rat	1:100

Table 2.3. Primary antibodies for embryo immunostaining.

Antibody	Fluorophore	Company	Catalogue number	Dilution
Goat anti-rat	Alexa Fluor 568	Invitrogen	A11077	1:300

Table 2.4. Secondary antibodies for embryo immunostaining.

2.4 Confocal microscopy

Sample imaging was done with a Leica TCS SP5 and SP8 confocal microscope using 10X and 40X objectives. Maximal projections were made for quantifications of retinas using Fiji/ImageJ. Fiji/ImageJ and Adobe Illustrator 2021 were used for quantification and image editing. Typically, at least 4 images per retinal area (vein with surrounding capillaries, artery with surrounding capillaries, capillary plexus, and sprouting front) were taken for each retina from at least 6 retinas per genotype from at least 3 independent experiments. For embryos, 10X tile scans were used to visualize the whole embryonic vascular structure.

2.5 Image analysis and quantification

2.5.1 Localization and quantification of vascular lesions

The identification of vascular lesions and their location was performed based on the observation of 10X images. Each image shows one of the petals of the retina, where the number of lesions was determined and classified as general or focal depending on their expanse. Retina petals would be divided in 4 “zones”, if a lesion spread out more than 1 of 4 “zones”; the lesion would be considered general.

2.5.2 Vascular area: IB4

The vascular area of the retinas was measured from the IB4 channel by adjusting the threshold to select the IB4+ area within the image. The mean percentage of the IB4-positive area was calculated for each retina (and for each retinal area when applicable) and compared between genotypes.

2.5.3 Recombinant endothelial cell area: GFP

The quantification of the extent of recombinant cells was carried out in animals carrying the *mTmG* allele. First, the IB4 channel was used as a mask for the vascular area. This mask was applied to the GFP channel, discarding any positive signal outside the applied selection. At this point, the GFP threshold was adjusted to quantify the GFP+ area within the mask. This approach enables the determination of the expansion of recombinant, specifically in the vascular area. The mean percentage of the GFP+/IB4+ area was calculated for each retina (and for each retinal area when applicable) and compared between genotypes.

2.5.4 Endothelial cell number: ERG

The number of endothelial cells was determined by manual counting of the ERG+ nuclei within the images. The mean percentage of the EC number was calculated for each retina and compared between genotypes.

2.5.5 PI3K α pathway activation: p-S6

The intensity of the p-S6 (S235/236) signal was used as an indicator of the activation level of the PI3K α pathway, as S6 is one of the effectors phosphorylated by AKT. The quantification of p-S6 (S235/236) was based on calculating the corrected total fluorescence (CTF) and comparing the CTF between mutant and control tissues, and it was represented as relative values or fold change. The integrated density of p-S6 and mean grey value of the background signal of p-S6 (S235/236) was measured within the p-S6 (S235/236) channel. The CTF was calculated as follows:

CTF = integrated density – (GFP+ area x mean grey value)

2.5.6 MAPK pathway activation: p-ERK

The intensity of the p-ERK (T202/Y204) signal was used as an indicator of the activation level of the MAPK pathway. The quantification of p-ERK (T202/Y204) was based on calculating the corrected total fluorescence (CTF) and comparing the CTF between mutant and control tissues, and it was represented as relative values or fold change. The integrated density of p-ERK (T202/Y204) and mean grey value of the background signal

of p-ERK (T202/Y204) was measured within the p-ERK (T202/Y204) channel. The CTF was calculated as follows:

$$\text{CTF} = \text{integrated density} - (\text{GFP+ area} \times \text{mean grey value})$$

p-ERK (T202/Y204) area was also calculated by adjusting the p-ERK (T202/Y204) threshold and measurement within the GFP+ area. The mean percentage of the p-ERK+/GFP+ area was calculated for each retina (and for each retinal area when applicable) and compared between genotypes.

3. Recombinant protein experiments

3.1 Generation of *PIK3CA* mutant plasmids

To express and purify the PI3K α wild-type (WT) and mutant proteins, we needed to create the correct for their expression. WT p110 α , H1047R p110 α , and p85 α plasmids were already created for other projects (Cambridge MTC Laboratory for Molecular Biology (LMB-MRC) plasmid number OP831, OP838, and OP809, respectively). We used the WT p110 α plasmid to create the p110 α E545K and E726K plasmids by mutagenesis, using the Q5 Site-Directed Mutagenesis Kit according to the manufacturer's protocol (New England Biolabs, NEB E05545). Briefly, exponential amplification through PCR was performed with primer pairs designed to change the WT sequence to the desired one (GAA into AAA to change glutamic acid to lysine) (**Table 3.1**). A KLD reaction ligated the primers and confirmed in an agarose gel. A transformation into TOP10 *E. coli* followed through heat shock. The *E. coli* cells were cultured in SOC and gently shaken at 37 °C for 1 hour and finally plated on agar selection plates containing 10 μ g gentamicin (ThermoFisher Scientific, 15750060) to select the transformed cells and incubated overnight at 37 °C. Colonies were selected and grown overnight in LB medium supplemented with 10 μ g of gentamicin at 37 °C. MiniPrep DNA isolation (ThermoFisher Scientific, K210002) was performed on the selected colonies to acquire the plasmid DNA, and they were sent for sequencing to verify the mutation. Once the mutations were confirmed, we performed MaxiPrep DNA isolation (ThermoFisher Scientific, K210007) on some colonies to acquire high concentrations of the plasmids for p110 α H1047R, E545K, and E726K.

PI3Kα mutant	Primer sequence (5'-3')
E545K	FW: TGAAATCACTaaaCAGGAGAAAGATTTTC RV: GAGAGAGGATCTCGTG
E726K	FW: GAAGAAGGATaaaACACAAAAGG RV: TCCTGTTTGAGAATGTCAG

Table 3.1. Primers designed for mutagenesis.

3.2 Bacmid transformation and preparation

The acquired plasmids needed to be combined into a Bacmid plasmid for expression in eukaryote cells. To prepare the bacmid plasmids, plasmids were diluted to 1-40 ng/ μ L and transformed into DH10EmBacY (DH10Bac with YFP reporter) competent cells through heat shock. Cells were spread on agar selective plates (50 ug/ml kanamycin, 7 ug/ml gentamicin, 10 ug/ml tetracycline, 100 ug/ml X-gal, and 40 ug/ml IPTG) and incubated at 37 °C for 2 days. White colonies for each variant were selected and grown overnight in 2X YT medium containing 50 ug/ml kanamycin, 7 ug/ml gentamicin, and 10 ug/ml tetracycline at 37 °C. Bacteria were then centrifuged, and DNA was isolated by suspending, lysing, and neutralization and separation using isopropanol and 70% ethanol and several centrifugation steps. Eventually, DNA pellets were resuspended in sterile EB on ice, concentration was measured, and the bacmids stored at 4 °C until further use.

3.3 Sf9 insect cell transfection and amplification

The PI3K α proteins will be produced in eukaryote *Spodoptera frugiperda* (Sf9) cells. were prepared by upscaling their growth in Insect-XPRESS with L-Glutamine medium shaking at 27 °C (Lonza, BE12-730Q). Once confluency reached 1.0×10^6 cells/ml in 500 mL, cells were plated in 6-well plates (2 mL) and FuGENE HD DNA mix (Promega, E2311) with the Bacmid plasmids was added for 15 mins at room temperature. The Sf9 cells now produce baculovirus containing the PI3K α plasmids that were be used for amplification and subsequent production of the proteins by the Sf9 cells. 2 rounds of amplification were performed by combining first 10 mL of Sf9 cells, then 20 mL of Sf9 cells to the baculovirus, virus was harvested after 2-3 days and washed with PBS (when cells reached 80% fluorescence through GFP expression). Eventually, Sf9 cells were frozen at -80 °C until protein purification. Western blot was performed to validate the presence of both subunits in the cell pellets for each variant.

3.4 Protein purification

To obtain the PI3K α proteins, sf9 cell pellets were resuspended in lysis Buffer (20 mM Tris, 150 mM NaCl, 5% glycerol, 2 mM β -mercaptoethanol, 0.02% CHAPS, pH 8.0) and sonicated at 4°C for 10 min in 10 sec intervals followed by a 10 sec pause. Ultracentrifugation for 45 mins at 45000 g at 4 °C created a cell debris pellet and the protein supernatant, which was filtered using a 0.45 μ M filter and passed through 5 mL StrepTrap column with S300 buffer (20 mM Tris, 300 mM NaCl, 5% glycerol, 2 mM TCEP, pH 8.0) (Cytiva, 29401322). The column was washed with buffer A (20 mM Tris, 100 mM NaCl, 5% glycerol, 1 mM TCEP, pH 8.0) and eluted using a gradient from 1-100% buffer B (buffer A containing 5 mM *d*-Desthiobiotin). The protein containing fractions were collected and diluted 1:2 with Salt dilution buffer (20 mM Tris pH 8.0, 1 mM DTT) to reduce NaCl concentration to 100 mM. The pooled protein solutions were passed over a HiTrap Heparin HP column washed with buffer A, and eluted with a gradient of 1-100% buffer C (20 mM Tris, 1 M NaCl, 1 mM TCEP, pH 8.0) (Cytiva, 17040601). Again, protein-containing fractions were collected and finally passed through a Superdex 200 26/60 HiLoad gel filtration column in gel filtration buffer (20 mM HEPES pH 7.4, 100 mM NaCl, 2 mM TCEP) (Cytiva, 28989336). All the previous steps for column separation were performed at 4 °C. The protein-containing fractions were collected, concentrated to 2.5 mg/mL and flash-frozen in liquid nitrogen and stored at -80 °C. Coomassie staining for each variant were performed to confirm purity of the protein.

3.5 ADP glo

ADP glo assays were performed using the ADP glo kinase assay kit according to the manufacturer's instructions (Promega, V6930). The enzymatic reaction was performed in reaction buffer containing 20 mM HEPES, 50 mM NaCl, 50 mM KCl, 3 mM MgCl₂, 1 mM EGTA, 1 mM TCEP, pH 7.4. Concentrations ranges for each PI3K α variant were selected based on predicted enzymatic velocity (potential kinase activity increase of mutations); 40 nM, 20 nM, 10 nM, and 5 nM for WT and E726K PI3K α , 20 nM, 10 nM, 5 nM, and 2.5 nM for E726K PI3K α , and 10 nM, 5 nM, 2.5 nM, and 1.25 nM for H1047R PI3K α in basal conditions (without phosphotyrosine pY), and 8 nM, 4 nM, 2 nM, and 1 nM for WT, E545K and E726K PI3K α , and 0.5 nM, 0.25 nM, 0.125 nM, and 0.0625 nM for H1047R PI3K α in pY-stimulated conditions. PIP2PS substrate was added at 75 μ M and ATP at 100 μ M, and pY at 1 μ M. The enzymatic reactions were precisely timed to 45 mins each and luminescence was read.

4. *In vitro* experiments

4.1 Mouse heart endothelial cell isolation and culture

Mouse heart endothelial cells (ECs) were isolated from adult mice between 3 and 6 weeks old. Hearts were homogenized with a scalpel and incubated with dispase II (4 U/mL) and collagenase A (10 mg/mL) in 5 mL of Hank's Balanced Salt Solution (1% P/S) for 30 minutes at 37 °C. The digested tissue was strained (cell strainer 40 µM) and the enzyme activity was halted by addition of DMEM (supplemented with 10% iFBS and 1% P/S). Cells were washed 2 times with PBS/BSA (0.5% BSA) and resuspended in 100 µL of PBS containing anti-CD31 antibody-coated magnetic beads for 30 mins at room temperature. The CD31+ fraction was selected and washed with PBS/BSA using a magnet. Cells were resuspended and cultured in 0.5% gelatin-coated 12-well plates in F12/DMEM medium (supplemented with 20% iFBS and 1% P/S). Once confluent, cells underwent a second round of selection to purify the CD31+ ECs by a second in-well incubation with anti-CD31 antibody-coated magnetic beads for 30 mins at room temperature. The cells were trypsinized, selected on the magnet, and resuspended in 6-well plates in F12/DMEM complete medium. ECs were cultured at 37 °C in 5% CO₂. Reagents can be found in **Table 4.1**.

Experiments were either done on freshly isolated ECs, or ECs could be cryopreserved in liquid nitrogen. ECs were trypsinized and resuspended in iFBS with 10% DMSO in cryotubes and transferred to a liquid nitrogen storage tank. To thaw the ECs, they were taken out of storage, thawed in a warm water bad at 37 °C, and mixed with DMEM. After centrifugation, ECs were resuspended in F12/DMEM complete medium and cultured as usual.

Reagent	Company	Catalogue number
30% BSA	Labclinics	A0296
DMEM	Gibco	41965-039
F12/DMEM	Gibco	21041-025
Endothelial Cell growth medium 2	Promocell	C-22111
Dispase II	Roche Diagnostics	4942078001
Dynabeads sheep a-Rat IgG	Invitrogen	110-35
FBS	Gibco	10270106
Porcine gelatin	Sigma-Aldrich	G1890
HBSS	Gibco	14170-112
P/S (Penicillin/streptomycin)	Gibco	15140-122
CD31	BD Pharmingen	555289
Trypsin	Gibco	15400054

Table 4.1. Reagents used for mouse heart EC isolation and culture.

4.2 *In vitro* Cre-mediated recombination of *Pik3ca* mutations

To induce recombination in cultured ECs, cells were treated with 2 μ M of 4-OHT for 24 hours, diluted in etOH. etOH-treated *Pdgfb-CreER^{T2}*; *Pik3ca^{Tg^{WT}}* controls were used for each variant in the experiments of Results Figures 2.3.1 - 2.3.3., while 4-OHT treated *Pdgfb-CreER^{T2}*; *Pik3ca^{WT/WT}* were used in Results Figures 2.3.4 - 2.3.6. For most experiments, we allowed for the recombined cells to expand by allowing more time before seeding the cells for the experiment. Moreover, in many experiments, starved conditions were used. These recombined cells were ultimately used for experimental treatments, such as immunocytochemistry and qPCR experiments, and re-seeded in the functional assays (confluency, EdU, scratch-wound assays).

4.3 Analysis of recombination with PCR

To determine if the *Pik3ca* mutant constructs were being recombined *in vitro*, primers were designed for each mutation (**Table 4.2**). For *Pik3ca^{H1047R}* and *Pik3ca^{E726K}*, the primers were designed to capture the recombination of the mini-gene by differentiating between the non-recombined, long sequence when the mini-gene is still present, and the recombined, short sequence when the mini-gene is excised. For *Pik3ca^{H1047R}*, the primers were designed around the LoxP-STOP-LoxP sequence to differentiate its excision in recombined conditions. We used 4-OHT-treated *Pdgfb+*; *Pik3ca^{WT/WT}* cells (WT) and etOH-treated *Pik3ca^{Tg^{WT}}* cells as controls for each variant. After 24 hours of etOH or 4-OHT treatment, the cells were centrifuged at 1500 g and the pellet was frozen at -20 °C. Afterwards, RNA was extracted (protocol and kit explained in chapter 4.5) and PCR was performed with the primers mentioned in Table 4.2. Untreated *Pik3ca^{WT/WT}* ECs were used as an additional control for each variant.

<i>Pik3ca</i> mutant gene	Primer sequence (5'-3')	PCR reaction	PCR conditions
<i>Pik3ca</i> ^{H1047R}	FW: AGCCAAGGGAGAGGAATGGT RV: CCGTGCCTAGCGTCGTTTCAT	2 µL DNA 3 µL 10X buffer w/o Mg ²⁺ 3 µL 15 µM MgCl ₂ 3 µL 10 µM dNTPs 3 µL 10 µM primers mix 0.25 µL EcoTaq DNA polymerase 15.75 µL H ₂ O	94 °C, 3 min 35X: - 94 °C, 30 sec - 60 °C, 30 sec - 72 °C, 45 sec 72 °C, 7 min
<i>Pik3ca</i> ^{E545K}	FW: GCGGATTCTGAGTCTAAGGG RV: AGATGGTTGCTCTAAACTAGGC	2 µL DNA 3 µL 10X buffer w/o Mg ²⁺ 3 µL 15 µM MgCl ₂ 3 µL 10 µM dNTPs 3 µL 10 µM primers mix 0.25 µL EcoTaq DNA polymerase 15.75 µL H ₂ O	94 °C, 5 min 35X: - 94 °C, 30 sec - 53 °C, 45 sec - 72 °C, 1 min 72 °C, 5 min
<i>Pik3ca</i> ^{E726K}	FW: ACTGCCTGGCTCCATGTATT RV: TGTGCTCCAACCTCAAGGGA	2 µL DNA 3 µL 10X buffer w/o Mg ²⁺ 3 µL 15 µM MgCl ₂ 3 µL 10 µM dNTPs 3 µL 10 µM primers mix 0.25 µL EcoTaq DNA polymerase 15.75 µL H ₂ O	95 °C, 10 min 35X: - 95 °C, 30 sec - 55 °C, 30 sec - 72 °C, 40 sec 72 °C, 5 min

Table 4.2. Primers and conditions to verify *Pik3ca* mutant construct recombination.

4.4 Protein extraction and immunoblotting

4.4.1 Signalling in basal, starved, and iFBS-stimulated conditions

After recombination, ECs were changed to full medium (F12/DMEM supplemented with 20% iFBS) without 4-OHT or to starvation medium (F12/DMEM pure) and starved overnight. Afterwards, ECs for stimulation were then supplemented with 20% iFBS for 15 mins. Control and starved cells would be supplemented with the same volume of either full or starvation medium, that way, the cells would always be manipulated equally. Then, cells were quickly washed with cold PBS Ca⁺/Mg⁺ and frozen at -80 °C or protein was extracted fresh.

4.4.2 Signalling in VEGFC and EGF-stimulated conditions

After recombination, ECs were changed to starvation medium (F12/DMEM pure) and starved overnight. Afterwards, ECs for stimulation were then supplemented with 75 ng/mL VEGFC (BioLegend, 775102) and 75 ng/mL EGF (R&D systems, 2028-EG) for 10 mins. Starved ECs and 20% iFBS-stimulated cells were used as controls. Starved cells would be supplemented with the same volume as the GF-stimulated cells, but with vehicle (sterile PBS) to keep the handling between conditions equal. Then, cells were quickly washed with cold PBS Ca⁺/Mg⁺ and frozen at -80 °C or protein was extracted fresh.

4.4.3 Protein extraction and immunoblotting

ECs were kept at 4 °C during the protein extraction process. ECs were lysed with 82 µL of cold lysis buffer (50mM Tris-HCl pH 7.4, 5mM EDTA, 150mM NaCl, and 1% Triton X-100, supplemented with phosphatase and protease inhibitors, Roche, 4906845001 and 11836153001) for 15 mins, followed by centrifugation at maximum speed for at 4 °C for 15 mins. Protein concentration for each sample was measured using the Pierce BCA Protein Assay Kit following manufacturer's instructions (ThermoFisher Scientific, 23225). Total cell lysates were resolved on 4 to 12 % Bis-Tris protein gels (ThermoFisher Scientific, WG1402BOX) using NuPage MOPS SDS running buffer (ThermoFisher Scientific, NP0001) for 2 hours at 170 V. Transfer onto nitrocellulose membranes was done in NuPage transfer buffer (ThermoFisher Scientific, PN00061) for 30 mins at 25V. The membranes were blocked in 5% milk in TBST (0.1% Tween 20 in TBS) for 1 hour followed by overnight incubation with specific primary antibodies diluted in TBST with 2% BSA and 1:1000 azida (**Table 4.3**) at 4 °C. After 3 washes with TBST, membranes were incubated with fluorescent secondary antibodies diluted in 5% milk in TBST for 1 hour at room temperature covered from light (**Table 4.4**).

Antigen	Company	Catalogue number	Species	Dilution
p-AKT (S473)	Cell Signalling Tech.	4060	Rabbit	1:1000
p-AKT (T308)	Cell Signalling Tech.	4056S	Rabbit	1:500
T-AKT	Cell Signalling Tech.	9272	Rabbit	1:2000
p-ERK (T202/Y204)	Cell Signalling Tech.	9101	Rabbit	1:1000
T-ERK	Cell Signalling Tech.	9102	Rabbit	1:1000
p-S6 (S235/6)	Cell Signalling Tech.	4857	Rabbit	1:1000
T-S6	Cell Signalling Tech.	2212	Rabbit	1:1000
Vinculin	Sigma-Aldrich	9131	Mouse	1:10000

Table 4.3. Primary antibodies used for immunoblotting.

Antibody	Company	Catalogue number	Species	Dilution
Anti-rabbit IRDye 800 CW	Licor	926-32211	Goat	1:5000
Anti-mouse IRDye 680 RD	Licor	926-68070	Goat	1:5000

Table 4.4. Fluorescent secondary antibodies used for immunoblotting.

4.5 RNA extraction and qPCR

4.5.1 Expression of *Ang2*, *Cxcr4*, *EphB4*, *Itga9*

After recombination, ECs were either immediately frozen for the 24 hours timepoint (24 hours since the start of 4-OHT treatment) or were changed to full medium (F12/DMEM supplemented with 20% iFBS) without 4-OHT and left to expand for another 48 hours for the 72 hours timepoint (24 hours since the start of 4-OHT treatment). Afterwards, cells were quickly washed with cold PBS Ca⁺/Mg⁺ and frozen at -80 °C until RNA extraction.

4.5.2 Expression of *Vegfr1*, *Vegfr2*, *Vegfr3*, and *Egfr* in starved and EGF-stimulated conditions

After recombination, ECs were changed to starvation medium (F12/DMEM pure) and starved overnight. Afterwards, ECs for stimulation were then supplemented with 75 ng/mL EGF for 10 mins. Starved cells would be supplemented with the same volume as the GF-stimulated cells, but with vehicle (sterile PBS) to keep the handling between conditions equal. Then, cells were quickly washed with cold PBS Ca⁺/Mg⁺ and frozen at -80 °C until RNA extraction.

4.5.3 RNA extraction, cDNA synthesis and qPCR

Total RNA was isolated from ECs using the Maxwell RSC simplyRNA Cells kit according to the manufacturer's protocol (Promega, AS1390). RNA concentration and quality were measured with a NanoDrop One spectrophotometer. RT-PCR was done with 0.5 µg of RNA in 10 µL H₂O for cDNA synthesis using the High Capacity cDNA Reverse Transcription kit following the manufacturer's protocol (Applied Biosystems, 4368814). Quantitative PCR was performed using the LightCycler 480 SYBR Green I Master kit and LightCycler 480 System (Roche, 4.707.516.001). *MI32* was used as a housekeeping gene (**Table 4.5**).

Gene	Protein	Primer sequence (5'-3')
<i>MI32</i>	MRPL32	FW: ACCCCAGAGGCATTGACAAC RV: ATTGTGGACCAGGAACTTGC
<i>Ang2</i>	ANG2	FW: CCTCGACTACGACGACTCAGT RV: TCTGCACCACATTCTGTTGGA
<i>Ephb4</i>	EPHB4	FW: CTGGATGGAGAACCCCTACA RV: CCAGGTAGAAGCCAGCTTTG
<i>Cxcr4</i>	CXCR4	FW: TCCTCCTGACTATACCTGACTTCATCT RV: CCTGTCATCCCCCTGACTGAT
<i>Itga9</i>	ITGA9	FW: GCCTGGAACCAATTAAGCAGACCTG RV: TCACGACGTCATTAAGCCATCCAC
<i>Vegfr1</i>	VEGFR1	FW: CACCCCTGTCACCACAATCA RV: CACCAATGTGCTAACCGTCTTA
<i>Vegfr2</i>	VEGFR2	FW: AAGTGATCCCAGATGACAGCC RV: GGTAGCCACTGGTCTGGTTG
<i>Vegfr3</i>	VEGFR3	FW: CGTGACATCACAGGCAATG RV: GCTCAGGTACCCACTTAGCC
<i>Egfr</i>	EGFR	FW: GGACTGTGTCTCCTGCCAGAAT RV: GGCAGACATTCTGGATGGCACT

Table 4.5. Primers used for qPCR.

4.6 Confluency assay

Confluency assays were performed to determine proliferation, cell growth, and survival. Here, cells were recombined for 48 hours with 2 μ M of 4-OHT, then plated in 96-well plates in triplicate per cell line and per biological replicate. ECs were plated at 4000 cells/well and kept in full medium (F12/DMEM supplemented) for the first experiment. They were left to grow for 96 hours, and medium was not replenished. For the experiment in starved conditions, the cells were seeded at 8000 cells/well and left overnight to attach in full medium, subsequently washed and changed to starvation medium (F12/DMEM pure). After plating, 96-well plates were placed in a Incucyte SX5 (Sartorius) where pictures were taken every 2 hours while cells were incubated at 37 °C in 5% CO₂. Images were processed and analysed with Fiji/ImageJ.

4.7 EdU-incorporation assay

EdU (5-ethynyl-2-deoxyuridine)-incorporation assays were performed to study EC proliferation *in vitro*. Briefly, 0.5x10⁵ ECs were seeded onto a gelatin-coated cover slip and incubated in full medium containing 2 μ M of etOH or 4-OHT for 24 hours at 37°C in 5% CO₂. The next day, cells were washed with PBS and replaced with new medium with EdU reagent for 2 hours at 10 μ M concentration according to manufacturer's instructions (Invitrogen, C10340). The cells were then fixed with 4% PFA for 15 minutes followed by triple wash with PBS. Cell were permeabilised with 0.2% Triton X-100 in PBS for 20 min and incubated with 2 M HCl for 10 minutes at room temperature. After 45 minutes of blocking in 3% BSA in PBS, cover slips were incubated with a primary mouse anti-EdU

antibody (diluted 1:50 in the blocking solution) overnight at 4°C. The following day, the cells were washed three times in 0.5% Tween-20 in PBS solution and incubated with a secondary Alexa Fluor 647-conjugated rat anti-mouse secondary antibody (1:200) for 1 hour at room temperature, followed by 5 minutes incubation with DAPI (1:10000, Invitrogen, S33025). Confocal images were taken and EdU+/DAPI+ cells were compared between the 4-OHT-treated *Pik3ca* mutants and their etOH-treated controls. Images were processed and analysed with Fiji/ImageJ.

4.8 Scratch-wound assay

Scratch-wound assays were performed to determine EC migration. Here, cells were recombined for 48 hours with 2 µM of 4-OHT, then plated in 96-well plates in six replicates per cell line and repeated 3 times per biological replicate. ECs were plated at 10000 cells/well and kept in full medium (F12/DMEM supplemented). They were left to grow until they were fully confluent. With the 96-well Woundmaker (Sartorius), a scratch was induced in the middle of the wells, and the damaged cells and debris were washed, and medium was replaced to either full medium (F12/DMEM supplemented) or starvation medium (F12/DMEM pure). 96-well plates were placed in a Incucyte SX5 (Sartorius) where pictures were taken every 2 hours while cells were incubated at 37 °C in 5% CO₂. Images were processed and analysed with Fiji/ImageJ.

5. Statistical analysis

Statistical analysis was performed using the GraphPad Prism 10 software. Statistical tests range from parametric (un)paired t-test to parametric one-way ANOVA depending on the experiment. Normality was tested for all experiments with Shapiro-Wilk's test. All figures showcase individual datapoint that indicate biological replicates with mean and s.e.m as error bars. Data is normalized to controls. In some cases, the incremental analysis was performed to analyse the trends rather than the mean values themselves, to study the changes in up- or downregulation of genes/proteins. P values were considered statistically significant if *p < 0.05, **p < 0.01, ***p < 0.001, and ****p < 0.0001.

Results

I. Objective 1: Studying the activating *PIK3CA* mutations in the developing vasculature in mice.

1.1. Vascular malformations generated by the *PIK3CA* variants during angiogenesis.

To study the role of *PIK3CA* variants in a tissue-specific and time-specific manner, inducible Cre-dependent mouse models were used. *Pik3ca* variants were expressed under the endogenous promoter (**Figure 1.1.1**). For *Pik3ca*^{H1047R} (268) and *Pik3ca*^{E726K}, the mini-gene strategy was used. A cassette containing the cDNA of exons from the wild-type gene (exon 20 for *Pik3ca*^{H1047R}, and exons 13-20 for *Pik3ca*^{E726K}) were inserted, flanked by LoxP sites to enable excision by Cre recombinase. These cassettes were followed by the remaining exons containing the mutation (in exon 20 for *Pik3ca*^{H1047R} and exon 13 for *Pik3ca*^{E726K}). For *Pik3ca*^{E545K} (269), a knock-in strategy was used, where the wild-type exon 9 was replaced with the mutant version. A LoxP-STOP-LoxP cassette was inserted upstream of the coding sequence to allow expression of the mutant gene when the stop-codon is excised by Cre recombinase. As a result, there is no *Pik3ca* expression on this allele when Cre recombinase is not active.

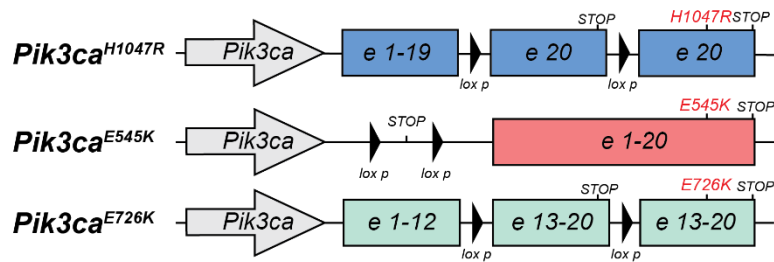


Figure 1.1.1. *In vivo* strategies for overactivation of PIK3CA with *Pik3ca* mutant mouse models. The 3 variant constructs of *Pik3ca*^{H1047R}, *Pik3ca*^{E545K}, and *Pik3ca*^{E726K}. *Pik3ca*^{H1047R} and *Pik3ca*^{E726K} use the mini-gene strategy, where Cre recombinase can excise the wild-type exons, resulting in expression of the mutations. *Pik3ca*^{E545K} uses the knock-in strategy, where recombination will remove a stop codon to express the mutation.

First, we wanted to study the effect of expressing the *PIK3CA* variant mutations on the development of the vasculature *in vivo*. We used the mouse retina as a model for angiogenesis since the blood vessels in the mouse retina develop postnatally over the span of 3 weeks. During the first week, active angiogenesis occurs, leading to the formation of a superficial vascular monolayer driven by abundant mitogenic signals from the environment. In the second week, two additional vascular layers develop beneath the first. By the third week, the vasculature matures, accompanied by a reduction in growth signals (273). To study the effect of heterozygous *Pik3ca*^{H1047R}, *Pik3ca*^{E545K}, or *Pik3ca*^{E726K} expression on the vascular bed in mouse retinas, we crossed the *Pik3ca* mutant mice with mice expressing CreERT² recombinase under the endothelial cell (EC)-specific *Pdgfb* promoter. This pan-endothelial Cre line will induce recombination in all ECs (270). The administration of 4-hydroxy-tamoxifen (4-OHT) will activate the Cre recombinase in ECs specifically, inducing the recombination of the mutant *Pik3ca* gene. To validate that recombination has taken place, we crossed the lines with the *Rosa26-mTmG* reporter line which will indicate non-recombined cells in red (TdTomato expression), and recombined cells in green (GFP expression) (272). Previous research in our lab determined that *Pik3ca*^{H1047R} expression resulted in massive hyperplasia of the vascular bed in mouse retinas with different doses of 4-OHT (73, 89) Here, we used the largest dose of 25 mg/kg 4-OHT ensure the recombination of the majority of all ECs and to compare the effects of *Pik3ca* variant expression on the development of the retinal vasculature during the first week of development (**Figure 1.1.2**).

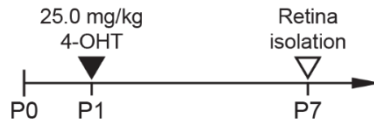


Figure 1.1.2. *in vivo* injections scheme to study overactivation of *PIK3CA* with *Pik3ca* mutant mouse models.

We induced recombination by intragastric injection of 25.0 mg/kg at postnatal day 1 (P1) and isolated the mouse retinas at P7.

To understand the differences in severity of the vascular phenotype that the 3 *Pik3ca* variants generated in mice, we compared the occurrence of vascular malformations (general and focal) in the petals of the studied retinas (**Figure 1.1.3**). We observed a general vascular malformation, characterized by massive hyperplasia, in 100% of EC-*Pik3ca*^{H1047R/WT} petals. In EC-*Pik3ca*^{E545K/WT} petals we noticed a general vascular malformation in 71% of cases, and smaller, focal vascular malformations in 21% of cases. Only 8% of all studied petals remained without vascular lesions. We observed a general vascular malformation in 10% of EC-*Pik3ca*^{E726K/WT} petals and 16% showcased smaller, focal vascular malformations, while 74% remained without vascular lesions. These data suggest that *Pik3ca*^{H1047R/WT} and *Pik3ca*^{E545K/WT} are mutations that generate a severe vascular phenotype, often resulting in vascular lesions when expressed in ECs, while *Pik3ca*^{E726K/WT} only generated a mild phenotype in rare cases.



Figure 1.1.3. Occurrence of *Pik3ca*^{H1047R}, *Pik3ca*^{E545K}, and *Pik3ca*^{E726K}-driven vascular malformations during angiogenesis.

Vascular malformations (VM) were counted in the petals of *Pik3ca*^{H1047R/WT}, *Pik3ca*^{E545K/WT}, and *Pik3ca*^{E726K/WT} mutant mice. Lesions were categorized depending on their size and expanse (general or focal). n ≥ 24 petals per genotype.

To investigate and quantify the vascular malformations caused by these *Pik3ca* variants, we analysed retinal vasculature using immunostaining and confocal microscopy. First, we validated previous findings on *Pik3ca*^{H1047R/WT} expression in retinas (73, 89).

Following a 25 mg/kg 4-OHT injection at P1, we isolated retinas at P7 and performed immunostaining with anti-IB4 to assess vascular area and anti-GFP to assess the recombined endothelium. We used 4-OHT-injected *Pdgfb-CreER^{T2}*; *Pik3ca^{WT/WT}* littermates as controls. We observed massive hyperplasia of the vasculature in the mutants compared to the controls (**Figure 1.1.4.A**). The vasculature displayed hyperplasia most evidently towards the sprouting front. This was reflected in the assessment of the IB4+ area, where we measured a significant increase in IB4+ in the mutants compared to the controls (**Figure 1.1.4.B**). Then, GFP+/IB4+ assessment revealed a recombination rate of >80% in both controls and mutants, in accordance with what was previously described for this model (73) (**Figure 1.1.4.C**). Mutants showed a significant increase in GFP+/IB4+ area, indicating clonal expansion of the recombined ECs. In summary, these findings demonstrate that *Pik3ca^{H1047R/WT}* expression in ECs leads to pronounced vascular hyperplasia, driven by the clonal expansion of recombined ECs in the retinal vasculature. This recapitulates well the data previously generated in our lab for this model (73).

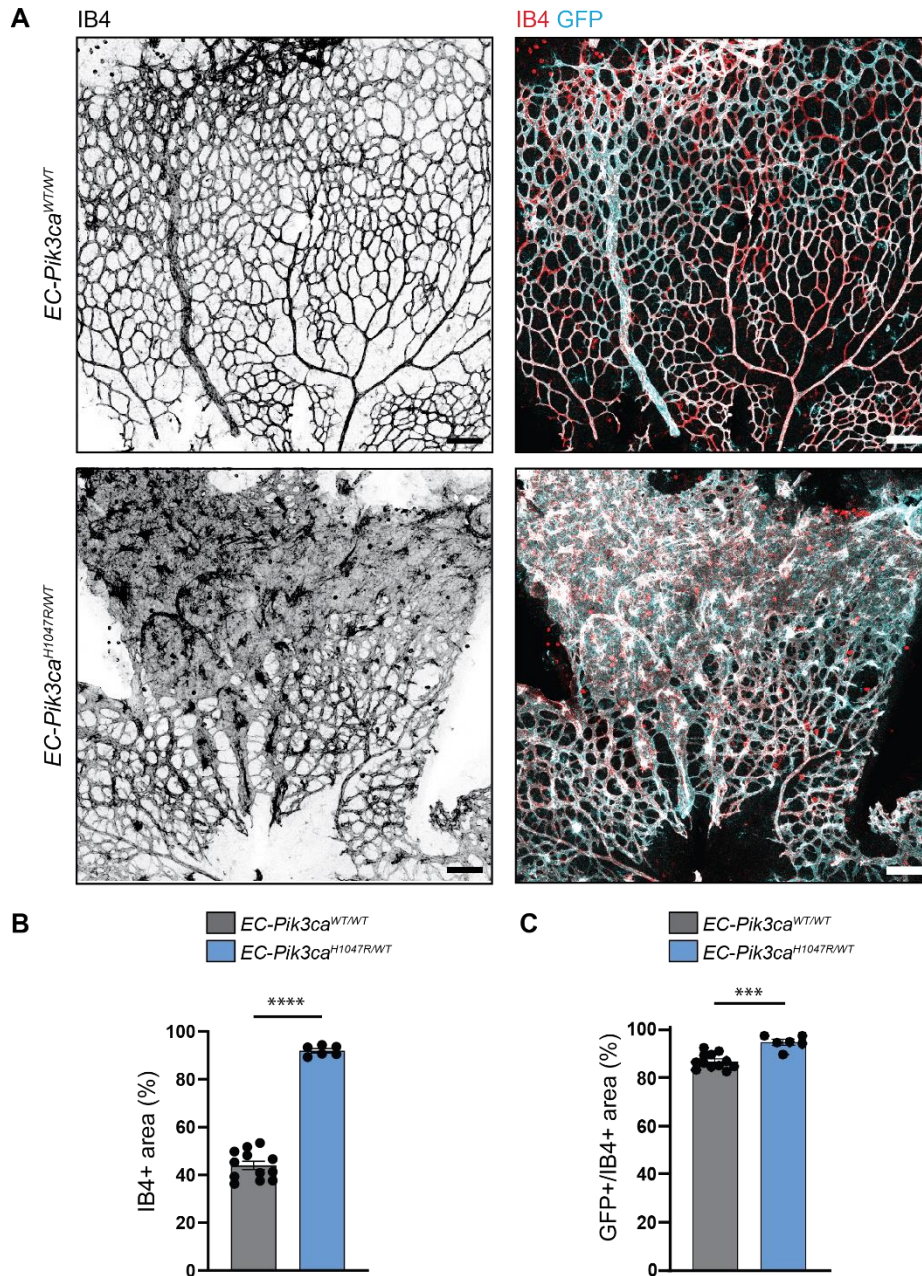


Figure 1.1.4. *Pik3ca*^{H1047R}-driven vascular malformations in mouse retinas.

(A) Representative confocal images of retinas immunostained with anti-IB4 and anti-GFP. Scale bar = 100 μm . $n \geq 6$ retinas per genotype. **(B)** Quantification of IB4+ area per 250000 μm^2 area per petal. Statistical analysis was performed by parametric unpaired t-test. **** $p < 0.0001$ was considered statistically significant. $n \geq 6$ retinas per genotype. **(C)** Quantification of GFP+/IB4+ area per 250000 μm^2 area per petal. Statistical analysis was performed by parametric unpaired t-test. *** $p < 0.001$ was considered statistically significant. $n \geq 6$ retinas per genotype.

To verify that hyperplasia occurred because of increased numbers of ECs, we stained P7 retinas with ERG and compared the EC number between *Pik3ca*^{WT/WT}-expressing controls and *Pik3ca*^{H1047R/WT}-expressing mutants (**Figure 1.1.5.A**). In the lesions, we observed a significant increase in EC number in mutants compared to controls (**Figure 1.1.5.B**). These data suggest that *Pik3ca*^{H1047R/WT} expression caused hyperplasia of the vasculature due to an enlarged number of ECs.

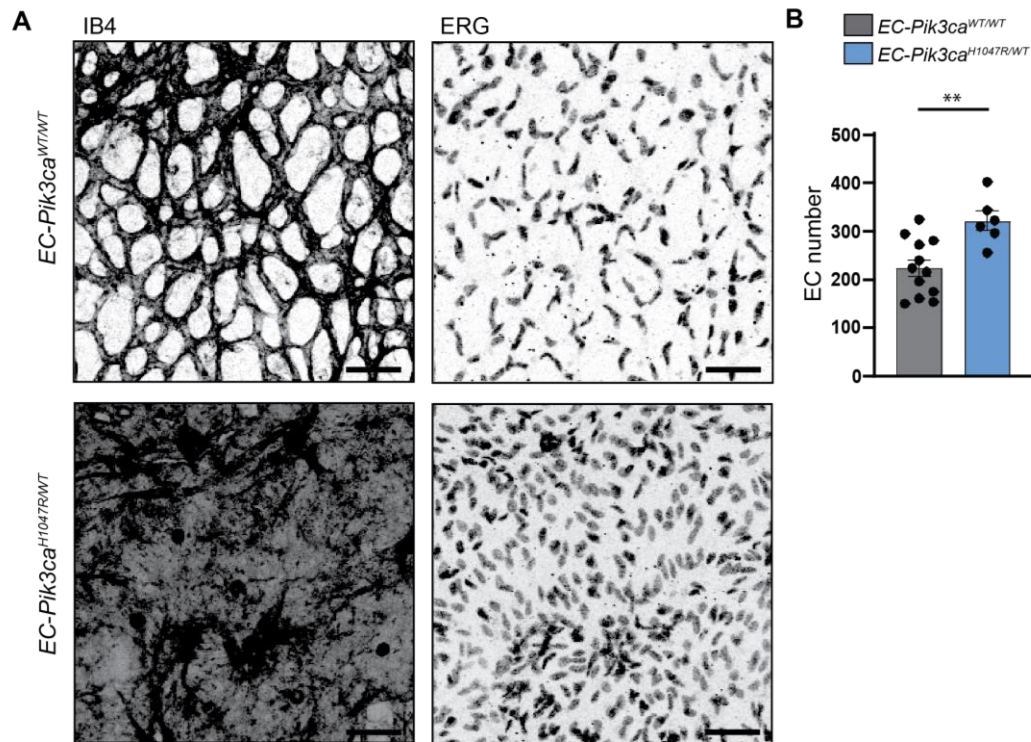


Figure 1.1.5. *Pik3ca*^{H1047R}-driven vascular malformations with increased amounts of endothelial cells in mouse retinas.

(A) Representative confocal images of retinas immunostained with anti-IB4 and anti-ERG. Scale bar = 50 μm. n ≥ 6 retinas per genotype. (B) Quantification of ERG+ nuclei per 250000 μm² area per petal. Statistical analysis was performed by parametric unpaired t-test. **p < 0.01 was considered statistically significant. n ≥ 6 retinas per genotype.

The *Pik3ca*^{E545K} variant is well-known for its oncogenic potential in various cancer types and is commonly found in VMs, where it activates the PI3Kα pathway to drive cell proliferation and tumorigenesis (60, 269, 274). However, its specific effects when expressed in ECs remain unexplored, making this study crucial for understanding its role in vascular development and pathology. We injected *Pdgfb-CreERT2*; *Pik3ca*^{E545K/WT} mice with 25 mg/kg 4-OHT at P1 and isolated the retinas at P7, followed by immunostaining with IB4 and GFP. We used 4-OHT-injected *Pdgfb-CreERT2*; *Pik3ca*^{WT/WT} littermates as controls. *Pik3ca*^{E545K/WT} expression resulted in large hyperplasia, mainly towards the sprouting front (**Figure 1.1.6.A**). The vascular phenotype was similar to that of *Pik3ca*^{H1047R/WT} expression. Here, we also quantified a significantly enlarged vascular

area (IB4+ area) in mutants compared to controls (**Figure 1.1.6.B**). As with *Pik3ca*^{H1047R/WT}, here we measured a recombination rate (GFP+/IB4+ area) of >80% in controls and mutants, and a significantly increased GFP+/IB4+ area in mutants compared to controls, indicating clonal expansion of recombined cells (**Figure 1.1.6.C**). Together, these data show a massive hyperplasia when we express *Pik3ca*^{E545K/WT} in de ECs of the developing retina. Malformations are driven by clonal expansion of recombined ECs, comparable to expression of *Pik3ca*^{H1047R/WT}.

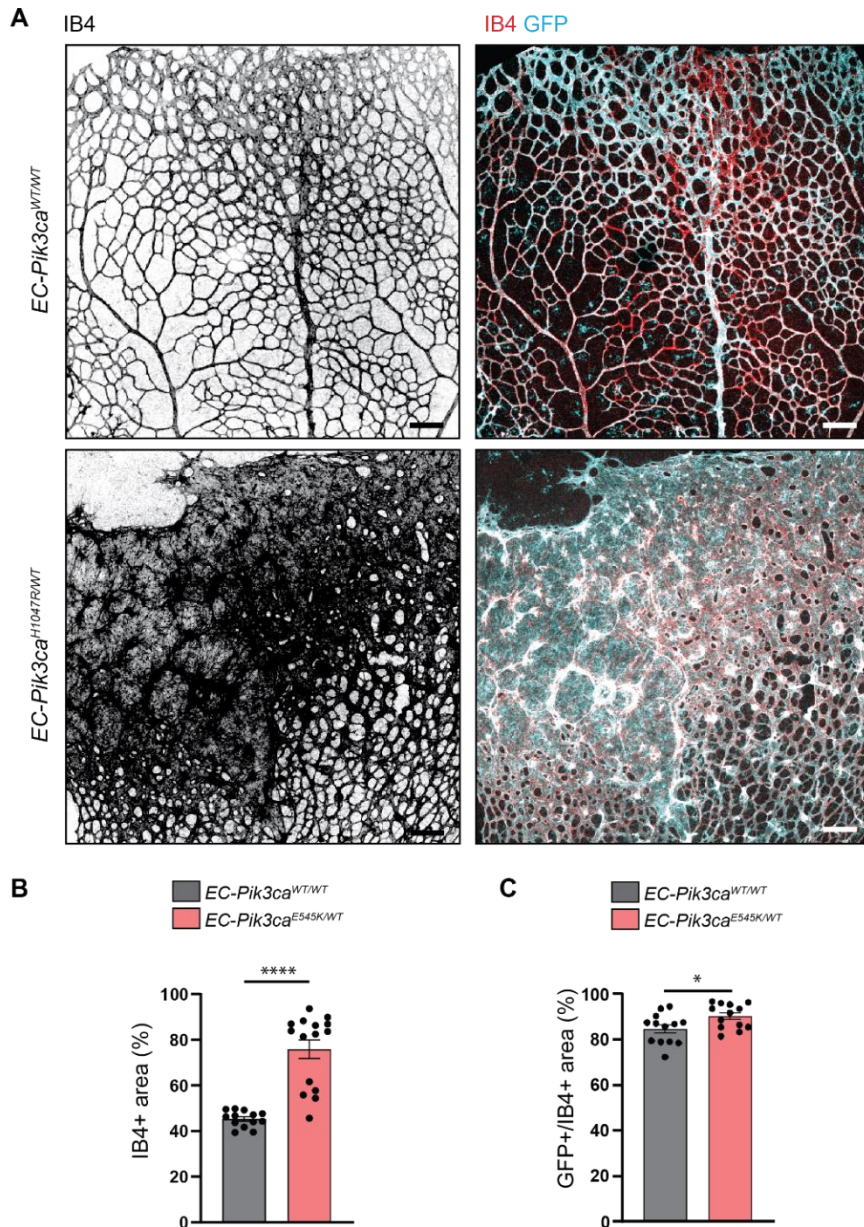


Figure 1.1.6. *Pik3ca*^{E545K}-driven vascular malformations in mouse retinas.

(A) Representative confocal images of retinas immunostained with anti-IB4 and anti-GFP. Scale bar = 100 μ m. $n \geq 13$ retinas per genotype. **(B)** Quantification of IB4+ area per 250000 μ m² area per petal. Statistical analysis was performed by parametric unpaired t-test. **** $p < 0.0001$ was considered statistically significant. $n \geq 13$ retinas per genotype. **(C)** Quantification of GFP+/IB4+ area per 250000 μ m² area per petal. Statistical analysis was performed by parametric unpaired t-test. * $p < 0.05$ was considered statistically significant. $n \geq 13$ retinas per genotype.

For *Pik3ca*^{E545K/WT}, we also verified if hyperplasia could be attributed to increased numbers of ECs. Therefore, we immunostained P7 retinas with ERG and compared the EC count with *Pik3ca*^{WT/WT}-expressing littermate controls (**Figure 1.1.7.A**). As in *Pik3ca*^{H1047R/WT}, we observed a significant increase in EC number (**Figure 1.1.7.B**). These data show that *Pik3ca*^{E545K/WT} expression caused hyperplasia of the vasculature due to an enlarged number of ECs, similar to *Pik3ca*^{H1047R/WT} expression.

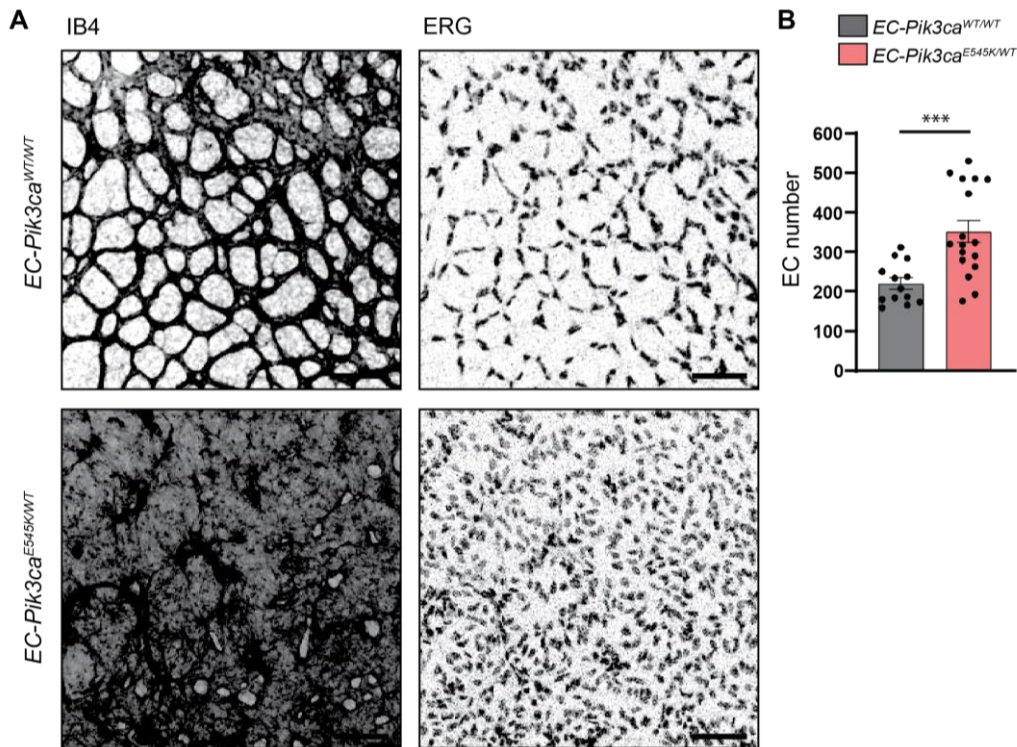


Figure 1.1.7. *Pik3ca*^{E545K}-driven vascular malformations with increased amounts of endothelial cells in mouse retinas.

(A) Representative confocal images of retinas immunostained with anti-IB4 and anti-ERG. Scale bar = 50 μm. n ≥ 13 retinas per genotype. (B) Quantification of ERG+ nuclei per 250000 μm² area per petal. Statistical analysis was performed by parametric unpaired t-test. ***p < 0.001 was considered statistically significant. n ≥ 13 retinas per genotype.

The *Pik3ca*^{E726K/WT} model was generated by our group for the purpose of studying the effect of non-hotspot variant expression on the vasculature. Here, we injected *Pdgfb-CreERT2*; *Pik3ca*^{E726K/WT} mice with 25 mg/kg 4-OHT at P1 and isolated the retinas at P7, followed by immunostaining with IB4 and GFP. We used 4-OHT-injected *Pdgfb-CreERT2*; *Pik3ca*^{WT/WT} littermates as controls. *Pik3ca*^{E726K/WT} expression resulted in hyperplasia of the vascular bed surrounding the vein and capillary areas, towards the active sprouting front (**Figure 1.1.8.A**). The size of the lesions was smaller compared to the lesions generated by *Pik3ca*^{H1047R/WT} and *Pik3ca*^{E545K/WT} expression. Although lesions were smaller, we measured a significant increase in IB4+ area in mutants compared to controls

(Figure 1.1.8.B). As for the other variants, recombination rates (GFP+/IB4+ area) were >80% in controls and mutants (Figure 1.1.8.C). The less pronounced lesions with *Pik3ca*^{E726K/WT} expression compared to the other variants can therefore not be attributed to less recombination. Here, there was no significant increase in GFP+/IB4+ area in mutants compared to controls, indicating that there is less or no clonal expansion of the recombined ECs. As a result, these data suggest that *Pik3ca*^{E726K/WT} expression results in an overgrown vascular bed, but lesions are milder and less frequent compared to *Pik3ca*^{H1047R/WT} or *Pik3ca*^{E545K/WT} expression. We also observed no competitive clonal expansion of ECs carrying the *Pik3ca*^{E726K/WT} variant.

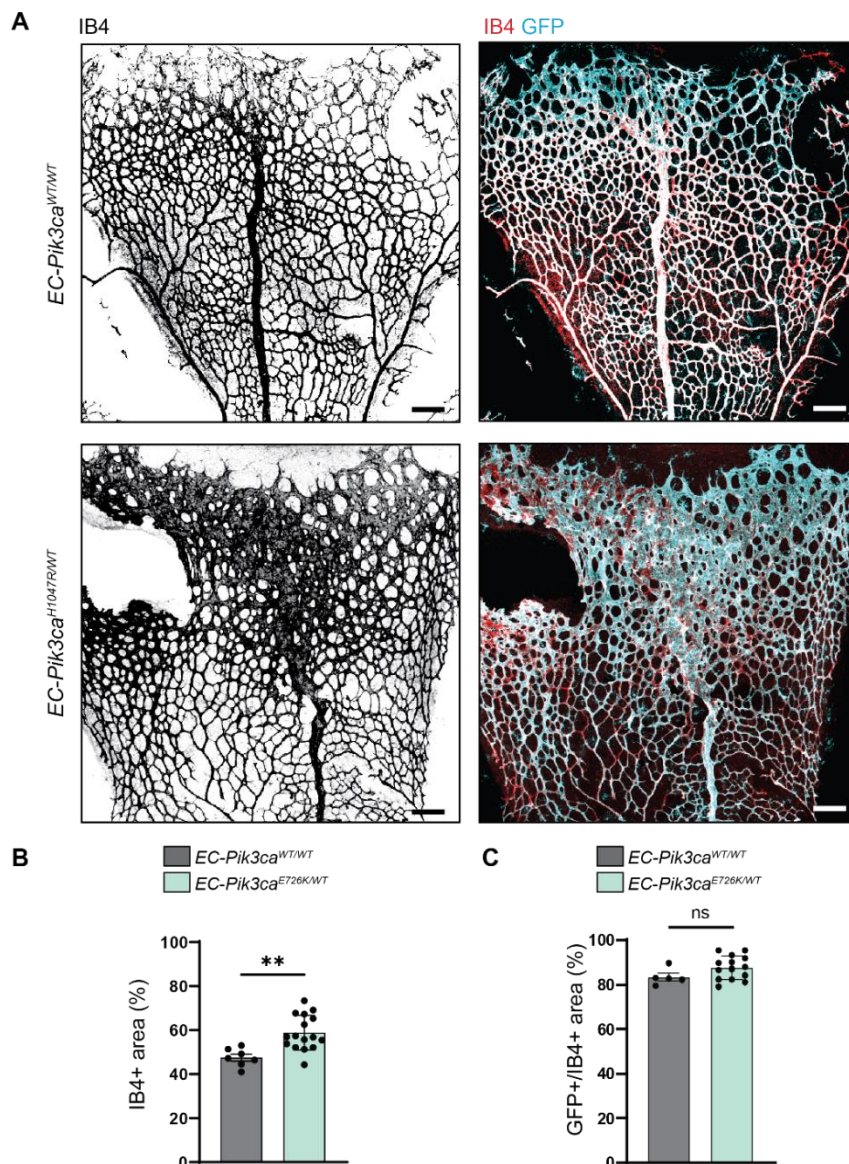


Figure 1.1.8. *Pik3ca*^{E726K}-driven vascular malformations in mouse retinas.

(A) Representative confocal images of retinas immunostained with anti-IB4 and anti-GFP. Scale bar = 100 μm . $n \geq 8$ retinas per genotype. (B) Quantification of IB4+ area per 250000 μm^2 area per petal. Statistical analysis was performed by parametric unpaired t-test. $**p < 0.01$ was considered statistically significant. $n \geq 8$ retinas per genotype. (C) Quantification of GFP+/IB4+ area per 250000 μm^2 area per petal. Statistical analysis was performed by parametric unpaired t-test. $n \geq 8$ retinas per genotype.

Although lesions with *Pik3ca*^{E726K/WT} expression are less frequent and milder compared to the other variants, we verified if this mild hyperplasia occurred because of increased numbers of ECs. We compared the EC number in P7 retinas between *Pik3ca*^{WT/WT}-expressing controls and *Pik3ca*^{E726K/WT}-expressing mutants after immunostaining with ERG (**Figure 1.1.9.A**). In the lesions, we observed a significant increase in EC number in mutants compared to controls (**Figure 1.1.9.B**). These data suggest that *Pik3ca*^{E726K/WT} expression causes local hyperplasia of the retina vasculature due to an increased number of ECs within the lesions compared to controls.

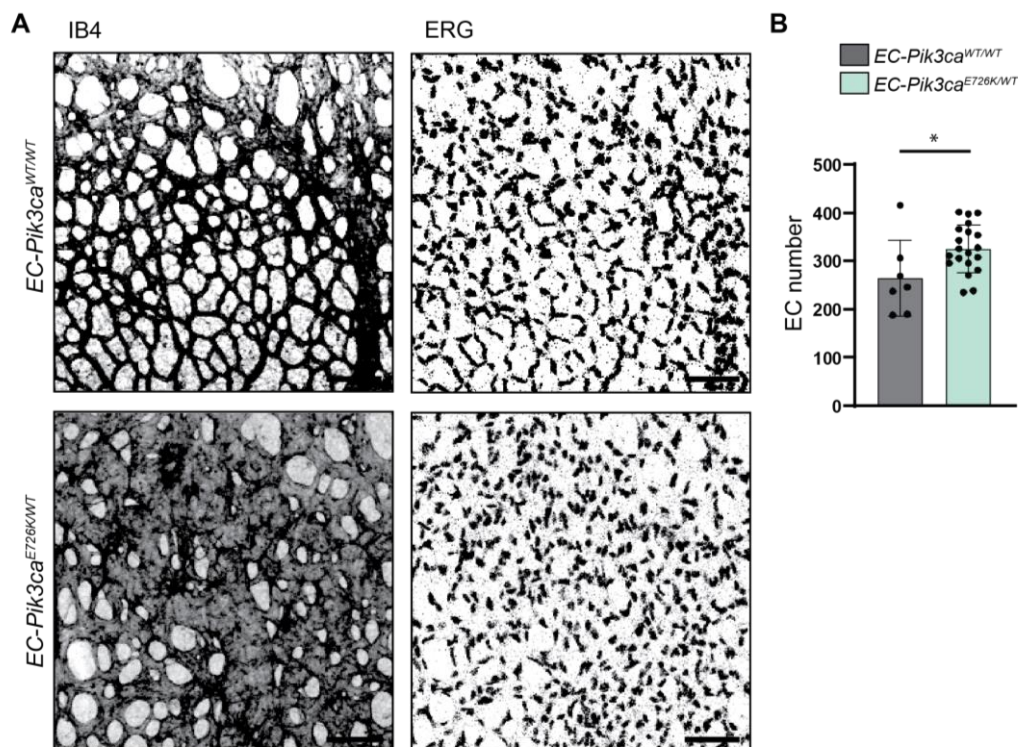


Figure 1.1.9. *Pik3ca*^{E726K}-driven vascular malformations with increased amounts of endothelial cells in mouse retinas.

(A) Representative confocal images of retinas immunostained with anti-IB4 and anti-ERG. Scale bar = 50 μm. n ≥ 8 retinas per genotype. (B) Quantification of ERG+ nuclei per 250000 μ² area per petal. Statistical analysis was performed by parametric unpaired t-test. *p < 0.05 was considered statistically significant. n ≥ 8 retinas per genotype.

1.2. Vascular malformations generated by the *PIK3CA* variants during vascular remodelling.

Here, we explored if *Pik3ca*^{E545K} was more likely to induce vascular malformations during the vascular remodelling process compared to the other variants. The remodelling phase is characterized by vascular pruning, mural cell maturation, vessel stabilization, and reduced angiogenic signals from the environment compared to the angiogenic phase (206, 273). Due to the different activating mechanisms between the variants, we

hypothesised that some variants might manifest a different phenotype during the remodelling phase. Specifically, *Pik3ca*^{E545K} has an activating mechanism independent of growth factor stimulation (46, 48). Vascular remodelling can be studied in the retina model by injecting 4-OHT at P15 and studying the fully matured retina at P21 (**Figure 1.2.1**).

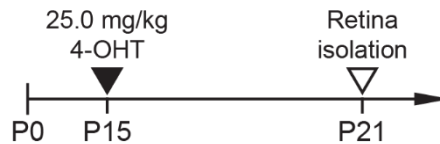


Figure 1.2.1. In vivo injection scheme to study overactivation of PIK3CA with *Pik3ca* mutant mouse models.

We induced recombination by intragastric injection of 25.0 mg/kg at postnatal day 15 (P15) and isolated the mouse retinas at P21.

We compared the occurrence of vascular malformations (general and focal) in the petals of the studied retinas (**Figure 1.2.2**). In EC-*Pik3ca*^{H1047R/WT} petals, we observed a general vascular malformation, characterized by massive hyperplasia, in 8% of cases. 27% of cases showcased a mild, focal malformation, and 65% had no observable phenotype compared to controls. In EC-*Pik3ca*^{E545K/WT} petals we noticed a general vascular malformation in 7% of cases, and smaller, focal vascular malformations in 7% of cases, while 86% of remained without vascular lesions. Then, we observed no vascular malformation in EC-*Pik3ca*^{E726K/WT}-expressing petals. This data suggests that expression of *Pik3ca*^{H1047R/WT}, *Pik3ca*^{E545K/WT}, or *Pik3ca*^{E545K/WT} generally does not cause vascular malformations during vascular remodelling. This indicates that the different mechanisms of activation are not causative for vascular malformations during the remodelling process where the amount of growth signals from the environment are decreased.

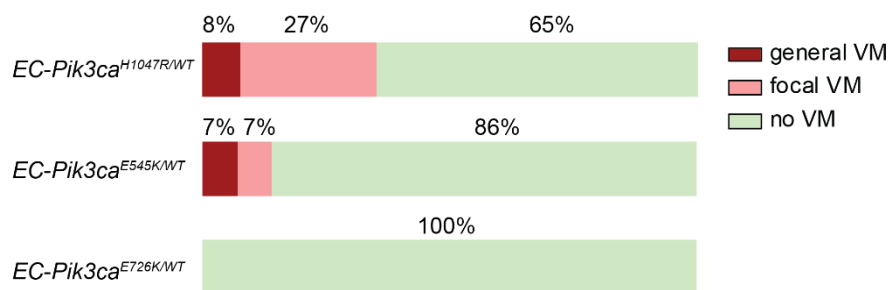


Figure 1.2.2. Occurrence of *Pik3ca*^{H1047R}, *Pik3ca*^{E545K}, and *Pik3ca*^{E726K}-driven vascular malformations during vascular remodelling.

Vascular malformations (VM) were counted in the petals of *Pik3ca*^{H1047R/WT}, *Pik3ca*^{E545K/WT}, and *Pik3ca*^{E726K/WT} mutant mice. Lesions were categorized depending on their size and expanse (general or focal). n ≥ 28 petals per genotype.

First, we studied the vasculature in P21 retinas with *Pik3ca*^{H1047R/WT} expression. We injected 25 mg/kg 4-OHT at P15, isolated the retina at P21, and immunostained for IB4 and GFP to measure vascular area and recombined endothelium. We used 4-OHT-injected *Pik3ca*^{WT/WT}-expressing littermates as controls. In most retinas, *Pik3ca*^{H1047R/WT} expression did not cause any apparent phenotype in the vasculature. Only some cases showed extensive hyperplasia of the vasculature (**Figure 1.2.3.A**). When quantifying the IB4+ area, we observed a significant increase in mutants compared to controls (**Figure 1.2.3.B**). Recombination rates (GFP+/IB4+ area) were measured to be >80% in controls and mutants and were not significantly changed in mutants compared to control (**Figure 1.2.3.C**). Together, these data show that *Pik3ca*^{H1047R/WT} expression does not typically generate a phenotype during vascular remodelling, and there is no clonal expansion of recombined ECs.

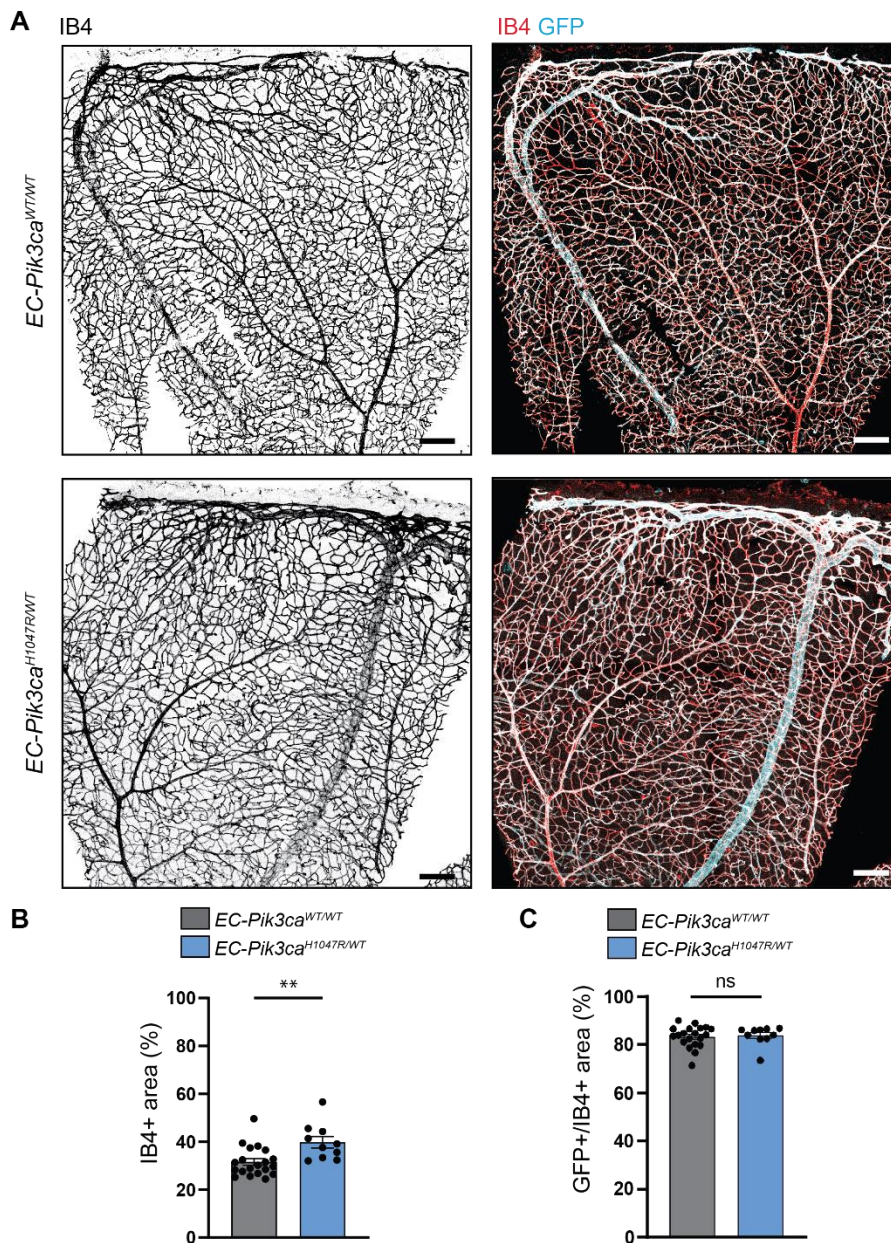


Figure 1.2.3. *Pik3ca^{H1047R}* expression during vascular remodeling in mouse retinas.

(A) Representative confocal images of retinas immunostained with anti-IB4 and anti-GFP. Scale bar = 150 μm . $n \geq 10$ retinas per genotype. (B) Quantification of IB4+ area per 250000 μm^2 area per petal. Statistical analysis was performed by parametric unpaired t-test. $**p < 0.01$ was considered statistically significant. $n \geq 10$ retinas per genotype. (C) Quantification of GFP+/IB4+ area per 250000 μm^2 area per petal. Statistical analysis was performed by parametric unpaired t-test. $n \geq 10$ retinas per genotype.

Then, we studied the impact of *Pik3ca^{E545K/WT}* expression in P21 retinas. We injected *Pdgfb-CreER^{T2}; Pik3ca^{E545K/WT}* mice with 25 mg/kg 4-OHT at P15 and isolated the retinas at P21, followed by immunostaining with IB4 and GFP. We used 4-OHT-injected *Pdgfb-CreER^{T2}; Pik3ca^{WT/WT}* littermates as controls. *Pik3ca^{E545K/WT}* expression did not cause any apparent phenotype in the vasculature of most retinas, only rare cases displayed large hyperplasia (Figure 1.2.4.A). Here, we measured no significantly enlarged

vascular area (IB4+ area) in mutants compared to controls (**Figure 1.2.4.B**). Recombination rates (GFP+/IB4+ area) were >80% for controls and mutants and were not significantly changed in mutants compared to controls (**Figure 1.2.4.C**). These data show that *Pik3ca*^{E545K/WT} expression does not typically generate a phenotype during vascular remodelling. This indicates that *Pik3ca*^{E545K/WT} expression is not more likely to cause malformations during vascular remodelling compared to other *Pik3ca* variants, even if the activating mechanism is independent of growth factors.

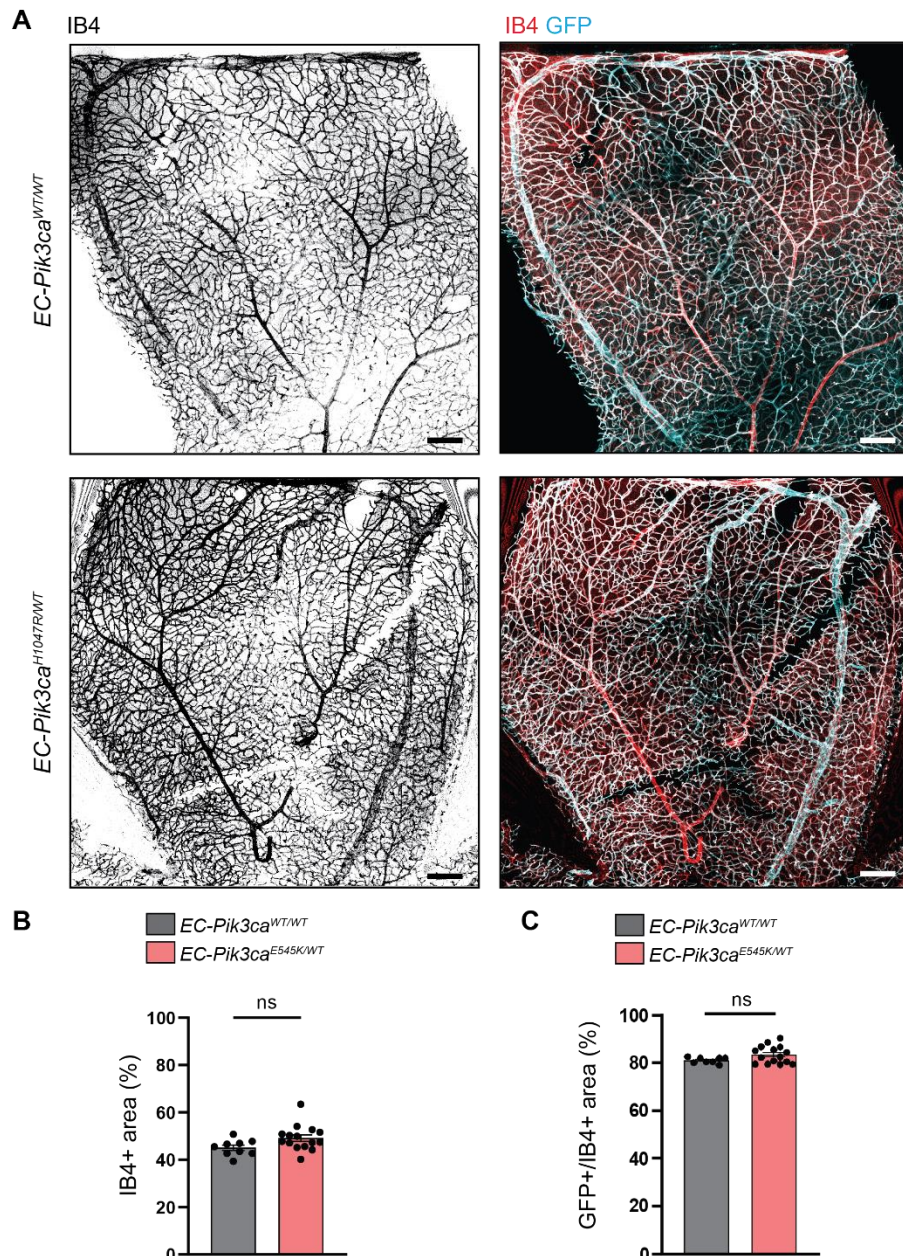


Figure 1.2.4. *Pik3ca*^{E545K} expression during vascular remodelling in mouse retinas.

(A) Representative confocal images of retinas immunostained with anti-IB4 and anti-GFP. Scale bar = 150 μ m. $n \geq 9$ retinas per genotype. (B) Quantification of IB4+ area per 250000 μ m² area per petal. Statistical analysis was performed by parametric unpaired t-test. ** $p < 0.01$ was considered statistically significant. $n \geq 9$ retinas per genotype. (C) Quantification of GFP+/IB4+ area per 250000 μ m² area per petal. Statistical analysis was performed by parametric unpaired t-test. $n \geq 9$ retinas per genotype.

Lastly, we studied *Pik3ca*^{E726K/WT} expression in P21 retinas. We injected *Pdgfb-CreER*^{T2}; *Pik3ca*^{E726K/WT} mice with 25 mg/kg 4-OHT at P15 and isolated the retinas at P7, followed by immunostaining with IB4 and GFP. We used 4-OHT-injected *Pdgfb-CreER*^{T2}; *Pik3ca*^{WT/WT} littermates as controls. *Pik3ca*^{E726K/WT} expression did not cause any apparent differences in the vasculature during the remodelling phase (**Figure 1.2.5.A**). IB4+ area quantification revealed no significant changes in vascular area in mutants compared to controls (**Figure 1.2.5.B**). GFP+/IB4+ area assessment displayed a recombination rate of >80% in controls and mutants, and there were no significant changes in mutants compared to controls (**Figure 1.2.5.C**). These data show that *Pik3ca*^{E726K/WT} expression does not contribute to the formation of any vascular phenotype during vascular remodelling. This differs from what we previously discovered with *Pik3ca*^{H1047R/WT} and *Pik3ca*^{E545K/WT} expression, where lesions could be observed in rare cases. Together, these data indicate that *Pik3ca*^{E545K/WT} expression is not more pathogenic than *Pik3ca*^{H1047R/WT} and *Pik3ca*^{E726K/WT} expression in the context of vascular remodelling when growth factors are scarce.

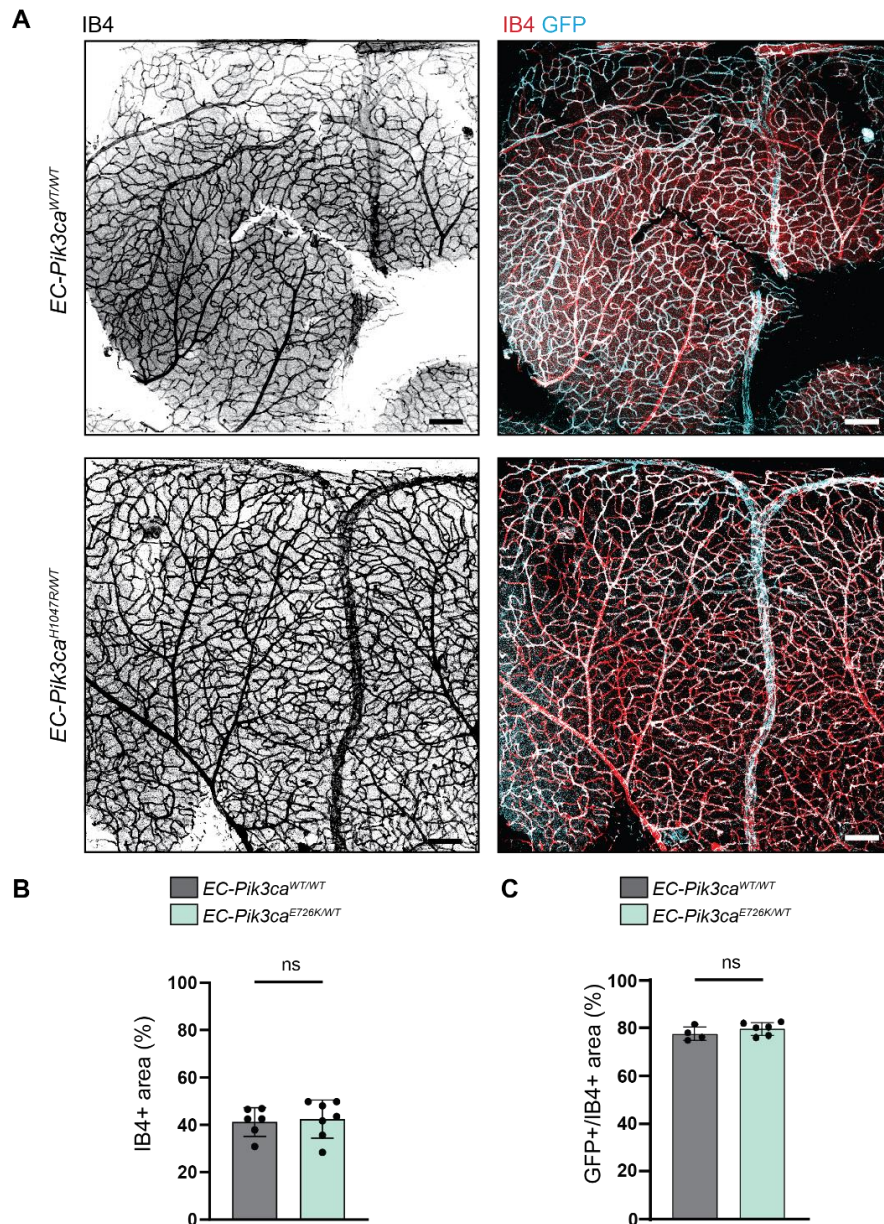


Figure 1.2.5. *Pik3ca*^{E726K} expression during vascular remodelling in mouse retinas.

(A) Representative confocal images of retinas immunostained with anti-IB4 and anti-GFP. Scale bar = 150 μm . $n \geq 9$ retinas per genotype. **(B)** Quantification of IB4+ area per 250000 μm^2 area per petal. Statistical analysis was performed by parametric unpaired t-test. $**p < 0.01$ was considered statistically significant. $n \geq 9$ retinas per genotype. **(C)** Quantification of GFP+/IB4+ area per 250000 μm^2 area per petal. Statistical analysis was performed by parametric unpaired t-test. $n \geq 9$ retinas per genotype.

1.3. Tolerability of *Pik3ca*^{E545K} expression during embryonic development.

Within the controlled context of the retina model, we established that EC-specific expression of *Pik3ca*^{H1047R/WT}, *Pik3ca*^{E545K/WT}, and *Pik3ca*^{E726K/WT} during angiogenesis leads to vascular malformations. In patients, activating *PIK3CA* mutations are typically acquired during the embryonic development, resulting into presence of vascular malformations at birth. Therefore, studying the effect of *Pik3ca* mutant expression during embryo development is crucial to understanding the pathologies generated by the

variants. The expression of *Pik3ca*^{H1047R/WT} during mouse embryogenesis and the resulting vascular phenotypes were already described in (71). They expressed *Pik3ca*^{H1047R/WT} ubiquitously and observed no survival past embryonic day 9.5. When they expressed *Pik3ca*^{H1047R/WT} in only the endothelial cells using the constitutive *Tie2*-Cre line, they observed complete embryonic lethality by E11.5.

We established that *Pik3ca*^{H1047R/WT} and *Pik3ca*^{E545K/WT} expression results in massive phenotypes in the vasculature. Given the distinct activating mechanisms of these variants, we examined if the *Pik3ca*^{E545K/WT} variant showcases the same lethality as previously described *Pik3ca*^{H1047R/WT} when expressed in ECs of the developing mouse embryo. We used the same pan-endothelial constitutive Cre line as in (271) by crossing the *Pik3ca*^{E545K/WT} mice with the *Tie2*-Cre mice. This line expresses the Cre recombinase under the endogenous *Tie2* promoter, which is expressed in the endothelial compartment and in hematopoietic stem cells very early during embryonic development, starting from day E7.5 onward (271). From this point forward, this cross will be referred to as *Tie2-Cre; Pik3ca*^{E545K/WT}.

First, we determined the precise timing of lethality during embryonic development. We began controlled matings between males and females, noting the presence of a vaginal plug as an indication of mating. Using this method, embryos were collected and analysed at different gestational stages, starting at E11.5. We analysed a total of 13 embryos at E11.5 and 34 embryos at E10.5 (Table 1.3.1). At E11.5, all *Tie2-Cre+; Pik3ca*^{E545K/WT} embryos were classified as reabsorbed and/or dead, chi-square analysis revealed significant deviation from the Mendelian ratios, indicating a loss of viability in these embryos when expressing *Pik3ca*^{E545K/WT}. At E10.5, chi-square analysis did not reveal a significant deviation from Mendelian ratios, however, a drop was observed in *Tie2-Cre+; Pik3ca*^{E545K/WT} viable embryos compared to Mendelian ratios. These data suggest that loss of viability in these embryos occurred around E10.5 and complete embryonic lethality by E11.5, similar to what *Hare et al.* discovered for *Tie2-Cre+; Pik3ca*^{H1047R/WT} (71).

Day	<i>Tie2-Cre+; Pik3ca</i> ^{E545K/WT}	<i>Tie2-Cre+; Pik3ca</i> ^{WT/WT}	<i>Tie2-Cre-; Pik3ca</i> ^{E545K/WT}	<i>Tie2-Cre-; Pik3ca</i> ^{WT/WT}	Number of embryos
E10.5	9%	21%	29%	41%	34
E11.5**	0%	62%	31%	7%	13

Table 1.3.1. Viability table of *Tie2-Cre; Pik3ca*^{E545K/WT} embryos.

Viable embryos from the cross *Tie2-Cre; Pik3ca*^{E545K/WT} with all allele combinations. Statistical analysis was performed with chi-square test. **p < 0.01 was considered statistically significant.

Hare *et al.* concluded that *Tie2-Cre+; Pik3ca^{H1047R/WT}* embryos collapsed at mid-gestation (i.e., E-10.5-E11.5) due to vascular defects. We reasoned that *Tie2-Cre+; Pik3ca^{E545K/WT}* embryos also underwent prominent defects in the development of blood vessels. Hence, we isolated *Tie2-Cre; Pik3ca^{E545K/WT}* embryos at E11.5 and immunostained for the vasculature with endomucin (EMCN) (**Figure 1.3.1**). We used *Tie2-Cre-; Pik3ca^{E545K/WT}* and *Tie2-Cre+; Pik3ca^{WT/WT}* as controls. The mutants were smaller in size, and showcased disorganized vasculature compared to controls. These data suggest that lethality at this stage is caused by severe disruption of vascular development.

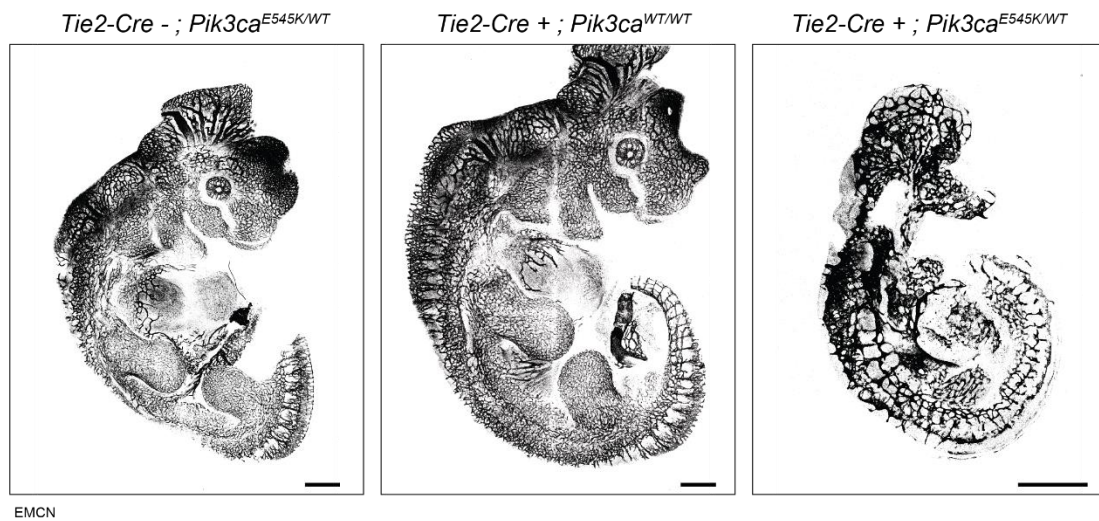


Figure 1.3.1. Embryos of *Tie2-Cre-; Pik3ca^{E545K/WT}*, *Tie2-Cre+; Pik3ca^{WT/WT}* and *Tie2-Cre+; Pik3ca^{E545K/WT}* at E11.5.

Representative embryo images immunostained with EMCN at stage E11.5 are shown. Scale bar = 500 μ m. Representative images for n = 2 litters.

Next, to study the effects of *Pik3ca^{E545K/WT}* expression at an earlier stage during development, we isolated *Tie2-Cre+; Pik3ca^{E545K/WT}* mutants and *Tie2-Cre-; Pik3ca^{E545K/WT}* and *Tie2-Cre+; Pik3ca^{WT/WT}* control embryos and examined the vasculature by staining for Emcn. At this stage, we observed little difference between mutants and controls. Stereomicroscopy images did reveal increased blood accumulation in some areas of the mutant embryo, such as the heart and brain (**Figure 1.3.2**). Confocal microscopy revealed no clear difference in embryo size or disorganized vasculature (**Figure 1.3.3**). Taken together, these data show that the vasculature of *Tie2-Cre; Pik3ca^{E545K/WT}* embryos developed normally until E10.5 and they remain viable up to this stage. However, at E11.5, *Tie2-Cre; Pik3ca^{E545K/WT}* embryos appeared smaller and had aberrant vessel development and were no longer viable. In *Tie2-Cre; Pik3ca^{H1047R/WT}* embryos, Hare *et al.* observed disorganized vessels in the brain and lack of vessels in the pharyngeal arch at E10.5, this phenotype is not entirely recapitulated in our *Tie2-*

Cre; Pik3ca^{E545K/WT} embryos, suggesting that *Tie2-Cre; Pik3ca^{H1047R/WT}* might generate more severe phenotypes in the vasculature of embryos during early developmental stages.

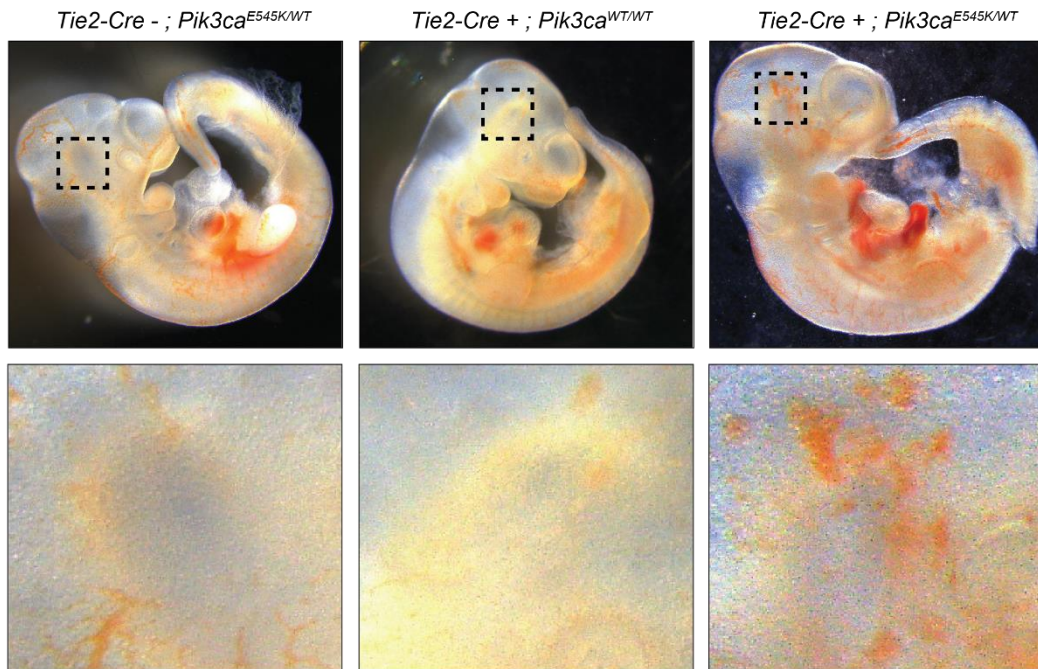


Figure 1.3.2. Stereoscopic images of embryos of *Tie2-Cre-; Pik3ca^{E545K/WT}*, *Tie2-Cre+; Pik3ca^{WT/WT}* and *Tie2-Cre+; Pik3ca^{E545K/WT}* at E10.5.
Representative stereomicroscopy images of E10.5 embryos. Upper panels show whole embryos. Lower panels show enlarged images from squares of upper panels.

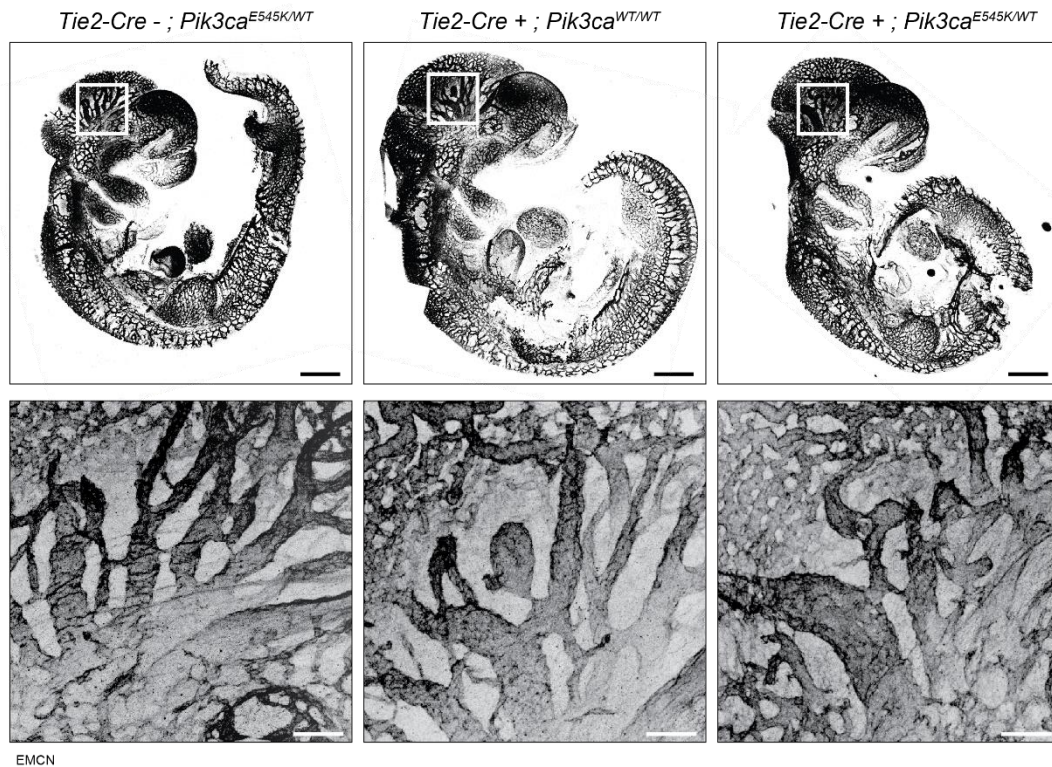


Figure 1.3.3. Confocal images of embryos of *Tie2-Cre-; Pik3ca^{E545K/WT}*, *Tie2-Cre+; Pik3ca^{WT/WT}* and *Tie2-Cre+; Pik3ca^{E545K/WT}* at E10.5.

Representative confocal microscopy images of E10.5 embryos stained for Emcn. Upper panels show whole embryos. Lower panels show enlarged images from squares of upper panels. Scale bar = 500 μ m. Representative images for n = 5 litters.

From our experiments in Objective I, we have gained critical insights into the effects of different *Pik3ca* variant expression on vascular development and pathology. First, we observed distinct phenotypes in the developing vasculature when we induced expression during angiogenesis. Namely, the expression of the oncogenic variants *Pik3ca^{H1047R/WT}* and *Pik3ca^{E545K/WT}* led to significant vascular hyperplasia, driven by increased EC numbers and expansion of the recombined clones. Increases in vessel area and EC number were also observed with *Pik3ca^{E726K/WT}* expression, but to a lesser extent. Therefore, we conclude this variant cannot generate the same strong vascular phenotypes as the other oncogenic hotspot variants. Secondly, *Pik3ca^{E545K/WT}* is known for its growth factor-independent activation mechanism (46, 48). However, when vascular phenotypes were examined in a mature vascular environment where growth factors are less abundant, no significant phenotypic differences were observed among the variants. This indicates that the activating mechanisms of the *Pik3ca* variants are less impactful in later stages of vascular development. Likely, vascular remodelling does not rely on PI3K α signalling, or other, unknown mechanisms influence PI3K α activity. We conclude that active angiogenesis is required for the formation of vascular malformations

caused by PI3K α overactivation. Lastly, the expression of the strong activator *Pik3ca*^{E545K/WT} in ECs of the developing mouse embryo resulted in embryonic lethality and vascular phenotypes comparable to those observed with *Pik3ca*^{H1047R/WT}, suggesting that both variants induce severe and similar disruptions during embryogenesis. These findings enhance our understanding of the capacity of the variants to generate a vascular malformation depending on the developmental stage and within the context of different transgenic mouse models.

II. Objective 2: Elucidating *PIK3CA* variant kinase activity and signalling differences in cultured endothelial cells.

2.1. Variant effect on PI3K α 's kinase activity.

The kinase activity of the mutant PI3K α H1047R and E545K proteins has already been studied (51, 275), revealing both hotspot mutations increase kinase activity and activate the PI3K α pathway through distinct mechanisms. However, the E726K mutation and its effect on the protein remains unknown. We wanted to use ADP glo kinase assays to study and directly compare the kinase activity of the 3 *PIK3CA* variants with the mutant PI3K α enzyme.

We evaluated the intrinsic change in kinase activity between wild-type (WT) PI3K α and the mutants H1047R, E545K, and E726K, by creating recombinant proteins for each of these variants. We transfected Sf9 insect cells with baculovirus containing the plasmids for each catalytic subunit (p110 α WT, H1047R, E545K, E726K) and co-transfected with the regulatory subunit p85 α . Protein was isolated and purified, and ADP Glo assays were performed to measure the enzyme velocity (nmol ADP generated per nmol enzyme per second), by mixing enzyme with 75 μ M of substrate (PIP2) and 100 μ M ATP.

First, we identified a concentration range where the enzymatic velocity remains within the linear phase for each variant enzyme. Here, the increase in product formation (ADP) remains proportional to time, and the enzymatic activity will be primarily determined by the rate of the reaction (velocity), not the enzyme concentration. We selected 4 concentrations for each variant ranging from 40 to 1.25 nM (**Figure 2.1.1.A**). We confirmed that the velocity remained similar within each concentration range for each variant. Based on these findings, optimal concentrations of 20 nM for WT and E726K, 10 nM for E545K, and 5 nM for H1047R were selected for the activity assays.

Then, we measured the velocity for each variant and compared it to the WT using previously determined enzyme concentrations (**Figure 2.1.1.B**). We observed an increase in basal kinase activity in H1047R compared to the WT. Also, the kinase activity of E545K showed an increased tendency compared to the WT. In contrast, the E726K variant showed no significant change.

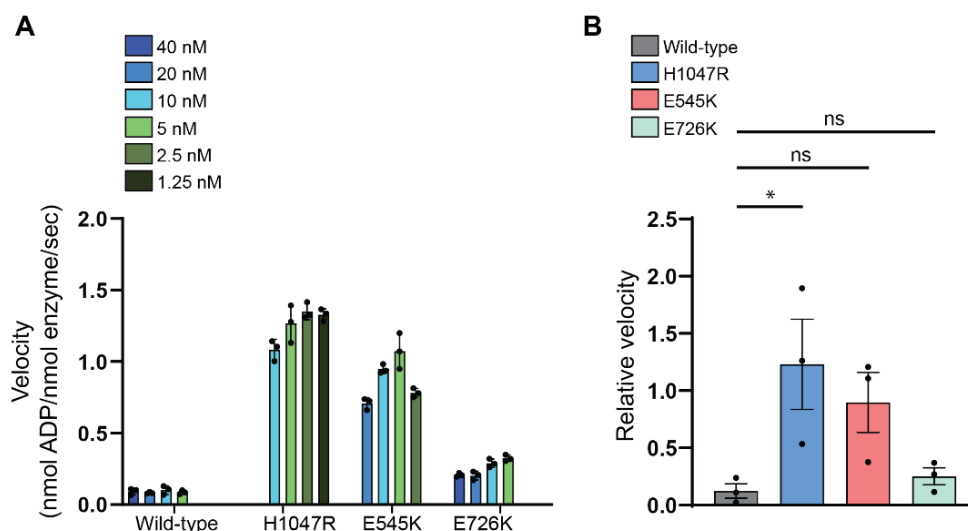


Figure 2.1.1. Determination of optimal enzyme concentration and comparison of enzyme activity for wild-type and mutant PI3K α in basal conditions.

(A) ADP Glo enzyme titration experiment to identify the appropriate enzyme concentration within the linear range. Various concentrations of WT and mutant (H1047R, E545K, E726K) PI3K α proteins ranging from 40 nM to 1.25 nM were tested. Datapoints represent mean values with s.e.m. for one assay. Graph is representative for n = 2. **(B)** Quantification of ADP glo activity assays comparing enzyme velocity between WT and mutant (H1047R, E545K, E726K) PI3K α proteins. Enzyme concentrations were 20 nM for WT and E726K, 10 nM for E545K, and 5 nM for H1047R. Data represented as fold change values relative to WT with s.e.m. Statistical analysis was performed by parametric one-way ANOVA. *p < 0.05 was considered statistically significant. n = 3 per variant.

Stimulation via RTKs plays an important role in the activation of the PI3K α complex. This stimulation is dependent on an interaction between p85 and phosphotyrosines (pY) on the receptors. With ADP Glo, we can administer 1 μ M of pY to the reaction mixture to imitate this activation stimulus. As for the basal condition, here too we first identified a concentration range where the enzymatic velocity remains within the linear phase for each enzyme. We selected 4 concentrations for each variant ranging from 8 to 0.25 nM (**Figure 2.1.2.A**). We confirmed that the velocity remained similar within each concentration range WT, E545K, and E726K. However, H1047R showed a decreased velocity with decreased enzyme concentration. Based on these findings, optimal concentration of 4 nM for WT and all variants was selected for the activity assays.

When we measured the velocity for each variant in the pY-stimulated conditions and compared it to the WT, we overall observed no significant changes (**Figure 2.1.2.B**). For

the H1047R mutation, this was surprising, since its activating mechanism has been reported to be dependent on p85-RTK interaction and similar experiments revealed a strong increase of H1047R kinase activity in the pY-stimulated condition (51, 275, 276). For E545K, it is described that the activating mechanism is RTK independent. Therefore, it is not surprising that the kinase activity is not changed. Lastly, it appears the E726K mutations has little effect on the kinase activity.

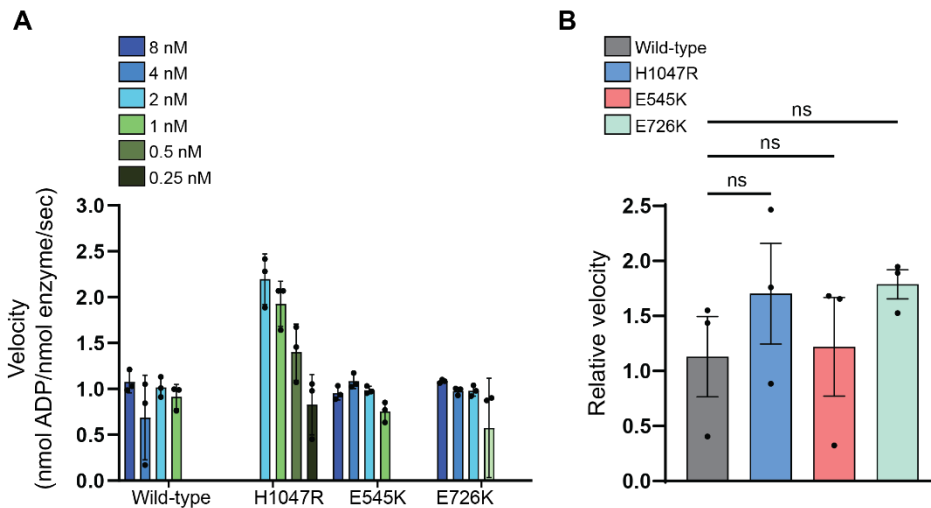


Figure 2.1.2. Determination of optimal enzyme concentration and comparison of enzyme activity for wild-type and mutant PI3K α in pY-stimulated conditions.

(A) ADP Glo enzyme titration experiment to identify the appropriate enzyme concentration within the linear range. Various concentrations of WT and mutant (H1047R, E545K, E726K) PI3K α proteins were tested. Datapoints represent mean values with s.e.m. for one assay. Graph is representative for $n = 2$. **(B)** Quantification of ADP glo activity assays comparing enzyme velocity between WT and mutant (H1047R, E545K, E726K) PI3K α proteins. Enzyme concentrations were 4 nM for WT, H1047R, E545K, and E726K. Data represented as fold change values relative to WT with s.e.m. Statistical analysis was performed by parametric one-way ANOVA. * $p < 0.05$ was considered statistically significant. $n = 3$ per variant.

2.2. Characterization of recombination between the different *Pik3ca* mutant constructs *in vitro*.

To study the effects of expressing the *PIK3CA* variants in cultured ECs, we used an *in vitro* model where we isolated heart ECs from the *Pdgfb-CreER^{T2}; Pik3ca^{Tg/WT}* mice (referred to as EC-*Pik3ca^{H1047R/WT}*, EC-*Pik3ca^{E545K/WT}*, and EC-*Pik3ca^{E726K/WT}*). We control activation of the *Pik3ca* mutation in these cultured ECs by inducing recombination by supplying 4-OHT in the medium.

The recombination of EC-*Pik3ca^{H1047R/WT}* was already confirmed in our laboratory *in vitro* with a treatment of 2 μ M 4-OHT for 6 hours (73). To assess if EC-*Pik3ca^{E545K/WT}* and EC-*Pik3ca^{E726K/WT}* recombined at similar rates, we treated them with 2 or 5 μ M 4-OHT for 6 or 24 hours and used ethanol-treated cells as controls. We wanted to verify

recombination by immunoblotting and measured p-AKT (S473) levels and p-S6 (S235/236) levels, downstream effectors of the PI3K α pathway. For both EC-*Pik3ca*^{E545K/WT} and EC-*Pik3ca*^{E726K/WT} we noticed elevated levels of p-AKT (S473) and p-S6 (S235/236), which confirmed the recombination in both variants (**Figure 2.2.1**). We already observed increased PI3K α signalling in both with 2 and 5 μ M 4-OHT after 6 hours. However, we used 2 μ M of 4-OHT during 24 hours in future experiments to allow more time to pass for recombination to occur and increase the amount of recombination, without inducing dose-related 4-OHT toxicity.

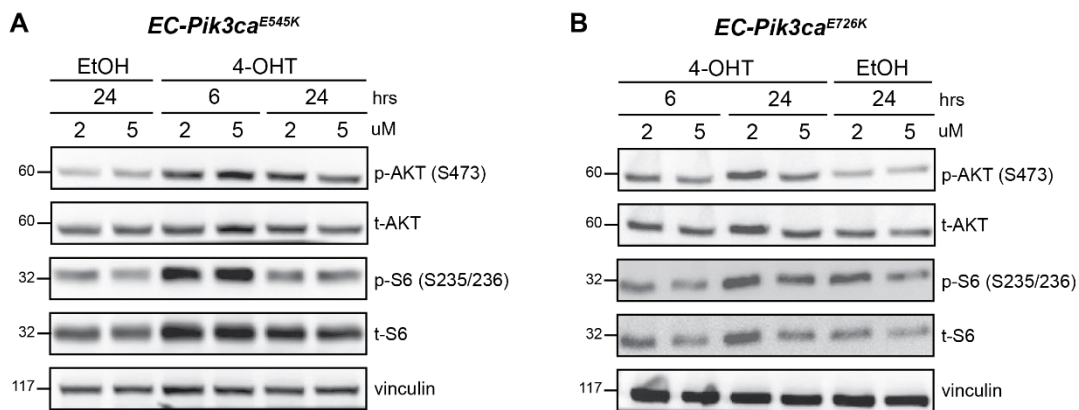


Figure 2.2.1. Determination of recombination in EC-*Pik3ca*^{E545K/WT} and EC-*Pik3ca*^{E726K/WT} with different treatments of 4-OHT.

(A) PI3K α signalling pathway assessment by immunoblotting of ethanol (etOH) and 4-OHT treated *Pik3ca*^{E545K/WT} mouse heart ECs. Cells were treated with etOH for 24 hours with 2 or 5 μ M, or with 4-OHT for 6 or 24 hours with 2 or 5 μ M. Immunoblot is representative for n = 2. (B) PI3K α signalling pathway assessment by immunoblotting of ethanol (etOH) and 4-OHT treated *Pik3ca*^{E726K/WT} mouse heart endothelial cells. Cells were treated with etOH for 24 hours with 2 or 5 μ M, or with 4-OHT for 6 or 24 hours with 2 or 5 μ M. Immunoblot is representative for n = 1.

Next, we validated that recombination took place in each variant line with the previously determined 4-OHT treatment regimen. We designed various primer pairs that can detect DNA from cultured ECs through PCR and which can differentiate between the WT or mutated sequences for each construct (**Figure 2.2.2**). We used 4-OHT-treated *Pdgfb*⁺; *Pik3ca*^{WT/WT} cells (WT) and etOH-treated *Pik3ca*^{Tg/WT} cells as controls for each variant. These were included to ensure the observed recombination were specific to the *Pik3ca* mutations and not a result of 4-OHT treatment itself, and so we could verify the recombination from etOH-treated to 4-OHT treated ECs. For EC-*Pik3ca*^{H1047R/WT} and EC-*Pik3ca*^{E726K/WT}, we detected the excision of the mini-gene in the 2 μ M 4-OHT-treated cells. The primer pairs were located to include the whole mini-gene, intron sequence differences between the mini-gene and the endogenous sequence allow to differentiate

them when recombination takes place. In EC-*Pik3ca*^{E545K/WT}, we detected the excision of the LoxP-STOP-LoxP sequence in the 4-OHT-treated cells.

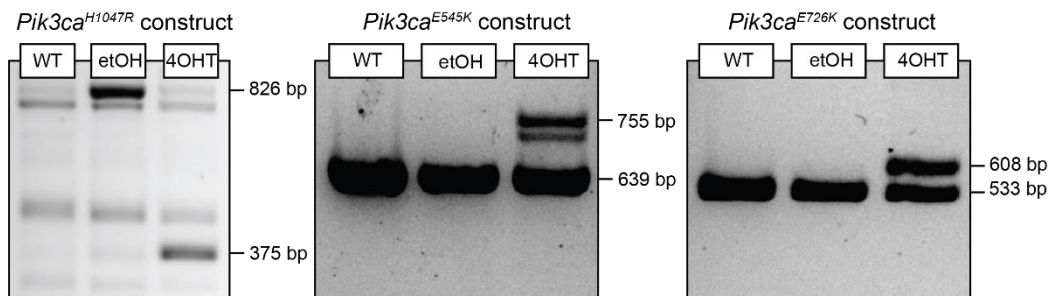


Figure 2.2.2. Validation of the recombination in the three heterozygous EC-*Pik3ca*^{H1047R/WT}, EC-*Pik3ca*^{E545K/WT}, and EC-*Pik3ca*^{E726K/WT}.

For each variant, WT cells and etOH-treated cells from mice heterozygous with the mutant constructs are used as controls. In EC-*Pik3ca*^{H1047R/WT}, the mutant construct without recombination is detected at 826 bp. When the mini-gene gets excised, the band appears at 375 bp. In EC-*Pik3ca*^{E545K/WT}, when the LoxP-STOP-LoxP is excised, the band appears at 755 bp. The WT sequence is visible at 639 bp. In EC-*Pik3ca*^{E726K/WT}, the mutant construct without recombination is detected at 2442 bp (not visible on gel). When the mini-gene gets excised, the band appears at 608 bp. The WT sequence is visible at 533 bp.

2.3 Signalling differences between the *PIK3CA* variants *in vitro*.

Upon determining the appropriate 4-OHT regimen *in vitro*, we wanted to compare the degree of PI3K α -AKT activation between the 3 variants in ECs. To clearly appreciate signalling differences and to mimic activating cues, we used 3 different conditions: full medium, starvation, and iFBS stimulation. EC-*Pik3ca*^{H1047R/WT}, EC-*Pik3ca*^{E545K/WT}, and EC-*Pik3ca*^{E726K/WT} were treated with 2 μ M etOH (controls) or 4-OHT for 24 hours. With immunoblotting, p-AKT (S473) was used as a readout of PI3K α pathway activation (**Figure 2.3.1.A**). Cells were left to expand for 24 hours after recombination in full medium, then either kept in full medium, or starved overnight. iFBS stimulation was done by treating cells in medium supplemented with 20% iFBS for 15 mins after overnight starvation.

In the full medium condition, both EC-*Pik3ca*^{H1047R/WT} and EC-*Pik3ca*^{E545K/WT} showed significantly increased p-AKT (S473) levels, whereas EC-*Pik3ca*^{E726K/WT} did not, although a tendency to increase p-AKT (S473) levels was observed (**Figure 2.3.1.B**). In the starvation condition, only EC-*Pik3ca*^{H1047R/WT} showed significantly increased p-AKT (S473) levels, whereas EC-*Pik3ca*^{E545K/WT} and EC-*Pik3ca*^{E726K/WT} did not, although a tendency to increase p-AKT (S473) levels was observed (**Figure 2.3.1.C**). In iFBS-stimulated conditions, no variants showed significant changes in p-AKT (S473) levels (**Figure 2.3.1.D**). These data suggest that expression of *Pik3ca*^{H1047R/WT}, and to a lesser

extent *Pik3ca*^{E545K/WT}, impact the PI3K α -AKT pathway in endothelial cells, while *Pik3ca*^{E726K/WT} does not.

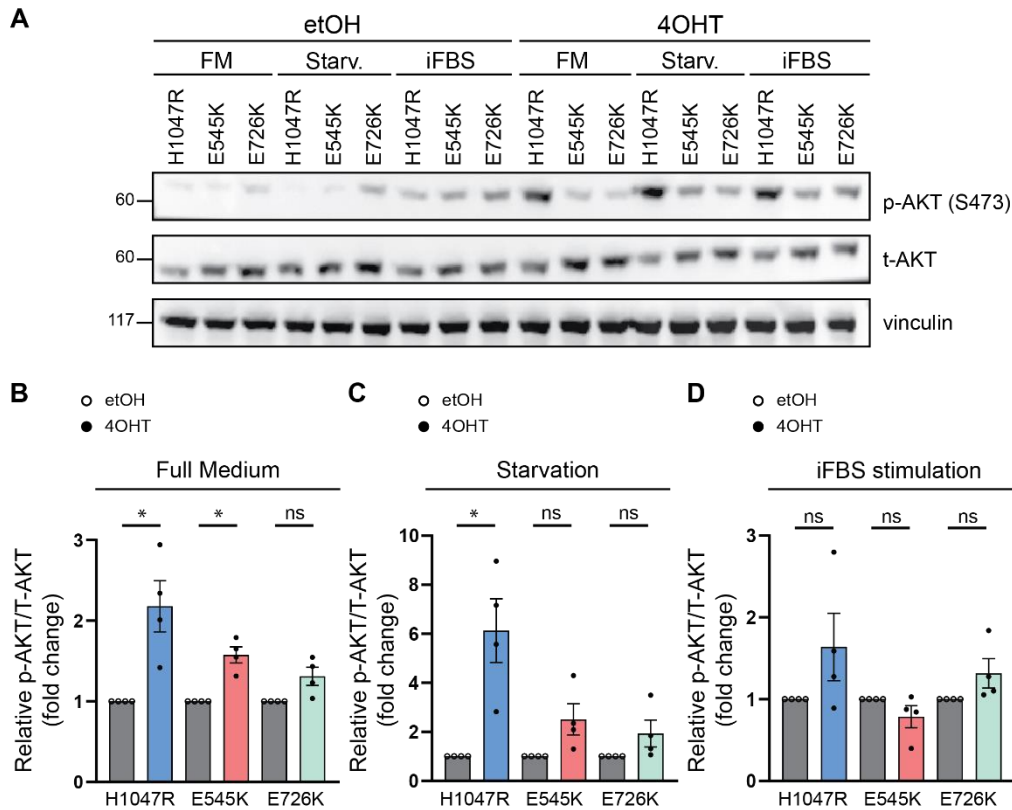


Figure 2.3.1. Comparison of PI3K α pathway activation between EC-*Pik3ca*^{H1047R/WT}, EC-*Pik3ca*^{E545K/WT}, and EC-*Pik3ca*^{E726K/WT} *in vitro*.

(A) Immunoblot of etOH-treated control and 4-OHT-treated mutant EC-*Pik3ca*^{H1047R/WT}, EC-*Pik3ca*^{E545K/WT}, and EC-*Pik3ca*^{E726K/WT} mouse heart ECs. Immunoblot is representative for n = 4. FM = full medium, starv. = starvation, iFBS is iFBS stimulation. (B) Quantification of relative p-AKT/t-AKT expression in full medium conditions. Data represented as fold change values relative to etOH-treated controls with s.e.m. Statistical analysis was performed by parametric paired t-test. *p < 0.05 was considered statistically significant. n = 4 per genotype. (C) Quantification of relative p-AKT/t-AKT expression in starved conditions. Data represented as fold change values relative to etOH-treated controls with s.e.m. Statistical analysis was performed by parametric paired t-test. *p < 0.05 was considered statistically significant. n = 4 per genotype. (D) Quantification of relative p-AKT/t-AKT expression in iFBS-stimulated conditions. Data represented as fold change values relative to etOH-treated controls with s.e.m. Statistical analysis was performed by parametric paired t-test. *p < 0.05 was considered statistically significant. n = 4 per genotype.

To better understand how *PIK3CA* variant expression affects signalling in ECs, we also examined the impact of expressing *Pik3ca*^{H1047R/WT}, *Pik3ca*^{E545K/WT}, and *Pik3ca*^{E726K/WT} on other intracellular pathways. The MAPK plays an important role in EC function; therefore, we analysed p-ERK (T202/204) levels in EC-*Pik3ca*^{H1047R/WT}, EC-*Pik3ca*^{E545K/WT}, and EC-*Pik3ca*^{E726K/WT} and compared them to etOH-treated controls. Cells were treated with 2 μ M etOH (controls) or 4-OHT for 24 hours and left to expand for 24 hours after recombination in full medium, then either kept in full medium, or starved overnight. iFBS

stimulation was done by treating cells in medium supplemented with 20% iFBS for 15 mins after overnight starvation.

In the full medium condition, EC-*Pik3ca*^{H1047R/WT} showed significantly decreased p-ERK (T202/204) levels, whereas EC-*Pik3ca*^{E545K/WT} and EC-*Pik3ca*^{E726K/WT} did not, although a tendency to decrease p-ERK (T202/204) levels was observed (**Figure 2.3.2.B**). In the starvation condition, only EC-*Pik3ca*^{E545K/WT} showed significantly decreased p-ERK (T202/204) levels, whereas EC-*Pik3ca*^{H1047R/WT} and EC-*Pik3ca*^{E726K/WT} did not, although a tendency to decrease p-ERK (T202/204) levels was observed (**Figure 2.3.2.C**). In iFBS-stimulated conditions, no variants showed significant changes in p-ERK (T202/204) levels (**Figure 2.3.2.D**). These data suggest that expression of the strong PI3K α -AKT activators *Pik3ca*^{H1047R/WT} and *Pik3ca*^{E545K/WT} can negatively impact the MAPK pathway in endothelial cells, while weak PI3K α -AKT activation by *Pik3ca*^{E726K/WT} expression does not.

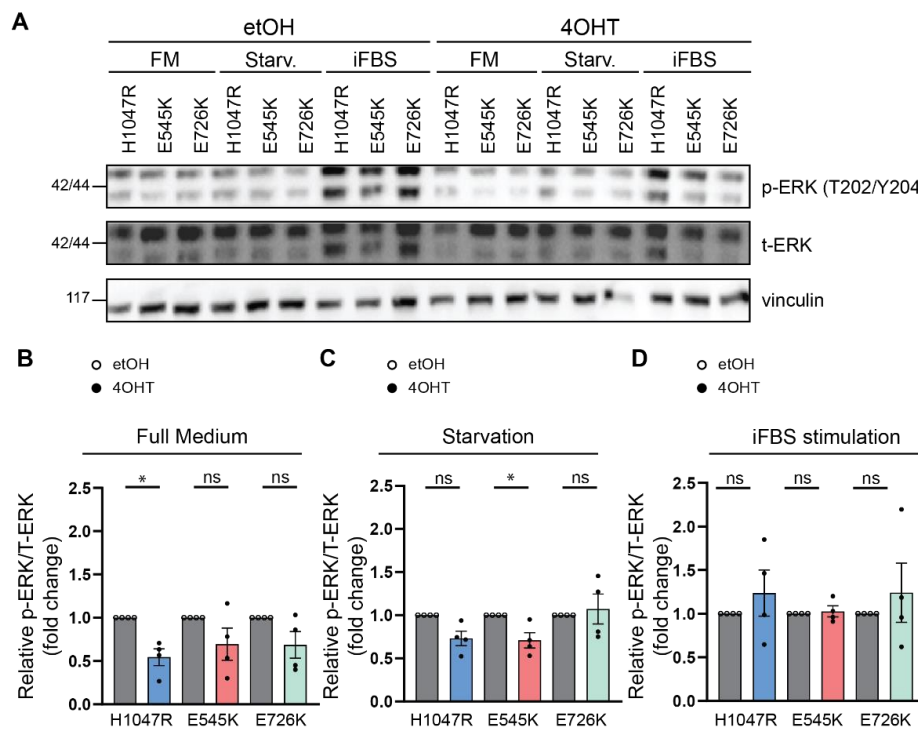


Figure 2.3.2. Comparison of MAPK pathway activation between EC-*Pik3ca*^{H1047R/WT}, EC-*Pik3ca*^{E545K/WT}, and EC-*Pik3ca*^{E726K/WT} *in vitro*.

(A) Immunoblot of etOH-treated control and 4-OHT-treated mutant EC-*Pik3ca*^{H1047R/WT}, EC-*Pik3ca*^{E545K/WT}, and EC-*Pik3ca*^{E726K/WT} mouse heart ECs. Immunoblot is representative for n = 4. FM = full medium, starv. = starvation, iFBS is iFBS stimulation. (B) Quantification of relative p-ERK/t-ERK expression in full medium conditions. Data represented as fold change values relative to etOH-treated controls with s.e.m. Statistical analysis was performed by parametric paired t-test. *p < 0.05 was considered statistically significant. n = 4 per genotype. (C) Quantification of relative p-ERK/t-ERK expression in starved conditions. Data represented as fold change values relative to etOH-treated controls with s.e.m. Statistical analysis was performed by parametric paired t-test. *p < 0.05 was considered statistically significant. n = 4 per genotype. (D) Quantification of relative p-ERK/t-ERK expression in iFBS-stimulated conditions. Data represented as fold change values relative to etOH-treated controls with s.e.m. Statistical analysis was performed by parametric paired t-test. *p < 0.05 was considered statistically significant. n = 4 per genotype.

PI3K α signaling regulates the expression of key endothelial cell (EC) genes, such as *Ang2* and *Cxcr4*, which are rapidly downregulated upon activation, while *EphB4* and *Itga9* are upregulated in these conditions (73). To investigate whether the extent of these transcriptional changes depends on the specific *Pik3ca* variant or its intrinsic signaling strength, we examined gene expression in heart ECs expressing *Pik3ca*^{H1047R/WT}, *Pik3ca*^{E545K/WT}, and *Pik3ca*^{E726K/WT}. We used 2 timepoints after induction of recombination to allow more time for the activation of the transcriptional programmes and to measure the kinetic changes in RNA expression of the target genes. We treated heart ECs with 2 μ M of 4-OHT for 24 hours and used etOH-treated cells as a control for each variant. Then, we either froze the cells directly after 4-OHT treatment, or left the cells to expand for another 48 hours in full medium (72 hours timepoint). RNA extraction was followed by cDNA synthesis and qPCR analysis, where the RNA levels of *Ang2*, *Cxcr4*, *EphB4*, and *Itga9* were measured.

At 24 hours, *Ang2* and *Cxcr4* expression both showed a decreasing trend in *EC-Pik3ca*^{H1047R/WT}, with *Cxcr4* significantly reduced. By 72 hours, *Ang2* expression was significantly decreased, while *Cxcr4* remained consistently downregulated. In contrast, *EC-Pik3ca*^{E545K/WT} and *EC-Pik3ca*^{E726K/WT} displayed no significant changes in *Ang2* or *Cxcr4* expression at 24 hours, although both showed a decreasing trend at 72 hours (**Figures 2.3.3.A** and **2.3.3.C**). For *EphB4*, no changes were observed in *EC-Pik3ca*^{H1047R/WT} at 24 hours, but expression significantly increased by 72 hours. However, *EC-Pik3ca*^{E545K/WT} and *EC-Pik3ca*^{E726K/WT} exhibited no changes at either time point (**Figure 2.3.3.B**). Meanwhile, *Itga9* expression remained largely unchanged across all conditions, except for a slight increasing trend observed in *EC-Pik3ca*^{H1047R/WT} at 72 hours (**Figure 2.3.3.D**). Together, these findings show that *EC-Pik3ca*^{H1047R/WT} consistently exerts a strong influence on the transcriptional regulation of the 4 target genes. Particularly, *EC-Pik3ca*^{H1047R/WT} reduces *Ang2* and *Cxcr4* while upregulating *EphB4*, compared to *EC-Pik3ca*^{E545K/WT} and *EC-Pik3ca*^{E726K/WT}. This is likely related to the degree in which these variants activate the PI3K α pathway, where *EC-Pik3ca*^{H1047R/WT} is stronger compared to *EC-Pik3ca*^{E545K/WT} and *EC-Pik3ca*^{E726K/WT}.

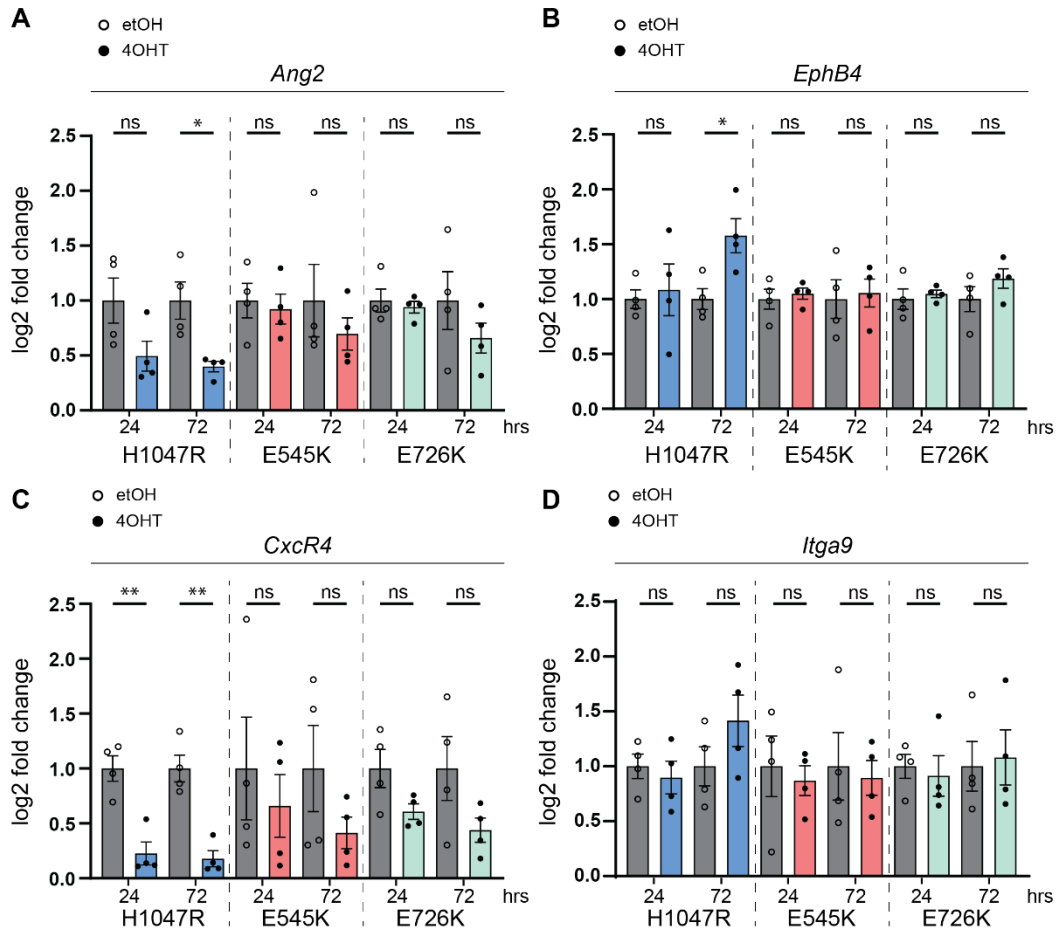


Figure 2.3.3. Impact of EC-*Pik3ca*^{H1047R/WT}, EC-*Pik3ca*^{E545K/WT}, and EC-*Pik3ca*^{E726K/WT} on transcription of *Ang2*, *EphB4*, *Cxcr4*, and *Itga9*.

(A) Comparison of *Ang2* gene expression in 24 or 72 hours expanded heart ECs from EC-*Pik3ca*^{H1047R/WT}, EC-*Pik3ca*^{E545K/WT}, and EC-*Pik3ca*^{E726K/WT} by quantitative PCR. Gene expression was normalized to the *MI32* housekeeping gene. Data represented as log₂ fold change values relative to etOH-treated controls with s.e.m. Statistical analysis was performed by parametric unpaired t-test. *p < 0.05 was considered statistically significant. n = 4 per genotype. **(B)** Comparison of *EphB4* gene expression in 24 or 72 hours expanded heart ECs from EC-*Pik3ca*^{H1047R/WT}, EC-*Pik3ca*^{E545K/WT}, and EC-*Pik3ca*^{E726K/WT} by quantitative PCR. Gene expression was normalized to the *MI32* housekeeping gene. Data represented as log₂ fold change values relative to etOH-treated controls with s.e.m. Statistical analysis was performed by parametric unpaired t-test. *p < 0.05 was considered statistically significant. n = 4 per genotype. **(C)** Comparison of *Cxcr4* gene expression in 24 or 72 hours expanded heart ECs from EC-*Pik3ca*^{H1047R/WT}, EC-*Pik3ca*^{E545K/WT}, and EC-*Pik3ca*^{E726K/WT} by quantitative PCR. Gene expression was normalized to the *MI32* housekeeping gene. Data represented as log₂ fold change values relative to etOH-treated controls with s.e.m. Statistical analysis was performed by parametric unpaired t-test. *p < 0.05 and **p < 0.01 was considered statistically significant. n = 4 per genotype. **(D)** Comparison of *Itga9* gene expression in 24 or 72 hours expanded heart ECs from EC-*Pik3ca*^{H1047R/WT}, EC-*Pik3ca*^{E545K/WT}, and EC-*Pik3ca*^{E726K/WT} by quantitative PCR. Gene expression was normalized to the *MI32* housekeeping gene. Data represented as log₂ fold change values relative to etOH-treated controls with s.e.m. Statistical analysis was performed by parametric unpaired t-test. *p < 0.05 was considered statistically significant. n = 4 per genotype.

Now we have studied the effects of expressing *Pik3ca*^{H1047R/WT}, *Pik3ca*^{E545K/WT}, and *Pik3ca*^{E726K/WT} on intracellular signalling in mouse heart ECs. However, signalling cues from the environment are crucial to the function of PI3K α . Therefore, we wanted to explore how the signalling changes caused by expression of *Pik3ca* variants would be

influenced by VEGFC and EGF stimulation, 2 important growth factors for ECs. Since EC-*Pik3ca*^{E726K/W} did not cause strong malformations (Objective 1) and did not strongly activate PI3K α -AKT signalling, we decided to only explore the two strong activators EC-*Pik3ca*^{H1047R/WT} and EC-*Pik3ca*^{E545K/WT}.

To optimize our signalling data, we changed our approach by using 4-OHT-treated *Pdgfb+*; *Pik3ca*^{WT/WT} mouse heart ECs (referred to as EC-*Pik3ca*^{WT/WT}) as controls for 4-OHT-treated EC-*Pik3ca*^{H1047R/WT} and EC-*Pik3ca*^{E545K/WT}. After the 2 μ M 4-OHT treatment of 24 hours, cells were starved overnight and subsequently stimulated with 75 ng/mL VEGFC or 75 ng/mL EGF for 10 mins. Starved cells and 20% iFBS-treated cells were used as internal controls for each *Pik3ca* variant. With immunoblotting, p-AKT (T308) and p-ERK (T202/204) levels were measured as readouts for PI3K α -AKT and MAPK signalling, respectively (**Figure 2.3.4.** and **Figure 2.3.5.**).

To evaluate PI3K α -AKT pathway activation, we compared p-AKT (T308) levels between the two mutant variants and the control across different conditions (starved, iFBS, VEGFC, and EGF stimulation). No significant changes in p-AKT (T308) levels were observed in any condition. However, EC-*Pik3ca*^{H1047R/WT} consistently showed a tendency toward increased p-AKT (T308) levels under all conditions, whereas EC-*Pik3ca*^{E545K/WT} displayed this tendency only under EGF-stimulated conditions (**Figure 2.3.4.B**). Then, we compared differences in p-AKT (T308) levels across the conditions within each cell line. In EC-*Pik3ca*^{WT/WT} controls, a slight tendency for increased p-AKT (T308) levels was observed under iFBS stimulation, but no such tendencies were evident under VEGFC or EGF stimulation. In EC-*Pik3ca*^{H1047R/WT}, p-AKT (T308) levels remained unchanged across all conditions. By contrast, EC-*Pik3ca*^{E545K/WT} showed a tendency for increased p-AKT (T308) levels under both iFBS and EGF stimulation, but not under VEGFC stimulation (**Figure 2.3.4.C**).

Together, these findings suggest that PI3K α -AKT signalling is mildly enhanced in EC-*Pik3ca*^{H1047R/WT} across all conditions, indicating a baseline activation independent of growth factor stimulation. In EC-*Pik3ca*^{E545K/WT}, PI3K α -AKT signalling enhancement is more context-dependent, with a tendency to activate primarily under EGF and iFBS stimulation.

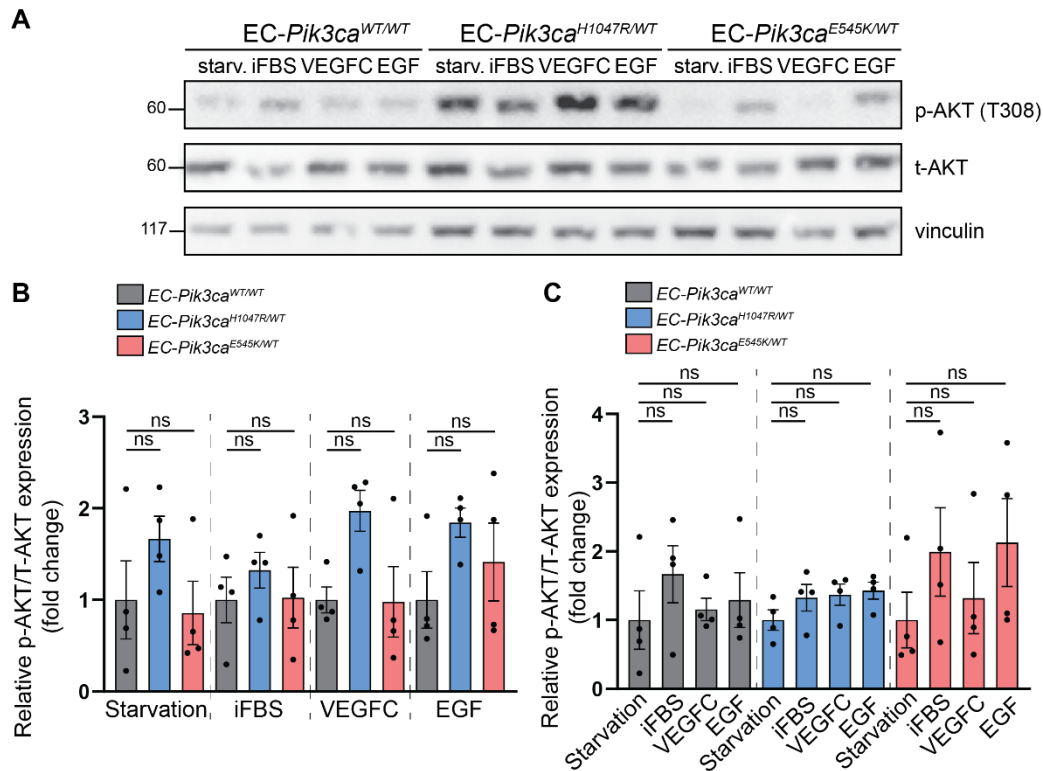


Figure 2.3.4. Regulation of PI3K α -AKT pathway activation in EC-*Pik3ca*^{H1047R/WT} and EC-*Pik3ca*^{E545K/WT} in VEGFC and EGF-stimulated conditions *in vitro*.

(A) Immunoblot of 4-OHT-treated control EC-*Pik3ca*^{WT/WT} and mutant EC-*Pik3ca*^{H1047R/WT} and EC-*Pik3ca*^{E545K/WT} mouse heart ECs. Immunoblot is representative for n = 4. starv. = starvation, iFBS is iFBS stimulation. (B) Quantification of relative p-AKT/t-AKT expression in the 4 conditions. Data represented as fold change values relative to EC-*Pik3ca*^{WT/WT} controls with s.e.m. Statistical analysis was performed by parametric one-way ANOVA. n = 4 per genotype. (C) Quantification of relative p-AKT/t-AKT expression in the 3 variants for each condition. Data represented as fold change values relative to each *Pik3ca* variant's starvation condition with s.e.m. Statistical analysis was performed by parametric one-way ANOVA. n = 4 per genotype.

To assess MAPK pathway activation, we compared p-ERK (T202/204) levels between the mutant and the control under different conditions (starved, iFBS, VEGFC, and EGF stimulation). No significant changes in p-ERK (T202/204) levels were observed across any condition. However, in the starved condition, both EC-*Pik3ca*^{H1047R/WT} and EC-*Pik3ca*^{E545K/WT} exhibited a tendency for reduced p-ERK (T202/204) levels compared to the control (**Figure 2.3.5.B**). Next, we compared p-ERK (T202/204) levels across different conditions within each cell line (**Figure 2.3.5.C**). In EC-*Pik3ca*^{WT/WT} controls, a tendency for reduced p-ERK (T202/204) levels was observed under VEGFC stimulation, while no notable changes were seen with iFBS or EGF stimulation compared to starvation. In EC-*Pik3ca*^{H1047R/WT}, p-ERK (T202/204) levels significantly increased under EGF stimulation and showed a tendency to increase with iFBS stimulation, but no changes were observed under VEGFC stimulation compared to starvation. Similarly, in

EC-Pik3ca^{E545K/WT}, significant increases in p-ERK (T202/204) levels were observed under both iFBS and EGF stimulation, with no changes under VEGFC stimulation.

Together, these findings suggest that in the starved condition, both *EC-Pik3ca*^{H1047R/WT} and *EC-Pik3ca*^{E545K/WT} exhibit a trend toward decreased MAPK signalling compared to the control. However, MAPK pathway activation is significantly enhanced in response to iFBS and EGF stimulation in both variants compared to starvation, whereas VEGFC stimulation does not result into a similar response.

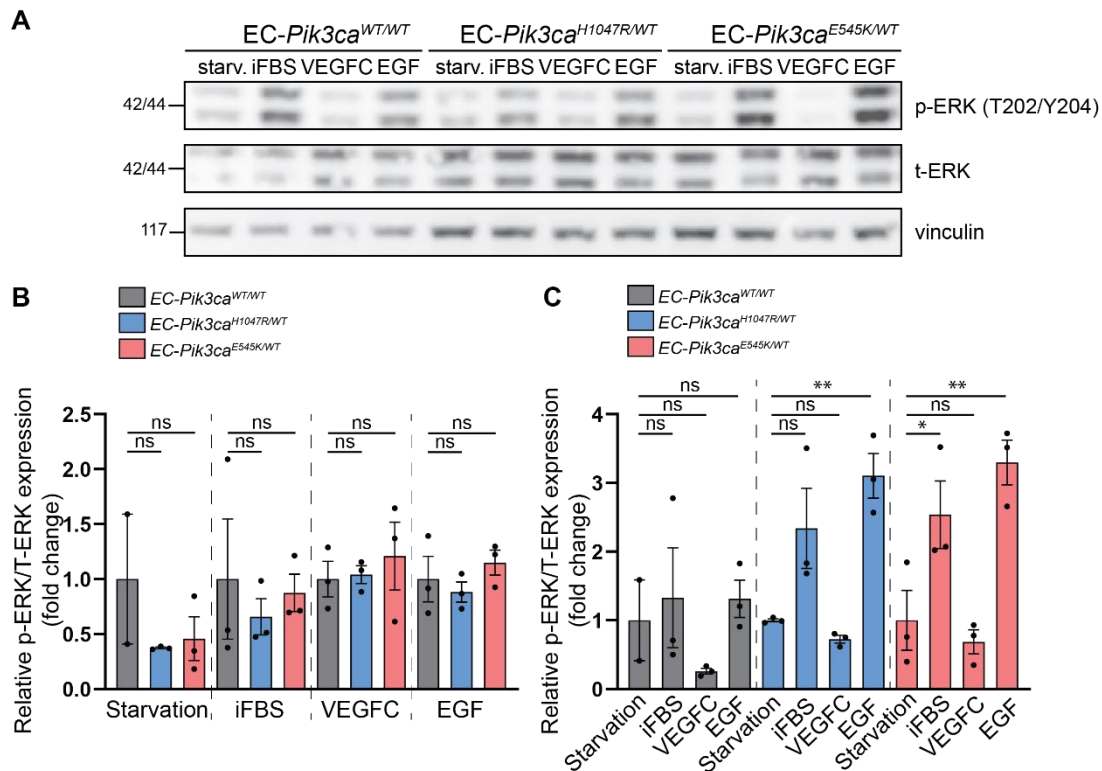


Figure 2.3.5. Regulation of MAPK pathway activation in *EC-Pik3ca*^{H1047R/WT} and *EC-Pik3ca*^{E545K/WT} in VEGFC and EGF-stimulated conditions *in vitro*.

(A) Immunoblot of 4-OHT-treated control *EC-Pik3ca*^{WT/WT} and mutant *EC-Pik3ca*^{H1047R/WT} and *EC-Pik3ca*^{E545K/WT} mouse heart ECs. Immunoblot is representative for n = 4. starv. = starvation, iFBS is iFBS stimulation (D) Quantification of relative p-ERK/t-ERK expression in the 4 conditions. Data represented as fold change values relative to *EC-Pik3ca*^{WT/WT} controls with s.e.m. Statistical analysis was performed by parametric one-way ANOVA. n = 3 per genotype, and n = 2 for starved *EC-Pik3ca*^{WT/WT} controls. (E) Quantification of relative p-ERK/t-ERK expression in the 3 variants for each condition. Data represented as fold change values relative to each *Pik3ca* variant's starvation condition with s.e.m. Statistical analysis was performed by parametric one-way ANOVA. *p < 0.05 and **p < 0.01 was considered statistically significant. n = 3 per genotype, and n = 2 for starved *EC-Pik3ca*^{WT/WT} controls.

It appeared that *Pik3ca*^{H1047R/WT} and *Pik3ca*^{E545K/WT} can respond differently to upstream VEGFC and EGF stimulation. We hypothesized that expression of the variants could sensitize the ECs to these stimuli by upregulation of the receptors of VEGFC and EGF, namely *Vegfr1*, *Vegfr2*, *Vegfr3*, and *Egfr*. Therefore, we examined the RNA levels of

these receptors with qPCR in starved and EGF-stimulated cells in 4-OHT-treated EC-*Pik3ca*^{H1047R/WT} and EC-*Pik3ca*^{E545K/WT} and compared them with 4-OHT-treated EC-*Pik3ca*^{WT/WT}. After the 2 µM 4-OHT treatment of 24 hours, cells were starved for 6 hours and subsequently stimulated with 75 ng/mL EGF for 10 mins (**Figure 2.3.6**).

Vegfr1, a negative regulator of VEGF signalling, exhibited no changes in expression across all conditions, remaining unchanged in both EC-*Pik3ca*^{H1047R/WT} and EC-*Pik3ca*^{E545K/WT} compared to EC-*Pik3ca*^{WT/WT} in both starved and EGF-stimulated conditions (**Figure 2.3.6.A**). In contrast, *Vegfr2* and *Vegfr3* expression showed clear differences between the variants. In EC-*Pik3ca*^{H1047R/WT}, *Vegfr2* expression was significantly upregulated in both starved and EGF-stimulated conditions. However, in EC-*Pik3ca*^{E545K/WT}, only a tendency to increase *Vegfr2* expression was observed in both conditions (**Figure 2.3.6.B**). Similarly, *Vegfr3* expression was significantly upregulated in EC-*Pik3ca*^{H1047R/WT} under starved conditions and showed a tendency to increase in the EGF-stimulated condition. In EC-*Pik3ca*^{E545K/WT}, *Vegfr3* expression demonstrated only a slight tendency to increase under both conditions (**Figure 2.3.6.C**). Then, *Egfr* expression displayed a distinct pattern compared to the VEGF receptors. In EC-*Pik3ca*^{H1047R/WT}, *Egfr* levels were unchanged in the starved condition but showed a slight tendency to decrease in the EGF-stimulated condition. In contrast, EC-*Pik3ca*^{E545K/WT} exhibited a tendency to upregulate *Egfr* expression in both the starved and EGF-stimulated conditions (**Figure 2.3.6.D**).

Together, these findings highlight notable differences between the 2 variants: EC-*Pik3ca*^{H1047R/WT} upregulates *Vegfr2* and *Vegfr3* expression in both starved and EGF-stimulated conditions, while EC-*Pik3ca*^{E545K/WT} shows only mild increases for these genes. Conversely, EC-*Pik3ca*^{E545K/WT} appears to uniquely upregulate *Egfr* expression under both starved and EGF-stimulated conditions, whereas EC-*Pik3ca*^{H1047R/WT} displayed no changes in starved conditions, and downregulation of *Egfr* in EGF-stimulated conditions.

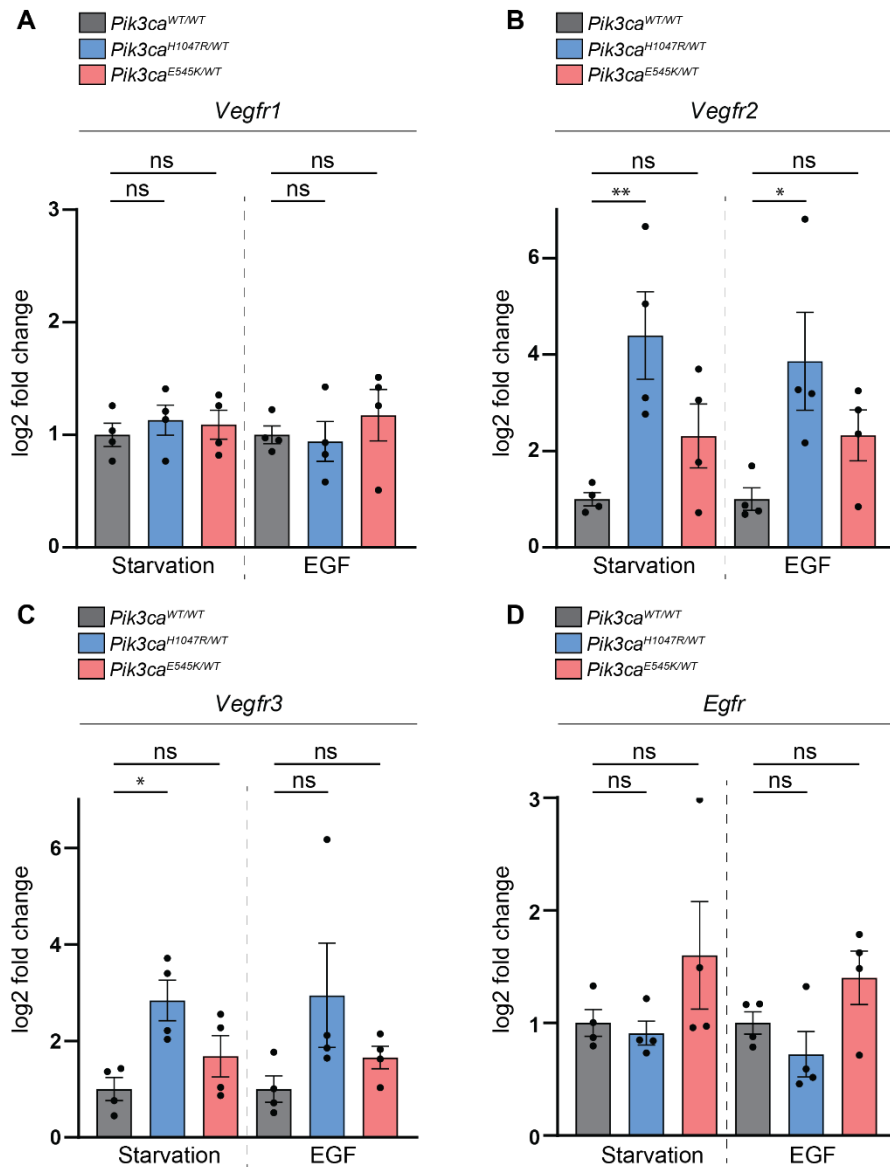


Figure 2.3.6. Impact of EC- $Pik3ca^{H1047R/WT}$ and EC- $Pik3ca^{E545K/WT}$ on transcription of *Vegfr1*, *Vegfr2*, *Vegfr3*, and *Egfr* expression in starved and EGF-stimulated conditions.

(A) Comparison of *Vegfr1* gene expression in control EC- $Pik3ca^{H1047R/WT}$ and mutant EC- $Pik3ca^{H1047R/WT}$ and EC- $Pik3ca^{E545K/WT}$ mouse heart ECs by quantitative PCR. Gene expression was normalized to the *MI32* housekeeping gene. Data represented as log₂ fold change values relative to EC- $Pik3ca^{WT/WT}$ with s.e.m. Statistical analysis was performed by parametric one-way ANOVA. n = 4 per genotype. (B) Comparison of *Vegfr2* gene expression in control EC- $Pik3ca^{H1047R/WT}$ and mutant EC- $Pik3ca^{H1047R/WT}$ and EC- $Pik3ca^{E545K/WT}$ mouse heart ECs by quantitative PCR. Gene expression was normalized to the *MI32* housekeeping gene. Data represented as log₂ fold change values relative to EC- $Pik3ca^{WT/WT}$ with s.e.m. Statistical analysis was performed by parametric one-way ANOVA. *p < 0.05 and **p < 0.01 was considered statistically significant. n = 4 per genotype. (C) Comparison of *Vegfr3* gene expression in control EC- $Pik3ca^{H1047R/WT}$ and mutant EC- $Pik3ca^{H1047R/WT}$ and EC- $Pik3ca^{E545K/WT}$ mouse heart ECs by quantitative PCR. Gene expression was normalized to the *MI32* housekeeping gene. Data represented as log₂ fold change values relative to EC- $Pik3ca^{WT/WT}$ with s.e.m. Statistical analysis was performed by parametric one-way ANOVA. *p < 0.05 was considered statistically significant. n = 4 per genotype. (D) Comparison of *Egfr* gene expression in control EC- $Pik3ca^{H1047R/WT}$ and mutant EC- $Pik3ca^{H1047R/WT}$ and EC- $Pik3ca^{E545K/WT}$ mouse heart ECs by quantitative PCR. Gene expression was normalized to the *MI32* housekeeping gene. Data represented as log₂ fold change values relative to EC- $Pik3ca^{WT/WT}$ with s.e.m. Statistical analysis was performed by parametric one-way ANOVA. n = 4 per genotype.

2.4 Cellular processes affected by *PIK3CA* variants *in vitro*.

Next, we wanted to examine the effects of the strong activating *PIK3CA* mutations on cellular processes such as growth, proliferation, and migration. These processes are important for EC function and therefore influential in the formation of vascular malformations. First, to study the effects of expressing *Pik3ca*^{H1047R/WT} and *Pik3ca*^{E545K/WT} on EC growth and proliferation, we performed a IncuCyte assay on 4-OHT-treated control EC-*Pik3ca*^{WT/WT} and mutant EC-*Pik3ca*^{H1047R/WT} and EC-*Pik3ca*^{E545K/WT} in normal growth conditions where the confluency was measured for 96 hours (**Figure 2.4.1**). When we examined the confluency curves, no significant changes between the mutants and controls were observed for the first 48 hours (**Figure 2.4.1.A**). Interestingly, EC-*Pik3ca*^{H1047R/WT} grows more confluent from 48 hours onward. Growth medium was not refreshed during the experiment, so with time, nutrients deplete, and waste accumulates in the wells. When we compare the confluency at the end of the 96 hours between the variants and controls, we noticed no significant changes, yet EC-*Pik3ca*^{H1047R/WT} showed a tendency for increased confluency (**Figure 2.4.1.B**). To explore if there are growth differences before and after the 48 hours, we studied the slopes of the confluency curves within the timeframes of 0 to 48 hours, and 48 to 96 hours (**Figure 2.4.1.C**). From 0 to 48 hours, there are no significant differences between the slopes of the variants compared to control. After 48 hours, EC-*Pik3ca*^{H1047R/WT} shows a tendency to increase the slope, while EC-*Pik3ca*^{E545K/WT} does not compared to controls. These data suggest that expressing *Pik3ca*^{H1047R/WT} and *Pik3ca*^{E545K/WT} in ECs does not affect the cell growth or proliferation in normal growing conditions compared to *Pik3ca*^{WT/WT} controls. However, when nutrients are depleted, *Pik3ca*^{H1047R/WT} showcased a steeper growth curve.

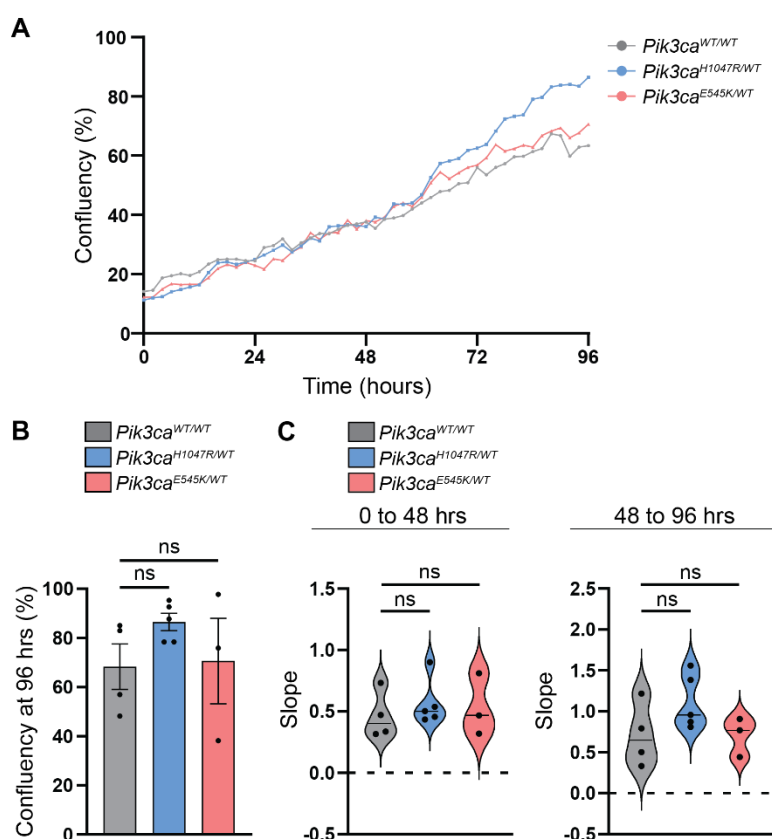


Figure 2.4.1. Impact of EC-*Pik3ca*^{H1047R/WT} and EC-*Pik3ca*^{E545K/WT} on confluency in normal growth conditions *in vitro*.

(A) EC-*Pik3ca*^{H1047R/WT}, EC-*Pik3ca*^{E545K/WT}, and EC-*Pik3ca*^{WT/WT} were plated at similar cell densities and left to grow for 96 hours, with images being taken every 2 hours. Data represents mean confluency % values in the well. $n \geq 3$ per genotype. (B) Comparison of confluency at 96 hours. Data represents mean confluency % values in the well with s.e.m. Statistical analysis was performed by parametric one-way ANOVA. $n \geq 3$ per genotype. (C) Linear regression analysis to compare the slope of the curves in (A). We analysed the slopes between 0 to 48 hours and from 48 to 96 hours. Data represents mean slope values. Statistical analysis was performed by parametric one-way ANOVA. $n \geq 3$ per genotype.

To study more in detail the growth behaviour of EC-*Pik3ca*^{H1047R/WT} and EC-*Pik3ca*^{E545K/WT} in medium-depleted conditions, we repeated the experiment by changing to starvation conditions 20 hours after plating (Figure 2.4.2). First, we compared the confluency at the timepoint before changing to starvation conditions. Although there is no significant difference, EC-*Pik3ca*^{H1047R/WT} showed a non-significant tendency to increase, while EC-*Pik3ca*^{E545K/WT} did not (Figure 2.4.2.B). When we compared the confluency at the final endpoint of 96 hours, we observed that EC-*Pik3ca*^{H1047R/WT} showed a significant increase, while EC-*Pik3ca*^{E545K/WT} showed a non-significant tendency to increase. Then, we compared the slopes of the confluency curves before the change to starvation conditions. Here, EC-*Pik3ca*^{H1047R/WT} showed a non-significant tendency to increase, while EC-*Pik3ca*^{E545K/WT} did not (Figure 2.4.2.C). When we looked at the slopes from the start of starvation onward, we observed that EC-*Pik3ca*^{H1047R/WT} showed a significant increase,

while EC-*Pik3ca*^{E545K/WT} showed a non-significant tendency to increase. Together, these data indicate that *PIK3CA* mutant expressing ECs withstand starvation conditions better than controls.

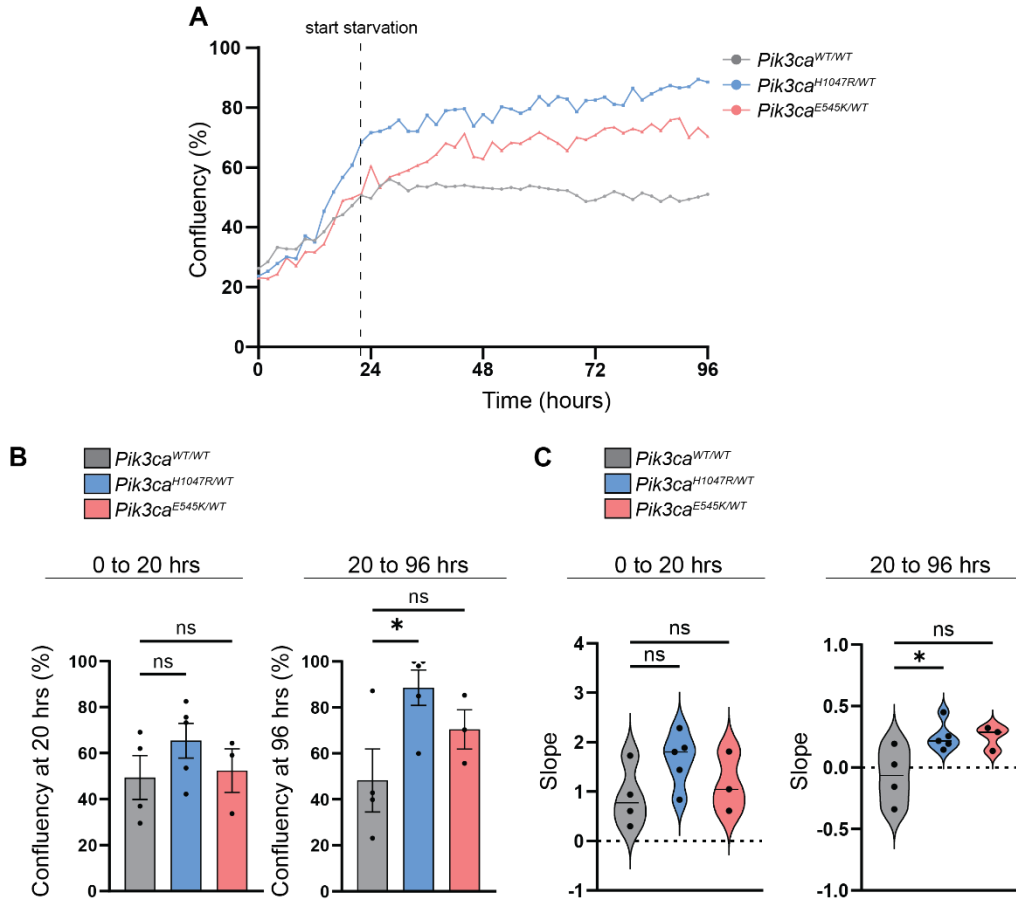


Figure 2.4.2. Impact of EC-*Pik3ca*^{H1047R/WT} and EC-*Pik3ca*^{E545K/WT} on confluency in starvation conditions *in vitro*.

(A) EC-*Pik3ca*^{H1047R/WT}, EC-*Pik3ca*^{E545K/WT}, and EC-*Pik3ca*^{WT/WT} were plated at similar cell densities and left to grow for 20 hours before changing to starvation medium, with images being taken every 2 hours. Data represents mean confluency % values in the well. $n \geq 3$ per genotype. (B) Comparison of confluency at 20 and 96 hours. Data represents mean confluency % values in the well with s.e.m. Statistical analysis was performed by parametric one-way ANOVA. * $p < 0.05$ was considered statistically significant. $n \geq 3$ per genotype. (C) Linear regression analysis to compare the slope of the curves in (A). We analysed the slopes between 0 to 20 hours and from 20 to 96 hours. Data represents mean slope values. Statistical analysis was performed by parametric one-way ANOVA. * $p < 0.05$ was considered statistically significant. $n \geq 3$ per genotype.

We wanted to study more specifically the impact of the *Pik3ca* mutations on proliferation. We did so by comparing the actively proliferating cells between etOH and 4-OHT-treated EC-*Pik3ca*^{H1047R/WT} and EC-*Pik3ca*^{E545K/WT} by EdU staining in normal growth conditions (Figure 2.4.3). Neither variant showcased a significant increase in proliferation compared to their etOH-treated control, though non-significant tendencies can be observed for both variants.

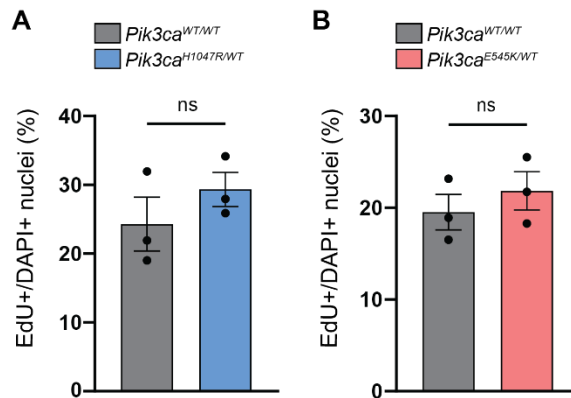


Figure 2.4.3. Impact of EC-*Pik3ca*^{H1047R/WT} and EC-*Pik3ca*^{E545K/WT} on proliferation in normal growth conditions *in vitro*.

(A) etOH and 4-OHT-treated EC-*Pik3ca*^{H1047R/WT} were plated at similar cell densities and used for the EdU-incorporation assay. Data represents mean EdU+/DAPI+ % values in the well. Statistical analysis was performed by parametric unpaired t-test. n = 3 per genotype. (B) etOH and 4-OHT-treated EC-*Pik3ca*^{E545K/WT} were plated at similar cell densities and used for the EdU-incorporation assay. Data represents mean EdU+/DAPI+ % values in the well. Statistical analysis was performed by parametric unpaired t-test. n = 3 per genotype.

Cell migration is another cellular process that could be relevant in the formation of vascular malformations. We studied the effect of EC-*Pik3ca*^{H1047R/WT} and EC-*Pik3ca*^{E545K/WT} expression on migration via scratch wound assays in normal growing conditions and compared them to 4-OHT-treated EC-*Pik3ca*^{WT/WT} controls (Figure 2.4.4). In normal growing conditions, we observed no differences in wound closure at the end point of the assay between EC-*Pik3ca*^{H1047R/WT} and EC-*Pik3ca*^{E545K/WT} with the control EC-*Pik3ca*^{WT/WT} (Figure 2.4.4.A). Full wound closure was reached around 50 hours. When we compared the wound healing throughout the experiment, we noticed no differences (Figure 2.4.4.B and C). These data suggest *Pik3ca*^{H1047R/WT} and EC-*Pik3ca*^{E545K/WT} expression do not affect migration in ECs in normal growth conditions.

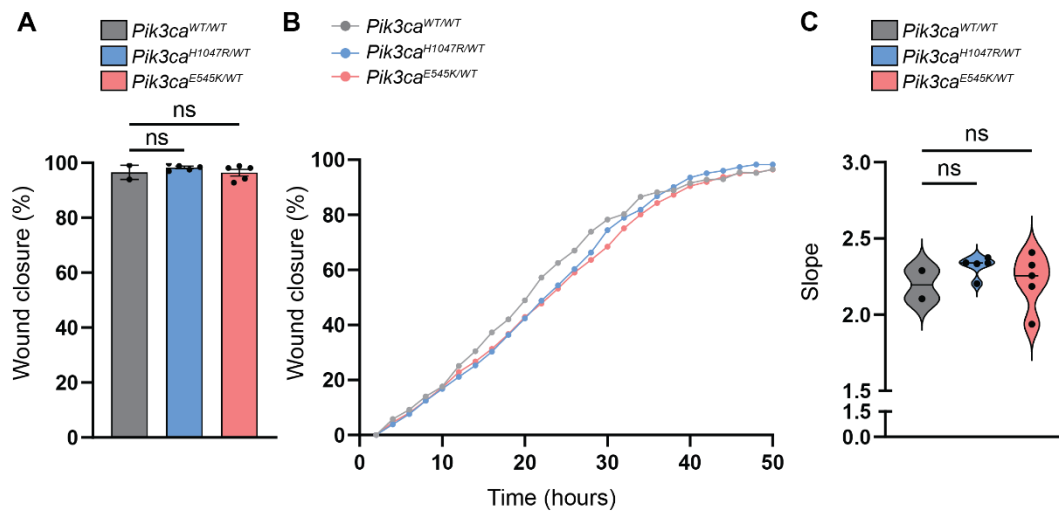


Figure 2.4.4. Impact of EC-*Pik3ca*^{H1047R/WT} and EC-*Pik3ca*^{E545K/WT} on migration in normal growth conditions *in vitro*.

EC-*Pik3ca*^{H1047R/WT}, EC-*Pik3ca*^{E545K/WT}, and EC-*Pik3ca*^{WT/WT} were plated at similar cell densities and left to grow until 100% monolayer confluency. Then, a scratch was performed, and images were taken every 2 hours. **(A)** Comparison of wound closure between variants at 50 hours. Data represents mean wound closure % values in the well at 50 hours. Statistical analysis was performed by parametric one-way ANOVA. $n = 3$ technical replicates per experiment, $n \geq 2$ per genotype. **(B)** Wound closure curves between variants. $n = 3$ technical replicates per experiment, $n \geq 2$ per genotype. **(C)** Linear regression analysis to compare the slope of the curves in (B). Data represents mean slope values. Statistical analysis was performed by parametric one-way ANOVA. $n = 3$ technical replicates per experiment, $n \geq 2$ per genotype.

To study exclusively the *PIK3CA* mutant effect on migration without growth factor influence, we repeated the experiment in starvation conditions and examined any changes in wound closure (**Figure 2.4.5**). In starvation conditions, we observed a significant increase in wound closure for EC-*Pik3ca*^{H1047R/WT}, and not EC-*Pik3ca*^{E545K/WT} (**Figure 2.4.5.A**). When we compared the wound healing throughout the experiment, we noticed a significant increase in wound closure for EC-*Pik3ca*^{H1047R/WT}, and not EC-*Pik3ca*^{E545K/WT} (**Figure 2.4.5.B and C**). This data suggests *Pik3ca*^{H1047R/WT} can enhance migration compared to *Pik3ca*^{WT/WT} in starvation conditions in ECs, while EC-*Pik3ca*^{E545K/WT} does not affect migration.

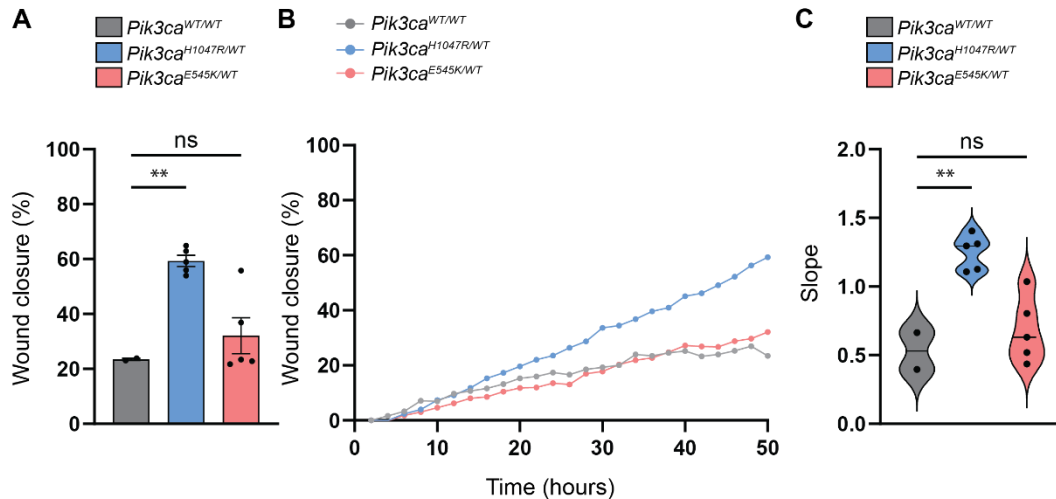


Figure 2.4.5. Impact of EC-*Pik3ca*^{H1047R/WT} and EC-*Pik3ca*^{E545K/WT} on migration in starvation conditions *in vitro*.

EC-*Pik3ca*^{H1047R/WT}, EC-*Pik3ca*^{E545K/WT}, and EC-*Pik3ca*^{WT/WT} were plated at similar cell densities and left to grow until 100% monolayer confluency. A scratch was performed and the medium changed to starvation medium, and images were taken every 2 hours. **(A)** Comparison of wound closure between variants at 50 hours. Data represents mean wound closure % values in the well at 50 hours. Statistical analysis was performed by parametric one-way ANOVA. * $p < 0.05$ and ** $p < 0.01$ were considered statistically significant. $n = 3$ technical replicates per experiment, $n \geq 2$ per genotype. **(B)** Wound closure curves between variants. $n = 3$ technical replicates per experiment, $n \geq 2$ per genotype. **(C)** Linear regression analysis to compare the slope of the curves in (B). Data represents mean slope values. Statistical analysis was performed by parametric one-way ANOVA. * $p < 0.05$ and ** $p < 0.01$ were considered statistically significant. $n = 3$ technical replicates per experiment, $n \geq 2$ per genotype.

To conclude objective II, we determined kinase activity under basal and pY-stimulated conditions and tested for signalling differences between the *PIK3CA* variants in different conditions in heart ECs *in vitro*. ADP glo assays showed that H1047R strongly increases basal kinase activity compared to the WT PI3K α enzyme, E545K also enhanced kinase activity, but to lesser extent than H1047R. Lastly, E726K showcased no significant difference. In pY-stimulated conditions, to mimic RTK interaction, we witnessed no further activation for any of the variants, although for H1047R, these results are questionable and not in line with what is known about this variant. *In vitro*, we first performed immunoblotting to verify PI3K α and MAPK activation and qPCR of PI3K α -controlled genes. It appeared that mainly EC-*Pik3ca*^{H1047R/WT} enhanced PI3K α -AKT signalling in basal, starved, and iFBS-stimulated conditions. Meanwhile, EC-*Pik3ca*^{E545K/WT} and EC-*Pik3ca*^{E726K/WT} did not significantly upregulate the PI3K α -AKT signalling pathway or showed the same extent of transcriptional control over the tested genes. For EC-*Pik3ca*^{E726K/WT}, this was in line with our results from objective I, namely, this variant likely activates the PI3K α -AKT signalling pathway to a lesser extent than the other variants, and therefore only results into mild phenotypes when expressed in the ECs of mice retinas. For EC-*Pik3ca*^{E545K/WT}, this was more surprising, since this variant caused strong

phenotypes when expressed in retinas and is known to be a strong and oncogenic activator of PI3K α -AKT signalling. This led us to compare the downstream signalling of the EC-*Pik3ca*^{H1047R/WT} and EC-*Pik3ca*^{E545K/WT} under conditions relevant to EC biology and function. Namely, we tested how they respond to stimulation with VEGFC and EGF. Here, we found that EC-*Pik3ca*^{H1047R/WT} activates the PI3K α -AKT signalling pathway in all conditions, in contrast to EC-*Pik3ca*^{E545K/WT} which scarcely activates PI3K α -AKT signalling, and mostly with EGF stimulation. Interestingly, MAPK signalling seemed to respond to EGF stimulation as well, although it was not clear if the variants played a major role in its activation. As a possible mechanism for these responses to the growth factors, we wanted to know if expression of the variants had any influence on the expression of the receptors for these growth factors. Interestingly, it appeared that EC-*Pik3ca*^{H1047R/WT} upregulated expression of *Vegfr2* and *Vegfr3* and showed a tendency to downregulate *Egfr* expression. EC-*Pik3ca*^{H1047R/WT} showed a tendency to upregulate *Vegfr2* and *Vegfr3* and significantly upregulated *Egfr* expression in EGF-stimulated conditions. We will explore the involvement of the MAPK pathway *in vivo* in objective III.

In vitro, we showed that the expression of these variants improved survival under nutrient-deprived circumstances. Proliferation did not seem to be affected upon expression of the variants, however, other research in many cell types showed that proliferation is enhanced with expression of either variant (277, 278). *In vivo*, it was shown that *Pik3ca*^{H1047R/WT} expression in the retinal vasculature also increased proliferation (73, 89). Scratch-wound assays revealed no enhanced migration, although under starved condition, *Pik3ca*^{H1047R/WT} showed a more migratory phenotype compared to *Pik3ca*^{E545K/WT} or *Pik3ca*^{WT/WT} controls.

III. Objective 3: Exploring the signalling differences between *Pik3ca*^{H1047R} and *Pik3ca*^{E545K} *in vivo* during vascular malformation development.

3.1. Validation of PI3K α activation in *Pik3ca*^{E545K}.

In objective II, we studied signalling differences between the *PIK3CA* variants under different circumstances *in vitro*. We noticed that *Pik3ca*^{H1047R} and *Pik3ca*^{E545K} expression can affect the expression of certain receptors differently, which could influence certain signalling pathways in cultured ECs. The effect of *Pik3ca*^{H1047R} and *Pik3ca*^{E545K} expression on the MAPK pathway has never been studied in the blood vasculature. Hence, we wanted to study the effect of *Pik3ca*^{H1047R} and *Pik3ca*^{E545K} expression on the

PI3K α and MAPK signalling in the developing vasculature of the mouse retina, to understand if there are signalling differences in an *in vivo* context.

To study the signalling in the developing vasculature, we injected *pdgfb-CreERT²*; *Pik3ca*^{H1047R} and *Pik3ca*^{E545K} (EC-*Pik3ca*^{Tg/WT} with *Rosa26-mTmG* reporter line) mice at P1 with 4-OHT and isolated the retinas at P6. To study the signalling, it is ideal to study smaller lesions with a select number of mutated cells and comparing to controls, therefore, full recombination such as in objective I is not required. We targeted less cells by adjusting to lower doses of 4-OHT. Recombination with lower 4-OHT doses was already performed in *Pik3ca*^{H1047R/WT} in (73). We tested the same doses (2.5 , 0.25 , and 0.125 mg/kg) in retinas expressing *Pik3ca*^{E545K/WT} in the ECs of the vasculature (**Figure 3.1.1**). We found that for both 0.125 and 0.25 mg/kg, there was little recombination in the mutant *Pik3ca*^{E545K/WT} retinas. The low number of recombined ECs did not result into any observable phenotype. With the higher dose of 2.5 mg/kg, there was more recombination, and hyperplasia of the vasculature was observed. To study the signalling differences, we require a clear phenotype, therefore we opted for the 2.5 mg/kg in future experiments (**Figure 3.1.2**).

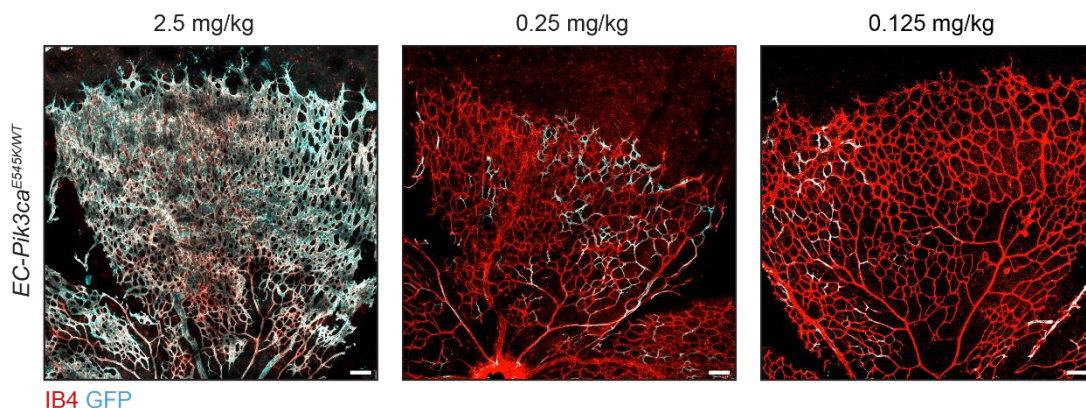


Figure 3.1.1. Recombination in *Pik3ca*^{E545K/WT} mouse retinas with different doses of 4-OHT. (A) P1 *Pik3ca*^{E545K/WT} mutant mice were injected with 2.50, 0.25, or 0.125 mg/kg 4-OHT, and retinas were isolated on P6 and immunostained with anti-IB4 and anti-GFP. Representative confocal ages are shown. Scale bar = 100 μ m. n \geq 6 retinas per genotype.

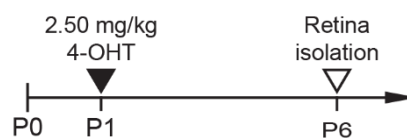


Figure 3.1.2. *In vivo* injection scheme to study overactivation of PIK3CA with *Pik3ca* mutant mouse models.

We induced recombination by intragastric injection of 2.50 mg/kg at postnatal day 1 (P1) and isolated the mouse retinas at P6.

We studied the formation of vascular malformations and quantified the rate of recombination in EC-*Pik3ca*^{H1047R/WT} retinas using 2.5 mg/kg 4-OHT. We immunostained the retinas for IB4 and GFP to quantify the vascular area and recombined endothelium. We used 4-OHT-injected *Pik3ca*^{WT/WT}-expressing retinas as controls. With the 2.5 mg/kg 4-OHT dose, *Pik3ca*^{H1047R/WT} expression resulted in massive hyperplasia of the vascular bed (**Figure 3.1.3.A**). We noticed a significantly enlarged vascular area (IB4+ area) in mutants compared to controls (**Figure 3.1.3.B**). Recombination (GFP+/IB4+ area) was not significantly altered in mutants compared to controls (**Figure 3.1.3.C**). These data show that even with less 4-OHT, *Pik3ca*^{H1047R/WT} expression still results in widespread recombination and a massive vascular lesion in the mouse retina.

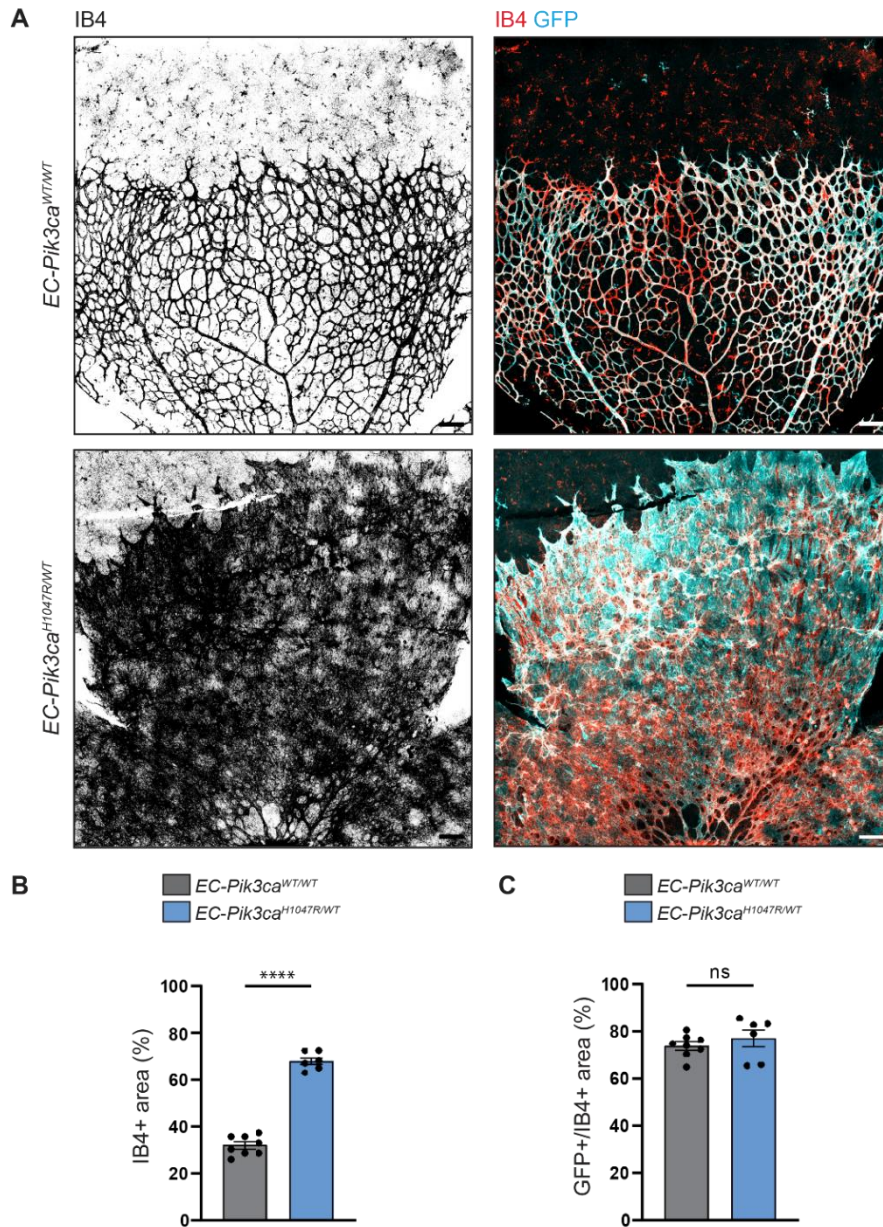


Figure 3.1.3. *Pik3ca^{H1047R}*-driven vascular malformations in mouse retinas with 2.5 mg/kg 4-OHT injection.

(A) P1 *Pik3ca^{WT/WT}* control and *Pik3ca^{H1047R/WT}* mutant mice were injected with 2.50 mg/kg 4-OHT, and retinas were isolated on P7 and immunostained with anti-IB4 and anti-GFP. Representative confocal images are shown. Scale bar = 100 μm . $n \geq 6$ retinas per genotype. **(B)** Quantification of IB4+ area per 180000 μm^2 area per petal. Statistical analysis was performed by parametric unpaired t-test. **** $p < 0.0001$ was considered statistically significant. $n \geq 6$ retinas per genotype. **(C)** Quantification of GFP+/IB4+ area per 180000 μm^2 area per petal. Statistical analysis was performed by parametric unpaired t-test. $n \geq 6$ retinas per genotype.

Then, we studied the formation of vascular malformations and the rate of recombination in EC-*Pik3ca*^{E545K/WT} retinas with the injection strategy from Figure 3.1.1. With the 2.5 mg/kg 4-OHT dose, *Pik3ca*^{E545K/WT} expression resulted into hyperplasia of the vascular bed, characterized by enlargement of ECs in the capillaries and sprouting front, and enlargement of the vein. Arteries remained unaffected, although they were less elongated due to the disorganized and hyperplastic tissue towards the sprouting front (**Figure 3.1.4.A**). We noticed a significantly enlarged vascular area (IB4+ area) in mutants compared to controls (**Figure 3.1.4.B**). Recombination (GFP+/IB4+ area) was not significantly altered in mutants compared to controls (**Figure 3.1.4.C**). These data show that with less 4-OHT, *Pik3ca*^{E545K/WT} expression still results in vascular lesions in the retina, though, to a lesser extent compared to the malformations found in EC-*Pik3ca*^{H1047R} retinas.

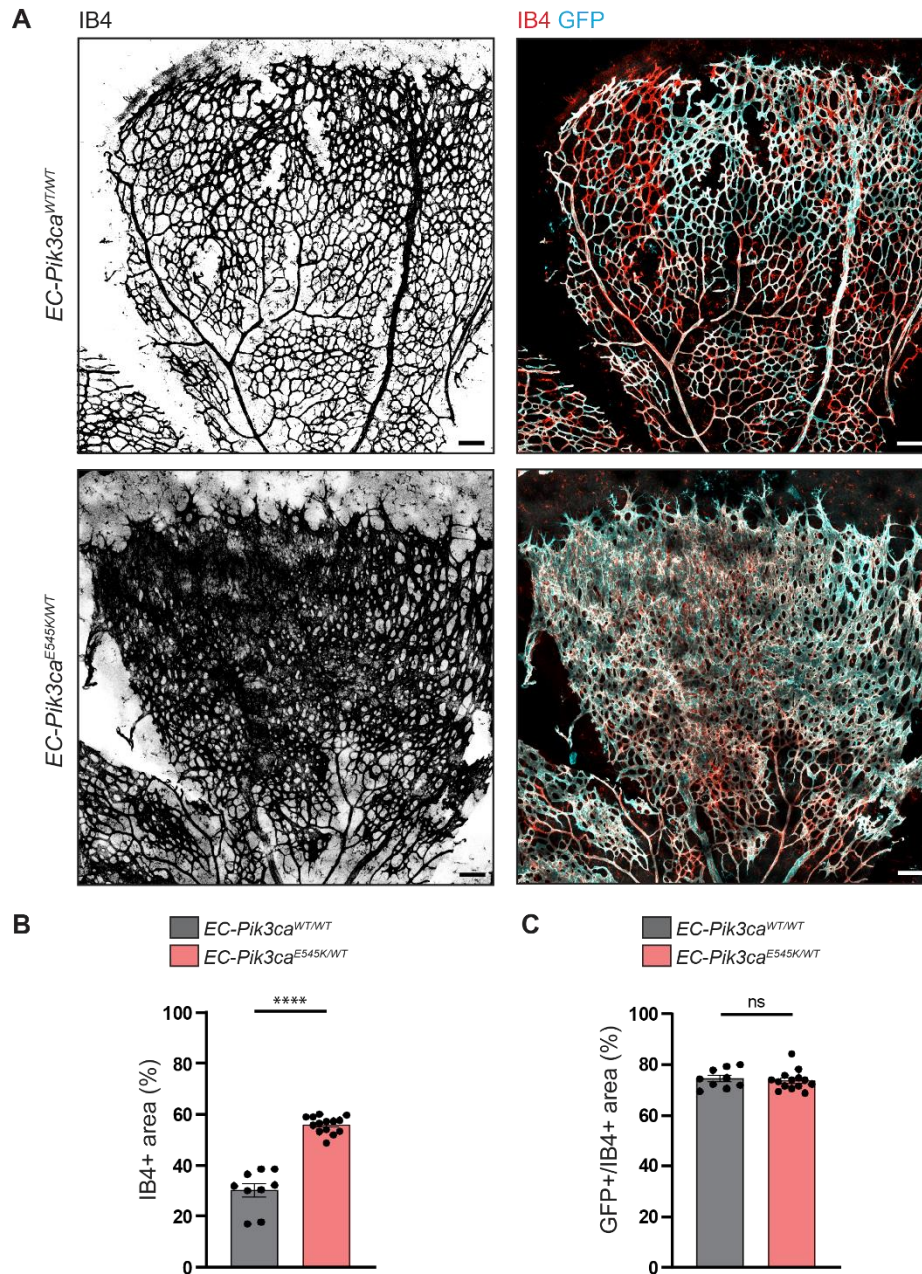


Figure 3.1.4. *Pik3ca*^{E545K}-driven vascular malformations in mouse retinas with 2.5 mg/kg 4-OHT injection.

(A) P1 *Pik3ca*^{WT/WT} control and *Pik3ca*^{E545K/WT} mutant mice were injected with 2.50 mg/kg 4-OHT, and retinas were isolated on P7 and immunostained with anti-IB4 and anti-GFP. Representative confocal images are shown. Scale bar = 100 μ m. $n \geq 9$ retinas per genotype. **(B)** Quantification of IB4+ area per 180000 μ m² area per petal. Statistical analysis was performed by parametric unpaired t-test. **** $p < 0.0001$ was considered statistically significant. $n \geq 9$ retinas per genotype. **(C)** Quantification of GFP+/IB4+ area per 180000 μ m² area per petal. Statistical analysis was performed by parametric unpaired t-test. $n \geq 9$ retinas per genotype.

Then, we wanted to verify PI3K α -AKT pathway activation *in vivo* with the expression of the *PIK3CA* variants. PI3K α -AKT pathway overactivation has already been studied in our lab by immunostaining with p-S6 (S235/236), a downstream effector of PI3K α -AKT (73, 89). It appeared p-S6 (S235/236) levels increased with expression of *Pik3ca*^{H1047R/WT}. Next, we examined the p-S6 (S235/236) levels in EC-*Pik3ca*^{E545K/WT} retinas by taking high-magnification images of 4 different areas in the retinal vasculature: vein and surrounding capillaries, artery and surrounding capillaries, at the capillary plexus, and capillaries at the sprouting front (**Figure 3.1.5.A**). When we compared the p-S6 (S235/236) intensity fold changes, no significant differences were observed by combining the data of the 4 areas (**Figure 3.1.5.B**). These data suggest that EC-*Pik3ca*^{E545K/WT} expression does not increase PI3K α -AKT pathway signalling via p-S6 (S235/236) in mouse retinas.

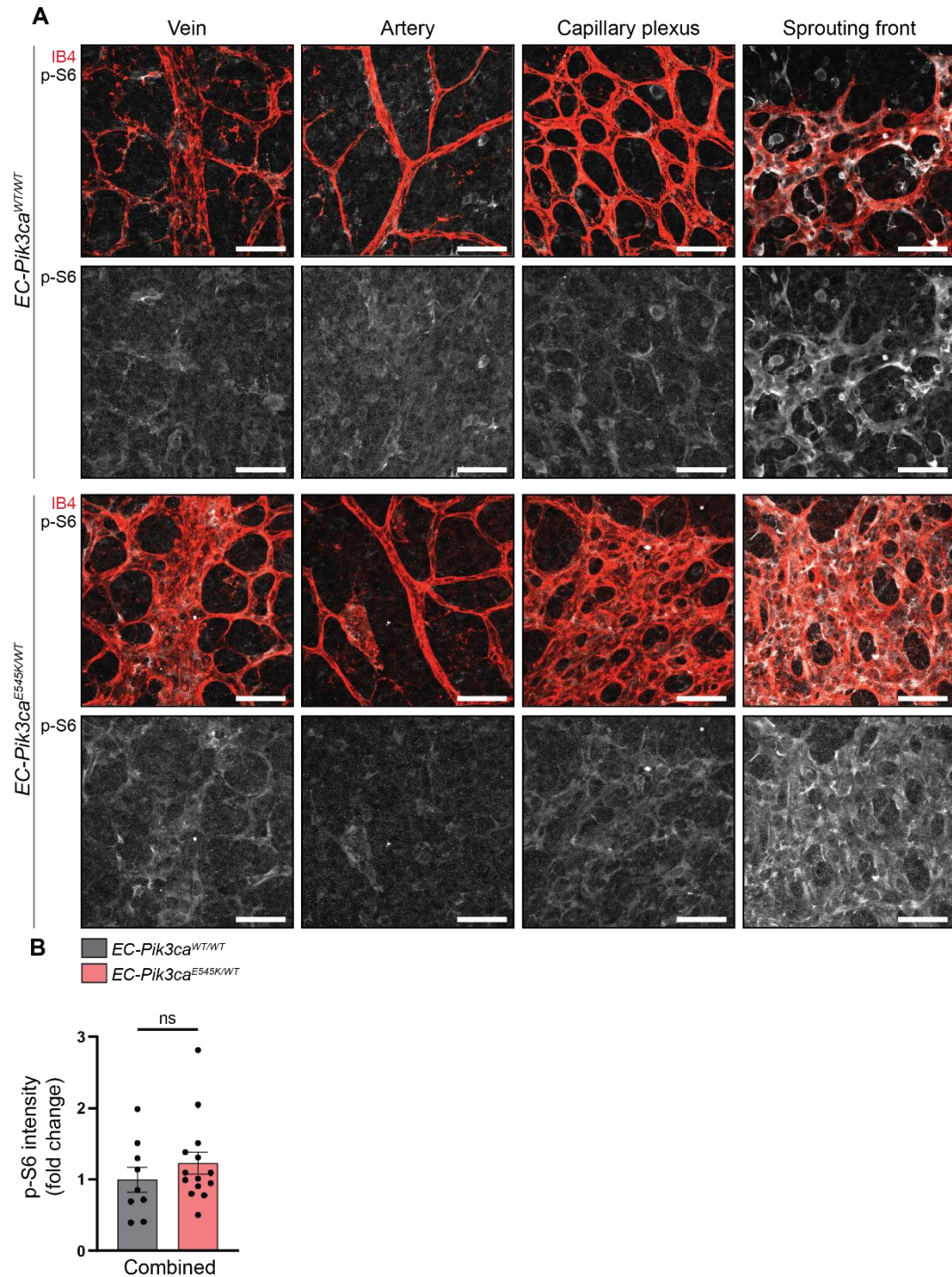


Figure 3.1.5. P-S6 (S235/236) levels in *Pik3ca^{E545K}*-expressing mouse retinas with 2.5 mg/kg 4-OHT injection.

(A) *Pik3ca^{WT/WT}* control and *Pik3ca^{E545K/WT}* mutant mice were injected with 2.50 mg/kg 4-OHT, and retinas were isolated on P7 and immunostained with anti-IB4 and anti-p-S6 (S235/236). Representative confocal images are shown. Scale bar = 50 μm . $n \geq 9$ retinas per genotype. **(C)** Quantification of p-S6 (S235/236) intensity per 180000 μm^2 area per petal. Data represented as fold change values relative to *Pik3ca^{WT/WT}* controls. Statistical analysis was performed by parametric unpaired t-test. $n \geq 9$ retinas per genotype.

3.2. Study of MAPK signalling in *Pik3ca*^{H1047R} and *Pik3ca*^{E545K}.

Next, we wanted to study MAPK pathway activation *in vivo* with the expression of the *PIK3CA* variants. First, we examined the p-ERK (T202/Y204) levels in EC-*Pik3ca*^{H1047R/WT} retinas by taking high-magnification images of 4 different areas in the retinal vasculature: vein and surrounding capillaries, artery and surrounding capillaries, at the capillary plexus, and capillaries at the sprouting front (**Figure 3.1.6.A**). When we compared the p-ERK (T202/Y204) levels in mutants relative to controls, the p-ERK (T202/Y204) levels were significantly increased (**Figure 3.1.6.B**). Additionally, to get a better idea of the p-ERK (T202/Y204) distribution, we measured the p-ERK+/GFP+ area. Here, we observed no significant differences between mutants and controls, although mutants show a tendency for higher p-ERK+ area. These data suggest that EC-*Pik3ca*^{H1047R/WT} expression increases MAPK pathway signalling in the ECs of mouse retinas.

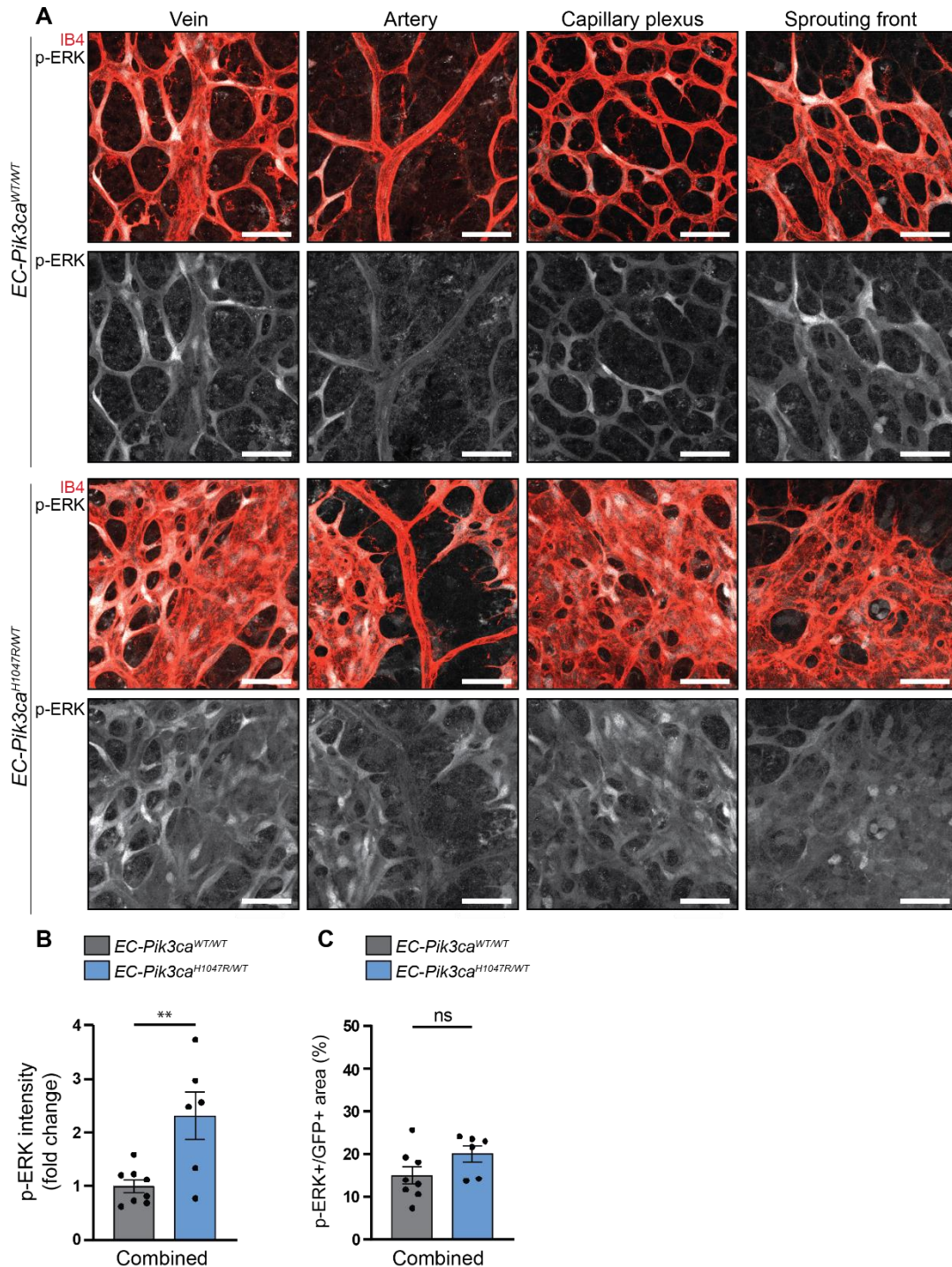


Figure 3.1.6. P-ERK (T202/Y204) levels in *Pik3ca^{H1047R}*-expressing mouse retinas with 2.5 mg/kg 4-OHT injection.

(A) P1 *Pik3ca^{WT/WT}* control and *Pik3ca^{H1047R/WT}* mutant mice were injected with 2.50 mg/kg 4-OHT, and retinas were isolated on P7 and immunostained with anti-IB4 and anti-p-ERK. Representative confocal images are shown. Scale bar = 50 μm . $n \geq 6$ retinas per genotype. (B) Quantification of p-ERK intensity per 180000 μm^2 area per petal. Data represented as fold change values relative to *Pik3ca^{WT/WT}* controls. Statistical analysis was performed by parametric unpaired t-test. $**p < 0.01$ was considered statistically significant. $n \geq 6$ retinas per genotype. (C) Quantification of p-ERK+/GFP+ area in *Pik3ca^{H1047R/WT}* retinas per 180000 μm^2 per petal. Data represented as mean area %. Statistical analysis was performed by parametric unpaired t-test. $n \geq 6$ retinas per genotype.

Next, we examined the p-ERK (T202/Y204) levels in EC-*Pik3ca*^{E545K/WT} retinas, as described above (**Figure 3.1.7.A**). We noticed no significant changes in the relative intensity of p-ERK (T202/Y204) expression in mutants relative to controls (**Figure 3.1.7.B**). When we measured the p-ERK+/GFP+ area, we saw a significant decrease in the p-ERK+ area. (**Figure 3.1.7.C**). These data suggest that EC-*Pik3ca*^{E545K/WT} expression affects MAPK signalling differently compared to EC-*Pik3ca*^{H1047R/WT} in the ECs of the mouse retina. It is possible that the p-ERK (T202/Y204) levels are generally downregulated or redistributed to more localized area in EC-*Pik3ca*^{E545K/WT} expression, hence the decrease in area while the intensity stays relatively similar.

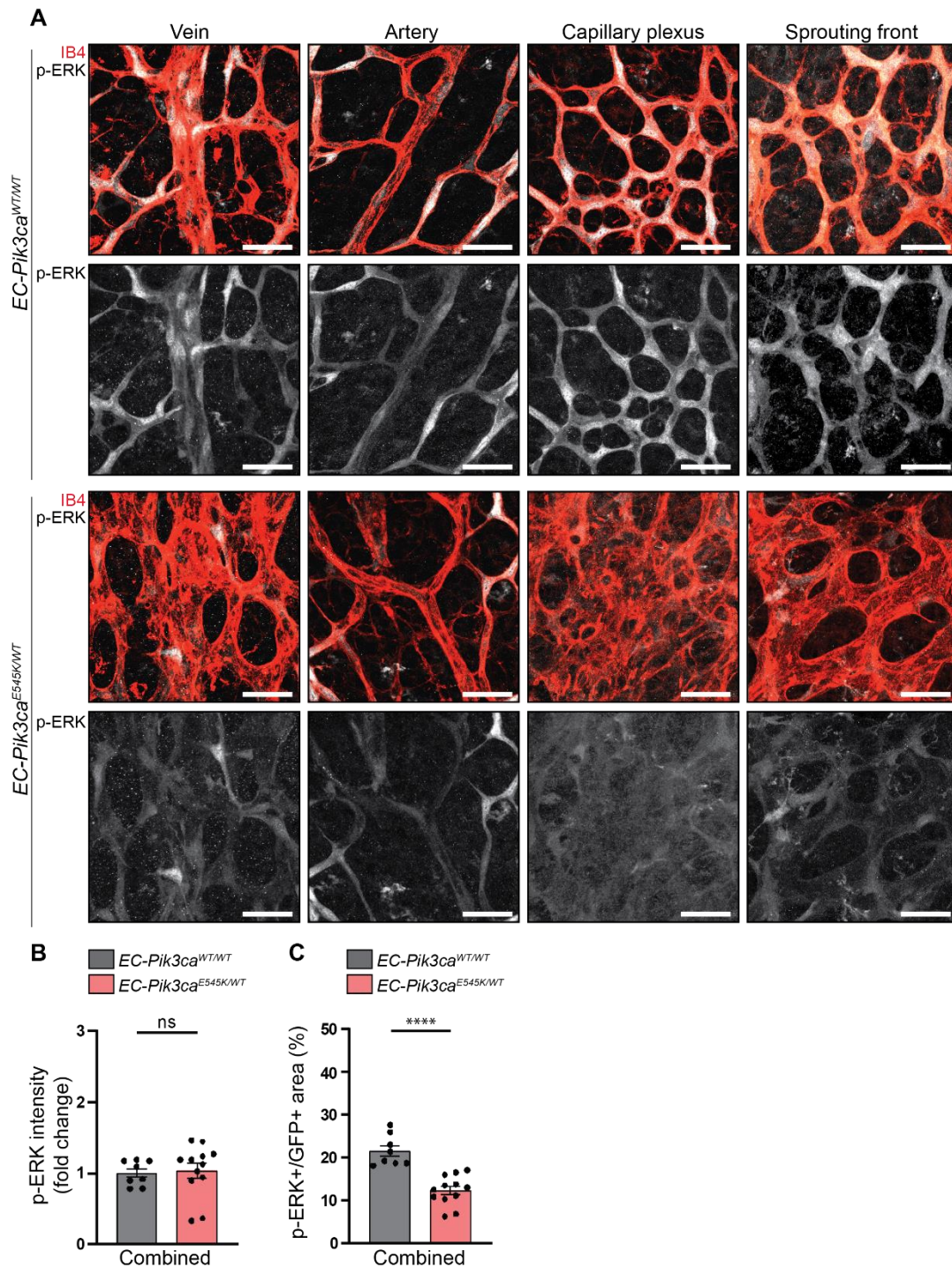


Figure 3.1.7. P-ERK levels in *Pik3ca^{E545K}*-expressing mouse retinas with 2.5 mg/kg 4-OHT injection. (A) P1 *Pik3ca^{WT/WT}* control and *Pik3ca^{E545K/WT}* mutant mice were injected with 2.50 mg/kg 4-OHT, and retinas were isolated on P7 and immunostained with anti-IB4 and anti-p-ERK. Representative confocal images are shown. Scale bar = 50 μm . $n \geq 8$ retinas per genotype. (B) Quantification of p-ERK intensity per 180000 μm^2 area per petal. Data represented as fold change values relative to *Pik3ca^{WT/WT}* controls. Statistical analysis was performed by parametric unpaired t-test. $n \geq 8$ retinas per genotype. (C) Quantification of p-ERK+/GFP+ area in *Pik3ca^{E545K/WT}* retinas per 180000 μm^2 per petal. Data represented as mean area %. Statistical analysis was performed by parametric unpaired t-test. $n \geq 6$ retinas per genotype.

To conclude objective III, we first established a different 4-OHT treatment regimen in retinas to obtain a less severe phenotype for the study of the signalling pathways *in vivo*. We observed that 4-OHT concentrations are not always directly proportional to the number of recombined cells. To still see phenotype with EC-*Pik3ca*^{E545K/WT} retinas, we opted to inject with 2.5 mg/kg of 4-OHT. Using this regimen, we still observed widespread recombination and hyperplasia of the vasculature in both EC-*Pik3ca*^{H1047R/WT} and EC-*Pik3ca*^{E545K/WT} retinas. In EC-*Pik3ca*^{H1047R/WT} retinas, previous research established that expression of this mutant results in augmented p-S6 (S235/236) levels, used as a readout for PI3K α activation (73, 89). In the EC-*Pik3ca*^{E545K/WT} retinas, we observed no activation of this pathway *in vivo*, in line with our results from objective II, where we observed relatively low PI3K α -AKT pathway activation compared to the *Pik3ca*^{H1047R/WT} variant. Interestingly, the *PIK3CA* mutations displayed a different pattern when studying their effect on the MAPK pathway, namely EC-*Pik3ca*^{H1047R/WT} retinas showed an activation of this pathway, while EC-*Pik3ca*^{E545K/WT} retinas showed predominantly no activation, or downregulation of p-ERK (T202/Y204) expression. Whether this difference plays a role in the pathology caused by the variants in vascular malformations remains unknown.

Discussion

Since the discovery of the PI3K family in 1988, extensive research has shed light on many aspects of the role of this family of kinases in physiology. PI3K's proved crucial for many cellular processes, such as survival, metabolism, migration, and proliferation, in various cell types. Over the years, mutations in the class IA *PIK3CA* gene have been associated with several cancers, ultimately revealing that *PIK3CA* is one of the most frequently mutated genes in cancer (41, 42). With time, the most common oncogenic mutations or “hotspots” of *PIK3CA* were discovered, and the mechanism by which they activate the PI3K α signalling pathway. Step by step, different pathway components were revealed and their crucial function in physiology and oncogenic transformation. This paved the way for the formation of molecular therapies.

Then, in 2008, *Graupera et al.* revealed that PI3K α is crucial for embryonic development, specifically due to its indispensable role in the formation of the vasculature (222). Additional studies revealed that *PIK3CA* is a key regulator of endothelial function, angiogenesis, and the maintenance of arteriovenous identity in ECs. By using a genetic mouse model for the oncogenic hotspot mutation *Pik3ca*^{H1047R}, *Castillo et al.* discovered that overactivation of the PI3K α pathway during embryonic development resulted in the formation of VMs (89). Then, activating *PIK3CA* mutations were observed in patients with VMs. Since then, many overgrowth disorders have been associated with oncogenic mutations in *PIK3CA*, and grouped under the umbrella term of PROS. Advances in sequencing techniques over the years have revealed many *PIK3CA* variants in patients with VMs and PROS, spanning the entirety of the gene. However, this field of study is young, and new discoveries are still being made about the relationship between *PIK3CA* variants and the phenotypic outcome. For many variants, the mechanism of activation and their impact on the associated pathology remains underexplored. Distinct activating mechanisms for the oncogenic hotspot variants H1047R and E545K (and E542K) have

been demonstrated, although how these distinct mechanisms influence downstream signalling remains elusive (46, 48). Notably, emerging epidemiological studies on VMs and PROS reveal a distinct pattern of mutation prevalence across PROS disorders (53-55). Namely, oncogenic hotspots were overrepresented in isolated lesions affecting a limited amount of tissue types, while non-hotspot variants such as E726K resulted in more widespread phenotypes. This led to the hypothesis that some mutational variants are tolerated at different stages throughout embryonic development depending on their activating potential.

In this thesis, we aimed to explore unanswered questions about how *PIK3CA* variants contribute to VM phenotypes. Our objective was to gain a deeper understanding of the genotype-phenotype relationship for three *PIK3CA* variants H1047R, E545K, and E726K. We employed several mice models and investigated variant expression in the endothelium during different stages of blood vessel development. First, we modelled the vascular phenotypes by expressing the variants in the endothelium of the developing retina during active angiogenesis and during vascular remodelling. After, we compared embryonic lethality between *Pi3kca*^{H1047R} (studied in 71) and *Pik3ca*^{E545K}. Then, we explored the intracellular signalling pathway effects of variant expression in mouse cultured heart ECs. *In vitro*, we mimicked different conditions relevant during angiogenesis and compared distinct signalling events. Lastly, we attempted to translate the findings from the *in vitro* data to *in vivo* by comparing the PI3K and MAPK signalling in vascular malformations in the retina model of mice expressing the hotspot variants *Pi3kca*^{H1047R} and *Pik3ca*^{E545K}.

I. Objective 1: Studying the activating *PIK3CA* mutations in the developing vasculature in mice.

The vast diversity of phenotypes in patients with VMs presents a challenge in modelling these diseases, to study their progression, and to conduct clinical testing. Some models to study VMs have been developed in the past, by introducing the oncogenes by viral transduction or by xenotransplantation of ECs expressing a mutation (279, 280). Although these models pioneered the study of VMs in mice, they do not recapitulate the natural disease progression in patients accurately. Moreover, the extensive process necessary for these models makes them unsuitable to efficiently model disease progression or for clinical applications.

Other models have since been developed to study the vasculature. The postnatal retina model is suitable for the study of VMs due to its reproducible nature and relative simplicity compared to xenograft models (281). The generation of conditional mice models that allow for spatiotemporal control of expression of the mutated gene under the endogenous locus further improved the possibilities of studying VMs (282). For *PIK3CA*-related VMs, *Castillo et al.* demonstrated that heterozygous expression of *Pik3ca*^{H1047R} in the mesoderm resulted in the formation of venous malformations (89). Then, *Kobialka et al.* demonstrated preclinical use of the inducible, EC-specific *Pdgfb*-CreER^{T2} system in combination with heterozygous expression of *Pik3ca*^{H1047R} in the mice retina (73). Specifically, they were able to control the number of recombined ECs and therefore elegantly recapitulate the mosaic aspect of VM onset and use this model for preclinical testing of the AKT inhibitor Miransertib.

We used the same conditional mouse model as *Kobialka et al.*; namely *Pdgfb*-CreER^{T2}; *Pik3ca*^{H1047R/WT}. To achieve our objectives, we expanded this system to other *PIK3CA* variants by crossing the *Pdgfb*-CreER^{T2} system with other *Pik3ca* mutant constructs. First, *Robinson et al.* generated a knock-in mouse model with a conditional *Pik3ca*^{E545K} allele controlled by the endogenous *Pik3ca* promoter to study medulloblastomas development (269). This model has since been used to study brain overgrowth and epilepsy (274). We employed this *Pik3ca*^{E545K} construct for the study of *PIK3CA*-related VMs. Lastly, the *Pik3ca*^{E726K} was developed by us, using the same mini-gene strategy that *Kinross et al.* used when they constructed *Pik3ca*^{H1047R} (268).

In objective I, we employed these models to study and compare VMs generated by the variants. Yet, there are limitation to this approach. We used different *Pik3ca* constructs, each with distinct mechanisms for expressing the mutation. Although all constructs are controlled by the endogenous *Pik3ca* promoter, their recombination efficiency may vary. Therefore, when comparing phenotypes, we must account for the possibility that differences in recombination efficiency results in varying numbers of recombined clones, which could influence lesion formation. Also, the timepoint at which the mutation takes place plays an important role in the generation of a lesion; if some constructs recombine slower than others, the recombined cells will not have the same amount of time to expand. We tried several approaches to mitigate these effects. First, *Kobialka et al.* already established a dose-response effect in *Pik3ca*^{H1047R} by treatment with increasing concentrations of 4-OHT. We used their highest dose of 25 mg/kg 4-OHT to compare the VMs, using 4-OHT-injected *Pik3ca*^{WT/WT} mice as controls for each variant. This way, we guaranteed maximum recombination in all variant constructs. To verify the activity of Cre recombinase, we crossed each *Pik3ca* variant line with the mTmG reporter line, which

allowed us to compare the recombination rates between the variants and their respective controls. We measured GFP+/IB4+ area to quantify the recombination rates between all variants and their respective controls. We observed a similar recombination rate of 80% or higher for all variants and controls. Interestingly, the oncogenic variants *Pik3ca*^{H1047R/WT} and *Pik3ca*^{E545K/WT} showcased an increase in recombined area, suggesting a clonal expansion of the recombined clones. This increase was not observed in *Pik3ca*^{E545K/WT}. These results suggest ECs carrying an oncogenic hotspot variant gain a competitive advantage resulting in their rapid expansion in the vascular tissue compared to control ECs. Nonetheless, the expression of GFP does not signify recombination of the mutant *Pik3ca* allele since the mTmG reporter line is located on a different locus. In the future, other methods can be applied to verify similar recombination rates between the *Pik3ca* variant constructs in the retina. For instance, simultaneous immunostaining for PI3K α could help assess the amount of PI3K α protein present in recombined clones. However, while this approach could indicate overall *PIK3CA* expression, it would not distinguish between wild-type and mutant *PIK3CA*. As a result, it would provide only a semi-quantitative assessment of whether the different variant constructs are expressed at similar levels. A more thorough approach would be the isolation of ECs from the retina tissue for subsequent downstream applications. Specifically, GFP+ clones are selected by FACS, and the number of recombined cells is counted. Further transcriptomic or proteomic analysis could be employed to study PI3K α pathway activation in detail. This is currently being attempted in our laboratory.

Injecting the high 25 mg/kg 4-OHT dose at P1 and studying the vascular architecture at P7 in retinas showed us that *Pik3ca*^{H1047R/WT} and *Pik3ca*^{E545K/WT} expression resulted into a massive hyperplasia of the vasculature due to increased amounts of ECs, while *Pik3ca*^{E726K/WT} expression only resulted into mild hyperplasia and more focal vascular malformations, due to locally increased numbers of ECs. This is accordance with the knowledge that *PIK3CA*^{H1047R} and *PIK3CA*^{E545K} are highly potent activators of the PI3K α pathway with oncogenic potential (52-54). Here, we showed that both caused similar severity of VM phenotype. *PIK3CA*^{E726K} has not been studied in many contexts and was hypothesized to cause less severe activation of the PI3K α pathway (69, 70). Together, these data enforce the knowledge about these variants and their behaviour in patients. Namely, the oncogenic hotspot variants *PIK3CA*^{H1047R} and *PIK3CA*^{E545K} are powerful activators and give rise to strong VM and PROS phenotypes, such as isolated VMs and LMs (69-71). Meanwhile, *PIK3CA*^{E726K} is not as often represented in isolated VMs, but more commonly found in widespread PROS phenotypes such as MCAP and CLOVES (58, 59, 84, 94).

Another genetic tool, the iSure-Cre model, can ensure recombination in mutated clones by inducing a second wave of Cre expression upon recombination. We used this model in the *Pik3ca*^{E726K/WT} retina to confirm that the milder phenotype was due to the mutation's lower activity rather than poor recombination of the mutant construct (data not shown). Although the comparison was limited to one mutant and one control animal, the retinas did not show any additional phenotype with this approach. This supports the conclusion that *Pik3ca*^{E726K/WT} expression causes focal lesions, unlike the more extensive phenotypes observed with *Pik3ca*^{H1047R/WT} and *Pik3ca*^{E545K/WT}, and that increasing recombination does not enlarge the lesions.

Studies revealed an important mechanistic difference between *PIK3CA*^{H1047R} and *PIK3CA*^{E545K}. As discussed, *PIK3CA*^{H1047R} strongly activates intrinsic kinase activity of the enzyme, while its oncogenic potential can be further increased by RTK activation and is independent of Ras activation (46, 48, 49). *PIK3CA*^{E545K}, on the other hand, reduces the enzyme to a basal activity, independent of further RTK activation, while still being activated further by Ras interaction (46, 48, 49, 238). *PIK3CA*^{E726K}'s mode of activation is not explored, although we hypothesize that this variant increases membrane interactions to negatively charged regions of the plasma membrane, this is based on the evidence that E726 is positioned in a flexible loop at the protein's surface, and structural data showed that this area interacts with the membrane (19, 46, 51). Knowing this, we theorised that *Pik3ca*^{E545K/WT} could produce a vascular lesion even when environmental growth cues were low during the final stage of retinal blood vessel formation. However, it appeared that during this remodelling phase, *Pik3ca*^{E545K/WT} expression was not more likely to cause VMs compared to *Pik3ca*^{H1047R/WT}. Meanwhile, *Pik3ca*^{E726K/WT} expression did not result into any lesion at all, likely because of its low activation potential. We speculate that the vascular remodelling process does not rely on PI3K α signalling as much, or other factors could mitigate PI3K α pathway activity during this developmental phase. We mentioned the lower amounts of mitogenic factors during vascular remodelling, this could result into a general decrease in PI3K activity while the ECs shift from a proliferative to a quiescent state (221). PTEN is active during vascular remodelling, so its activity might be mitigating the effects of *PIK3CA* variant expression during vascular remodelling (283). Moreover, when the vessel develops, blood flow will induce the activity of other signalling elements such as eNOS and Notch (284). These have been shown to inhibit PI3K α pathway activity in certain contexts (285). Additional research regarding the interplay between these pathways in developmental context is required to understand why PI3K overactivation during vascular remodelling does not commonly manifest a malformation. All together, we conclude that active angiogenesis

is important for the generation of vascular malformations caused by PI3K α overactivation.

Even though we can distinguish phenotypic differences between the variants in the developing retina, there are drawbacks to using the 25 mg/kg 4-OHT. Mainly, VMs in patients are typically characterized by a high degree of mosaicism. This mosaic pattern is not reflected well when we maximize recombination. Furthermore, VMs in patients don't typically occur in the eye, but in skin, adipose, brain, or muscular tissues. Given the large heterogeneity of blood vessels within different tissues, the mouse retina does not necessarily translate into the different disease phenotypes that occur in patients in these tissues. Other factors, such as interaction with the immune system, have been shown to contribute to VMs (81), and remain underexplored in the retinal model. Regardless of its limitations, the retinal model remains an important tool to study vascular lesions in a reproducible manner. In combination with other experimental techniques, the retina model can be employed to examine specific cellular processes relevant for VM development *in vivo*. For instance, EdU-incorporation assays in the *Pik3ca*^{H1047R/WT} retina model already revealed increased EC proliferation in *PIK3CA*-related VMs (73, 89). Moreover, the retina model can be combined with other genetic tools to further advance our understanding of VMs in patients. Recently, the iFlu-mosaic *Pik3ca*^{H1047R} model was developed by Dr. Rui Benedito, in which the WT and mutant *Pik3ca* gene are expressed on the same allele, both coupled to a different fluorophore. This will introduce a higher level of mosaicism in the lesion but also allow tracing of the mutant clones. This model is already being used in our lab to better understand certain aspects of VM pathology caused by PI3K α overactivation, specifically, why *PIK3CA* mutant clones don't populate the artery. However, since we lack similar models for the other variants, we can't use this model to compare lesion properties with other variants.

VMs in patients typically occur during embryonic development. Mouse models to express the variants during the embryonic development have been generated as well, including to target the endothelium using the *Tie2-Cre* system (271). *Hare et al.* already used the constitutive *Tie2-Cre* system in combination with the endogenous *Pik3ca*^{H1047R/WT} to study the lethality in mouse embryos and the related vascular properties. We found that when we expressed *Pik3ca*^{E545K/WT} in all ECs of the developing mouse embryo, we observed embryonic death around E10.5 and full embryonic lethality at E11.5, similar as *Hare et al.* observed with *Pik3ca*^{H1047R/WT}. We conclude that expression of both oncogenic hotspot variants in the vasculature results into embryonic lethality at mid-gestation due to vascular defects. Due to the similar timing of lethality, we conclude these variants possess a similar PI3K α pathway activating potential. This confirmed our findings in

retinas, namely that *Pik3ca*^{H1047R/WT} and *Pik3ca*^{E545K/WT} expression are similarly capable of generating massive vascular lesions. Even though we studied 47 embryos in total, we only performed immunofluorescence on a couple of these embryos to demonstrate some obvious developmental differences between mutants and controls. Immunostaining a higher number of embryos or examining cross-sections to observe the vessel sizes at certain locations, could reveal more details about the disease phenotype generated by *Pik3ca*^{E545K/WT} expression. We wanted to explore lethality with *Pik3ca*^{E726K/WT} as well. This could have demonstrated that this “weaker” mutation could be tolerated earlier throughout embryonic development and therefore support the hypothesis that “weaker” mutations can be tolerated at earlier developmental stages, hence, giving rise to more widespread phenotypes as observed in patients (58, 59, 84, 94). However, due to breeding problems with this mouse model, these experiments could not be performed.

II. Objective 2: Elucidating *PIK3CA* variant kinase activity and signalling differences in cultured endothelial cells.

In objective II, we first explored the intrinsic changes in the PI3K α enzyme when the mutations are present in basal and pY-stimulated conditions to mimic RTK activation cues. Previous studies revealed increased kinase activity for some variants (and combinations of those variants) and increased lipid binding (51, 275). Specifically, *Vasan et al.* performed radioactive *in vitro* kinase assays and showed increased kinase activity for H1047R and E545K, and less for E726K, compared to WT. However, their research question was more focused on double PI3K α mutants, and although these data provide interesting qualitative data for these double mutants, it is lacking a quantitative approach to compare the kinase activity for our variants of interest. ADP glo provides a more quantitative approach and was used by *Gong et al.* to study the kinase activity in basal and pY-stimulated conditions for E545K and H1047R. With their help, we repeated the ADP glo experiments and included E726K. Of note, one important difference is that *Gong et al.* used PIP2 embedded in liposomes to perform the enzymatic reaction, which mimics the natural environment of the plasma membrane. We used soluble PIP2 instead, because these specialized liposomes are expensive and time-consuming to produce. The data in basal conditions revealed that H1047R had the strongest lipid kinase activity, followed by E545K, and lastly E726K, which barely displayed an increased kinase activity compared to WT. Therefore, it appears that H1047R and E545K can cause conformational changes in the protein complex that intrinsically enhance kinase activity, whereas E726K does not. This corroborates the hypothesis that E726K improved kinase

activity by enhanced binding to the plasma membrane, though this cannot be tested by ADP glo. Additional membrane-binding assays should be performed to verify this, though *Vasan et al.* already performed such assays and indeed saw improved membrane binding for every variant. In pY-stimulated conditions, we saw no enhanced kinase activity for any of the variants compared to WT. For E545K, this was expected because of its activation mechanism and in line with *Gong et al.* E726K did not improve kinase activity in basal conditions compared to WT, therefore it is not surprising that pY stimulation does not increase the kinase activity further. The results for H1047R were most surprising, *Gong et al.* clearly showed a significant increase in lipid kinase activity for H1047R in pY-stimulated conditions. During the kinase titration, we did not witness a linear phase for this variant, instead we witnessed velocity directly correlated with enzyme concentration. One explanation could be the depletion of ATP during the reaction. However, this depletion was not observed, therefore we likely encountered technical problems during this replicate. Perhaps we used too little substrate for the reaction, there were pipetting errors, or the protein was not stable at these low concentrations. Of note, the Sf9 cells displayed high lethality when we expressed H1047R in contrast to the other variants or the WT. Therefore, we were not able to isolate this variant ourselves, and it was kindly given to us by Dr. Grace Gong. Technical problems could have occurred during the handling of this protein.

Kobialka et al. studied the transcriptomic profile of isolated mouse lung ECs with *Pik3ca*^{H1047R/WT} expression and revealed up- and downregulation of genes important for cell division, mitosis and cell cycle progression (73). We explored the signalling related to these cellular processes in heart ECs expressing *Pik3ca*^{H1047R/WT}, *Pik3ca*^{E545K/WT}, and *Pik3ca*^{E726K/WT} by studying the activation of PI3K or MAPK pathway components under different developmental conditions. First, the same limitation as in objective I needs to be discussed, namely, we compared signalling differences between 3 variant constructs that might recombine at different rates. Therefore, we first attempted to verify that PI3K α pathway activation took place with different 4-OHT treatment regimens. Then, using primers designed to bind specific regions of the variant constructs, which produce different DNA fragments upon Cre-mediated excision, we confirmed recombination occurred in each variant after treatment with 2 μ M 4-OHT for 24 hours. However, this does not reveal quantitative data about the number of cells that are recombined, neither about the kinetics of recombination for each variant construct *in vitro*. Surely, more characterization is necessary to fully understand these constructs' properties.

Next, the isolation of ECs from mice provides a compelling model to study intracellular signalling or to perform cell functional assays. However, there are limitations to what an

in vitro model can recapitulate about complicated physiological processes. Angiogenesis and vessel maturation during embryonic development are complicated processes that rely heavily on growth factor signalling in the context of their specific environments. Here, we isolated ECs from adult mice and hereby removed them from their natural environment. Moreover, the process of isolation is damaging to the ECs since they undergo multiple rounds of digestion and lysis before the culture is pure. Usually, cultured ECs can only be passaged 6/7 times before experiencing significant senescence. Therefore, we need to remain vigilant when translating *in vitro* data to an *in vivo* context. Additionally, because we isolated the entire heart tissue, we could not precisely control the specific tissues or cell types included in our cultures. This could result in a mix of EC subpopulations, ranging from arterial to lymphatic ECs and from differentiated cells to progenitors. Previous work in our lab attempted to identify these subpopulations through marker immunostaining in lung and heart ECs (unpublished data). However, the findings were inconclusive due to the heterogeneity of the populations. Moreover, we hypothesize that ECs in culture may alter their expression of certain markers when transitioned to an *in vitro* environment. This could lead to less-defined specification or a loss of key identity characteristics, further complicating the interpretation of their properties and behaviour.

Nonetheless, our signalling study in cultured ECs did reveal some interesting differences between the variants. Mainly, immunoblotting and transcriptomic analysis of PI3K α -controlled genes revealed that *Pik3ca*^{H1047R/WT} expression activated the PI3K α -AKT pathway in full medium and starvation conditions, while *Pik3ca*^{E545K/WT} and *Pik3ca*^{E726K/WT} expression showed little activation. We already demonstrated in objective I that *Pik3ca*^{E726K/WT} expression did not cause massive lesions in the vasculature compared to *Pik3ca*^{H1047R/WT} and *Pik3ca*^{E545K/WT} expression. From the kinase activity assays, we also showed no increase in kinase activity for E726K compared to WT. Therefore, we propose a correlation between E726K's poor activation of the enzyme, resulting into little PI3K α -AKT pathway activation, causing only a mild phenotype in the retina model. With this conclusion, we ended our investigation of this variant. Surprisingly, *Pik3ca*^{E545K/WT} expression did not show a strong increase in p-AKT (S473) levels either. Since this variant showed strong vascular lesions and high kinase activity, we expected PI3K α -AKT pathway activation similar to *Pik3ca*^{H1047R/WT} expression. Consequently, we hypothesized this variant might be inducing VMs by manipulating different pathways than PI3K α -AKT. However, when we studied the MAPK pathway, we showed that both *Pik3ca*^{H1047R/WT} and *Pik3ca*^{E545K/WT} expression decreased MAPK pathway signalling in full medium and

starvation conditions. This is supported by previous research showing that augmented PI3K activity can downregulate MAPK signalling by multiple interactions (226-228).

As a consequence, we examined how *Pik3ca*^{E545K/WT} expression could generate a strong phenotype in the vasculature without strong activation of the PI3K α -AKT pathway. We hypothesized that *in vivo*, *Pik3ca*^{E545K/WT}-expressing ECs receive specific growth factors from their environment contributing to the formation of a VM, which is not recapitulated well in the *in vitro* context in normal or starvation medium. Supplying these growth factors *in vitro* might therefore reveal further pathway activation in *Pik3ca*^{E545K/WT}-expressing ECs. We treated cultured ECs with VEGFC and EGF, 2 important growth factors for vascular development. Both families of receptors for these ligands (VEGFR and EGFR) have been shown to regulate PI3K signalling directly or indirectly (56, 175, 232, 237, 286) Specifically, VEGFRs can activate PI3K α -AKT pathway signalling, however, they typically don't do this directly and navigate the pathway via Ras. EGFR has pY-sites that can activate both Ras-ERK signalling and PI3K α -AKT pathway signalling depending on the adaptor molecules (242).

We found that *Pik3ca*^{H1047R/WT} expression increased PI3K α -AKT pathway signalling in all conditions (starved, iFBS-, VEGFC-, and EGF-stimulated) compared to control cells. However, p-AKT (T308) levels were not significantly changed between the conditions in *Pik3ca*^{H1047R/WT}-expressing ECs, showing that the PI3K α -AKT pathway is not further activated by these growth factors. *Pik3ca*^{E545K/WT}-expressing ECs showed little PI3K α -AKT pathway activation, only with EGF stimulation is there a mild increase in p-AKT (T308) levels. Therefore, EGFR could play an important role in the activation of this variant. Before, we observed downregulation of MAPK signalling with activated PI3K α signalling. Since both VEGFC and EGF activation have been associated with MAPK pathway activation through Ras, we explored p-ERK(T202/Y204) levels as well. When we compared the p-ERK(T202/Y204) levels in the variants to the control cells, we did not witness any changes. However, when we compared the conditions within each variant, we remarked that iFBS and EGF stimulation, and not VEGFC stimulation, increased p-ERK(T202/Y204) levels.

We theorized the different signal activation with these growth factors could be influenced by availability of the receptors for VEGFC and EGF. Namely, variant expression could modify transcriptomic expression of these receptors and alter the response to their stimulation. qPCR revealed that *Pik3ca*^{H1047R/WT} expression significantly upregulated the expression of VEGFR2 and VEGFR3, while *Pik3ca*^{E545K/WT} expression only slightly augmented expression of these receptors. Interestingly, increased VEGFA and VEGFR2

expression levels have been shown in embryos expressing *Pik3ca*^{H1047R/WT} ubiquitously (71). Interestingly, the EGFR was negatively regulated by *Pik3ca*^{H1047R/WT} expression and upregulated with *Pik3ca*^{E545K/WT} expression. This distinct control of *Egfr* in ECs could have interesting implications for the intracellular signalling activation by these variants. Interestingly, paracrine upregulation of EGF signalling by *PIK3CA* mutations has been observed in breast cancer cell lines (287). Whether the upregulation of *Egfr* expression, plays any role in the phenotypes generated by the *Pik3ca*^{E545K/WT} variant remains to be explored.

It should be noted that treatments in cultured ECs and subsequent western blotting are subjected to high variation between replicates. In-well confluency, the number of recombined ECs, the timing of treatment, and the western blot procedure all influence the outcome. Although we kept experimental handling as uniformly as possible, variation between replicates is evident, and therefore, we propose more replicates should be added to these results to solidify our conclusions.

In the cell functional assays, we mainly noted a difference in EC survival with *Pik3ca*^{H1047R/WT} and *Pik3ca*^{E545K/WT} expression in nutrient-deprived conditions. No changes in proliferation or migration were observed. It is important to acknowledge that these experiments were conducted at a different institute due to the availability of specialized expertise and access to the IncuCyte system. As a result, the ECs were subjected to cryopreservation and transport prior to experimentation. Based on prior experience, the ECs exhibited altered behaviour at the external location, including slower growth and a less healthy morphology compared to their typical behaviour at the home institute. These factors may have influenced the experimental observations and should be considered when interpreting the results. We expected an increase in proliferation with expression of the variants in ECs, as has been observed in other cell types (277, 278). Yet, we observed no significant proliferation in the cultured ECs. In contrast to our findings, research on vascular malformations caused by PI3K α overactivation *in vivo* did reveal increased proliferation of ECs (73, 89). Therefore, we propose that *in vitro* EdU-incorporation assays might not be optimal to study cellular proliferation. The confluency of the ECs and the timing of EdU-incorporation can influence the outcome and could explain why we don't see increased levels of proliferation. Further optimization is required to determine the optimal conditions for this experimental technique.

Next, we observed no changes in migratory capacity in the *Pik3ca*^{H1047R/WT} and *Pik3ca*^{E545K/WT} expression ECs. In starvation, *Pik3ca*^{H1047R/WT}-expressing ECs did migrate better than *Pik3ca*^{E545K/WT}-expressing ECs or controls, this could be due to the high PI3K α

activity we observed for this variant. Of note, *PIK3CA*^{E545K} expression in HeLa and cervical cancer (CaSki) cell lines did increase their migratory phenotype (288).

As mentioned, other assays could reveal important characteristics of the vascular phenotypes generated by the variants. *In vitro*, paxillin immunostaining could be used to study cell adhesion, and beta-catenin immunostaining could be used to measure EC size. These processes could be influenced by variant expression and reveal important aspects of *PIK3CA* pathology. As mentioned, *in vivo* models might be more useful to study functional differences in mutated clones. For example, EdU-incorporation assays in the retina model are useful to study proliferation. The use of certain reporter mouse lines and combinations with different doses of 4-OHT can reveal other characteristics, such as clonal expansion, cell size, cell differentiation into different subpopulation, etc. Therefore, we conclude additional research could reveal new insights in the specific pathogenicity of the studied variants.

III. Objective 3: Exploring the signalling differences between *Pik3ca*^{H1047R} and *Pik3ca*^{E545K} *in vivo* during vascular malformation development.

We employed the retina model for the purpose of translating the signalling differences from objective II. The 4-OHT dose we used in objective I was to promote maximum recombination to accurately compare the severity of the phenotype between variants. To study the signalling, maximum recombination is not required, and more isolated lesions are preferred to measure certain markers in recombined clones. *Kobialka et al.* already tested several 4-OHT doses to achieve more isolated lesions for *Pik3ca*^{H1047R/WT} (73). They still noticed vascular lesions when reducing the 4-OHT dose to 0.125 mg/kg. We attempted to study the dose-response for *Pik3ca*^{E545K/WT} and detected no vascular lesions and only a small number of recombined clones with 0.125 and 0.25 mg/kg 4-OHT doses. This could be attributed to *Pik3ca*^{E545K/WT}-expressing ECs not being as potent to expand and generate a vascular phenotype like *Pik3ca*^{H1047R/WT}, or it could be that the *Pik3ca*^{E545K/WT} construct does not recombine as well as the *Pik3ca*^{H1047R/WT} construct with these low 4-OHT concentrations. However, we required vascular lesions to study the signalling differences, so we opted for the 2.5 mg/kg 4-OHT dose, where lesions were observed with *Pik3ca*^{E545K/WT} expression. Though, these lesions were massive and similar to the full dose (25 mg/kg) lesions from objective I. This substantiates that 4-OHT dose is not always directly correlated to the number of recombined clones. Due to time constraints, we could not explore other 4-OHT doses, although it would be interesting to

have tried several more and compare the phenotypes between *Pik3ca*^{H1047R/WT} and *Pik3ca*^{E545K/WT} to better understand dose-responses for both variants. This approach could provide valuable insights into the recombination kinetics of both constructs, the expansion dynamics of recombined cells, and their contribution to lesion size and preferred endothelial subpopulations.

First, we examined PI3K α -AKT pathway activation by staining for p-S6 (S235/236). Of note, S6 is a downstream effector of AKT, but there are several molecular regulators between PI3K α and S6. More direct markers would be more insightful to study PI3K α -AKT activation. Staining for p-AKT (S473) was attempted, but not successful. Increased PI3K α -AKT pathway activation by immunostaining for p-S6 (S235/236) in *Pik3ca*^{H1047R/WT} mouse retinas was already confirmed (73, 89). We managed to do the immunostaining for p-S6 (S235/236) in *Pik3ca*^{E545K/WT} mouse retinas and observed no increase in p-S6 (S235/236) intensity compared to controls. The lack of increased p-S6 (S235/236) levels could indicate that *Pik3ca*^{E545K/WT} expression does not activate p-S6 but may signal through alternative pathways and therefore immunostaining for this marker may not reflect PI3K α activation. Otherwise, perhaps the experimental conditions and immunostaining protocol were not optimal to verify p-S6 activation. However, this does corroborate our *in vitro* results, where we observed little PI3K α -AKT pathway activation with *Pik3ca*^{E545K/WT} expression. Ideally, more biological replicates should be added to confirm if there is indeed no augmentation of p-S6 (S235/236) levels.

Differences in MAPK signalling were observed with variant expression *in vivo*, which highlight distinct pathway activation patterns for *Pik3ca*^{H1047R/WT} and *Pik3ca*^{E545K/WT}. Specifically, we observed augmented p-ERK (T202/Y204) intensity levels relative to controls in *Pik3ca*^{H1047R/WT} and not *Pik3ca*^{E545K/WT}. When we quantified p-ERK+/GFP+ area to measure the distribution of p-ERK (T202/Y204) signalling, we observed no significant change in *Pik3ca*^{H1047R/WT} and a decrease in *Pik3ca*^{E545K/WT}.

In objective II, we noticed a decrease in p-ERK (T202/Y204) levels *in vitro* with *Pik3ca*^{H1047R/WT} expression starved conditions, however, in contrast to what we observe in the retina. We did notice increased expression of *Vegfr2* and *Vegfr3*, perhaps this upregulation is present in mouse retinas as well and could be for MAPK pathway activation in this context. The activation of both PI3K α -AKT and MAPK pathway in the mouse retina with *Pik3ca*^{H1047R/WT} signalling might explain why this variant generates massive vascular lesions.

Objective II showed little PI3K α -AKT and MAPK pathway activation in cultured ECs for the *Pik3ca*^{E545K/WT} variant, and *in vivo* we observed no PI3K α -AKT or MAPK pathway

activation. The significant decrease in p-ERK+/GFP+ area is interesting though, this could indicate an overall downregulation of MAPK signalling. This could be possible due to previous research in cultured EC lines that demonstrated that activated PI3K α -AKT can inhibit Raf1 phosphorylation (226-228). Immunostaining *in vivo* or western blotting in cultured ECs for p-Raf1 could corroborate this hypothesis and explain why MAPK signalling is downregulated with *Pik3ca*^{E545K/WT} expression. Another explanation for the decrease in p-ERK+/GFP+ area could be the redistribution of p-ERK in the ECs of the retina, with p-ERK becoming more concentrated in certain areas, for example in lesions, or in the nuclei of recombined ECs. Interestingly, nuclear translocation of p-ERK is essential for promoting proliferation (289). However, we didn't observe the concentration of p-ERK in any regions when inspecting the generated images. This phenomenon could be quantified by co-staining with ERG (a marker for EC nuclei) and measurements of p-ERK+/ERG+ area.

The conditional mouse retina model we employed during this thesis are helpful tools to study VM onset in a reproducible manner. Kobińska et al. already showed the preclinical use of the *Pik3ca*^{H1047R} retina model for the treatment of VMs with the AKT inhibitor Miransertib (73). The retina models for the other variants can be exploited for this purpose as well. Specifically, the distinct mechanisms of signalling activation between *Pik3ca*^{H1047R/WT} and *Pik3ca*^{E545K/WT} could be of interest when considering the treatment of VMs. We wanted to test the impact of Trametinib, a MEK1/2 inhibitor, on the rescue of the vascular phenotype in both variants, unfortunately, we did not manage to include it in this thesis due to time constraints. In *Pik3ca*^{H1047R/WT} mouse retinas, treatment with trametinib could have been used to verify that the MAPK pathway plays a role in the formation of the vascular lesions caused by the variant's expression. Potentially, Trametinib could prove beneficial for the treatment of lesions caused by *Pik3ca*^{H1047R/WT} expression. Interestingly, Trametinib already proved beneficial in the treatment of arteriovenous malformations caused by oncogenic KRAS mutations in mice, and in some rare cases with patient with arteriovenous malformations or advanced CCLA (central conducting lymphatic anomaly) (290-293).

Other approaches could be beneficial as well, we have seen *in vitro* that *Pik3ca*^{H1047R/WT} expression, and to a lesser extent *Pik3ca*^{E545K/WT} expression, upregulates *Vegfr2* and *Vegfr3* gene expression. VEGFR inhibitors have already been used to treat certain cancers, and over 340 clinical trials related to VEGFR inhibitors in cancer are ongoing (294). Perhaps, VEGFR inhibitors could be useful as well in the treatment of PI3K α -related VMs, with or without the combination of PI3K α inhibitors. The same could be considered for *Pik3ca*^{E545K/WT}-related VMs, where we noticed upregulation of *Egfr* gene

expression with this variant in cultured ECs. EGFR inhibitors are already approved by the FDA for the treatment of non small cell lung carcinoma, breast cancer, and pancreatic cancer among other, and several clinical trials for EGFR inhibitors to treat other cancers are still ongoing (295). So far, neither VEGFR nor EGFR inhibitors have been tested for treatment of VMs.

To conclude, this thesis investigated three PROS hotspots by use of conditional mouse models allowing spatiotemporal control of variant expression. *in vivo*, *Pik3ca*^{H1047R/WT} and *Pik3ca*^{E545K/WT} expression revealed massive hyperplasia and increased EC number. We also revealed that active angiogenesis is required for VM formation. Interestingly, these variants showcased distinct activation pathways intracellularly, with *Pik3ca*^{H1047R/WT} expression strongly activating PI3K α -AKT and MAPK signalling, upregulating VEGFR2 and VEGFR3, and slightly downregulating EGFR. *Pik3ca*^{E545K/WT} expression, on the other hand, showed less PI3K α -AKT activation and potentially downregulation of MAPK *in vivo*, while slightly upregulating VEGFR2 and VEGFR3 and EGFR. These signalling differences could be exploited for therapeutic intervention. *Pik3ca*^{E726K/WT} expression only resulted in mild vascular phenotypes, and mild PI3K α -AKT activation, supporting the hypothesis that this variant results in milder PROS phenotypes because of earlier embryonic tolerance, though this should be further investigated.

Conclusions

- Expression of *Pik3ca*^{H1047R} and *Pik3ca*^{E545K} in ECs during retinal angiogenesis results in profound vascular malformations. Instead, expression of these variants during vascular remodelling leads to minor phenotypes in vessels.
- Expression of *Pik3ca*^{E726K} in ECs only results in minor vascular overgrowth when the mutation is expressed during retinal angiogenesis.
- Expression of *Pik3ca*^{E545K} in all ECs during embryonic development results in embryonic lethality at mid-gestation.
- Kinase activity assays, and signalling and transcriptomic analyses showed that *PIK3CA*^{H1047R}, compared to *PIK3CA*^{E545K} and *PIK3CA*^{E726K}, is the strongest activating *PIK3CA* mutation.
- VEGFC and EGF prominently activate PI3K signalling upon expression of *Pik3ca*^{H1047R} in cultured ECs. Instead, EGF but not VEGFC activates PI3K signalling downstream of *Pik3ca*^{E545K} in cultured ECs.
- Expression of *Pik3ca*^{H1047R} and *Pik3ca*^{E545K} improve endothelial cell survival in starved medium conditions.
- *Pik3ca*^{H1047R/WT} retinas show robust MAPK pathway activation, while *Pik3ca*^{E545K/WT} retinas exhibit minimal PI3K α -AKT and MAPK activation.

References

1. Whitman M, Downes CP, Keeler M, Keller T, Cantley L. Type I phosphatidylinositol kinase makes a novel inositol phospholipid, phosphatidylinositol-3-phosphate. *Nature*. 1988;332(6165):644-646. doi:10.1038/332644a0
2. Fruman DA, Chiu H, Hopkins BD, Bagrodia S, Cantley LC, Abraham RT. The PI3K Pathway in Human Disease. *Cell*. 2017;170(4):605-635. doi:10.1016/j.cell.2017.07.029
3. Goncalves MD, Hopkins BD, Cantley LC. Phosphatidylinositol 3-Kinase, Growth Disorders, and Cancer. *N Engl J Med*. 2018;379(21):2052-2062. doi:10.1056/NEJMra1704560
4. Burke JE, Triscott J, Emerling BM, Hammond GRV. Beyond PI3Ks: targeting phosphoinositide kinases in disease. *Nat Rev Drug Discov*. 2023;22(5):357-386. doi:10.1038/s41573-022-00582-5
5. Mellor P, Furber LA, Nyarko JN, Anderson DH. Multiple roles for the p85 α isoform in the regulation and function of PI3K signalling and receptor trafficking. *Biochem J*. 2012;441(1):23-37. doi:10.1042/BJ20111164
6. Rathinaswamy MK, Dalwadi U, Fleming KD, et al. Structure of the phosphoinositide 3-kinase (PI3K) p110 γ -p101 complex reveals molecular mechanism of GPCR activation. *Sci Adv*. 2021;7(35):eabj4282. Published 2021 Aug 27. doi:10.1126/sciadv.abj4282
7. Fox M, Mott HR, Owen D. Class IA PI3K regulatory subunits: p110-independent roles and structures. *Biochem Soc Trans*. 2020;48(4):1397-1417. doi:10.1042/BST20190845
8. Bilanges B, Posor Y, Vanhaesebroeck B. PI3K isoforms in cell signalling and vesicle trafficking. *Nat Rev Mol Cell Biol*. 2019;20(9):515-534. doi:10.1038/s41580-019-0129-z
9. Campa CC, Franco I, Hirsch E. PI3K-C2 α : One enzyme for two products coupling vesicle trafficking and signal transduction. *FEBS Lett*. 2015;589(14):1552-1558. doi:10.1016/j.febslet.2015.05.001
10. Gulluni F, Martini M, De Santis MC, et al. Mitotic Spindle Assembly and Genomic Stability in Breast Cancer Require PI3K-C2 α Scaffolding Function. *Cancer Cell*. 2017;32(4):444-459.e7. doi:10.1016/j.ccell.2017.09.002
11. Kobiialka P, Llana J, Deleyto-Seldas N, et al. PI3K-C2 β limits mTORC1 signaling and angiogenic growth. *Sci Signal*. 2023;16(813):eadg1913. doi:10.1126/scisignal.adg1913
12. Braccini L, Ciruolo E, Campa CC, et al. PI3K-C2 γ is a Rab5 effector selectively controlling endosomal Akt2 activation downstream of insulin signalling. *Nat Commun*. 2015;6:7400. Published 2015 Jun 23. doi:10.1038/ncomms8400
13. Jaber N, Dou Z, Chen JS, et al. Class III PI3K Vps34 plays an essential role in autophagy and in heart and liver function. *Proc Natl Acad Sci U S A*. 2012;109(6):2003-2008. doi:10.1073/pnas.1112848109
14. Bilanges B, Alliouachene S, Pearce W, et al. Vps34 PI 3-kinase inactivation enhances insulin sensitivity through reprogramming of mitochondrial metabolism. *Nat Commun*. 2017;8(1):1804. Published 2017 Nov 27. doi:10.1038/s41467-017-01969-4
15. Vanhaesebroeck B, Guillermet-Guibert J, Graupera M, Bilanges B. The emerging mechanisms of isoform-specific PI3K signalling. *Nat Rev Mol Cell Biol*. 2010;11(5):329-341. doi:10.1038/nrm2882
16. Burke JE, Williams RL. Dynamic steps in receptor tyrosine kinase mediated activation of class IA phosphoinositide 3-kinases (PI3K) captured by H/D exchange (HDX-MS). *Adv Biol Regul*. 2013;53(1):97-110. doi:10.1016/j.jbior.2012.09.005
17. Madsen RR, Vanhaesebroeck B. Cracking the context-specific PI3K signaling code. *Sci Signal*. 2020;13(613):eaay2940. Published 2020 Jan 7. doi:10.1126/scisignal.aay2940
18. Rathinaswamy MK, Burke JE. Class I phosphoinositide 3-kinase (PI3K) regulatory subunits and their roles in signaling and disease. *Adv Biol Regul*. 2020;75:100657. doi:10.1016/j.jbior.2019.100657

19. Liu X, Yang S, Hart JR, et al. Cryo-EM structures of PI3K α reveal conformational changes during inhibition and activation. *Proc Natl Acad Sci U S A*. 2021;118(45):e2109327118. doi:10.1073/pnas.2109327118
20. Jenkins ML, Ranga-Prasad H, Parson MAH, Harris NJ, Rathinaswamy MK, Burke JE. Oncogenic mutations of PIK3CA lead to increased membrane recruitment driven by reorientation of the ABD, p85 and C-terminus. *Nat Commun*. 2023;14(1):181. Published 2023 Jan 12. doi:10.1038/s41467-023-35789-6
21. Murillo MM, Zelenay S, Nye E, et al. RAS interaction with PI3K p110 α is required for tumor-induced angiogenesis. *J Clin Invest*. 2014;124(8):3601-3611. doi:10.1172/JCI74134
22. Siempelkamp BD, Rathinaswamy MK, Jenkins ML, Burke JE. Molecular mechanism of activation of class IA phosphoinositide 3-kinases (PI3Ks) by membrane-localized HRas. *J Biol Chem*. 2017;292(29):12256-12266. doi:10.1074/jbc.M117.789263
23. Buckles TC, Ziemba BP, Masson GR, Williams RL, Falke JJ. Single-Molecule Study Reveals How Receptor and Ras Synergistically Activate PI3K α and PIP₃ Signaling. *Biophys J*. 2017;113(11):2396-2405. doi:10.1016/j.bpj.2017.09.018
24. Denley A, Kang S, Karst U, Vogt PK. Oncogenic signaling of class I PI3K isoforms. *Oncogene*. 2008;27(18):2561-2574. doi:10.1038/sj.onc.1210918
25. Pacold ME, Suire S, Perisic O, et al. Crystal structure and functional analysis of Ras binding to its effector phosphoinositide 3-kinase gamma. *Cell*. 2000;103(6):931-943. doi:10.1016/s0092-8674(00)00196-3
26. Engelman JA, Luo J, Cantley LC. The evolution of phosphatidylinositol 3-kinases as regulators of growth and metabolism. *Nat Rev Genet*. 2006;7(8):606-619. doi:10.1038/nrg1879
27. Manning BD, Cantley LC. AKT/PKB signaling: navigating downstream. *Cell*. 2007;129(7):1261-1274. doi:10.1016/j.cell.2007.06.009
28. Manning BD, Toker A. AKT/PKB Signaling: Navigating the Network. *Cell*. 2017;169(3):381-405. doi:10.1016/j.cell.2017.04.001
29. Huang J, Manning BD. A complex interplay between Akt, TSC2 and the two mTOR complexes. *Biochem Soc Trans*. 2009;37(Pt 1):217-222. doi:10.1042/BST0370217
30. Calnan DR, Brunet A. The FoxO code. *Oncogene*. 2008;27(16):2276-2288. doi:10.1038/onc.2008.21
31. Cross DA, Alessi DR, Cohen P, Andjelkovich M, Hemmings BA. Inhibition of glycogen synthase kinase-3 by insulin mediated by protein kinase B. *Nature*. 1995;378(6559):785-789. doi:10.1038/378785a0
32. Sano H, Kane S, Sano E, et al. Insulin-stimulated phosphorylation of a Rab GTPase-activating protein regulates GLUT4 translocation. *J Biol Chem*. 2003;278(17):14599-14602. doi:10.1074/jbc.C300063200
33. Zhou, B., Liao, Y., Xia, W. *et al.* HER-2/*neu* induces p53 ubiquitination via Akt-mediated MDM2 phosphorylation. *Nat Cell Biol* **3**, 973–982 (2001). <https://doi.org/10.1038/ncb1101-973>
34. Krugmann S, Williams R, Stephens L, Hawkins PT. ARAP3 is a PI3K- and rap-regulated GAP for RhoA. *Curr Biol*. 2004;14(15):1380-1384. doi:10.1016/j.cub.2004.07.058
35. Kiyokawa E, Hashimoto Y, Kobayashi S, Sugimura H, Kurata T, Matsuda M. Activation of Rac1 by a Crk SH3-binding protein, DOCK180. *Genes Dev*. 1998;12(21):3331-3336. doi:10.1101/gad.12.21.3331
36. Bruhn MA, Pearson RB, Hannan RD, Sheppard KE. AKT-independent PI3-K signaling in cancer - emerging role for SGK3. *Cancer Manag Res*. 2013;5:281-292. Published 2013 Aug 26. doi:10.2147/CMAR.S35178
37. Desiderio S. Role of Btk in B cell development and signaling. *Curr Opin Immunol*. 1997;9(4):534-540. doi:10.1016/s0952-7915(97)80107-0

38. Hopkins BD, Hodakoski C, Barrows D, Mense SM, Parsons RE. PTEN function: the long and the short of it. *Trends Biochem Sci.* 2014;39(4):183-190. doi:10.1016/j.tibs.2014.02.006
39. Samuels Y, Wang Z, Bardelli A, et al. High frequency of mutations of the PIK3CA gene in human cancers. *Science.* 2004;304(5670):554. doi:10.1126/science.1096502
40. Arafeh R, Samuels Y. PIK3CA in cancer: The past 30 years. *Semin Cancer Biol.* 2019;59:36-49. doi:10.1016/j.semcancer.2019.02.002
41. Kandoth C, McLellan MD, Vandin F, et al. Mutational landscape and significance across 12 major cancer types. *Nature.* 2013;502(7471):333-339. doi:10.1038/nature12634
42. Lawrence MS, Stojanov P, Mermel CH, et al. Discovery and saturation analysis of cancer genes across 21 tumour types. *Nature.* 2014;505(7484):495-501. doi:10.1038/nature12912
43. Van Keymeulen A, Lee MY, Ousset M, et al. Reactivation of multipotency by oncogenic PIK3CA induces breast tumour heterogeneity. *Nature.* 2015;525(7567):119-123. doi:10.1038/nature14665
44. Koren S, Reavie L, Couto JP, et al. PIK3CA(H1047R) induces multipotency and multi-lineage mammary tumours. *Nature.* 2015;525(7567):114-118. doi:10.1038/nature14669
45. Koren S, Bentires-Alj M. Mouse models of PIK3CA mutations: one mutation initiates heterogeneous mammary tumors. *FEBS J.* 2013;280(12):2758-2765. doi:10.1111/febs.12175
46. Liu X, Zhou Q, Hart JR, et al. Cryo-EM structures of cancer-specific helical and kinase domain mutations of PI3K α . *Proc Natl Acad Sci U S A.* 2022;119(46):e2215621119. doi:10.1073/pnas.2215621119
47. Liu X, Yang S, Hart JR, et al. Cryo-EM structures of PI3K α reveal conformational changes during inhibition and activation. *Proc Natl Acad Sci U S A.* 2021;118(45):e2109327118. doi:10.1073/pnas.2109327118
48. Burke JE, Perisic O, Masson GR, Vadas O, Williams RL. Oncogenic mutations mimic and enhance dynamic events in the natural activation of phosphoinositide 3-kinase p110 α (PIK3CA). *Proc Natl Acad Sci U S A.* 2012;109(38):15259-15264. doi:10.1073/pnas.1205508109
49. Zhao L, Vogt PK. Hot-spot mutations in p110 α of phosphatidylinositol 3-kinase (p13K): differential interactions with the regulatory subunit p85 and with RAS. *Cell Cycle.* 2010;9(3):596-600. doi:10.4161/cc.9.3.10599
50. Carson JD, Van Aller G, Lehr R, et al. Effects of oncogenic p110 α subunit mutations on the lipid kinase activity of phosphoinositide 3-kinase. *Biochem J.* 2008;409(2):519-524. doi:10.1042/BJ20070681
51. Vasan N, Razavi P, Johnson JL, et al. Double PIK3CA mutations in cis increase oncogenicity and sensitivity to PI3K α inhibitors. *Science.* 2019;366(6466):714-723. doi:10.1126/science.aaw9032
52. Keppler-Noreuil KM, Sapp JC, Lindhurst MJ, et al. Clinical delineation and natural history of the PIK3CA-related overgrowth spectrum. *Am J Med Genet A.* 2014;164A(7):1713-1733. doi:10.1002/ajmg.a.36552
53. Madsen RR, Vanhaesebroeck B, Semple RK. Cancer-Associated PIK3CA Mutations in Overgrowth Disorders. *Trends Mol Med.* 2018;24(10):856-870. doi:10.1016/j.molmed.2018.08.003
54. Mussa A, Leoni C, Iacoviello M, et al. Genotypes and phenotypes heterogeneity in PIK3CA-related overgrowth spectrum and overlapping conditions: 150 novel patients and systematic review of 1007 patients with PIK3CA pathogenetic variants. *J Med Genet.* 2023;60(2):163-173. doi:10.1136/jmedgenet-2021-108093
55. Angulo-Urarte A, Graupera M. When, where and which PIK3CA mutations are pathogenic in congenital disorders. *Nat Cardiovasc Res.* 2022;1(8):700-714. doi:10.1038/s44161-022-00107-8

56. Rivière JB, Mirzaa GM, O'Roak BJ, et al. De novo germline and postzygotic mutations in AKT3, PIK3R2 and PIK3CA cause a spectrum of related megalencephaly syndromes. *Nat Genet.* 2012;44(8):934-940. Published 2012 Jun 24. doi:10.1038/ng.2331
57. Park HJ, Shin CH, Yoo WJ, et al. Detailed analysis of phenotypes and genotypes in megalencephaly-capillary malformation-polymicrogyria syndrome caused by somatic mosaicism of PIK3CA mutations. *Orphanet J Rare Dis.* 2020;15(1):205. Published 2020 Aug 10. doi:10.1186/s13023-020-01480-y
58. Mirzaa G, Timms AE, Conti V, et al. PIK3CA-associated developmental disorders exhibit distinct classes of mutations with variable expression and tissue distribution. *JCI Insight.* 2016;1(9):e87623. doi:10.1172/jci.insight.87623
59. Brouillard P, Schlögel MJ, Hoday N, et al. Non-hotspot PIK3CA mutations are more frequent in CLOVES than in common or combined lymphatic malformations. *Orphanet J Rare Dis.* 2021;16(1):267. Published 2021 Jun 10. doi:10.1186/s13023-021-01898-y
60. Dogruluk T, Tsang YH, Espitia M, et al. Identification of Variant-Specific Functions of PIK3CA by Rapid Phenotyping of Rare Mutations. *Cancer Res.* 2015;75(24):5341-5354. doi:10.1158/0008-5472.CAN-15-1654
61. Gymnopoulos M, Elsliger MA, Vogt PK. Rare cancer-specific mutations in PIK3CA show gain of function. *Proc Natl Acad Sci U S A.* 2007;104(13):5569-5574. doi:10.1073/pnas.0701005104
62. Jansen LA, Mirzaa GM, Ishak GE, et al. PI3K/AKT pathway mutations cause a spectrum of brain malformations from megalencephaly to focal cortical dysplasia. *Brain.* 2015;138(Pt 6):1613-1628. doi:10.1093/brain/awv045
63. Usui H, Tsurusaki Y, Shimbo H, et al. A novel method for isolating lymphatic endothelial cells from lymphatic malformations and detecting PIK3CA somatic mutation in these isolated cells. *Surg Today.* 2021;51(3):439-446. doi:10.1007/s00595-020-02122-3
64. Hafner C, López-Knowles E, Luis NM, et al. Oncogenic PIK3CA mutations occur in epidermal nevi and seborrheic keratoses with a characteristic mutation pattern. *Proc Natl Acad Sci U S A.* 2007;104(33):13450-13454. doi:10.1073/pnas.0705218104
65. Lindhurst MJ, Parker VE, Payne F, et al. Mosaic overgrowth with fibroadipose hyperplasia is caused by somatic activating mutations in PIK3CA. *Nat Genet.* 2012;44(8):928-933. Published 2012 Jun 24. doi:10.1038/ng.2332
66. Rivière JB, Mirzaa GM, O'Roak BJ, et al. De novo germline and postzygotic mutations in AKT3, PIK3R2 and PIK3CA cause a spectrum of related megalencephaly syndromes. *Nat Genet.* 2012;44(8):934-940. Published 2012 Jun 24. doi:10.1038/ng.2331
67. Kurek KC, Luks VL, Ayturk UM, et al. Somatic mosaic activating mutations in PIK3CA cause CLOVES syndrome. *Am J Hum Genet.* 2012;90(6):1108-1115. doi:10.1016/j.ajhg.2012.05.006
68. Mirzaa G, Graham JM Jr, Keppler-Noreuil K. PIK3CA-Related Overgrowth Spectrum. In: Adam MP, Feldman J, Mirzaa GM, Pagon RA, Wallace SE, Amemiya A, eds. *GeneReviews®*. Seattle (WA): University of Washington, Seattle; August 15, 2013.
69. Canaud G, Hammill AM, Adams D, Vikkula M, Keppler-Noreuil KM. A review of mechanisms of disease across PIK3CA-related disorders with vascular manifestations. *Orphanet J Rare Dis.* 2021;16(1):306. Published 2021 Jul 8. doi:10.1186/s13023-021-01929-8
70. De Graer C, Marangoni M, Romnée S, et al. Novel features of PIK3CA-Related Overgrowth Spectrum: Lesson from an aborted fetus presenting a de novo constitutional PIK3CA mutation. *Eur J Med Genet.* 2020;63(4):103775. doi:10.1016/j.ejmg.2019.103775
71. Hare LM, Schwarz Q, Wiszniak S, et al. Heterozygous expression of the oncogenic Pik3ca(H1047R) mutation during murine development results in fatal embryonic and extraembryonic defects. *Dev Biol.* 2015;404(1):14-26. doi:10.1016/j.ydbio.2015.04.022

72. Berenjano IM, Piñeiro R, Castillo SD, et al. Oncogenic PIK3CA induces centrosome amplification and tolerance to genome doubling. *Nat Commun.* 2017;8(1):1773. Published 2017 Nov 24. doi:10.1038/s41467-017-02002-4
73. Kobińska P, Sabata H, Vilalta O, et al. The onset of PI3K-related vascular malformations occurs during angiogenesis and is prevented by the AKT inhibitor miransertib. *EMBO Mol Med.* 2022;14(7):e15619. doi:10.15252/emmm.202115619
74. Boscolo E, Coma S, Luks VL, et al. AKT hyper-phosphorylation associated with PI3K mutations in lymphatic endothelial cells from a patient with lymphatic malformation. *Angiogenesis.* 2015;18(2):151-162. doi:10.1007/s10456-014-9453-2
75. Kuentz P, St-Onge J, Duffourd Y, et al. Molecular diagnosis of PIK3CA-related overgrowth spectrum (PROS) in 162 patients and recommendations for genetic testing. *Genet Med.* 2017;19(9):989-997. doi:10.1038/gim.2016.220
76. Kłaniewska M, Rydzanicz M, Kosińska J, et al. CLOVES syndrome caused by mosaic mutation in the PIK3CA gene identified in fibroblasts. *Pediatrics Polska - Polish Journal of Paediatrics.* 2021;96(2):148-152. doi:10.5114/polp.2021.107401.
77. Ranieri C, Di Tommaso S, Loconte DC, et al. In vitro efficacy of ARQ 092, an allosteric AKT inhibitor, on primary fibroblast cells derived from patients with PIK3CA-related overgrowth spectrum (PROS). *Neurogenetics.* 2018;19(2):77-91. doi:10.1007/s10048-018-0540-1
78. Sun B, Jiang Y, Cui H, et al. Activating PIK3CA mutation promotes adipogenesis of adipose-derived stem cells in macrodactyly via up-regulation of E2F1. *Cell Death Dis.* 2020;11(7):600. Published 2020 Jul 30. doi:10.1038/s41419-020-02806-1
79. Couto JA, Konczyk DJ, Vivero MP, et al. Somatic PIK3CA mutations are present in multiple tissues of facial infiltrating lipomatosis. *Pediatr Res.* 2017;82(5):850-854. doi:10.1038/pr.2017.155
80. Martinez-Corral I, Zhang Y, Petkova M, et al. Blockade of VEGF-C signaling inhibits lymphatic malformations driven by oncogenic PIK3CA mutation. *Nat Commun.* 2020;11(1):2869. Published 2020 Jun 8. doi:10.1038/s41467-020-16496-y
81. Petkova M, Kraft M, Stritt S, et al. Immune-interacting lymphatic endothelial subtype at capillary terminals drives lymphatic malformation. *J Exp Med.* 2023;220(4):e20220741. doi:10.1084/jem.20220741
82. Cox JA, Bartlett E, Lee EI. Vascular malformations: a review. *Semin Plast Surg.* 2014;28(2):58-63. doi:10.1055/s-0034-1376263
83. Alhazzab A, Alkhaibary A, Khairy S, Alshaya W. CLOVES syndrome and cervical arteriovenous fistula: a unique association managed by combined microsurgical and endovascular therapy. *J Surg Case Rep.* 2021;2021(4):rjab122. Published 2021 Apr 19. doi:10.1093/jscr/rjab122
84. Martinez-Lopez A, Blasco-Morente G, Perez-Lopez I, et al. CLOVES syndrome: review of a PIK3CA-related overgrowth spectrum (PROS). *Clin Genet.* 2017;91(1):14-21. doi:10.1111/cge.12832
85. Borst AJ, Nakano TA, Blei F, Adams DM, Duis J. A Primer on a Comprehensive Genetic Approach to Vascular Anomalies. *Front Pediatr.* 2020;8:579591. Published 2020 Oct 19. doi:10.3389/fped.2020.579591
86. Limaye N, Wouters V, Uebelhoer M, et al. Somatic mutations in angiopoietin receptor gene TEK cause solitary and multiple sporadic venous malformations. *Nat Genet.* 2009;41(1):118-124. doi:10.1038/ng.272
87. Soblet J, Limaye N, Uebelhoer M, Boon LM, Vikkula M. Variable Somatic TIE2 Mutations in Half of Sporadic Venous Malformations. *Mol Syndromol.* 2013;4(4):179-183. doi:10.1159/000348327
88. Limaye N, Kangas J, Mendola A, et al. Somatic Activating PIK3CA Mutations Cause Venous Malformation. *Am J Hum Genet.* 2015;97(6):914-921. doi:10.1016/j.ajhg.2015.11.011

89. Castillo SD, Tzouanacou E, Zaw-Thin M, et al. Somatic activating mutations in *Pik3ca* cause sporadic venous malformations in mice and humans. *Sci Transl Med*. 2016;8(332):332ra43. doi:10.1126/scitranslmed.aad9982
90. Castel P, Carmona FJ, Grego-Bessa J, et al. Somatic PIK3CA mutations as a driver of sporadic venous malformations. *Sci Transl Med*. 2016;8(332):332ra42. doi:10.1126/scitranslmed.aaf1164
91. Luks VL, Kamitaki N, Vivero MP, et al. Lymphatic and other vascular malformative/overgrowth disorders are caused by somatic mutations in PIK3CA. *J Pediatr*. 2015;166(4):1048-54.e545. doi:10.1016/j.jpeds.2014.12.069
92. Rodriguez-Laguna L, Agra N, Ibañez K, et al. Somatic activating mutations in *PIK3CA* cause generalized lymphatic anomaly. *J Exp Med*. 2019;216(2):407-418. doi:10.1084/jem.20181353
93. Martinez-Corral I, Zhang Y, Petkova M, et al. Blockade of VEGF-C signaling inhibits lymphatic malformations driven by oncogenic PIK3CA mutation. *Nat Commun*. 2020;11(1):2869. Published 2020 Jun 8. doi:10.1038/s41467-020-16496-y
94. Goss JA, Konczyk DJ, Smits P, et al. Diffuse capillary malformation with overgrowth contains somatic PIK3CA variants. *Clin Genet*. 2020;97(5):736-740. doi:10.1111/cge.13702
95. Reynolds G, Cardaropoli S, Carli D, et al. Epidemiology of the disorders of the *Pik3ca*-related overgrowth spectrum (Pros). *Eur J Hum Genet*. 2023;31(11):1333-1336. doi:10.1038/s41431-023-01414-9
96. Blagosklonny MV. Cancer prevention with rapamycin. *Oncotarget*. 2023;14:342-350. Published 2023 Apr 14. doi:10.18632/oncotarget.28410
97. Ricci KW, Hammill AM, Mobberley-Schuman P, et al. Efficacy of systemic sirolimus in the treatment of generalized lymphatic anomaly and Gorham-Stout disease. *Pediatr Blood Cancer*. 2019;66(5):e27614. doi:10.1002/pbc.27614
98. Maruani A, Tavernier E, Boccara O, et al. Sirolimus (Rapamycin) for Slow-Flow Malformations in Children: The Observational-Phase Randomized Clinical PERFORMUS Trial. *JAMA Dermatol*. 2021;157(11):1289-1298. doi:10.1001/jamadermatol.2021.3459
99. Hammer J, Seront E, Duez S, et al. Sirolimus is efficacious in treatment for extensive and/or complex slow-flow vascular malformations: a monocentric prospective phase II study. *Orphanet J Rare Dis*. 2018;13(1):191. Published 2018 Oct 29. doi:10.1186/s13023-018-0934-z
100. Adams DM, Trenor CC 3rd, Hammill AM, et al. Efficacy and Safety of Sirolimus in the Treatment of Complicated Vascular Anomalies. *Pediatrics*. 2016;137(2):e20153257. doi:10.1542/peds.2015-3257
101. Parker VER, Keppler-Noreuil KM, Faivre L, et al. Safety and efficacy of low-dose sirolimus in the PIK3CA-related overgrowth spectrum. *Genet Med*. 2019;21(5):1189-1198. doi:10.1038/s41436-018-0297-9
102. Forde K, Resta N, Ranieri C, et al. Clinical experience with the AKT1 inhibitor miransertib in two children with PIK3CA-related overgrowth syndrome. *Orphanet J Rare Dis*. 2021;16(1):109. Published 2021 Feb 27. doi:10.1186/s13023-021-01745-0
103. Ours CA, Sapp JC, Hodges MB, de Moya AJ, Biesecker LG. Case report: five-year experience of AKT inhibition with miransertib (MK-7075) in an individual with Proteus syndrome. *Cold Spring Harb Mol Case Stud*. 2021;7(6):a006134. Published 2021 Dec 9. doi:10.1101/mcs.a006134
104. Biesecker LG, Edwards M, O'Donnell S, et al. Clinical report: one year of treatment of Proteus syndrome with miransertib (ARQ 092). *Cold Spring Harb Mol Case Stud*. 2020;6(1):a004549. Published 2020 Feb 3. doi:10.1101/mcs.a004549
105. Liu N, Rowley BR, Bull CO, et al. BAY 80-6946 is a highly selective intravenous PI3K inhibitor with potent p110 α and p110 δ activities in tumor cell lines and xenograft

models. *Mol Cancer Ther.* 2013;12(11):2319-2330. doi:10.1158/1535-7163.MCT-12-0993-T

106. Luu M, Vabres P, Devilliers H, et al. Safety and efficacy of low-dose PI3K inhibitor taselisib in adult patients with CLOVES and Klippel-Trenaunay syndrome (KTS): the TOTEM trial, a phase 1/2 multicenter, open-label, single-arm study. *Genet Med.* 2021;23(12):2433-2442. doi:10.1038/s41436-021-01290-y
107. André F, Ciruelos E, Rubovszky G, et al. Alpelisib for *PIK3CA*-Mutated, Hormone Receptor-Positive Advanced Breast Cancer. *N Engl J Med.* 2019;380(20):1929-1940. doi:10.1056/NEJMoa1813904
108. Venot Q, Blanc T, Rabia SH, et al. Targeted therapy in patients with *PIK3CA*-related overgrowth syndrome [published correction appears in *Nature*. 2019 Apr;568(7752):E6. doi: 10.1038/s41586-019-1109-3]. *Nature.* 2018;558(7711):540-546. doi:10.1038/s41586-018-0217-9
109. Pagliuzzi A, Oranges T, Traficante G, et al. *PIK3CA*-Related Overgrowth Spectrum From Diagnosis to Targeted Therapy: A Case of CLOVES Syndrome Treated With Alpelisib. *Front Pediatr.* 2021;9:732836. Published 2021 Sep 9. doi:10.3389/fped.2021.732836
110. Garreta Fontelles G, Pardo Pastor J, Grande Moreillo C. Alpelisib to treat CLOVES syndrome, a member of the *PIK3CA*-related overgrowth syndrome spectrum. *Br J Clin Pharmacol.* 2022;88(8):3891-3895. doi:10.1111/bcp.15270
111. Morin G, Degrugillier-Chopin C, Vincent M, et al. Treatment of two infants with *PIK3CA*-related overgrowth spectrum by alpelisib. *J Exp Med.* 2022;219(3):e20212148. doi:10.1084/jem.20212148
112. LBA23 EPIK-P1: Retrospective chart review study of patients (pts) with *PIK3CA*-related Overgrowth Spectrum (PROS) who have received alpelisib (ALP) as part of a compassionate use programme. Canaud, G. et al. *Annals of Oncology*, Volume 32, S1297
113. Delestre F, Venot Q, Bayard C, et al. Alpelisib administration reduced lymphatic malformations in a mouse model and in patients [published correction appears in *Sci Transl Med.* 2024 May 29;16(749):eadq3820. doi: 10.1126/scitranslmed.adq3820]. *Sci Transl Med.* 2021;13(614):eabg0809. doi:10.1126/scitranslmed.abg0809.
114. US Food Drug Adm. **2022**.. FDA approves alpelisib for *PIK3CA*-related overgrowth spectrum. . *US Food and Drug Administration.* <https://www.fda.gov/drugs/resources-information-approved-drugs/fda-approves-alpelisib-pik3ca-related-overgrowth-spectrum>
115. Morin GM, Zerbib L, Kaltenbach S, et al. *PIK3CA*-Related Disorders: From Disease Mechanism to Evidence-Based Treatments. *Annu Rev Genomics Hum Genet.* 2024;25(1):211-237. doi:10.1146/annurev-genom-121222-114518
116. Burke JE, Triscott J, Emerling BM, Hammond GRV. Beyond PI3Ks: targeting phosphoinositide kinases in disease. *Nat Rev Drug Discov.* 2023;22(5):357-386. doi:10.1038/s41573-022-00582-5
117. Loredana Puca, Anke Klippel. LOXO-783: A potent, highly mutant selective and brain-penetrant allosteric PI3K α H1047R inhibitor in combination with standard of care (SOC) treatments in preclinical PI3K α H1047R-mutant breast cancer models [abstract]. In: Proceedings of the 2022 San Antonio Breast Cancer Symposium; 2022 Dec 6-10; San Antonio, TX. Philadelphia (PA): AACR; Cancer Res 2023;83(5 Suppl):Abstract nr P4-08-02.
118. Wang, YX; Wang, ZH (Wang, Zhenghe). GENES & DISEASES 12, 2. DOI 10.1016/j.gendis.2024.101430 MAR 2025
119. Anke Klippel, Rui Wang, Barbara J. Brandhuber; Abstract P142: Preclinical characterization of LOX-22783, a highly potent, mutant-selective and brain-penetrant allosteric PI3K α H1047R inhibitor. *Mol Cancer Ther* 1 December 2021; 20 (12_Supplement): P142. <https://doi.org/10.1158/1535-7163.TARG-21-P142>
120. Andreas Varkaris, Komal Jhaveri, Alison M. Schram; Abstract CT017: Pan-mutant and isoform selective PI3K α inhibitor, RLY-2608, demonstrates selective targeting in a first-in-

human study of *PIK3CA*-mutant solid tumor patients, ReDiscover trial. *Cancer Res* 15 April 2023; 83 (8_Supplement): CT017. <https://doi-org.sire.ub.edu/10.1158/1538-7445.AM2023-CT017>

121. Eelen G, Treppe L, Li X, Carmeliet P. Basic and Therapeutic Aspects of Angiogenesis Updated. *Circ Res*. 2020;127(2):310-329. doi:10.1161/CIRCRESAHA.120.316851
122. Carmeliet P. Angiogenesis in health and disease. *Nat Med*. 2003;9(6):653-660. doi:10.1038/nm0603-653
123. Tucker WD, Arora Y, Mahajan K. Anatomy, Blood Vessels. [Updated 2023 Aug 8]. In: StatPearls [Internet]. Treasure Island (FL): StatPearls Publishing; 2025 Jan-. Available from: <https://www.ncbi.nlm.nih.gov/books/NBK470401/>
124. Null M, Arbor TC, Agarwal M. Anatomy, Lymphatic System. [Updated 2023 Mar 6]. In: StatPearls [Internet]. Treasure Island (FL): StatPearls Publishing; 2025 Jan-. Available from: <https://www.ncbi.nlm.nih.gov/books/NBK513247/>
125. Johnston-Cox H, Fuster V, Kovacic JC. Biology of the Vessel Wall. In: Fuster V, Harrington RA, Narula J, Eapen ZJ. eds. *Hurst's The Heart*, 14e. McGraw Hill; 2017. Accessed 7/10/2022.
126. Krüger-Genge A, Blocki A, Franke RP, Jung F. Vascular Endothelial Cell Biology: An Update (<https://pubmed.ncbi.nlm.nih.gov/31500313/>). *Int J Mol Sci*. 2019;20(18):4411. Accessed 7/10/2022.
127. Lin A, Peiris NJ, Dhaliwal H, et al. Mural Cells: Potential Therapeutic Targets to Bridge Cardiovascular Disease and Neurodegeneration. *Cells*. 2021;10(3):593. Published 2021 Mar 8. doi:10.3390/cells10030593
128. van Splunder H, Villacampa P, Martínez-Romero A, Graupera M. Pericytes in the disease spotlight. *Trends Cell Biol*. 2024;34(1):58-71. doi:10.1016/j.tcb.2023.06.001
129. Gerecht-Nir S, Osenberg S, Nevo O, Ziskind A, Coleman R, Itskovitz-Eldor J. Vascular development in early human embryos and in teratomas derived from human embryonic stem cells. *Biol Reprod*. 2004;71(6):2029-2036. doi:10.1095/biolreprod.104.031930
130. Monga I, Kaur K, Dhanda SK. Revisiting hematopoiesis: applications of the bulk and single-cell transcriptomics dissecting transcriptional heterogeneity in hematopoietic stem cells. *Brief Funct Genomics*. 2022;21(3):159-176. doi:10.1093/bfpg/elac002
131. Gonzalez-Crussi F. Vasculogenesis in the chick embryo. An ultrastructural study. *Am J Anat*. 1971;130(4):441-460. doi:10.1002/aja.1001300406
132. Risau W, Flamme I. Vasculogenesis. *Annu Rev Cell Dev Biol*. 1995;11:73-91. doi:10.1146/annurev.cb.11.110195.000445
133. Plein A, Fantin A, Denti L, Pollard JW, Ruhrberg C. Erythro-myeloid progenitors contribute endothelial cells to blood vessels. *Nature*. 2018;562(7726):223-228. doi:10.1038/s41586-018-0552-x
134. Nikolova G, Lammert E. Interdependent development of blood vessels and organs. *Cell Tissue Res*. 2003;314(1):33-42. doi:10.1007/s00441-003-0739-8
135. Sato Y. Dorsal aorta formation: separate origins, lateral-to-medial migration, and remodeling. *Dev Growth Differ*. 2013;55(1):113-129. doi:10.1111/dgd.12010
136. Makanya AN, Hlushchuk R, Djonov VG. Intussusceptive angiogenesis and its role in vascular morphogenesis, patterning, and remodeling. *Angiogenesis*. 2009;12(2):113-123. doi:10.1007/s10456-009-9129-5
137. Hlushchuk R, Ehrbar M, Reichmuth P, et al. Decrease in VEGF expression induces intussusceptive vascular pruning. *Arterioscler Thromb Vasc Biol*. 2011;31(12):2836-2844. doi:10.1161/ATVBAHA.111.231811
138. Hlushchuk R, Riesterer O, Baum O, et al. Tumor recovery by angiogenic switch from sprouting to intussusceptive angiogenesis after treatment with PTK787/ZK222584 or ionizing radiation. *Am J Pathol*. 2008;173(4):1173-1185. doi:10.2353/ajpath.2008.071131

139. Eming SA, Martin P, Tomic-Canic M. Wound repair and regeneration: mechanisms, signaling, and translation. *Sci Transl Med.* 2014;6(265):265sr6. doi:10.1126/scitranslmed.3009337
140. Wilgus TA. Vascular Endothelial Growth Factor and Cutaneous Scarring. *Adv Wound Care (New Rochelle).* 2019;8(12):671-678. doi:10.1089/wound.2018.0796
141. Boeldt DS, Bird IM. Vascular adaptation in pregnancy and endothelial dysfunction in preeclampsia. *J Endocrinol.* 2017;232(1):R27-R44. doi:10.1530/JOE-16-0340
142. Massri N, Loia R, Sones JL, Arora R, Douglas NC. Vascular changes in the cycling and early pregnant uterus. *JCI Insight.* 2023;8(11):e163422. Published 2023 Jun 8. doi:10.1172/jci.insight.163422
143. Barrasa-Ramos S, Dessalles CA, Hautefeuille M, Barakat AI. Mechanical regulation of the early stages of angiogenesis. *J R Soc Interface.* 2022;19(197):20220360. doi:10.1098/rsif.2022.0360
144. Phng LK, Gerhardt H. Angiogenesis: a team effort coordinated by notch. *Dev Cell.* 2009;16(2):196-208. doi:10.1016/j.devcel.2009.01.015
145. Jakobsson L, Franco CA, Bentley K, et al. Endothelial cells dynamically compete for the tip cell position during angiogenic sprouting. *Nat Cell Biol.* 2010;12(10):943-953. doi:10.1038/ncb2103
146. Leslie JD, Ariza-McNaughton L, Bermange AL, McAdow R, Johnson SL, Lewis J. Endothelial signalling by the Notch ligand Delta-like 4 restricts angiogenesis. *Development.* 2007;134(5):839-844. doi:10.1242/dev.003244
147. Hellström M, Phng LK, Hofmann JJ, et al. Dll4 signalling through Notch1 regulates formation of tip cells during angiogenesis. *Nature.* 2007;445(7129):776-780. doi:10.1038/nature05571
148. Suchting S, Freitas C, le Noble F, et al. The Notch ligand Delta-like 4 negatively regulates endothelial tip cell formation and vessel branching. *Proc Natl Acad Sci U S A.* 2007;104(9):3225-3230. doi:10.1073/pnas.0611177104
149. Krueger J, Liu D, Scholz K, et al. Flt1 acts as a negative regulator of tip cell formation and branching morphogenesis in the zebrafish embryo. *Development.* 2011;138(10):2111-2120. doi:10.1242/dev.063933
150. Blanco R, Gerhardt H. VEGF and Notch in tip and stalk cell selection. *Cold Spring Harb Perspect Med.* 2013;3(1):a006569. Published 2013 Jan 1. doi:10.1101/cshperspect.a006569
151. Fischer A, Schumacher N, Maier M, Sendtner M, Gessler M. The Notch target genes Hey1 and Hey2 are required for embryonic vascular development. *Genes Dev.* 2004;18(8):901-911. doi:10.1101/gad.291004
152. Phng LK, Potente M, Leslie JD, et al. Nrarp coordinates endothelial Notch and Wnt signaling to control vessel density in angiogenesis. *Dev Cell.* 2009;16(1):70-82. doi:10.1016/j.devcel.2008.12.009
153. Bentley, K., Franco, C., Philippides, A. et al. The role of differential VE-cadherin dynamics in cell rearrangement during angiogenesis. *Nat Cell Biol* **16**, 309–321 (2014). <https://doi.org/10.1038/ncb2926>
154. Fantin A, Vieira JM, Gestri G, et al. Tissue macrophages act as cellular chaperones for vascular anastomosis downstream of VEGF-mediated endothelial tip cell induction. *Blood.* 2010;116(5):829-840. doi:10.1182/blood-2009-12-257832
155. Charpentier MS, Conlon FL. Cellular and molecular mechanisms underlying blood vessel lumen formation. *Bioessays.* 2014;36(3):251-259. doi:10.1002/bies.201300133
156. Iruela-Arispe ML, Davis GE. Cellular and molecular mechanisms of vascular lumen formation. *Dev Cell.* 2009;16(2):222-231. doi:10.1016/j.devcel.2009.01.013
157. Lubarsky B, Krasnow MA. Tube morphogenesis: making and shaping biological tubes. *Cell.* 2003;112(1):19-28. doi:10.1016/s0092-8674(02)01283-7

158. Strilić B, Kucera T, Eglinger J, et al. The molecular basis of vascular lumen formation in the developing mouse aorta. *Dev Cell*. 2009;17(4):505-515. doi:10.1016/j.devcel.2009.08.011
159. Wang Y, Kaiser MS, Larson JD, et al. Moesin1 and Ve-cadherin are required in endothelial cells during in vivo tubulogenesis. *Development*. 2010;137(18):3119-3128. doi:10.1242/dev.048785
160. Nielsen JS, McNagny KM. Novel functions of the CD34 family [published correction appears in *J Cell Sci*. 2008 Dec 15;121(Pt 24):4145]. *J Cell Sci*. 2008;121(Pt 22):3683-3692. doi:10.1242/jcs.037507
161. Lampugnani MG, Orsenigo F, Rudini N, et al. CCM1 regulates vascular-lumen organization by inducing endothelial polarity. *J Cell Sci*. 2010;123(Pt 7):1073-1080. doi:10.1242/jcs.059329
162. Strilić B, Eglinger J, Krieg M, et al. Electrostatic cell-surface repulsion initiates lumen formation in developing blood vessels. *Curr Biol*. 2010;20(22):2003-2009. doi:10.1016/j.cub.2010.09.061
163. Lampugnani MG. Endothelial cell-to-cell junctions: adhesion and signaling in physiology and pathology. *Cold Spring Harb Perspect Med*. 2012;2(10):a006528. Published 2012 Oct 1. doi:10.1101/cshperspect.a006528
164. Haddad-Tóvolli R, Dragano NRV, Ramalho AFS, Velloso LA. Development and Function of the Blood-Brain Barrier in the Context of Metabolic Control. *Front Neurosci*. 2017;11:224. Published 2017 Apr 21. doi:10.3389/fnins.2017.00224
165. Dejana E. Endothelial cell-cell junctions: happy together. *Nat Rev Mol Cell Biol*. 2004;5(4):261-270. doi:10.1038/nrm1357
166. Carmeliet P, Lampugnani MG, Moons L, et al. Targeted deficiency or cytosolic truncation of the VE-cadherin gene in mice impairs VEGF-mediated endothelial survival and angiogenesis. *Cell*. 1999;98(2):147-157. doi:10.1016/s0092-8674(00)81010-7
167. Gory-Fauré S, Prandini MH, Pointu H, et al. Role of vascular endothelial-cadherin in vascular morphogenesis. *Development*. 1999;126(10):2093-2102. doi:10.1242/dev.126.10.2093
168. Red-Horse K, Siekmann AF. Veins and Arteries Build Hierarchical Branching Patterns Differently: Bottom-Up versus Top-Down. *Bioessays*. 2019;41(3):e1800198. doi:10.1002/bies.201800198
169. Red-Horse K, Ueno H, Weissman IL, Krasnow MA. Coronary arteries form by developmental reprogramming of venous cells. *Nature*. 2010;464(7288):549-553. doi:10.1038/nature08873
170. Hou S, Li Z, Dong J, et al. Heterogeneity in endothelial cells and widespread venous arterialization during early vascular development in mammals. *Cell Res*. 2022;32(4):333-348. doi:10.1038/s41422-022-00615-z
171. Rhee S, Wu JC. Vein to artery: the first arteriogenesis in the mammalian embryo. *Cell Res*. 2022;32(4):325-326. doi:10.1038/s41422-022-00629-7
172. Paik DT, Tian L, Williams IM, et al. Single-Cell RNA Sequencing Unveils Unique Transcriptomic Signatures of Organ-Specific Endothelial Cells. *Circulation*. 2020;142(19):1848-1862. doi:10.1161/CIRCULATIONAHA.119.041433
173. Xu C, Hasan SS, Schmidt I, et al. Arteries are formed by vein-derived endothelial tip cells. *Nat Commun*. 2014;5:5758. Published 2014 Dec 15. doi:10.1038/ncomms6758
174. Pitulescu ME, Schmidt I, Giaimo BD, et al. Dll4 and Notch signalling couples sprouting angiogenesis and artery formation. *Nat Cell Biol*. 2017;19(8):915-927. doi:10.1038/ncb3555
175. Shibuya M. Vascular Endothelial Growth Factor (VEGF) and Its Receptor (VEGFR) Signaling in Angiogenesis: A Crucial Target for Anti- and Pro-Angiogenic Therapies. *Genes Cancer*. 2011;2(12):1097-1105. doi:10.1177/1947601911423031

176. Akeson A, Herman A, Wiginton D, Greenberg J. Endothelial cell activation in a VEGF-A gradient: relevance to cell fate decisions. *Microvasc Res.* 2010;80(1):65-74. doi:10.1016/j.mvr.2010.02.001
177. Carmeliet P, Ferreira V, Breier G, et al. Abnormal blood vessel development and lethality in embryos lacking a single VEGF allele. *Nature.* 1996;380(6573):435-439. doi:10.1038/380435a0
178. Shalaby F, Rossant J, Yamaguchi TP, et al. Failure of blood-island formation and vasculogenesis in Flk-1-deficient mice. *Nature.* 1995;376(6535):62-66. doi:10.1038/376062a0
179. Fong GH, Rossant J, Gertsenstein M, Breitman ML. Role of the Flt-1 receptor tyrosine kinase in regulating the assembly of vascular endothelium. *Nature.* 1995;376(6535):66-70. doi:10.1038/376066a0
180. Ho VC, Duan LJ, Cronin C, Liang BT, Fong GH. Elevated vascular endothelial growth factor receptor-2 abundance contributes to increased angiogenesis in vascular endothelial growth factor receptor-1-deficient mice. *Circulation.* 2012;126(6):741-752. doi:10.1161/CIRCULATIONAHA.112.091603
181. Carmeliet P, Moons L, Lutun A, et al. Synergism between vascular endothelial growth factor and placental growth factor contributes to angiogenesis and plasma extravasation in pathological conditions. *Nat Med.* 2001;7(5):575-583. doi:10.1038/87904
182. McColl BK, Paavonen K, Karnezis T, et al. Proprotein convertases promote processing of VEGF-D, a critical step for binding the angiogenic receptor VEGFR-2. *FASEB J.* 2007;21(4):1088-1098. doi:10.1096/fj.06-7060com
183. Benedito R, Rocha SF, Woeste M, et al. Notch-dependent VEGFR3 upregulation allows angiogenesis without VEGF-VEGFR2 signalling. *Nature.* 2012;484(7392):110-114. Published 2012 Mar 18. doi:10.1038/nature10908
184. Alitalo K, Carmeliet P. Molecular mechanisms of lymphangiogenesis in health and disease. *Cancer Cell.* 2002;1(3):219-227. doi:10.1016/s1535-6108(02)00051-x
185. Dumont DJ, Jussila L, Taipale J, et al. Cardiovascular failure in mouse embryos deficient in VEGF receptor-3. *Science.* 1998;282(5390):946-949. doi:10.1126/science.282.5390.946
186. Cao Y, Linden P, Farnebo J, et al. Vascular endothelial growth factor C induces angiogenesis in vivo. *Proc Natl Acad Sci U S A.* 1998;95(24):14389-14394. doi:10.1073/pnas.95.24.14389
187. Marconcini L, Marchio S, Morbidelli L, et al. c-fos-induced growth factor/vascular endothelial growth factor D induces angiogenesis in vivo and in vitro. *Proc Natl Acad Sci U S A.* 1999;96(17):9671-9676. doi:10.1073/pnas.96.17.9671
188. Witzensbichler B, Asahara T, Murohara T, et al. Vascular endothelial growth factor-C (VEGF-C/VEGF-2) promotes angiogenesis in the setting of tissue ischemia. *Am J Pathol.* 1998;153(2):381-394. doi:10.1016/S0002-9440(10)65582-4
189. Tammela T, Zarkada G, Wallgard E, et al. Blocking VEGFR-3 suppresses angiogenic sprouting and vascular network formation. *Nature.* 2008;454(7204):656-660. doi:10.1038/nature07083
190. Korhonen EA, Murtomäki A, Jha SK, et al. Lymphangiogenesis requires Ang2/Tie/PI3K signaling for VEGFR3 cell-surface expression. *J Clin Invest.* 2022;132(15):e155478. doi:10.1172/JCI155478
191. Heinolainen K, Karaman S, D'Amico G, et al. VEGFR3 Modulates Vascular Permeability by Controlling VEGF/VEGFR2 Signaling. *Circ Res.* 2017;120(9):1414-1425. doi:10.1161/CIRCRESAHA.116.310477
192. Hori K, Sen A, Artavanis-Tsakonas S. Notch signaling at a glance. *J Cell Sci.* 2013;126(Pt 10):2135-2140. doi:10.1242/jcs.127308
193. Pedrosa AR, Trindade A, Fernandes AC, et al. Endothelial Jagged1 antagonizes DLL4 regulation of endothelial branching and promotes vascular maturation downstream of

- Dll4/Notch1. *Arterioscler Thromb Vasc Biol.* 2015;35(5):1134-1146. doi:10.1161/ATVBAHA.114.304741
194. Adams RH, Wilkinson GA, Weiss C, et al. Roles of ephrinB ligands and EphB receptors in cardiovascular development: demarcation of arterial/venous domains, vascular morphogenesis, and sprouting angiogenesis. *Genes Dev.* 1999;13(3):295-306. doi:10.1101/gad.13.3.295
 195. Yang C, Guo Y, Jadlowiec CC, et al. Vascular endothelial growth factor-A inhibits EphB4 and stimulates delta-like ligand 4 expression in adult endothelial cells. *J Surg Res.* 2013;183(1):478-486. doi:10.1016/j.jss.2013.01.009
 196. Wang HU, Chen ZF, Anderson DJ. Molecular distinction and angiogenic interaction between embryonic arteries and veins revealed by ephrin-B2 and its receptor Eph-B4. *Cell.* 1998;93(5):741-753. doi:10.1016/s0092-8674(00)81436-1
 197. Poliakov A, Cotrina ML, Pasini A, Wilkinson DG. Regulation of EphB2 activation and cell repulsion by feedback control of the MAPK pathway. *J Cell Biol.* 2008;183(5):933-947. doi:10.1083/jcb.200807151
 198. Mertens-Walker I, Fernandini BC, Maharaj MS, et al. The tumour-promoting receptor tyrosine kinase, EphB4, regulates expression of integrin- β 8 in prostate cancer cells. *BMC Cancer.* 2015;15:164. Published 2015 Mar 22. doi:10.1186/s12885-015-1164-6
 199. Wolf K, Hu H, Isaji T, Dardik A. Molecular identity of arteries, veins, and lymphatics. *J Vasc Surg.* 2019;69(1):253-262. doi:10.1016/j.jvs.2018.06.195
 200. Pitulescu ME, Adams RH. Regulation of signaling interactions and receptor endocytosis in growing blood vessels. *Cell Adh Migr.* 2014;8(4):366-377. doi:10.4161/19336918.2014.970010
 201. Polvani S, Pepe S, Milani S, Galli A. COUP-TFII in Health and Disease. *Cells.* 2019;9(1):101. Published 2019 Dec 31. doi:10.3390/cells9010101
 202. Li W, Liu C, Burns N, et al. Alterations in the spatiotemporal expression of the chemokine receptor CXCR4 in endothelial cells cause failure of hierarchical vascular branching. *Dev Biol.* 2021;477:70-84. doi:10.1016/j.ydbio.2021.05.008
 203. Siekmann AF, Standley C, Fogarty KE, Wolfe SA, Lawson ND. Chemokine signaling guides regional patterning of the first embryonic artery. *Genes Dev.* 2009;23(19):2272-2277. doi:10.1101/gad.1813509
 204. Tachibana K, Hirota S, Iizasa H, et al. The chemokine receptor CXCR4 is essential for vascularization of the gastrointestinal tract. *Nature.* 1998;393(6685):591-594. doi:10.1038/31261
 205. Dekker RJ, van Soest S, Fontijn RD, et al. Prolonged fluid shear stress induces a distinct set of endothelial cell genes, most specifically lung Krüppel-like factor (KLF2). *Blood.* 2002;100(5):1689-1698. doi:10.1182/blood-2002-01-0046
 206. Jain RK. Molecular regulation of vessel maturation. *Nat Med.* 2003;9(6):685-693. doi:10.1038/nm0603-685
 207. Kuo CT, Veselits ML, Barton KP, Lu MM, Clendenin C, Leiden JM. The LKLF transcription factor is required for normal tunica media formation and blood vessel stabilization during murine embryogenesis. *Genes Dev.* 1997;11(22):2996-3006. doi:10.1101/gad.11.22.2996
 208. Dyer LA, Patterson C. Development of the endothelium: an emphasis on heterogeneity. *Semin Thromb Hemost.* 2010;36(3):227-235. doi:10.1055/s-0030-1253446
 209. Yamazaki T, Mukoyama YS. Tissue Specific Origin, Development, and Pathological Perspectives of Pericytes. *Front Cardiovasc Med.* 2018;5:78. Published 2018 Jun 27. doi:10.3389/fcvm.2018.00078
 210. Gaengel K, Genové G, Armulik A, Betsholtz C. Endothelial-mural cell signaling in vascular development and angiogenesis. *Arterioscler Thromb Vasc Biol.* 2009;29(5):630-638. doi:10.1161/ATVBAHA.107.161521

211. Hellström M, Kalén M, Lindahl P, Abramsson A, Betsholtz C. Role of PDGF-B and PDGFR-beta in recruitment of vascular smooth muscle cells and pericytes during embryonic blood vessel formation in the mouse. *Development*. 1999;126(14):3047-3055. doi:10.1242/dev.126.14.3047
212. Hirschi KK, Rohovsky SA, Beck LH, Smith SR, D'Amore PA. Endothelial cells modulate the proliferation of mural cell precursors via platelet-derived growth factor-BB and heterotypic cell contact. *Circ Res*. 1999;84(3):298-305. doi:10.1161/01.res.84.3.298
213. Lindahl P, Johansson BR, Levéen P, Betsholtz C. Pericyte loss and microaneurysm formation in PDGF-B-deficient mice. *Science*. 1997;277(5323):242-245. doi:10.1126/science.277.5323.242
214. Potente M, Gerhardt H, Carmeliet P. Basic and therapeutic aspects of angiogenesis. *Cell*. 2011;146(6):873-887. doi:10.1016/j.cell.2011.08.039
215. Marchand M, Monnot C, Muller L, Germain S. Extracellular matrix scaffolding in angiogenesis and capillary homeostasis. *Semin Cell Dev Biol*. 2019;89:147-156. doi:10.1016/j.semcdb.2018.08.007
216. Mongiat M, Andreuzzi E, Tarticchio G, Paulitti A. Extracellular Matrix, a Hard Player in Angiogenesis. *Int J Mol Sci*. 2016;17(11):1822. Published 2016 Nov 1. doi:10.3390/ijms17111822
217. Korn C, Augustin HG. Mechanisms of Vessel Pruning and Regression. *Dev Cell*. 2015;34(1):5-17. doi:10.1016/j.devcel.2015.06.004
218. Alon T, Hemo I, Itin A, Pe'er J, Stone J, Keshet E. Vascular endothelial growth factor acts as a survival factor for newly formed retinal vessels and has implications for retinopathy of prematurity. *Nat Med*. 1995;1(10):1024-1028. doi:10.1038/nm1095-1024
219. Franco CA, Jones ML, Bernabeu MO, et al. Dynamic endothelial cell rearrangements drive developmental vessel regression [published correction appears in PLoS Biol. 2015 May 14;13(5):e1002163. doi: 10.1371/journal.pbio.1002163]. *PLoS Biol*. 2015;13(4):e1002125. Published 2015 Apr 17. doi:10.1371/journal.pbio.1002125
220. Blancas AA, Wong LE, Glaser DE, McCloskey KE. Specialized tip/stalk-like and phalanx-like endothelial cells from embryonic stem cells. *Stem Cells Dev*. 2013;22(9):1398-1407. doi:10.1089/scd.2012.0376
221. Ricard N, Bailly S, Guignabert C, Simons M. The quiescent endothelium: signalling pathways regulating organ-specific endothelial normalcy. *Nat Rev Cardiol*. 2021;18(8):565-580. doi:10.1038/s41569-021-00517-4
222. Graupera M, Guillermet-Guibert J, Foukas LC, et al. Angiogenesis selectively requires the p110alpha isoform of PI3K to control endothelial cell migration. *Nature*. 2008;453(7195):662-666. doi:10.1038/nature06892
223. Bi L, Okabe I, Bernard DJ, Wynshaw-Boris A, Nussbaum RL. Proliferative defect and embryonic lethality in mice homozygous for a deletion in the p110alpha subunit of phosphoinositide 3-kinase. *J Biol Chem*. 1999;274(16):10963-10968. doi:10.1074/jbc.274.16.10963
224. Lelievre E, Bourbon PM, Duan LJ, Nussbaum RL, Fong GH. Deficiency in the p110alpha subunit of PI3K results in diminished Tie2 expression and Tie2(-/-)-like vascular defects in mice. *Blood*. 2005;105(10):3935-3938. doi:10.1182/blood-2004-10-3955
225. Angulo-Urarte A, Casado P, Castillo SD, et al. Endothelial cell rearrangements during vascular patterning require PI3-kinase-mediated inhibition of actomyosin contractility. *Nat Commun*. 2018;9(1):4826. Published 2018 Nov 16. doi:10.1038/s41467-018-07172-3
226. Hong CC, Kume T, Peterson RT. Role of crosstalk between phosphatidylinositol 3-kinase and extracellular signal-regulated kinase/mitogen-activated protein kinase pathways in artery-vein specification. *Circ Res*. 2008;103(6):573-579. doi:10.1161/CIRCRESAHA.108.180745
227. Ren B, Deng Y, Mukhopadhyay A, et al. ERK1/2-Akt1 crosstalk regulates arteriogenesis in mice and zebrafish. *J Clin Invest*. 2010;120(4):1217-1228. doi:10.1172/JCI39837

228. Hong CC, Peterson QP, Hong JY, Peterson RT. Artery/vein specification is governed by opposing phosphatidylinositol-3 kinase and MAP kinase/ERK signaling. *Curr Biol*. 2006;16(13):1366-1372. doi:10.1016/j.cub.2006.05.046
229. Yuan TL, Choi HS, Matsui A, et al. Class 1A PI3K regulates vessel integrity during development and tumorigenesis. *Proc Natl Acad Sci U S A*. 2008;105(28):9739-9744. doi:10.1073/pnas.0804123105
230. Ghigo A. Cell-specific roles of p110 β in myocardial ischaemia. *Cardiovasc Res*. 2019;115(8):1264-1265. doi:10.1093/cvr/cvz051
231. Whitehead MA, Bombardieri M, Pitzalis C, Vanhaesebroeck B. Isoform-selective induction of human p110 δ PI3K expression by TNF α : identification of a new and inducible PIK3CD promoter. *Biochem J*. 2012;443(3):857-867. doi:10.1042/BJ20112214
232. Ruan GX, Kazlauskas A. VEGF-A engages at least three tyrosine kinases to activate PI3K/Akt. *Cell Cycle*. 2012;11(11):2047-2048. doi:10.4161/cc.20535
233. Figueiredo AM, Villacampa P, Diéguez-Hurtado R, et al. Phosphoinositide 3-Kinase-Regulated Pericyte Maturation Governs Vascular Remodeling. *Circulation*. 2020;142(7):688-704. doi:10.1161/CIRCULATIONAHA.119.042354
234. Shibuya M. Vascular endothelial growth factor receptor-1 (VEGFR-1/Flt-1): a dual regulator for angiogenesis. *Angiogenesis*. 2006;9(4):225-231. doi:10.1007/s10456-006-9055-8
235. Graupera M, Potente M. Regulation of angiogenesis by PI3K signaling networks. *Exp Cell Res*. 2013;319(9):1348-1355. doi:10.1016/j.yexcr.2013.02.021
236. Olsson AK, Dimberg A, Kreuger J, Claesson-Welsh L. VEGF receptor signalling - in control of vascular function. *Nat Rev Mol Cell Biol*. 2006;7(5):359-371. doi:10.1038/nrm1911
237. Ruan GX, Kazlauskas A. Axl is essential for VEGF-A-dependent activation of PI3K/Akt. *EMBO J*. 2012;31(7):1692-1703. doi:10.1038/emboj.2012.21
238. Gupta S, Ramjaun AR, Haiko P, et al. Binding of ras to phosphoinositide 3-kinase p110 α is required for ras-driven tumorigenesis in mice. *Cell*. 2007;129(5):957-968. doi:10.1016/j.cell.2007.03.051
239. Augustin HG, Koh GY, Thurston G, Alitalo K. Control of vascular morphogenesis and homeostasis through the angiopoietin-Tie system. *Nat Rev Mol Cell Biol*. 2009;10(3):165-177. doi:10.1038/nrm2639
240. Papapetropoulos A, Fulton D, Mahboubi K, et al. Angiopoietin-1 inhibits endothelial cell apoptosis via the Akt/survivin pathway. *J Biol Chem*. 2000;275(13):9102-9105. doi:10.1074/jbc.275.13.9102
241. Makki N, Thiel KW, Miller FJ Jr. The epidermal growth factor receptor and its ligands in cardiovascular disease. *Int J Mol Sci*. 2013;14(10):20597-20613. Published 2013 Oct 15. doi:10.3390/ijms141020597
242. Bjorge JD, Chan TO, Antczak M, Kung HJ, Fujita DJ. Activated type I phosphatidylinositol kinase is associated with the epidermal growth factor (EGF) receptor following EGF stimulation. *Proc Natl Acad Sci U S A*. 1990;87(10):3816-3820. doi:10.1073/pnas.87.10.3816
243. Karar J, Maity A. PI3K/AKT/mTOR Pathway in Angiogenesis. *Front Mol Neurosci*. 2011;4:51. Published 2011 Dec 2. doi:10.3389/fnmol.2011.00051
244. Tabernero J. The role of VEGF and EGFR inhibition: implications for combining anti-VEGF and anti-EGFR agents. *Mol Cancer Res*. 2007;5(3):203-220. doi:10.1158/1541-7786.MCR-06-0404
245. Phung TL, Ziv K, Dabydeen D, et al. Pathological angiogenesis is induced by sustained Akt signaling and inhibited by rapamycin. *Cancer Cell*. 2006;10(2):159-170. doi:10.1016/j.ccr.2006.07.003
246. Ola R, Dubrac A, Han J, et al. PI3 kinase inhibition improves vascular malformations in mouse models of hereditary haemorrhagic telangiectasia. *Nat Commun*. 2016;7:13650. Published 2016 Nov 29. doi:10.1038/ncomms13650

247. Lee MY, Luciano AK, Ackah E, et al. Endothelial Akt1 mediates angiogenesis by phosphorylating multiple angiogenic substrates. *Proc Natl Acad Sci U S A*. 2014;111(35):12865-12870. doi:10.1073/pnas.1408472111
248. Luo Z, Fujio Y, Kureishi Y, et al. Acute modulation of endothelial Akt/PKB activity alters nitric oxide-dependent vasomotor activity in vivo. *J Clin Invest*. 2000;106(4):493-499. doi:10.1172/JCI9419
249. Yamamoto N, Oyaizu T, Enomoto M, et al. VEGF and bFGF induction by nitric oxide is associated with hyperbaric oxygen-induced angiogenesis and muscle regeneration. *Sci Rep*. 2020;10(1):2744. Published 2020 Feb 17. doi:10.1038/s41598-020-59615-x
250. Potente M, Urbich C, Sasaki K, et al. Involvement of Foxo transcription factors in angiogenesis and postnatal neovascularization. *J Clin Invest*. 2005;115(9):2382-2392. doi:10.1172/JCI23126
251. Wilhelm K, Happel K, Eelen G, et al. FOXO1 couples metabolic activity and growth state in the vascular endothelium. *Nature*. 2016;529(7585):216-220. doi:10.1038/nature16498
252. Furuyama T, Kitayama K, Shimoda Y, et al. Abnormal angiogenesis in Foxo1 (Fkhr)-deficient mice. *J Biol Chem*. 2004;279(33):34741-34749. doi:10.1074/jbc.M314214200
253. Hosaka T, Biggs WH 3rd, Tieu D, et al. Disruption of forkhead transcription factor (FOXO) family members in mice reveals their functional diversification. *Proc Natl Acad Sci U S A*. 2004;101(9):2975-2980. doi:10.1073/pnas.0400093101
254. Dharaneeswaran H, Abid MR, Yuan L, et al. FOXO1-mediated activation of Akt plays a critical role in vascular homeostasis [published correction appears in *Circ Res*. 2014 Aug 1;115(4):e9]. *Circ Res*. 2014;115(2):238-251. doi:10.1161/CIRCRESAHA.115.303227
255. Kim J, Guan KL. mTOR as a central hub of nutrient signalling and cell growth. *Nat Cell Biol*. 2019;21(1):63-71. doi:10.1038/s41556-018-0205-1
256. Saxton RA, Sabatini DM. mTOR Signaling in Growth, Metabolism, and Disease [published correction appears in *Cell*. 2017 Apr 6;169(2):361-371. doi:10.1016/j.cell.2017.03.035]. *Cell*. 2017;168(6):960-976. doi:10.1016/j.cell.2017.02.004
257. Ding Y, Shan L, Nai W, et al. DEPTOR Deficiency-Mediated mTORc1 Hyperactivation in Vascular Endothelial Cells Promotes Angiogenesis. *Cell Physiol Biochem*. 2018;46(2):520-531. doi:10.1159/000488619
258. Fan W, Han D, Sun Z, et al. Endothelial deletion of mTORC1 protects against hindlimb ischemia in diabetic mice via activation of autophagy, attenuation of oxidative stress and alleviation of inflammation. *Free Radic Biol Med*. 2017;108:725-740. doi:10.1016/j.freeradbiomed.2017.05.001
259. Dormond O, Madsen JC, Briscoe DM. The effects of mTOR-Akt interactions on anti-apoptotic signaling in vascular endothelial cells. *J Biol Chem*. 2007;282(32):23679-23686. doi:10.1074/jbc.M700563200
260. Wang, Y., Li, Q., Zhang, Z. *et al.* mTOR contributes to endothelium-dependent vasorelaxation by promoting eNOS expression and preventing eNOS uncoupling. *Commun Biol* 5, 726 (2022). <https://doi.org/10.1038/s42003-022-03653-w>
261. Laplante M, Sabatini DM. mTOR signaling in growth control and disease. *Cell*. 2012;149(2):274-293. doi:10.1016/j.cell.2012.03.017
262. Hamada K, Sasaki T, Koni PA, et al. The PTEN/PI3K pathway governs normal vascular development and tumor angiogenesis. *Genes Dev*. 2005;19(17):2054-2065. doi:10.1101/gad.1308805
263. Choorapoikayil S, Weijts B, Kers R, de Bruin A, den Hertog J. Loss of Pten promotes angiogenesis and enhanced vegfaa expression in zebrafish. *Dis Model Mech*. 2013;6(5):1159-1166. doi:10.1242/dmm.012377
264. Serra H, Chivite I, Angulo-Urarte A, et al. PTEN mediates Notch-dependent stalk cell arrest in angiogenesis. *Nat Commun*. 2015;6:7935. Published 2015 Jul 31. doi:10.1038/ncomms8935

265. Herbert SP, Huisken J, Kim TN, et al. Arterial-venous segregation by selective cell sprouting: an alternative mode of blood vessel formation. *Science*. 2009;326(5950):294-298. doi:10.1126/science.1178577
266. Blum S, Issbrücker K, Willuweit A, et al. An inhibitory role of the phosphatidylinositol 3-kinase-signaling pathway in vascular endothelial growth factor-induced tissue factor expression. *J Biol Chem*. 2001;276(36):33428-33434. doi:10.1074/jbc.M105474200
267. Chu M, Li T, Shen B, et al. Angiopoietin receptor Tie2 is required for vein specification and maintenance via regulating COUP-TFII. *Elife*. 2016;5:e21032. Published 2016 Dec 22. doi:10.7554/eLife.21032
268. Kinross KM, Montgomery KG, Kleinschmidt M, et al. An activating Pik3ca mutation coupled with Pten loss is sufficient to initiate ovarian tumorigenesis in mice. *J Clin Invest*. 2012;122(2):553-557. doi:10.1172/JCI59309
269. Robinson G, Parker M, Kranenburg TA, et al. Novel mutations target distinct subgroups of medulloblastoma. *Nature*. 2012;488(7409):43-48. doi:10.1038/nature11213
270. Claxton S, Kostourou V, Jadeja S, Chambon P, Hodivala-Dilke K, Fruttiger M. Efficient, inducible Cre-recombinase activation in vascular endothelium. *Genesis*. 2008;46(2):74-80. doi:10.1002/dvg.20367
271. Kisanuki YY, Hammer RE, Miyazaki J, Williams SC, Richardson JA, Yanagisawa M. Tie2-Cre transgenic mice: a new model for endothelial cell-lineage analysis in vivo. *Dev Biol*. 2001;230(2):230-242. doi:10.1006/dbio.2000.0106
272. Muzumdar MD, Tasic B, Miyamichi K, Li L, Luo L. A global double-fluorescent Cre reporter mouse. *Genesis*. 2007;45(9):593-605. doi:10.1002/dvg.20335
273. Stahl A, Connor KM, Sapieha P, et al. The mouse retina as an angiogenesis model. *Invest Ophthalmol Vis Sci*. 2010;51(6):2813-2826. doi:10.1167/iovs.10-5176
274. Roy A, Skibo J, Kalume F, et al. Mouse models of human PIK3CA-related brain overgrowth have acutely treatable epilepsy. *Elife*. 2015;4:e12703. Published 2015 Dec 3. doi:10.7554/eLife.12703
275. Gong GQ, Bilanges B, Allsop B, et al. A small-molecule PI3K α activator for cardioprotection and neuroregeneration. *Nature*. 2023;618(7963):159-168. doi:10.1038/s41586-023-05972-2
276. Krimmer SG, Schlessinger J. Unveiling molecular insights into the mechanism of activation of oncogenic phosphoinositide 3-kinase mutants. *Proc Natl Acad Sci U S A*. 2022;119(50):e2218237119. doi:10.1073/pnas.2218237119
277. Jiang W, He T, Liu S, et al. The PIK3CA E542K and E545K mutations promote glycolysis and proliferation via induction of the β -catenin/SIRT3 signaling pathway in cervical cancer. *J Hematol Oncol*. 2018;11(1):139. Published 2018 Dec 14. doi:10.1186/s13045-018-0674-5
278. Zhao S, Cao Y, Liu SB, et al. The E545K mutation of PIK3CA promotes gallbladder carcinoma progression through enhanced binding to EGFR. *J Exp Clin Cancer Res*. 2016;35(1):97. Published 2016 Jun 18. doi:10.1186/s13046-016-0370-7
279. Wang YA, Zheng JW, Fei ZL, et al. A novel transgenic mice model for venous malformation. *Transgenic Res*. 2009;18(2):193-201. doi:10.1007/s11248-008-9224-1
280. Goines J, Boscolo E. A Xenograft Model for Venous Malformation. *Methods Mol Biol*. 2021;2206:179-192. doi:10.1007/978-1-0716-0916-3_13
281. Pitulescu ME, Schmidt I, Benedito R, Adams RH. Inducible gene targeting in the neonatal vasculature and analysis of retinal angiogenesis in mice. *Nat Protoc*. 2010;5(9):1518-1534. doi:10.1038/nprot.2010.113
282. Castillo SD, Baselga E, Graupera M. PIK3CA mutations in vascular malformations. *Curr Opin Hematol*. 2019;26(3):170-178. doi:10.1097/MOH.0000000000000496

283. Moulton KS, Li M, Strand K, et al. PTEN deficiency promotes pathological vascular remodeling of human coronary arteries. *JCI Insight*. 2018;3(4):e97228. Published 2018 Feb 22. doi:10.1172/jci.insight.97228
284. Abdelilah-Seyfried S, Ola R. Shear stress and pathophysiological PI3K involvement in vascular malformations. *J Clin Invest*. 2024;134(10):e172843. Published 2024 May 15. doi:10.1172/JCI172843
285. Liu ZJ, Xiao M, Balint K, et al. Inhibition of endothelial cell proliferation by Notch1 signaling is mediated by repressing MAPK and PI3K/Akt pathways and requires MAML1. *FASEB J*. 2006;20(7):1009-1011. doi:10.1096/fj.05-4880fje
286. Wee P, Wang Z. Epidermal Growth Factor Receptor Cell Proliferation Signaling Pathways. *Cancers (Basel)*. 2017;9(5):52. Published 2017 May 17. doi:10.3390/cancers9050052
287. Young CD, Zimmerman LJ, Hoshino D, et al. Activating PIK3CA Mutations Induce an Epidermal Growth Factor Receptor (EGFR)/Extracellular Signal-regulated Kinase (ERK) Paracrine Signaling Axis in Basal-like Breast Cancer. *Mol Cell Proteomics*. 2015;14(7):1959-1976. doi:10.1074/mcp.M115.049783
288. Arjumand W, Merry CD, Wang C, et al. Phosphatidylinositol-3 kinase (PIK3CA) E545K mutation confers cisplatin resistance and a migratory phenotype in cervical cancer cells. *Oncotarget*. 2016;7(50):82424-82439. doi:10.18632/oncotarget.10955
289. Maik-Rachline G, Hacoheh-Lev-Ran A, Seger R. Nuclear ERK: Mechanism of Translocation, Substrates, and Role in Cancer. *Int J Mol Sci*. 2019;20(5):1194. Published 2019 Mar 8. doi:10.3390/ijms20051194
290. Nguyen HL, Boon LM, Vikkula M. Trametinib as a promising therapeutic option in alleviating vascular defects in an endothelial KRAS-induced mouse model. *Hum Mol Genet*. 2023;32(2):276-289. doi:10.1093/hmg/ddac169
291. Nicholson CL, Flanagan S, Murati M, et al. Successful management of an arteriovenous malformation with trametinib in a patient with capillary-malformation arteriovenous malformation syndrome and cardiac compromise. *Pediatr Dermatol*. 2022;39(2):316-319. doi:10.1111/pde.14912
292. Cooke, Daniel L.a; Frieden, Ilona J.b; Shimano, Kristin A.c. Angiographic Evidence of Response to Trametinib Therapy for a Spinal Cord Arteriovenous Malformation. *Journal of Vascular Anomalies* 2(3):p e018, September 2021. | DOI: 10.1097/JOVA.0000000000000018
293. Li D, March ME, Gutierrez-Uzquiza A, et al. ARAF recurrent mutation causes central conducting lymphatic anomaly treatable with a MEK inhibitor. *Nat Med*. 2019;25(7):1116-1122. doi:10.1038/s41591-019-0479-2
294. Liu Y, Li Y, Wang Y, et al. Recent progress on vascular endothelial growth factor receptor inhibitors with dual targeting capabilities for tumor therapy. *J Hematol Oncol*. 2022;15(1):89. Published 2022 Jul 7. doi:10.1186/s13045-022-01310-7
295. Zubair T, Bandyopadhyay D. Small Molecule EGFR Inhibitors as Anti-Cancer Agents: Discovery, Mechanisms of Action, and Opportunities. *Int J Mol Sci*. 2023;24(3):2651. Published 2023 Jan 31. doi:10.3390/ijms24032651